# Light-Driven Multielectron Chemical Transformations with Tailored Nanoparticles

विद्या वाचस्पति की

उपाधि की अपेक्षाओं की आंशिक पूर्ति में प्रस्तुत शोध प्रबंध

A thesis submitted in partial fulfillment of the requirements of the degree of Doctor of Philosophy

द्वारा / By

वंशिका जैन / Vanshika Jain

पंजीकरण सं. २०१९३६७७/ Registration No.: 20193677

शोध प्रबंध पर्यवेक्षक / Thesis Supervisor:

प्रो. प्रमोद पी. पिल्लई/ Prof. Pramod P. Pillai


भारतीय विज्ञान शिक्षा एवं अनुसंधान संस्थान पुणे

INDIAN INSTITUTE OF SCIENCE EDUCATION AND RESEARCH PUNE

2025

# Certificate

I certify that the thesis entitled "***Light-Driven Multielectron Chemical Transformations with Tailored Nanoparticles***" presented by Ms. Vanshika Jain represents her original work, which was carried out by her at IISER, Pune, under my guidance and supervision during the period from August 2019 to June 2025. The work presented here or any part of it has not been included in any other thesis submitted previously for the award of any degree or diploma from any other University or institutions.

I further certify that the above statements made by her in regard to her thesis are correct to the best of my knowledge.

**Date**: 05/06/2025

**Place**: Pune, India

**Prof. Pramod P. Pillai**

*Thesis Supervisor*

# Declaration

I declare that this written submission represents my idea in my own words and where others' ideas have been included; I have adequately cited and referenced the original sources. I also declare that I have adhered to all principles of academic honesty and integrity and have not misrepresented or fabricated or falsified any idea/data/fact/source in my submission. I understand that violation of the above will be cause for disciplinary action by the Institute and can also evoke penal action from the sources which have thus not been properly cited or from whom proper permission has not been taken when needed. The work reported in this thesis is the original work done by me under the guidance of Prof. Pramod P. Pillai.

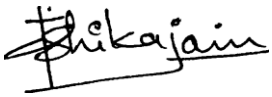

**Date**: 05/06/2025

**Vanshika Jain**

**Place**: Pune, India

Registration I.D.: 20193677

# Acknowledgments

To the outside world, a PhD is often seen as traveling lonesome on a long crusade to reach a singular goal. I am lucky that the tables have turned, and I found some great people on this journey to add the prefix *"Dr."* to my name. A mere *"thank you"* to people who have been a part of this journey, directly or indirectly, would be highly embarrassing and utterly inadequate. I am immensely grateful for all the love, support, guidance, and constant motivation from *everyone* involved. The acknowledgments section of the thesis is always accompanied by the risk of forgetting to thank all people in the way they might expect, but I will try my best with my pretty decent memory.

Firstly, my thesis supervisor- ***Prof. Pramod P. Pillai***; "Death is the only equilibrium state, rest everything is non-equilibrium…" I still remember this sentence from the PhD orientation session, which completely blew my mind and persuaded me to join your group. I must mention to the readers that I would not have enjoyed doing a PhD if it weren't for the Nano Alchemy Lab. Not only did I learn the way of doing science, but also the important life skills, be it man-management or handling failures and rejections, or celebrating small wins. For me, the past 5 years or so have been a time of tremendous growth and have shaped me as a person who can dream big without any fear. I must admit that I continue to admire your ability to communicate the scientific work with a mix of enthusiasm, slick slides, and structure, and making sure each one of us delivers our best. I would like to thank you for being so patient (with ~ 3 years of no positive results, and then never-ending revisions of almost all the projects) and, at the same time, for encouraging me, and, most importantly, for having faith in me when the road was tough. I am grateful for your unwavering support throughout. Thank you for being a fantastic mentor and an amazing human. I will forever cherish our mentor-mentee relationship.

Next, I thank my RAC members, ***Dr. C. S. Gopinath*** and ***Prof. Shabana Khan***, for all the wonderful discussions from time to time. I would like to mention I was introduced to research by Gopinath Sir in 2016 when I joined his group as a summer research fellow and the experience was so fulfilling that I continue to cherish the same till now. Thank you

for all the inspiration and encouragement. I hope I will get opportunities to interact with both of you.

I consider myself fortunate to have joined the lab at the correct time as I could spend the initial few months working with three incredible seniors of Nanoalchemy lab, ***Anish***, ***Gayathri***, and ***Soumendu***. The virtues I learned (*and still learning*) from these three guys have shaped me scientifically and non-scientifically. Thank you all of you for being such kind mentors and awesome humans.

Then comes the next generation seniors, Sumit and Indra.

***Sumit***- I still can't believe that we didn't talk for at least 2 months after I joined and suddenly became gossipmongers after the 2019 Kerala trip. Thankfully, I came along with you guys by not appearing for the mid-sem exam. Countless stories about you; I hope the stories with all the necessary *'masala'* will be told to juniors in the lab. I am in awe of your expressions while dancing, the art of storytelling, your commitment to saving TMA and enzymes after the fire accident, and many more. *S*poiler alert** If you see a picture of three men in helmets somewhere in C214, know that Sumit Roy was the mastermind!

***Indra***- So my first thought about you that of a lab technician and assistant turned out to be true **pun intended**. But honestly, thank you for always being there, on both professional and personal fronts. You have been such an immense emotional support throughout and continue to remain till now. I still need to learn certain things from you, for instance, having all the possible technological advances, cracking up the best jokes, and keeping up with *'n'* hobbies **pun intended again**. Thank you, guys, for keeping me sane during the last 5 years.

Next in line are *Pradyut* and *Kashyap*, who technically are seniors but nobody cares :P

***Pradyut***- You have taught me so much and a lot more is left to learn from you. If I was stuck somewhere, I always knew that I could always come to you for the rescue. A big thank you for always being there, be it a new project discussion, or experiment, or any kind of professional/personal support. Also, your life's motto has been pretty helpful for survival and moving on *(IYKYK)*. Thank you for being there in need, and I will cherish our friendship forever.

***Kashyap Ji***- I was lucky because gone are the days when everyone looked forward to the lab tour by Kashyap G. Over the past few years, I learned from you how complex things can be taught in a simplistic manner, how a simple idea can be brought to a prototype, and how leadership skills can be effectively utilized. Thank you for keeping the lab environment jolly and lively, else the journey would have been too unforgiving.

While the Covid-19 pandemic was still going on, ***Ankit*** became part of C-214 *virtually*. And the day he came to the lab, my projects came to a standstill. I will remember this, okay! *(just kidding)*. Your dedication towards picking up others' personalities has finally transformed you into a perfect doppelganger. I must admit that I am jealous of your ability to sleep anytime and anywhere, just in the blink of an eye. The lab would have been very monotonous if you weren't there with updated memes and reels. With such beautiful hands, I hope we all will see many more exotic nanostructures in future.

I am grateful to have met two amazing juniors- ***Shreya*** (Tyagi) and ***Adhra*** (ChiChi). Spending time with you guys felt like family: warm, cozy, and pure bliss. Thank you for listening to my rants every single day, and tolerating my ability to pass on existential crisis. I cannot imagine now how the journey would have been without you two. And I don't know how my academic journey will go on without your physical presence.

***Tyagi*** - You were the only one in 2022 and now as well. And you own the title of the *ultrafast* woman in IISER Pune very well. Your general knowledge is beyond comparison, your energy is unmatchable, and your eagle's eyes in finding typos are at par with Sir. I must mention that I was the only one who got to eat the tastiest *Bhindi Do Pyaza by Tyagi* during my PhD tenure. Thank you for being that annoying younger sister until now.

***ChiChi***- You have definitely let your journey decide your fate; else we wouldn't have met, and you would have to drink chai all alone (*ha ha ha*). I always wonder how come you are so talented- perfect meme model, emerging cricketer, trained dancer, singer, blackbelt holder, and so on. But, I have learnt and still learning many life skills from you, be it emotional maturity, calmness under challenging situations, or the ability to turn deaf and blind. As we got along, I found an academic sibling whom I can bully and irritate all the time. The prospect of opening a bakery cum café cum bookstore and so on still remains, OK?

Then comes the youngest member (feeling really old now)- ***Anushree***. I really wish I had the confidence you have right now in the beginning. I am sure you are going to rock in this journey.

Another fun part was usually the summers with a lab full of young science enthusiasts (Aiswarya, Aparna, Shruthy, Sandhra, Shreya, Hisham, Anju, Anuradha, Ajinkya, Thrisha, Madhusmita, Namitha, Mridul, Ashmita, Rachit). I thoroughly enjoyed their company and spirits and, on some occasions, a potluck with them.

On top of that, I had an opportunity to mentor pretty smart brains for their MS thesis.

***Rohit***: While I was still in the initial phase of PhD, mentoring you felt like a big responsibility. But it was such an enriching experience as we had something or other to teach or learn from each other.

***Namitha***- You are the sweetest of all, Namikutta, and made my mentoring experience so much fun. The constant influx of your questions and excellent time management made me work a lot *(literally!)*. I want the readers to make a guess about how much time it takes for one absorption spectrum to be recorded, and then guess how much time Namitha would have taken. I'm still amazed that you managed to carry out water splitting through NMR. Even though you questioned the connection in my thesis, I managed to pull it off, okay! Thank you for introducing us to the world of Blender, shaky videos, portrait photography, and the poorest dad jokes. You are going to slay, girl!

***Angela***- While I wasn't officially your mentor, *but then*, you were fun to work with. Thank you for treating us with delicious Marathi food during Omkarotsav (*trust issues for lifetime*). I appreciate your efforts in convincing all of us that misal pav is real food and can taste nice. *But then*, NO! I am still not over the fact that you could manage to balance centrifuge with one tube and send raw data to a professor. Also, I would like to mention to all that she has been the most racist BSMS, *but then*, also a rockstar.

***Hisham***- Well, it was so much fun working with you towards the end of my PhD on some exciting projects. With your utmost sincerity, you literally kept me on my toes. And of course, the best punch lines that anybody could deliver to Ankit!

All of you have been the best mentees and made mentoring a wholesome and fun experience for me. I would rate this experience 10/10 and the best of this journey.

And of course, I am grateful to our extended Nano Alchemy family member ***Riteeka*** for making our lives so vibrant. Thanks for all the pookie Vanshika Ji's reel throughout 2024 and providing the best content from the department throughout!!!

I extend my gratitude to ***Prof. Vivek Polshettiwar*** and ***Rishi*** for helping us with the gas-phase mass analysis.

I would like to thank all Department staff for their direct or indirect help, especially for all the purchase-related stuff after the unfortunate fire accident.

I thank IISER Pune and PMRF for fellowships. I also thank ***Prof. Srabanti Chaudhury*** and ***Sayalee*** for all the PMRF-related matters.

I am lucky to have met some amazing women when I started my journey in Science- ***Aashi, Sonam****, and* ***Kanika*** (along with me, it's *Fantastic Four*). You girls are the best people I could have asked for. Even though I have missed the major events of our group, you have always understood and encouraged me to do my best. Special thanks to *Aashi* for always being there, whatever the time on the clock, and also for joining PhD to back up each other at family events. Another person I would like to thank is ***Vikrant*** for constantly annoying me for all 5 years or so. Thank you for being my cheerleader. I don't know how you managed not to meet every single time I was there at home. I am holding grudges against that now! Also, I thank two of my long-distance friends- ***Dipti*** *&* ***Atanu***. You guys are my constant motivation to do good science and pursue a research career. Hopefully, we guys are gonna collaborate academically and industrially in the future!

At last, I wouldn't have reached here without my family (***Daddy, Mummy, Bhai, & Bhabhi***), who always believed in me and let me choose my path. You are all precious like stardust. Being a first-generation PhD, I feel it was way harder for you people to accommodate yourselves with my lifestyle and get along with me on my terms (with all my stubbornness till now), yet with no complaints. As a kid, I remember telling to everyone that how I want to become a scientist when I grow up. Thank you all for nurturing me with so much patience and love so that I fulfill my dreams. A special thanks to my brother- ***Vaibhav***, and sister-in-law ***Pankhuri***, for never letting me worry about home and defending me against all odds. I hope I made you all a little proud! (*happy tears*). A special mention and heartfelt thanks to you, ***Naani***, for your unconditional love and

secret prayers. And finally, I would like to thank ***Abhinav***, who became a part of this journey only towards the end, but also for forever. Thank you for showering so much love, believing in my dreams, and encouraging me to do what I love, and that I am sure gonna take me to greater heights.

Looking back at this journey, what a thriller it was! Took off in 2019, worked out through the multiple waves of the pandemic, came out stronger after the fire accident, and finally landed upon this degree in 2025! I humbly acknowledge all the generous help, guidance, support, and love that nurtured and empowered me to become an ambitious, confident, humane, and compassionate scientist!

- Vanshika

# Thesis Synopsis

Attaining sustainability in chemical synthesis is an important step to achieving the UN Sustainable Development Goals (SDGs) of Climate Action and Responsible Consumption and Production. The diligent utilization of solar energy by plants offers an excellent way for sustainable chemical production in a perpetual manner. The four key steps in photosynthesis, starting from light absorption leading to charge generation, charge separation, and charge transfer (process I) to water oxidation (process II) on one end and proton/electron storage in the form of NADPH (process III) on the other and finally reduction of $CO_2$ to biomass (process IV), can be coupled or decoupled for implementation of different solar utilization technologies. Among them, solar-to-chemical energy conversion in photosynthesis has gained substantial popularity, and hence, the area of photocatalysis is at the forefront of modern research. At the core of all photocatalytic transformations are the three fundamental steps: generation of charge carriers, separation, and charge transfer/utilization. Based on the physical parameters dictating these fundamental steps, combined with unique optoelectronic properties and rich surface chemistry, our choice of photocatalysts is plasmonic metal nanoparticles (NPs) and quantum dots (QDs). This thesis deals with maximizing the efficiency of each fundamental step through the rational design of both the core and the surface of the chosen photocatalysts for challenging and industrially relevant multielectron chemical transformations.

The present thesis begins with an introduction to photocatalysis, its fundamentals, and its advantages over thermal catalysis. This is followed by a discussion over our choice of photocatalyst cores - plasmonic metal nanoparticles and semiconductor quantum dots, their unique optoelectronic properties, and the associated challenges, respectively. Next, we summarize the significant role of ligands on the surface of the chosen photocatalysts in dictating the fundamental processes involved in photocatalysis. Finally, we discuss the impact of appropriately designed photocatalyst cores and surface ligands in driving challenging multielectron chemical transformations, which the present thesis revolves around.

With this objective, **Chapter 3** focuses on deciphering the role of light excitation attributes in light-driven nicotinamide cofactor regeneration with plasmonic metal nanoparticles. The choice of anisotropic gold nanorod core as the plasmonic photocatalyst allowed us to understand the exclusive role of interband vs intraband transitions in NADH photoregeneration. This work emphasizes the need for an appropriately chosen catalyst–reactant system and reaction conditions to gain meaningful insights into various factors controlling the product yield and selectivity in plasmonic photocatalysis.

With the aim of synthesizing important commodity chemicals such as ammonia, we fine-tuned the photocatalyst design in **Chapter 4a** to arrive at indium phosphide (InP) QDs with appropriate surface chemistry to drive selective nitrate-to-ammonia conversion. Photocatalytic nitrate-to-ammonia conversion is a multiproton and multielectron transformation and demands photocatalysts that generate long-lived surplus charge carriers and allow optimum surface interaction with the N-sources. Due to the challenges associated with a short lifetime in plasmonic metal nanoparticles, we changed the core from metal to semiconductor quantum dots (QDs). A rational choice of indium phosphide (InP) QDs and its appropriate surface functionalization, along with a preferential affinity of N-sources towards surface In atoms and ligands on InP QD photocatalysts, led to the selective and efficient ammonia production under visible-light irradiation at room temperature. We gained an in-depth understanding of important pathways involved in photocatalytic nitrate reduction in **Chapter 4b** to establish InP QD as a potential visible-light photocatalyst for ammonia synthesis. We listed key findings associated with reaction rate, competing reactions, proton source, and the fate of photoexcited holes in the multielectron transformation of nitrate to ammonia.

In **Chapter 5**, we attempted to enhance the efficiency of charge extraction by the appropriate choice of inorganic surface ligands on the InP QDs for light-driven ammonia synthesis. A positively charged metal-solvent complex was chosen as the ligand to maintain favorable catalyst-reactant interactions, while the inorganic nature of the ligand helps in improving charge extraction and transfer processes. The inorganic metal-solvent complex-capped InP QDs exhibited 16x rate enhancement for nitrate-to-ammonia transformation compared to organic long-alkyl ligands employed in the previous chapter.

Consequently, there was ~8x enhancement in quantum efficiency. This is one of the first reports where cationic inorganic ligands are employed in quantum dot photocatalyzed chemical transformations.

In summary, the present thesis showcases the need for the appropriate design of core and surface ligands to maximize each fundamental step in photocatalysis for challenging multielectron transformations. The concepts developed in this thesis can be easily extended to complex molecule/material synthesis in a sustainable manner, including multicomponent reactions.

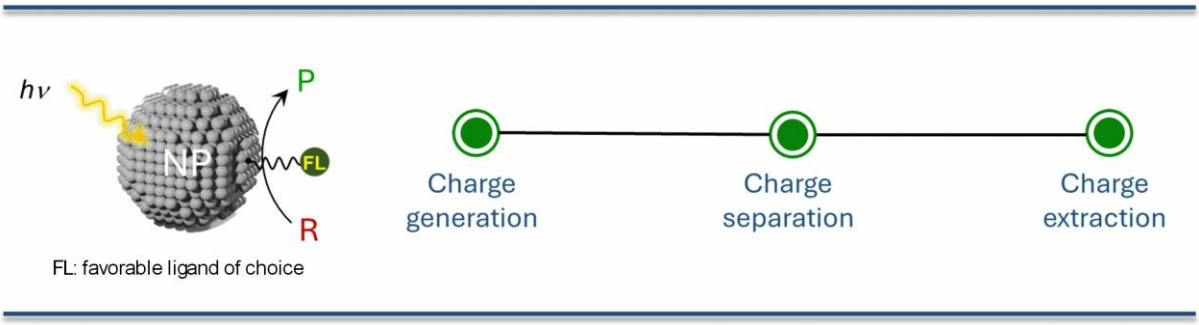

# Contents

## Chapter 6: Summary and Future Outlook



## Scientific output

*Lights, Catalyst, & Action…*

# Chapter – 1

## Introduction to Photocatalysis with Tailored Metal Nanoparticles and Quantum Dots

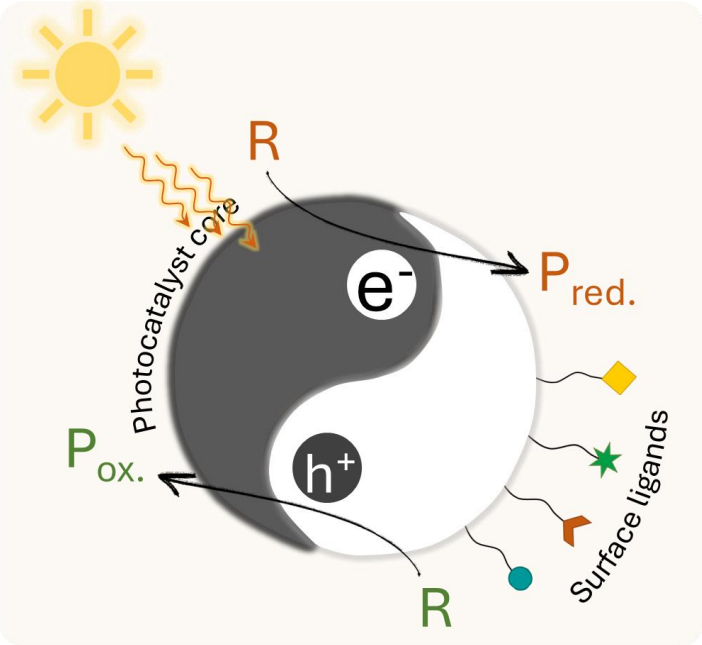


A part of this Chapter has been adapted from the following paper with permission. Copyright 2022, American Chemical Society.

**Jain, V.**; Roy, S.; Roy, P.; Pillai, P. P. When Design Meets Function: The Prodigious Role of Surface Ligands in Regulating Nanoparticle Chemistry. *Chem. Mater.* **2022**, *34*, 7579-7597.

# 1.1. Introduction

Chemical synthesis is an endergonic process, often relying on conventional non-renewable energy sources to meet the production demands.[1] The ever-increasing demand for chemical products across different supply chains is related to the production of high-value primary chemicals- methanol, ammonia, ethylene, propylene, and benzene/toluene/xylenes (BTX).[1-3] Not only do these commodity chemicals consume the largest proportion of energy to supply high temperatures, pressures, or purification, but they are also associated with the largest greenhouse gas emissions (**Figure 1.1**), arising from the enormous burning of fossil fuels.[3,4] Stipulated by the Paris Agreement, attaining sustainability in chemical synthesis and processing has sparked the urgent need for sustainable and low-carbon solutions. Utilizing surplus energy supplied by the Sun is considered one of the most sustainable and affordable solutions to reach these goals. Consequently, the development and implementation of various solar harvesting technologies are of great interest to the scientific community.[5-9]

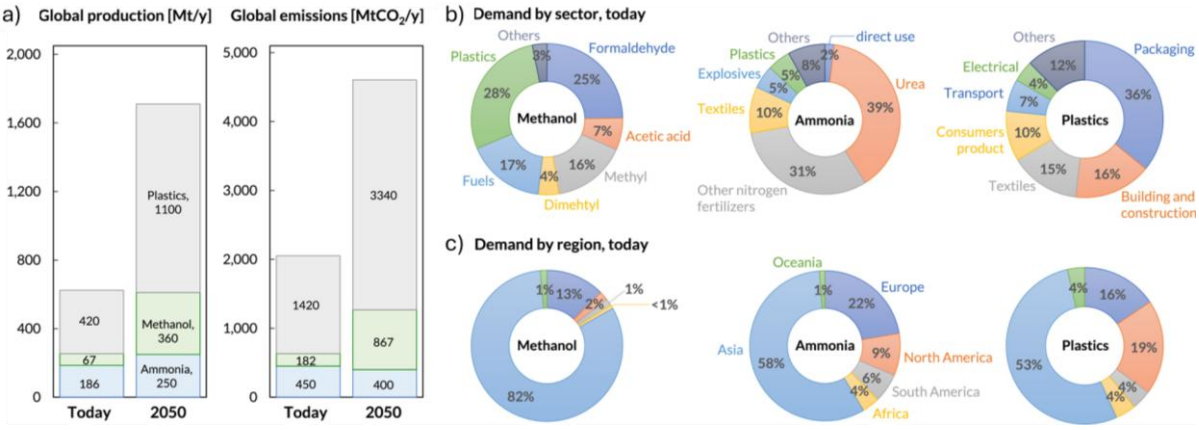


**Figure 1.1.** The global production and emissions per year associated with primary chemicals, along with their demands in different market sectors in different parts of the world. Reproduced with permission from reference 2. Copyright 2023 Elsevier Inc.

The attractive design principles catering to the modern solar energy research originate from the process of natural photosynthesis (**Figure 1.2**).[9] The four key steps of the natural photosynthetic process: I) charge generation, charge separation, and charge extraction, II) catalytic $H_2O$ oxidation, III) $H^+/e^-$ transfer and energy storage in the form of NAD(P)H and ATP, and IV) catalytic $CO_2$ fixation, can be coupled or decoupled for the

implementation of various solar utilization technologies, such as solar-to-thermal, solar -to-power or solar-to-chemical energy conversion.[9-11] The present thesis is primarily focused on solar-to-chemical energy transformation, which is widely achieved via the process of *photocatalysis*. In fact, photocatalysis is considered to be one of the most sustainable ways to make and break chemical bonds. In natural photosynthesis, the light cycle is associated with the catalytic oxidation of $H_2O$ to produce $O_2$, with simultaneous storage of hydride ions in the form of reactive nicotinamide cofactor, NAD(P)H.[12-15] This reduced cofactor enters the light-independent Calvin cycle for the catalytic fixation of $CO_2$ into biomass in a ceaseless manner.[15] This process prompted the development of artificial mimics of the natural photosynthetic systems, which require an appropriate choice and design of the light-harvesting materials with continuous catalytic function for sustainable chemical production. Furthermore, an in-depth understanding of the underlying fundamental principles behind photocatalyst design, its interaction with light, related photophysical processes, and interaction with substrates/reactants of choice is crucial to build photocatalytic platforms.

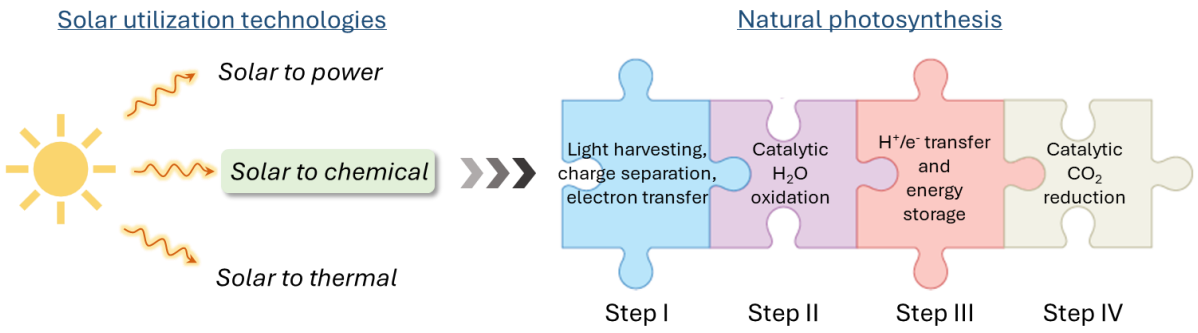


**Figure 1.2.** Schematics illustrating the key processes of natural photosynthesis that serve as the basis for the development of modern solar utilization technologies. The present *thesis* is focused on the transformation of solar energy into chemical bonds via *photocatalysis*.

In this thesis, we have uncovered the design principles pertaining to the photocatalyst core and modulation of its surface to drive important and challenging chemical transformations involving multiple electrons and protons. In this direction, the first section of this Chapter presents a brief overview of the photocatalysis- the past and the present, with its advantages for sustainable chemical synthesis. This is followed by a brief discussion on the fundamental processes involved in any photocatalytic

transformations, followed by an overview of emerging areas of plasmonic and quantum dot photocatalysis. With plasmonic metal nanoparticles (NPs) and quantum dots (QDs) as the photocatalyst of our choice, we will discuss the meticulous design strategies to arrive at the champion photocatalyst. These strategies will be utilized in the subsequent Chapters to make and break chemical bonds using visible light.

## 1.2. The dawn of photocatalysis

The beginning of the era of photocatalysis dates to the early 1900s, with Eibner, Kozak, and Ciamician being considered the early proponents of photochemistry.[5,16-18] The term '*photocatalysis'* first appeared in 1911 in a study by Kozak, which discussed the decomposition of oxalic acid in the presence of uranyl salts ($UO^{2+}$) when exposed to sunlight.[16] In the same year, Eibner independently reported the bleaching of Prussian blue in the presence of zinc oxide (ZnO) under light illumination.[17] Numerous reports on light-driven chemical transformations appeared at the beginning of the 20$^{th}$ century, but with the term 'photocatalytic reaction' being used with a more general meaning of 'photochemical reaction' as no catalyst was employed in several of them.[19-22] Nevertheless, all these works sparked a great interest in performing 'chemistry with light', and gradually the area was dominated by semiconductor oxides (ZnO, $TiO_2$, $Sb_2O_3$) as the photocatalyst, with interesting reports on photocatalytic activities of oxides appearing from the 1940s by Markham.[23-25] A strong push to the area was given in the 1970s when Honda and Fujishima reported photoelectrochemical water splitting assisted by $TiO_2$ photocatalyst and Pt cocatalyst.[26] And in the past 50 years, the area has expanded its limits to drive exotic and challenging chemical transformations, spanning across different classes such as solar fuels production, organic synthesis, wastewater treatment, $CO_2$ utilization, and so on.[27-32]

Not only does photocatalysis provide an alternate route for sustainable chemical synthesis, but it also offers added advantages. One of the key highlights is to drive thermodynamically uphill reactions or photosynthetic reactions under milder conditions.[27,33] While the excitation of the catalyst by light can enhance the kinetics of the exergonic reaction bearing $\Delta G < 0$, endergonic or thermodynamically non-

spontaneous reactions with ΔG > 0 can also be performed (**Figure 1.3a**).[27,33] In a stricter sense, the reactions bearing a positive value of ΔG are categorized as *photosynthetic* reactions. The key distinction is that photocatalysts promote the reactions with ΔG < 0 without storing the solar energy, whereas products of photosynthetic reactions are higher in energy, which makes reverse photosynthetic reactions thermodynamically feasible. Hence, photosynthetic reactions must suppress the reverse pathway along with facilitating non-spontaneous reactions in the forward direction by using and storing solar energy. Some of the prominent examples of photosynthetic reactions include overall water splitting into $H_2$ and $O_2$, $N_2$ fixation accompanied by water splitting, $CO_2$ reduction to methanol and methane with water oxidation, etc.[27,33,34]

In an interesting study by Fujita, Abe, Miyauchi, and coworkers, the thermodynamically uphill process of methane dry reforming ($CH_4 + CO_2 \rightarrow 2H_2 + 2CO$, $\Delta G_{298K}$ = +171 kJ $mol^{-1}$) under photocatalytic conditions was found to break the thermal limitation of the thermal catalysis at 450 °C.[35] Typically, the reaction requires high temperatures in the range of 800-900 °C to achieve substantial conversion greater than 50 %. By using rhodium NPs modified strontium titanate (Rh/$SrTiO_3$) as the photocatalyst, more than 50 % conversion could be achieved under light irradiation without any additional heat input (**Figure 1.3 b**). More interestingly, $H_2$ production was ~50 % even at mild temperatures below 200 °C under photocatalytic conditions. Control experiment with Rh/$SrTiO_3$ carried out under thermal conditions in the absence of light displayed lower performance (grey line in **Figure 1.3b**) than the limitations of the thermal catalyst (black dashed line in **Figure 1.3b**). Bare $SrTiO_3$ did not yield any $H_2$, confirming the active role of Rh catalytic sites (green line in **Figure 1.3b**). Detailed electron spin resonance and Kelvin probe force microscopy studies confirmed the active participation of photoexcited charge carriers in driving dry reforming of methane.

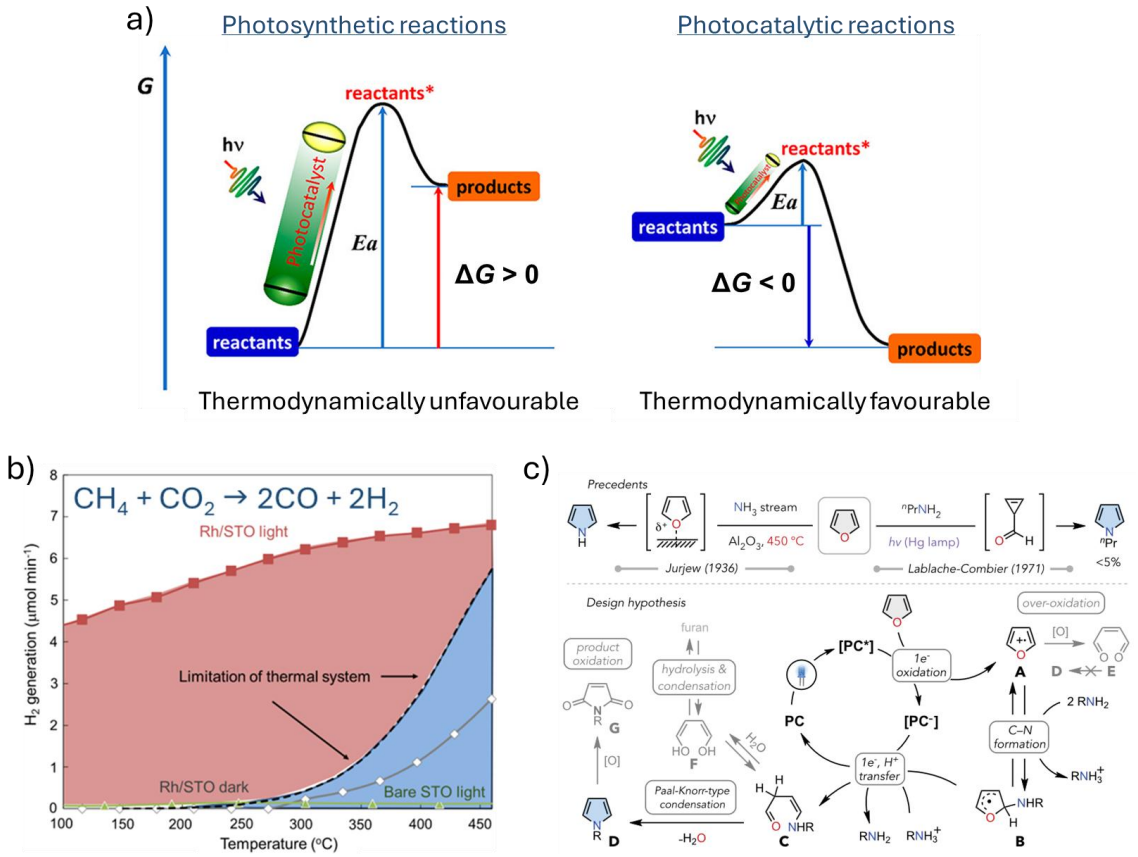


**Figure 1.3.** Distinct advantages of photocatalysis for sustainable chemical synthesis. a) Schematics showing the thermodynamics of uphill and downhill light-assisted catalytic reactions. With the help of photocatalysis, thermodynamically non-spontaneous reactions can be carried out under milder conditions. Reproduced with permission from reference 27. Copyright 2018 American Chemical Society. b) Photocatalytic uphill process of dry reforming of methane performed under light illumination in the presence of Rh/$SrTiO_3$ photocatalysts at much lower temperatures and high yields. The black dashed line depicts the limitation of the thermal system, which suggests the need for at least 400-450 °C to achieve decent $H_2$ production. The red squares show excellent $H_2$ production even at milder temperatures in the presence of Rh/$SrTiO_3$ photocatalyst under light irradiation, showcasing the potential of photocatalysis in achieving sustainability. Reproduced with permission from reference 35. Copyright 2020 Springer Nature. c) Conversion of furan to pyrrole in a single step under photocatalytic conditions. A distinct reaction mechanism allows selective furan to pyrrole conversion with excellent yields at room temperature. Reproduced with permission from reference 36. Copyright 2024 American Association of the Advancement of Science.

Another added advantage lies in molecular skeletal editing, where complex organic synthesis can be carried out in fewer steps than conventional routes under photocatalytic conditions.[36] One such example is the conversion of furan to pyrrole, which is highly challenging, as furan is highly stable due to its aromaticity. Classical methods for this chemical transformation include pyrolysis of furan in an ammonia stream over activated alumina at 450 °C or photolytic conversion using high-energy

ultraviolet (UV) irradiation.[36-38] The former method requires extremely high temperatures, while the latter strategy results in poor product yields.[36-38] In a seminal work by Park and coworkers, heteroatom swapping was done at ease to convert furan to pyrrole in a single step under photocatalytic conditions (**Figure 1.3c**).[36] A distinctly different reaction mechanism than the conventional routes was the key behind a single-shot conversion of O-atom to N-atom. Herein, an acridinium-based photocatalyst under blue light irradiation initiates one-electron oxidation of furan to yield furanic cation (**Figure 1.3c**). The electron-deficient furanic cation enables nucleophilic addition of amine to form an adduct, which in the next step accepts an electron from the reduced photoexcited photocatalyst. Subsequent proton transfer yields a ring-opened intermediate, followed by Paal-Knorr-type condensation to construct pyrrole (**Figure 1.3c**). The photocatalytic pathway resulted in an excellent yield of 92 % without any overoxidized or side products. The strategy was extended to synthesize naturally occurring products and pharmaceutical drugs, such as diosbulbin B, cafestol acetate, furosemide, etc.

All the fundamental studies and collective efforts till now have resulted in the translation of photocatalytic strategies to pilot scale, which is quite a remarkable feat. Recently, Syzygy Plasmonics- a Houston-based startup, produced its first batch of liquid fuel using Rigel photoreactors that drive chemical reactions in the presence of light. All these examples clearly demonstrate the power of photocatalysis for sustainable synthesis and the crucial role of fundamental research in achieving the same.

## 1.3. Fundamentals involved in photocatalysis

At the core of all these photocatalytic transformations lies three key steps: I) absorption of light leading to the generation of charge carriers, II) separation of photoexcited charge carriers, and III) charge extraction or transfer to the reactant of interest (**Figure 1.4**).[27,39-42] Various physical parameters dictate these key steps for all the photocatalysts, which impact the overall photocatalytic efficiency. Absorption of light is unambiguously the foremost step for any photocatalytic reaction, as without light input, no photocatalysis will occur. The interaction of light with the photocatalyst can be expressed as follows:[42]

$$I_0 = A_{\%} + T + R_s + S + R_d \qquad (\mathbf{1.1})$$

where, $I_0$ is the photon flux of incident light, $A_{\%}$ is the absorptance or the ratio of the absorbed to incident light, $T$ is the transmitted light, $R_s$ is the specularly reflected light, $S$ is the forward-scattered light, and $R_d$ is the backward-scattered light.

a)

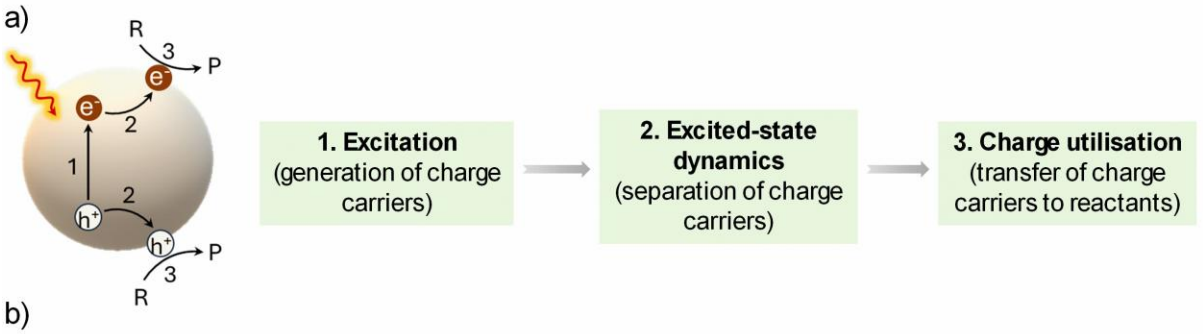


b)

| Photocatalyst | Absorption coefficient ($M^{-1}$ $cm^{-1}$) | Carrier concentration ($cm^{-3}$) | Lifetime of charge carriers | Diffusion length |
|---|---|---|---|---|
| Molecular systems | $10^3$-$10^5$ | low | A few ns | - |
| Bulk semiconductors | $10^4$-$10^6$ | $10^{12}$-$10^{16}$ | ps to a few ns | 10 - few 100s nm |
| Plasmonic NPs | $10^8$-$10^{10}$ | $10^{23}$ | 1-100 fs | 5-50 nm |
| Quantum dots | $10^4$-$10^6$ | $10^{18}$-$10^{20}$ | A few ns to 200 ns | 10-100 nm |
| Perovskites | $10^4$-$10^6$ | $10^{10}$ - $10^{18}$ | 200-500 ns | Few nm-mm |

**Figure 1.4.** a) Schematic illustration of the key steps involved in photocatalytic transformations. b) Table summarizing the key photophysical parameters of commonly used photocatalysts.

Out of all, it is the absorption of light that dictates the subsequent process of charge generation and is determined by the absorption coefficient ($\alpha$ ($\lambda$)) of the material. The absorption coefficients of different classes of photocatalysts are summarized in **Figure 1.4.** Amongst them, plasmonic metal nanoparticles (NPs) stand out with their exceptionally high molar absorption coefficient in the range of $10^8$-$10^{10}$ $M^{-1}$ $cm^{-1}$, arising from strong light-matter interactions due to the unique phenomenon of localized surface plasmon resonance (*vide infra*). Now, the number of electron-hole pairs generated per absorbed photon as a function of wavelength ($\lambda$) and light penetration depth ($x$), is described by the generation rate, $G$, as follows:[43,44]

$$G = \alpha I_0 e^{-\alpha x} \qquad (\mathbf{1.2})$$

Once charge carriers are generated, they must be spatially separated to reach their respective surface sites before they undergo recombination. The separation of photoexcited charge carriers is associated with various parameters such as exciton binding energy, effective mass of the charge carriers, carrier lifetime, carrier mobility, and diffusion length.[42] Based on the photoabsorbers, two distinct modes of charge separation are involved: asymmetric energetics (AE) and asymmetric kinetics (AK) (**Figure 1.5**).[39] For photoabsorbers possessing continuous energy bands, AE is the preferred mode of charge separation. Under AE, the charge carriers drift towards the respective surface reaction sites under the influence of the electric field within the photoabsorber, which enables the spatial separation.[39,45] Consequently, tuning of energy levels at the surface sites becomes necessary. Such a modulation can be achieved via varying the doping, constructing solid-solid interfaces, appropriately designing the crystal facets of varying surface energies, or by tuning the extrinsic and intrinsic dipoles of surface sites (**Figure 1.5a,b**).[39] For photoabsorbers that cannot sustain internal electric fields, such as molecular catalysts and quantum-confined materials, AK is the way to achieve charge separation.[39] In AK mode, the difference in the charge transfer rate is the driving force to achieve charge separation (**Figure 1.5c,d**). Once one of the charge carriers is utilized, there is an excess accumulation of the other carrier, thereby creating a gradient of charge carrier concentration.[39,46] As a result, the overall process becomes diffusion-limited and necessitates that the diffusion length of the charge carriers is larger than the size of the photocatalyst to avoid charge recombination before reaching the surface reaction sites. Based on Marcus' model, the modulation of charge transfer rates by varying the donor-acceptor distance is one of the ways to achieve charge separation under the AK regime.[47,48] Another commonly used strategy is to incorporate redox couples or sacrificial agents to remove the charge carriers, or by varying the free energy of the charge transfer process by tuning the acceptor energy levels. An interesting approach to tuning the local concentration of the acceptor near the photocatalyst reaction sites also facilitates charge separation.[39]

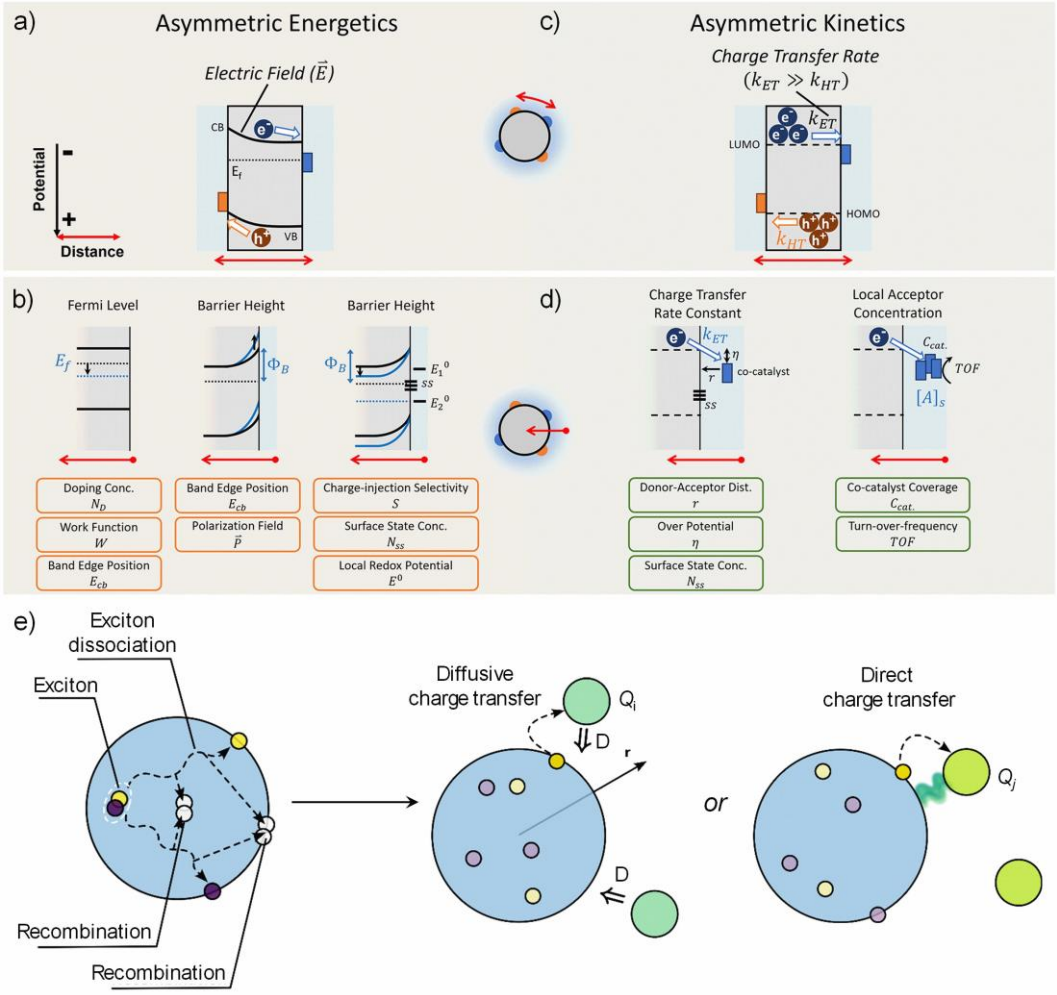


**Figure 1.5.** Schematics of different modes of charge separation in different photocatalysts: a, b) asymmetric energetics and c, d) asymmetric kinetics. a) and c) depict the ideal scenario for charge separation, while b) and d) represent various physical parameters that dictate charge separation under asymmetric energetics and asymmetric kinetics, respectively. Reproduced with permission from reference 39. Copyright 2022 American Chemical Society. e) Scheme showing the modes of photoinduced charge transfer from the semiconductor to the acceptor molecules. Reproduced with permission from reference 41. Copyright 2024 American Chemical Society.

Once the charge carriers reach the respective surface sites before the recombination, the final step involves the extraction of the charge carriers by the reactant molecules. For homogeneous photocatalysts, charge transfer occurs through diffusive collisions and is commonly described by either Smoluchowski or Collins-Kimball theory.[41] As diffusion occurs on longer time scales, generally, photocatalysts bearing triplet states are employed for effective charge transfer. When it comes to the heterogeneous photocatalysts, the phenomenon of charge transfer becomes more complex due to the

involvement of an interface. The charge transfer can occur via either surface binding (direct charge transfer) or reactant diffusion (diffusive charge transfer) (**Figure 1.5e**), depending on the photocatalyst and reactant of choice.[41,49,50] While the first two steps of photocatalysis are highly dependent on the photocatalysts' design, the process of charge extraction is significantly affected by the external environment as well.[50,51]

Based on some of the key parameters affecting the key steps in photosynthesis (**Figure 1.4b**), we have chosen *plasmonic metal NPs* and *semiconductor NPs (quantum dots, QDs)* as the photocatalysts of our choice. The subsequent section of this Chapter will discuss the light-matter interactions with plasmonic metal NPs and semiconductor QDs, their distinct features, charge transfer mechanisms, and the associated challenges. With these two classes of photocatalysts, we will discuss the design strategies to maximize each fundamental step in photocatalysis, which forms the objective of the present Thesis.

## 1.4. Introduction to plasmonic photocatalysis

Accelerating chemical transformations under plasmonic excitation is the crux of the area of plasmonic photocatalysis. What makes these plasmonic excitations exciting lies in the way metal NPs interact with the incoming electromagnetic radiation. When the frequency of incoming electromagnetic radiation matches the frequency of oscillating free electrons of metal NPs, a resonant condition is achieved.[43] This phenomenon is known as surface plasmon resonance (SPR). For metal NPs of the size range of 1-100 nm, SPR is confined to a small volume, which is commonly referred to as localized surface plasmon resonance (LSPR).[52] For metal NPs of size much smaller than the wavelength of light, only the dipolar mode of interaction is taken into consideration.[52] Under this assumption, the polarizability of spherical NPs of volume V is given by Clausius-Mossotti relation:[43]

$$\alpha = 3\varepsilon_0 V \left(\frac{\varepsilon - \varepsilon_m}{\varepsilon + 2\varepsilon_m}\right) \qquad (\mathbf{1.3})$$

where $\alpha$ is the polarizability, $\varepsilon_0$ is the permittivity of vacuum, $\varepsilon_m$ is the dielectric constant of the medium, and $\varepsilon$ is the dielectric function of metal, which is complex and frequency dependent. $\varepsilon$ can be expressed as $\varepsilon(\omega) = \varepsilon_r(\omega) + i\varepsilon_i(\omega)$, where $\varepsilon_r$ and $\varepsilon_i$ are the real and imaginary parts of the dielectric function, respectively.

From **eq. 1.3**, it can be seen that polarizability is maximum when $\varepsilon_r = -2\varepsilon_m$ under the assumption that $\varepsilon_i$ is small or weakly dependent on frequency. For most of the metals, the real part of the dielectric function is negative (**Figure 1.6a, b**). The absorption and scattering cross-sections ($C_{ext}$ and $C_{sca}$, respectively) can be related to dipolar polarizability as:[43,53]

$$C_{ext} = k\, Im(\alpha) \qquad (\mathbf{1.4})$$

$$C_{sca} = \frac{k^4(\alpha)^2}{6\pi} \qquad (\mathbf{1.5}), \qquad \text{where } k = \frac{2\pi\varepsilon_m^{1/2}}{\lambda}$$

For very small particles ($r << \lambda$), the scattering cross-section can be neglected, and the extinction cross-section is dominated by absorption, which can be expressed as:[53,54]

$$C_{ext} = \frac{24\pi^2 r^3 \varepsilon_m^{3/2}}{\lambda} \frac{\varepsilon_i}{(\varepsilon_r + 2\varepsilon_m)^2 + \varepsilon_i^2} \qquad (\mathbf{1.6})$$

Thus, the extinction cross-section becomes maximum at the resonant conditions and can even exceed the geometric cross-section of metal NPs by ten times.[55] As a result, NPs are able to absorb enormous light, which makes them highly desirable for photocatalysis. Of all metals, NPs of coinage metals such as Au, Ag, and Cu are highly interesting as the plasmon resonance frequency lies in the visible region of the electromagnetic spectrum (**Figure 1.6a, b**). For instance, AuNPs of size 10 nm exhibit strong absorption features at ~520 nm.[55] It is evident from **eqs. 1.3** and **1.6** that the extinction cross-section is sensitive to the size and shape of the NP and the dielectric constant of the materials and the surroundings.[55-57] Thus, light absorption can be tuned across the visible light spectrum by modifying these parameters.

Once a plasmon is excited, it undergoes dephasing within 1-10 fs via radiative or non-radiative relaxation pathways.[53,58,59] For small metal NPs (< 50 nm), non-radiative relaxation dominates and is relevant for photocatalysis (**Figure 1.6c**).[53,55] The dephasing of LSPR leads to the formation of highly energetic non-thermal charge carriers, which undergo thermalization by electron-electron scattering on the time scale of 100 fs to form a hot Fermi-Dirac distribution of charge carriers (**Figure 1.6c**).[53,59] Till this point, the hot charge carriers can be extracted to perform photocatalytic reactions and form the basis of the area of plasmonic photocatalysis. If hot charge carriers are not extracted, electron-phonon scattering events will occur on a time scale of 1-10 ps, after which the hot Fermi-Dirac distribution thermalizes to heat up the NP lattice (**Figure 1.6c**).[53,59] At this point, the local temperature at the surface of metal NPs can reach hundreds of Kelvins. The heated NP ultimately dissipates the energy to the surroundings by phonon-phonon scattering on a 100 ps timescale (**Figure 1.6c**).[53,59] In order to perform photocatalytic reactions, the hot charge carriers formed during the relaxation must be extracted before the energy is dissipated in the form of heat, and this is a core challenge in the area of plasmonic photocatalysis.[59,60]

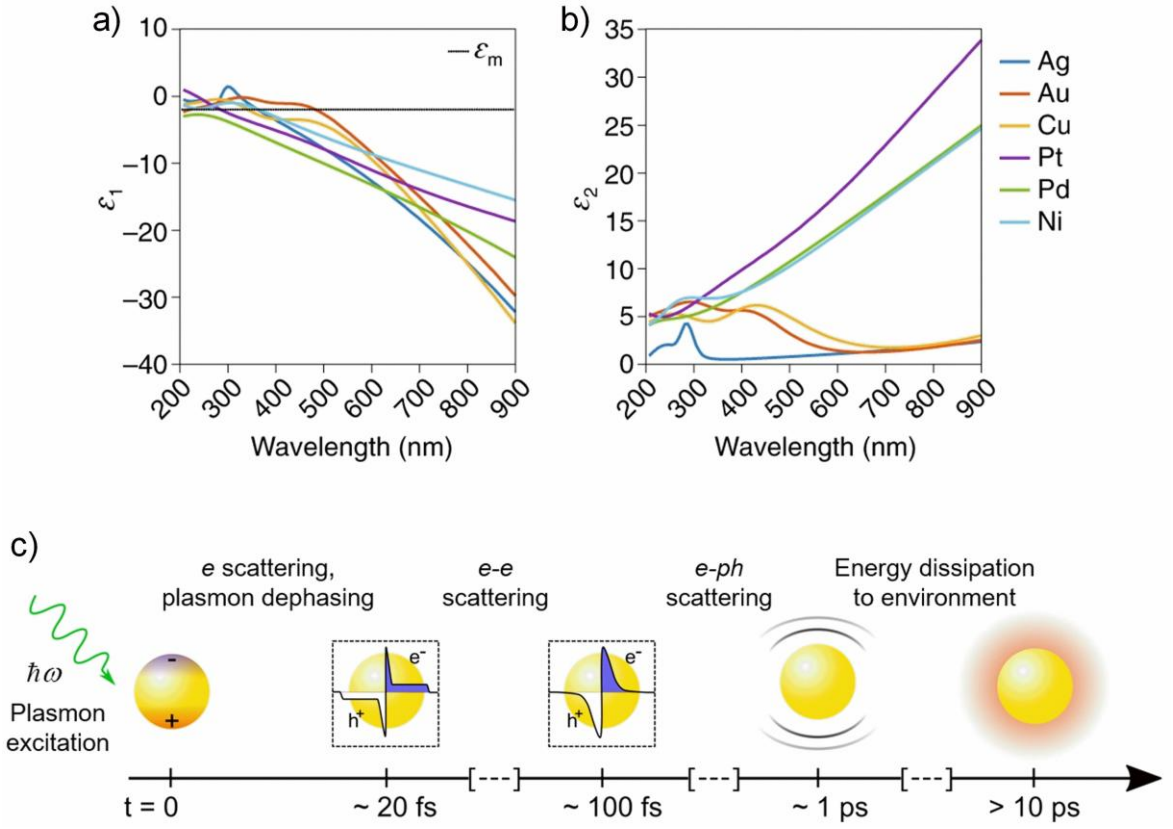

**Figure 1.6.** a) The real and b) imaginary part of the dielectric function of different metals as a function of wavelength. The black line in a) represents the resonant condition where $\varepsilon_r = -2\varepsilon_m$ with negligible or small contribution from the imaginary part of the dielectric function. Reproduced with permission from reference 54. Copyright 2018 Springer Nature. c) Scheme showing the plasmon relaxation dynamics, where the plasmonic excitation leads to the formation of highly energetic charge carriers, which dissipate their energy via electron-electron, electron-phonon, and phonon-phonon scattering events. Reproduced with permission from reference 59. Copyright 2021 Wiley-VCH.

The efficiency of charge generation in plasmonic NPs depends on both intrinsic and extrinsic factors such as geometrical shape and size of NP, light frequency and intensity, hot-spot generation between adjacent NPs, etc.[59,61-63] Since a small window of time exists between hot charge carrier generation and their thermalization, charge extraction must be carried out efficiently within the timescales of relaxation (within 10's of ps). There are two distinct mechanisms for charge transfer between plasmonic NPs and the reactants: I) indirect and II) direct charge carrier transfer.[59,64-66] In indirect charge injection, the charge carriers are first generated within the metal NP core, as discussed above, followed by their transfer to the acceptor molecules (**Figure 1.7**). Herein, the energy of the generated charge carriers is of prime importance as the potential barrier needs to be overcome to eject charge carriers out of the NP. As the highly energetic non-thermal charge carriers thermalize within a ps time scale, the concentration of low-energy charge carriers is higher.[64] This essentially suggests that charge transfer will be more favorable to the acceptor's energy levels that are close to the Fermi level of metal NPs, which limits the reaction yield. On the other hand, direct charge transfer is proposed to occur in a single step where the charge carriers are directly excited into the adsorbate's energy level, triggering the chemical reactivity (**Figure 1.7**).[64-66] This is also referred to as chemical interface damping (CID). The direct charge transfer mechanism is thought to have an intrinsic 100 % charge injection efficiency, as excited charge carriers do not stay inside the metal NPs to lose their energy via different scattering events.[59] This mechanism is found to dominate in systems where there is strong hybridization between the metal surface and the adsorbates' energy levels. Such strong electronic hybridization can also be utilized to achieve selectivity in the chemical transformations by targeting specific adsorbate energy levels.[67]

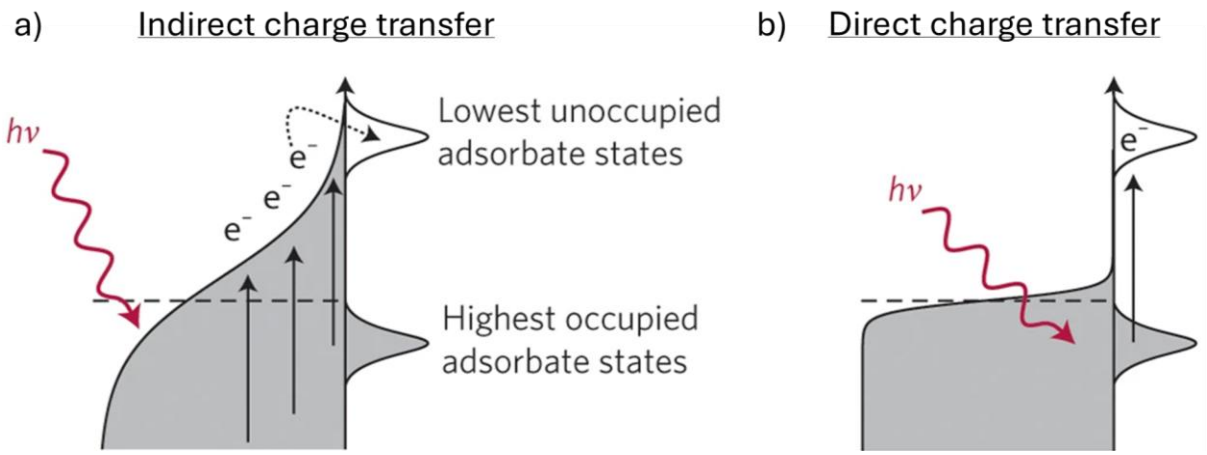


**Figure 1.7.** Mechanisms of charge transfer in plasmonic photocatalysis. a) In indirect charge transfer, hot charge carriers are first formed within the metal core and then transferred to the acceptor molecules. b) Direct charge transfer involves the transfer of photoexcited charge carriers in a single step by direct excitation of an electron from the metal to the adsorbate unoccupied orbital upon plasmon relaxation. Reproduced with permission from reference 65. Copyright 2015 Springer Nature.

## 1.5. Introduction to quantum dot photocatalysis

Quantum dots (QDs) are semiconductor nanoparticles having their size comparable to their bulk exciton Bohr radius.[68] This size regime is the quantum confined regime, where the exciton begins to feel the presence of the particle's boundaries.[68-70] As a consequence of the quantum confinement effect, the continuous energy levels collapse to give rise to discrete and quantized energy levels.[70,71] In general, the extent of confinement is manipulated by changing the size of QDs, which dramatically alters the optoelectronic properties.[68-71] With the decrease in the size of the QDs leading to a higher degree of confinement, the band gap increases (**Figure 1.8**).[70-72] Brus' equation describes the relation between the band gap ($E_g$) of the QDs to its bulk band gap as follows:[73]

$$E_g = E_{bulk} + \frac{h^2}{8R^2}\left(\frac{1}{m_e^*} + \frac{1}{m_h^*}\right) - \frac{1.786e^2}{4\pi\varepsilon_o\varepsilon_r R} \qquad (\mathbf{1.7})$$

where, $h$ is the Planck's constant, $R$ is the radius of the QD, $m_e^*$ and $m_h^*$ are the effective masses of electrons and holes in the QD, respectively, $\varepsilon_o$ is the permittivity of vacuum and $\varepsilon_r$ is the relative permittivity.

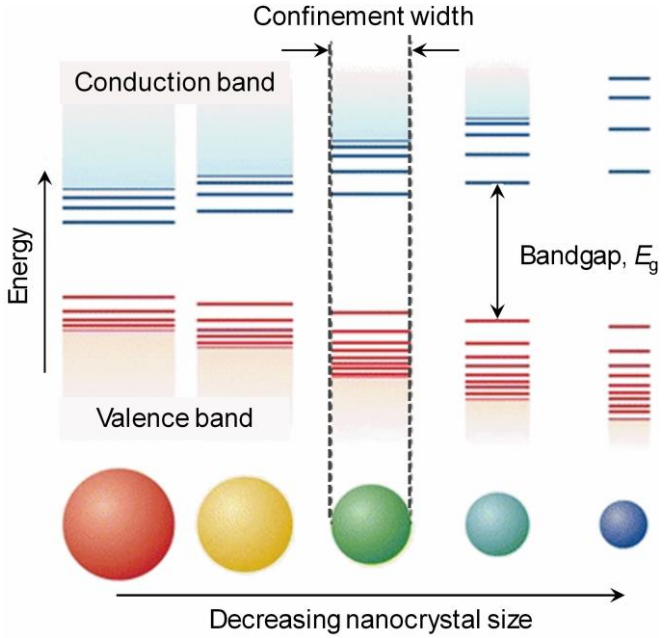


**Figure 1.8.** Schematics representing the quantum confinement effect leading to the change in the band gap of semiconductor nanoparticles as a function of their size. Reproduced with permission from reference 72. Copyright 2017 Springer.

From the photocatalytic point of view, QDs offer enormous flexibility to tune the band positions with respect to the thermodynamics of the desired reaction, just by varying the size of the QD. In addition, QDs exhibit a wide and tunable absorption range, large extinction coefficient, and high photostability - all of which make QDs attractive to be employed as photocatalysts.[74-76] Unlike molecular photocatalysts that follow Kasha's rule, QDs often involve higher excited states under photocatalytic conditions (**Figure 1.9**). Thus, high-energy charge carriers can be directly extracted by reactants.[77,78] However, the defect states are often present in QDs, which significantly affect the charge transfer by trapping the photoexcited charge carriers and can either act as a relay or a point of charge recombination (**Figure 1.9**).[79] Interestingly, QDs are susceptible to multiexcitonic processes as well due to the presence of degenerate and quasi-discrete energy levels.[41,80] This results in exciting non-trivial non-linear charge transfer processes across the interface (**Figure 1.9**). Another interesting process by which charge transfer can occur in QDs is through an Auger-assisted mechanism, in which electron transfer is promoted by virtue of hole excitation to deeper energy levels (**Figure 1.9**).[41,81] With such distinct charge carrier dynamics, albeit intricate, QDs serve as a unique photocatalytic platform for performing a wide array of chemical transformations.[82-85]

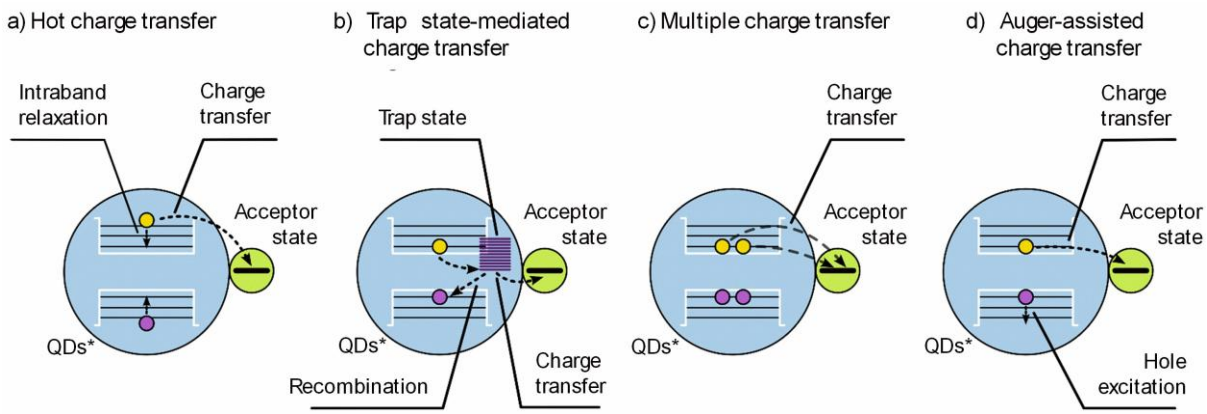


**Figure 1.9.** Schematics showing the different pathways of charge transfer from quantum dots to the acceptor. Reproduced with permission from reference 41. Copyright 2024 American Chemical Society.

## 1.6. *Surface* as a template for tuning photocatalysis

As the famous saying goes, *"God made the bulk, surfaces were invented by the devil"* by Wolfgang Pauli, the surface effects are quite phenomenal in the area of catalysis and photocatalysis.[85-103] The chosen photocatalysts, plasmonic metal NPs and QDs, not only offer intriguing optoelectronic properties, but the high surface-to-volume ratio of these nanostructures renders them a rich surface chemistry. Anatomically, metal NPs or QDs have two distinct parts: I) the core, which imparts photophysical properties, and II) the surface ligands, which act as stabilizing agents and provide dispersion in different media (**Figure 1.10a**).[76,86] A typical ligand comprises three parts: a binding group that attaches to the NP/QD surface, a spacer that determines the length between the NP/QD and the surroundings, and a terminal group from which various covalent and noncovalent forces emanate (**Figure 1.10a**).[51,86] Ligands form a self-assembled monolayer (SAM) on the surfaces of NP/QD, which decides how a NP/QD will interact with its surroundings.

From a photocatalysis point of view, ligands are often undesirable. The long-chain alkyl ligands hinder the approach of reactants towards the catalyst's surface, and their insulating nature restricts the flow of photoexcited charge carriers.[86,87-89] Taking inspiration from enzymes that employ a complex network of interactions to drive catalytic chemical reactions, the ligands on the surface of NP/QD can bring various interparticle forces into action, which can directly regulate the catalyst–reactant

interactions. By attaching the *ligand of choice* to the surface of NP/QD, favourable catalyst-reactant interactions can be installed to channel the reactants toward the NP/QD surface, thereby increasing the local concentration and, hence, the efficiency of the catalytic reaction (**Figure 1.10b**).[86,90-93] Thus, ligands can act as '*gatekeepers*' in plasmonic metal NPs and QDs photocatalyzed chemical reactions such as $H_2$ evolution, $CO_2$ reduction, biological cofactor regeneration, carbon-carbon coupling, etc.

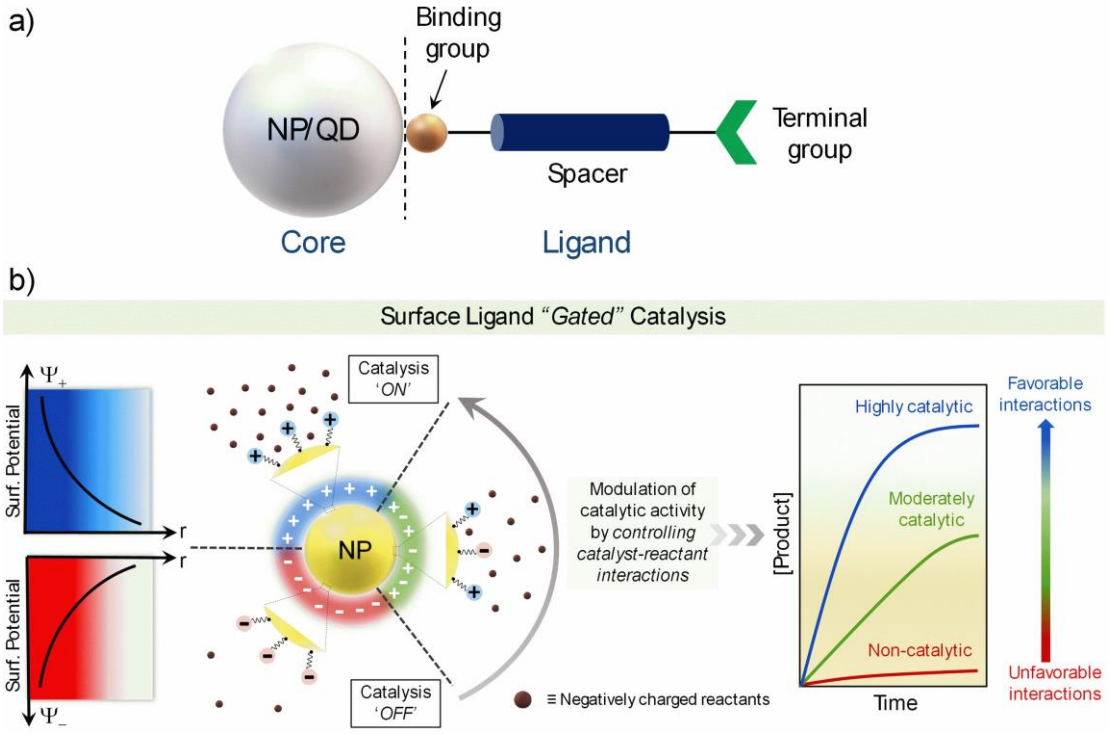


**Figure 1.10.** a) Schematic representation showing the anatomy of an NP/QD comprising core and surface ligands. A typical ligand comprises three parts: a binding group, a spacer, and a terminal group. b) Surface ligand "gated" catalysis. The graph on the left shows the exponential variation in the surface potential of the NP, arising from the charged ligands, as a function of distance. A favorable electrostatic interaction can channelize the flow of the reactants and increase their local concentration near the NP catalyst surface, thereby enhancing the catalytic activity. The catalyst–reactant interaction can be fine-tuned by varying the ratio of the [+] and [−] ligands on the NP surface, which has the power to modulate the catalytic activity as per the demand: highly catalytic, moderately catalytic, and noncatalytic. Reproduced with permission from reference 86. Copyright 2022 American Chemical Society.

Apart from improving the catalytic activity, surface ligands can play a crucial role in accomplishing other desirable functions in catalysis as well, such as product selectivity, switchability, and recyclability.[94-102] In an interesting study by Reisner and coworkers, product selectivity for the reduction of $CO_2$ to CO was achieved by stabilizing a particular

reaction intermediate with the help of smartly chosen ligands.[97] Here, the surface of ZnSe QDs was modified with imidazole ligands that stabilize the surface-bound $*CO_2^-$, which is a key intermediate in the formation of CO (**Figure 1.11a**). A 4-fold and 13-fold increase in the product yield and selectivity were obtained using imidazole functionalized ZnSe QDs, respectively. In a similar study, the same group has achieved CO product selectivity by inhibiting the $H_2$ evolution using dithiolated ligands having long chain lengths.[98] These preliminary studies indicate that the surface ligands have the power to control the adsorption–desorption kinetics of reactants, intermediates, and products. On a different note, Weiss and coworkers functionalized $CuInS_2$ QDs with distinct ligands terminated with amine to improve the photocatalytic $CO_2$ reduction activity in the presence of cobalt porphyrin catalyst (**Figure 1.11b**).[101] Here, the amine functional groups capture $CO_2$ as carbamic acid to enhance $CO_2$ solubility in water, and the electrostatic attraction between protonated amine groups and negatively charged cobalt porphyrin enables fast multielectron transfer from QD to the catalyst. As a result of finely tuned ligand chemistry, $CO_2$ photoreduction proceeded with unprecedented efficiency, with turnover number reaching >80000 with 5.2 % quantum yield and > 99 % selectivity.

Additionally, surface ligands also play a pivotal role in dictating the intrinsic properties of NP/QDs.[51,103-109] For instance, the electronic structure of the QD was found to be perturbed by surface ligands, resulting in a shift in the band edge positions.[104-106] The direct impact of this could be useful in modulating the free energy for charge transfer from photocatalysts to the reactant molecules. More importantly, ligands are known to significantly alter charge carrier dynamics, can introduce or eliminate trap states, modulate intrinsic conductivity, or even impact the stability under photoirradiation conditions.[107-111] Hence, it is clear that along with designing the photocatalyst core, it is crucial to optimize the ligand shell to obtain maximum efficiency in light-assisted chemical transformations.

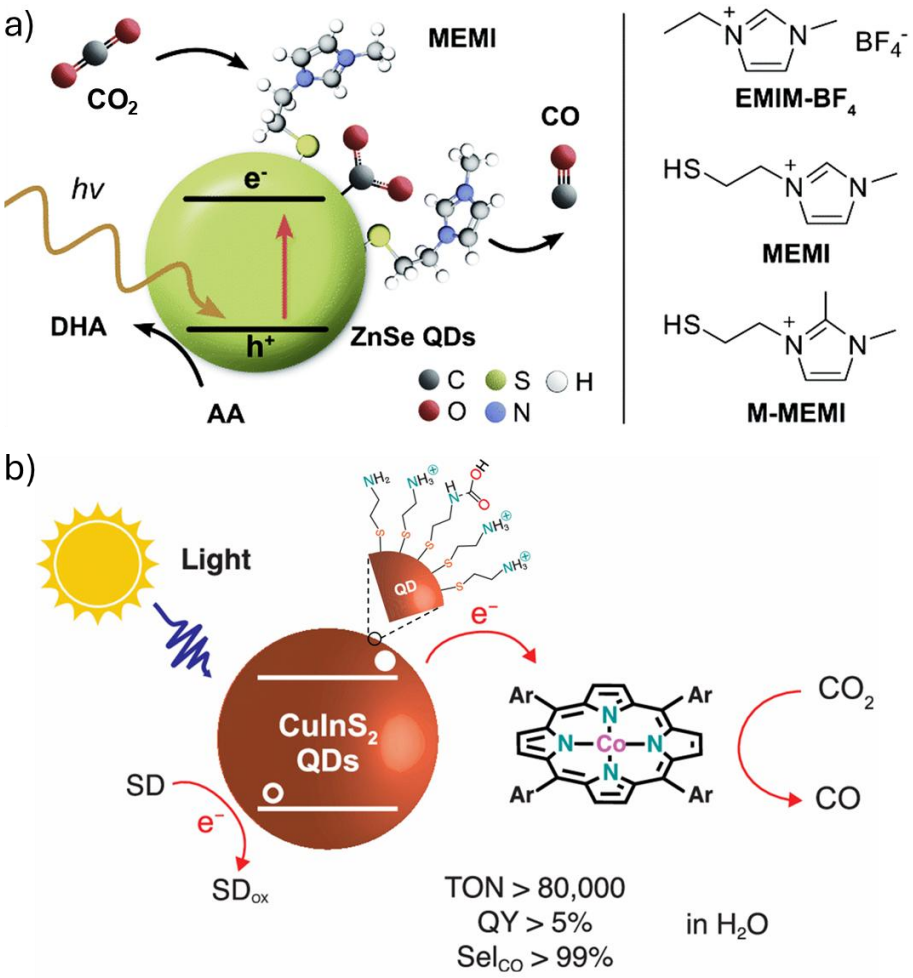


**Figure 1.11.** Surface ligand-mediated product selectivity in photocatalysis. a) Scheme representing the stabilization of the surface-bound $*CO_2^-$ intermediate by the imidazole ligand, resulting in a selective photocatalytic reduction of $CO_2$ to CO by ZnSe QDs. Reproduced with permission from reference 97. Copyright 2021 The Royal Society of Chemistry. b) Schematic illustration of photocatalytic $CO_2$ reduction with $CuInS_2$ QDs as photosensitizer and Co-porphyrin catalyst. The use of alkyl ligands bearing primary amine functional groups enables $CO_2$ capture in the form of carbamic acid, leading to higher solubility of $CO_2$, and the strong electrostatic interactions between oppositely charged surface ligands and Co-porphyrin catalyst ensure efficient electron transfer from QD to the catalyst under light irradiation. Reproduced with permission from reference 101. Copyright 2021 American Chemical Society.

## 1.7. Objective of the thesis

As seen in this Chapter, doing chemistry with light involves intricate underlying mechanisms for charge generation, separation, and their utilization in order to achieve desired chemical transformations. The main focus of the present *thesis* is to maximize the efficiency of the key fundamental steps in photocatalysis by rational design of the photocatalyst core and its surface ligands, to drive challenging multielectron reactions,

in particular. We believe that tuning the core properties (plasmonic metal NPs vs QDs) will allow us to regulate and maximize charge carrier generation and their dynamics in the excited states, whereas a meticulous choice of the surface ligands will dictate the interaction with reactants for effective utilization of photoexcited charge carriers. As discussed in this Chapter, a large number of studies focus on the fundamental aspects of charge generation, separation, and extraction independently. Despite extensive fundamental photophysical studies, these have not been translated to photocatalytic transformations to a sufficient extent.

In light of this, the present *thesis* will showcase the impact of rationally designed core and surface ligands in dictating the photocatalytic efficiencies in driving challenging multielectron transformations. In **Chapter 2**, the details of the chemical reagents used, the synthetic protocols followed, and the instrumentation methods are discussed. **Chapter 3** is focused on understanding the role of light excitation attributes in plasmon-photocatalyzed nicotinamide cofactor regeneration, which requires a rationally designed plasmonic core and surface. Appropriate design of the light-harvesting components was crucial to maximize the key photocatalytic steps and distinguish amongst various plasmon activation mechanisms under different light excitations. With an increase in the complexity of the reaction, from $2e^-/H^+$ driven regeneration of nicotinamide cofactors to $8e^-/9H^+$ reduction of nitrate ions to ammonia, we switched from plasmonic metal core to QDs to increase the charge separation process in **Chapter 4a**. Herein, we established indium phosphide (InP) QDs as an excellent visible light photocatalyst for ammonia synthesis at room temperature. The key mechanistic details involved in photocatalytic nitrate to ammonia conversion are listed in **Chapter 4b**. With the goal of increasing the efficiency of InP QD photocatalyzed nitrate to ammonia conversion, organic long-alkyl ligands were replaced with inorganic surface ligands to improve the charge utilization step in **Chapter 5**. The modifications in surface ligands on the InP QD surface led to a multifold enhancement in reaction rate and quantum efficiency. We envision that the areas of plasmonic photocatalysis and QD photocatalysis will surely benefit from adopting the existing fundamental concepts or even advance beyond our predictions.

## 1.8. References


1) Davis, S. J.; Lewis, N. S.; Shaner, M.; Aggarwal, S.; Arent, D.; Azevedo, I. L.; Benson, S. M.; Bradley, T.; Brouwer, J.; Chiang, Y. M.; Clack, C. T. M.; Cohen, A.; Doig, S.; Edmonds, J.; Fennell, P.; Field, C. B.; Hannegan, B.; Hodge, B.-M.; Hoffert, M. I.; Ingersoll, E.; Jaramillo, P.; Lackner, K. S.; Mach, K. J.; Mastrandrea, M.; Ogden, J.; Peterson, P. F.; Sanchez, D. L.; Sperling, D.; Stagner, J.; Trancik, J. E.; Yang, C. -J.; Caldeira, K. Net-Zero Emissions Energy Systems. *Science* **2018**, *360*, eaas9793.

2) Gabrielli, P.; Rosa, L.; Gazzani, M.; Meys, R.; Bardow, A.; Mazzotti, M.; Sansavini, G. Net-Zero Emissions Chemical Industry in a World of Limited Resources. *One Earth* **2023**, *6*, 682-704.

3) Schiffer, Z. J.; Manthiram, K. Electrification and Decarbonization of the Chemical Industry. *Joule* **2017**, *1*, 10-14.

4) Friend, C. M.; Xu, B. Heterogeneous Catalysis: A Central Science for a Sustainable Future. *Acc. Chem. Res.* **2017**, *50*, 517-521.

5) Ciamician, G. The Photochemistry of the Future. *Science* **1912**, *36*, 385-394.

6) Nocera, D. G. The Artificial Leaf. *Acc. Chem. Res.* **2012**, *45*, 767-776.

7) Lewis, N. S. Research Opportunities to Advance Solar Energy Utilization. *Science* **2016**, *351*, aad1920.

8) Wang, Q.; Pornrungroj, C.; Linley, S.; Reisner, E. Strategies to Improve Light Utilization in Solar Fuel Synthesis. *Nat. Energy* **2022**, *7*, 13-24.

9) Lv, J.; Xie, J.; Mohamed, A. G. A.; Zhang, X.; Feng, Y.; Jiao, L.; Zhou, E.; Yuan, D.; Wang, Y. Solar Utilization Beyond Photosynthesis. *Nat. Rev. Chem.* **2023**, *7*, 91-105.

10) Barber, J. Photosynthetic Energy Conversion: Natural and Artificial. *Chem. Soc. Rev.* **2009**, *38*, 185-196.

11) Armaroli, N.; Balzani, V. Solar Electricity and Solar Fuels: Status and Perspectives in the Context of the Energy Transition. *Chem. Eur. J.* **2016**, *22*, 32-57.

12) Barber, J. Photosynthetic Energy Conversion: Natural and Artificial. *Chem. Soc. Rev.* **2009**, *38*, 185-196.

13) Hill, R.; Bendall, F. A. Y. Function of the Two Cytochrome Components in Chloroplasts: A Working Hypothesis. *Nature* **1960**, *186*, 136-137.

14) Duysens, L. N. M.; Amesz, J.; Kamp, B. M. Two Photochemical Systems in Photosynthesis. *Nature* **1961**, *190*, 510-511.

15) Calvin, M. The Path of Carbon in Photosynthesis. *Science* **1962**, *135*, 3507.

16) Bruner, L.; Kozak, J. Information on the Photocatalysis I The Light Reaction in Uranium Salt Plus Oxalic Acid Mixtures. *Z. Elektrochem. Angew. Phys. Chem.* **1911**, *17*, 354-360.

17) Eibner, A. Action of Light on Pigments I. *Chem-Ztg* **1911**, *35*, 753–755.

18) Kamat, P. V. Unsung Heroes of Energy Research. *ACS Energy Lett.* **2018**, *3*, 1394-1395.

19) Baly, E. C. C.; Heilbron, I. M.; Barker, W. F. CX.—Photocatalysis. Part I. The Synthesis of Formaldehyde and Carbohydrates from Carbon Dioxide and Water. *J. Chem. Soc. Trans.* **1921**, *119*, 1025–1035.

20) Landau, M. Le Phénomène de La Photocatalyse. *Compt. Rend.* **1913**, *156*, 1894–1896.

21) Baly, E.C.C.; Heilbron, I.M.; Hudson, D.P. Photocatalysis. Part II. The Photosynthesis of Nitrogen Compounds from Nitrates and Carbon Dioxide. *J. Chem. Soc. Trans.* **1922**, *121*, 1078–1088.

22) Baly, E.C.C.; Heilbron, I.M.; Stern, H.J. Photocatalysis. Part III. The Photosynthesis of Naturally Occurring Nitrogen Compounds from Carbon Dioxide and Ammonia. *J. Chem. Soc. Trans.* **1923**, *123*, 185–197.

23) Markham, M.C.; Hannan, M.C.; Paternostro, R.M.; Rose, C.B. Oxidation of Alcohols Catalyzed by Zinc Oxide and Light. *J. Am. Chem. Soc.* **1958**, *80*, 5394–5397.

24) Markham, M.C.; Hannan, M.C.; Evans, S.W. Factors Influencing the Oxidation of Phenols, Catalyzed by Zinc Oxide and Light. *J. Am. Chem. Soc.* **1954**, *76*, 820–823.

25) Markham, M. C. Photocatalytic Properties of Oxides. *J. Chem. Educ.* **1955**, *32*, 540–543.

26) Fujishima, A.; Honda, K. Electrochemical Photolysis of Water at a Semiconductor Electrode. *Nature* **1972**, *238*, 37–38.

27) Yang, X.; Wang, D. Photocatalysis: From Fundamental Principles to Materials and Applications. *ACS Appl. Energy Mater.* **2018**, *1*, 6657-6693.

28) Chen, S.; Takata, T.; Domen, K. Particulate Photocatalysts for Overall Water Splitting. *Nat. Rev. Mater.* **2017**, *2*, 17050.

29) Voiry, D.; Shin, H. S.; Loh, K. P.; Chhowalla, M. Low-dimensional Catalysts for Hydrogen Evolution and $CO_2$ Reduction. *Nat. Rev. Chem.* **2018**, *2*, 0105.

30) Yuan, Y. C.; Jin, N.; Saghy, P.; Dube, L.; Zhu, H.; Chen, O. Quantum Dot Photocatalysts for Organic Transformations. *J. Phys. Chem. Lett.* **2021**, *12*, 7180-7193.

31) Vaiano, V.; Sacco, O.; Sannino, D.; Ciambelli, P. Photocatalytic Removal of Spiramycin from Wastewater under Visible Light with N-doped $TiO_2$ Photocatalysts. *Chem. Eng. J.* **2015**, *261*, 3-8.

32) Wei, Y. X.; Jiang, W. J.; Liu, Y.; Bai, X. J.; Hao, D.; Ni, B. J. Recent Advances in Photocatalytic Nitrogen Fixation and Beyond. *Nanoscale* **2022**, *14*, 2990– 2997.

33) Osterloh, F. E. Photocatalysis versus Photosynthesis: A Sensitivity Analysis of Devices for Solar Energy Conversion and Chemical Transformations. *ACS Energy Lett.* **2017**, *2*, 445-453.

34) Kulandaivalu, T.; Mohamed, A. R.; Ali, K. A.; Mohammadi, M. Photocatalytic Carbon Dioxide Reforming of Methane as an Alternative Approach for Solar Fuel Production-A Review. *Renewable Sustainable Energy Rev.* **2020**, *134*, 110363.

35) Shoji, S.; Peng, X.; Yamaguchi, A.; Watanabe, R.; Fukuhara, C.; Cho, Y.; Yamamoto, T.; Matsumura, S.; Yu, M.-W.; Ishii, S. Photocatalytic Uphill Conversion of Natural Gas beyond the Limitation of Thermal Reaction Systems. *Nat. Catal.* **2020**, *3*, 148-153.

36) Kim, D.; You, J.; Lee, D. H.; Hong, H.; Kim, D.; Park, Y. Photocatalytic Furan-to-Pyrrole Conversion. *Science* **2024**, *386*, 99-105.

37) Tao, L.; Wang, Z.-J.; Yan, T.-H.; Liu, Y.-M.; He, H.-Y.; Cao, Y. Direct Synthesis of Pyrroles via Heterogeneous Catalytic Condensation of Anilines with Bioderived Furans. *ACS Catal.* **2017**, *7*, 959-964.

38) Tamelen, E. E. V.; Whitesides, G. H. Photolytic Isomerization of Aromatic Species. Poly-tert-butylfurans. *J. Am. Chem. Soc.* **1968**, *90*, 3894–3896.

39) Yanagi, R.; Zhao, T.; Solanki, D.; Pan, Z.; Hu, S. Charge Separation in Photocatalysts: Mechanisms, Physical Parameters, and Design Principles. *ACS Energy Lett.* **2022**, *7*, 432-452.

40) Zhang, L.; Mohamed, H. H.; Dillert, R.; Bahnemann, D. Kinetics and Mechanisms of Charge Transfer Processes in Photocatalytic Systems: A Review *J. Photochem. Photobiol., C* **2012**, *13*, 263-276.

41) Ye, C.; Zhang, D.-S.; Chen, B.; Tung, C.-H.; Wu, L.-Z. Interfacial Charge Transfer Regulates Photoredox Catalysis. *ACS Cent. Sci.* **2024**, *10*, 529-542.

42) Takanabe, K. Photocatalytic Water Splitting: Quantitative Approaches toward Photocatalyst by Design. *ACS Catal.* **2017**, *7*, 8006-8022.

43) *Absorption and Scattering of Light by Small Particles;* Bohren, C. F.; Huffman, D. R., Eds.; Wiley-VCH, Weinheim, **2004**,: pp 1-476.

44) Bae, D.; Pedersen, T.; Seger, B.; Malizia, M.; Kuznetsov, A.; Hansen, O.; Chorkendorff, I.; Vesborg, P. C. K. Back-Illuminated Si Photocathode: A Combined Experimental and Theoretical Study for Photocatalytic Hydrogen Evolution. *Energy Environ. Sci.* **2015**, 8, 650-660.

45) Li, L.; Salvador, P. A.; Rohrer, G. S. Photocatalysts with Internal Electric Fields. *Nanoscale* **2014**, *6*, 24-42.

46) Proppe, A. H.; Li, Y. C.; Aspuru-Guzik, A.; Berlinguette, C. P.; Chang, C. J.; Cogdell, R.; Doyle, A. G.; Flick, J.; Gabor, N. M.; van Grondelle, R.; Hammes-Schiffer, S.; Jaffer, S. A.; Kelley, S. O.; Leclerc, M.; Leo, K.; Mallouk, T. E.; Narang, P.; Schlau-Cohen, G. S.; Scholes, G. D.; Vojvodic, A.; Yam, V. W.-W.; Yang, J. Y.; Sargent, E. H. Bioinspiration in Light Harvesting and Catalysis. *Nat. Rev. Mater.* **2020**, *5*, 828-846.

47) Reynal, A.; Willkomm, J.; Muresan, N. M.; Lakadamyali, F.; Planells, M.; Reisner, E.; Durrant, J. R. Distance Dependent Charge Separation and Recombination in Semiconductor/Molecular Catalyst Systems for Water Splitting. *Chem. Commun.* **2014**, *50*, 12768-12771.

48) Sudrajat, H.; Nobatova, M. Heterojunction Photocatalysts: Where Are They Headed? *RSC Appl. Interfaces* **2025**, *2*, 599-619.

49) Knowles, K. E.; Malicki, M.; Weiss, E. A. Dual-Time Scale Photoinduced Electron Transfer from PbS Quantum Dots to a Molecular Acceptor. *J. Am. Chem. Soc.* **2012**, *134*, 12470-12473.

50) Prather, K. V.; Stoffel, J. T.; Tsui, E. Y. Redox Reactions at Colloidal Semiconductor Nanocrystal Surfaces. *Chem. Mater.* **2023**, *35*, 3386-3403.

51) Huang, Y.; Cohen, T. A.; Sperry, B. M.; Larson, H.; Nguyen, H. A.; Homer, M. K.; Dou, F. Y.; Jacoby, L. M.; Cossairt, B. M.; Gamelin, D. R.; Luscombe, C. K. Organic Building Blocks at Inorganic Nanomaterial Interfaces. *Mater. Horizons* **2022**, *9*, 61-87.

52) Kelly, K. L.; Coronado, E.; Zhao, L. L.; Schatz, G. C. The Optical Properties of Metal Nanoparticles: The Influence of Size, Shape, and Dielectric Environment. *J. Phys. Chem. B* **2003**, *107*, 668-677.

53) Link, S.; El-Sayed, M. A. Spectral Properties and Relaxation Dynamics of Surface Plasmon Electronic Oscillations in Gold and Silver Nanodots and Nanorods. *J. Phys. Chem. B* **1999**, *103*, 8410-8426.

54) Aslam, U.; Rao, V. G.; Chavez, S.; Linic, S. Catalytic Conversion of Solar to Chemical Energy on Plasmonic Metal Nanostructures. *Nat. Catal.* **2018**, *1*, 656-665.

55) Jain, P. K.; Lee, K. S.; El-Sayed, I. H.; El-Sayed, M. A. Calculated Absorption and Scattering Properties of Gold Nanoparticles of Different Size, Shape, and Composition: Applications in Biological Imaging and Biomedicine. *J. Phys. Chem. B* **2006**, *110*, 7238-7248.

56) El-Sayed, M. A. Some Interesting Properties of Metals Confined in Time and Nanometer Space of Different Shapes. *Acc. Chem. Res.* **2001**, *34*, 257–264.

57) Jain, P. K.; Huang, X.; El-Sayed, I. H.; El-Sayed, M. A. Noble Metals on the Nanoscale: Optical and Photothermal Properties and Some Applications in Imaging, Sensing, Biology, and Medicine. *Acc. Chem. Res.* **2008**, *41*, 1578–1586.

58) Brongersma, M. L.; Halas, N. J.; Nordlander, P. Plasmon-Induced Hot Carrier Science and Technology. *Nat. Nanotech.* **2015**, *10*, 25–34.

59) Camargo, P. H. C.; Cortés, E. *Plasmonic Catalysis: From Fundamentals to Applications*; Wiley-VCH, **2021**.

60) Cortés, E.; Besteiro, L. V.; Alabastri, A.; Baldi, A.; Tagliabue, G.; Demetriadou, A.; Narang, P. Challenges in Plasmonic Catalysis. *ACS Nano* **2020**, *14*, 16202–16219.

61) Brown, A. M.; Sundararaman, R.; Narang, P.; Goddard, W. A.; Atwater, H. A. Nonradiative Plasmon Decay and Hot Carrier Dynamics: Effects of Phonons, Surfaces, and Geometry. *ACS Nano* **2016**, *10*, 957–966.

62) Yu, S. J.; Wilson, A. J.; Heo, J.; Jain, P. K. Plasmonic Control of Multi-Electron Transfer and C-C Coupling in Visible-Light-Driven $CO_2$ Reduction on Au Nanoparticles. *Nano Lett.* **2018**, *18*, 2189-2194.

63) Kim, Y.; Smith, J. G.; Jain, P. K. Harvesting Multiple Electron-Hole Pairs Generated through Plasmonic Excitation of Au Nanoparticles. *Nat. Chem.* **2018**, *10*, 763-769.

64) Linic, S.; Christopher, P.; Ingram, D. B. Plasmonic-Metal Nanostructures for Efficient Conversion of Solar to Chemical Energy. *Nat. Mater.* **2011**, *10*, 911– 921.

65) Linic, S.; Aslam, U.; Boerigter, C. & Morabito, M. Photochemical Transformations on Plasmonic Metal Nanoparticles. *Nat. Mater.* **2015**, *14*, 567-576.

66) Devasia, D.; Das, A.; Mohan, V.; Jain, P. K. Control of Chemical Reaction Pathways by Light–Matter Coupling. *Annu. Rev. Phys. Chem.* **2021**, *72*, 423-443.

67) Kale, M. J.; Avanesian, T.; Xin, H. L.; Yan, J.; Christopher, P. Controlling Catalytic Selectivity on Metal Nanoparticles by Direct Photoexcitation of Adsorbate-Metal Bonds. *Nano Lett.* **2014**, *14*, 5405-5412.

68) Jungnickel, V.; Henneberger, F. Luminescence Related Processes in Semiconductor Nanocrystals —The Strong Confinement Regime. *J. Lumin.* **1996**, *70*, 238–252.

69) Bawendi, M. G.; Steigerwald, L.; Brus, L. E. The Quantum Mechanics of Larger Semiconductor Clusters ("Quantum Dots"). *Annu. Rev. Phys. Chem.* **1990**, *4*, 477–496.

70) Alivisatos, A. P. Semiconductor Clusters, Nanocrystals, and Quantum Dots. *Science*, **1996**, *271*, 933-937.

71) Rossetti, R.; Nakahara, S.; Brus, L. E. Quantum Size Effects in the Redox Potentials, Resonance Raman Spectra, and Electronic Spectra of CdS Crystallites in Aqueous Solution. *J. Chem. Phys.* **1983**, *79*, 1086–1088.

72) Rabouw, F. T.; de Mello Donega, C. Excited-State Dynamics in Colloidal Semiconductor Nanocrystals; Springer: **2017**.

73) Brus, L. E. Electron–Electron and Electron-hole Interactions in Small Semiconductor Crystallites: The Size Dependence of the Lowest Excited Electronic State. *J. Chem. Phys.* **1984**, *80*, 4403–4409.

74) Medintz, I. L.; Mattoussi, H. Quantum Dot-Based Resonance Energy Transfer and Its Growing Application in Biology. *Phys. Chem. Chem. Phys.* **2009**, *11*, 17-45.

75) Bruchez Jr., M.; Moronne, M.; Gin, P.; Weiss, S.; Alivisatos, A. P. Semiconductor Nanocrystals as Fluorescent Biological Labels. *Science* **2013**, *281*, 2013–2016.

76) Chakraborty, I. N.; Roy, P.; Rao, A.; Devatha, G.; Roy, S.; Pillai, P. P. The Unconventional Role of Surface Ligands in Dictating the Light Harvesting Properties of Quantum Dots. *J. Mater. Chem. A* **2021**, *9*, 7422–7457.

77) Tisdale, W. A.; Williams, K. J.; Timp, B. A.; Norris, D. J.; Aydil, E. S.; Zhu, X.-Y. Hot-Electron Transfer from Semiconductor Nanocrystals. *Science* **2010**, *328*, 1543-1547.

78) Singh, R.; Liu, W.; Lim, J.; Robel, I.; Klimov, V. I. Hot-Electron Dynamics in Quantum Dots Manipulated by Spin-Exchange Auger Interactions. *Nat. Nanotechnol.* **2019**, *14*, 1035-1041.

79) Vishnu, E. K.; Thomas, E. M.; Prasad, L.; Thomas, K. G. Trap States in Semiconductor Quantum Dots: Friends or Foes. *J. Phys. Chem. C* **2024**, *128*, 4373-4382.

80) Luo, X.; Liang, G.; Wang, J.; Liu, X.; Wu, K. Picosecond Multi-Hole Transfer and Microsecond Charge-Separated States at the Perovskite Nanocrystal/Tetracene Interface. *Chem. Sci.* **2019**, *10*, 2459– 2464.

81) Zhu, H.; Yang, Y.; Hyeon-Deuk, K.; Califano, M.; Song, N.; Wang, Y.; Zhang, W.; Prezhdo, O. V.; Lian, T. Auger-Assisted Electron Transfer from Photoexcited Semiconductor Quantum Dots. *Nano Lett.* **2014**, *14*, 1263-1269.

82) Li, X.-B.; Tung, C.-H.; Wu, L.-Z. Semiconducting Quantum Dots for Artificial Photosynthesis. *Nat. Rev. Chem.* **2018**, *2*, 160-173.

83) Wu, K.; Lian, T. Quantum Confined Colloidal Nanorod Heterostructures for Solar-To-Fuel Conversion. *Chem. Soc. Rev.* **2016**, *45*, 3781– 3810.

84) Liang, W. F.; Nie, C. M.; Du, J.; Han, Y. Y.; Zhao, G. H.; Yang, F.; Liang, G. J.; Wu, K. F. Near-Infrared Photon Upconversion and Solar Synthesis Using Lead-Free Nanocrystals. *Nat. Photonics* **2023**, *17*, 346– 353.

85) Weiss, E. A. Designing the Surfaces of Semiconductor Quantum Dots for Colloidal Photocatalysis. *ACS Energy Lett.* **2017**, *2*, 1005-1013.

86) Jain, V.; Roy, S.; Roy, P.; Pillai, P. P. When Design Meets Function: The Prodigious Role of Surface Ligands in Regulating Nanoparticle Chemistry. *Chem. Mater.* **2022**, *34*, 7579-7597.

87) Smith, J. G.; Jain, P. K. The Ligand Shell as an Energy Barrier in Surface Reactions on Transition Metal Nanoparticles. *J. Am. Chem. Soc.* **2016**, *138*, 6765– 6773.

88) Kim, Y.; Wilson, A. J.; Jain, P. K. The Nature of Plasmonically Assisted Hot-Electron Transfer in a Donor-Bridge-Acceptor Complex. *ACS Catal.* **2017**, *7*, 4360– 4365.

89) Ansar, S. M.; Kitchens, C. L. Impact of Gold Nanoparticle Stabilizing Ligands on the Colloidal Catalytic Reduction of 4-Nitrophenol. *ACS Catal.* **2016**, *6*, 5553– 5560.

90) Roy, S.; Roy, S.; Rao, A.; Devatha, G.; Pillai, P. P. Precise Nanoparticle-Reactant Interaction Outplays Ligand Poisoning in Visible-Light Photocatalysis. *Chem. Mater.* **2018**, *30*, 8415– 8419.

91) Roy, S.; Jain, V.; Kashyap, R. K.; Rao, A.; Pillai, P. P. Electrostatically Driven Multielectron Transfer for the Photocatalytic Regeneration of Nicotinamide Cofactor. *ACS Catal.* **2020**, *10*, 5522– 5528.

92) Roy, S.; Rao, A.; Devatha, G.; Pillai, P. P. Revealing the Role of Electrostatics in Gold-Nanoparticle-Catalyzed Reduction of Charged Substrates. *ACS Catal.* **2017**, *7*, 7141– 7145.

93) Shirin, S.; Roy, S.; Rao, A.; Pillai, P. P. Accelerated Reduction of 4-Nitrophenol: Bridging Interaction Outplays Reducing Power in the Model Nanoparticle-Catalyzed Reaction. *J. Phys. Chem. C* **2020**, *124*, 19157-19165.

94) im, M.; Dygas, M.; Sobolev, Y. I.; Beker, W.; Zhuang, Q.; Klucznik, T.; Ahumada, G.; Ahumada, J. C.; Grzybowski, B. A. On-Nanoparticle Gating Units Render an Ordinary Catalyst Substrate- and Site-Selective. *J. Am. Chem. Soc.* **2021**, *143*, 1807-1815.

95) Kahsar, K. R.; Schwartz, D. K.; Medlin, J. W. Control of Metal Catalyst Selectivity through Specific Noncovalent Molecular Interactions. *J. Am. Chem. Soc.* **2014**, *136*, 520– 526.

96) Ung, D.; Murphy, I. A.; Cossairt, B. M. Designing Nanoparticle Interfaces for Inner-Sphere Catalysis. *Dalton Trans.* **2020**, *49*, 4995– 5005.

97) Sahm, C. D.; Mates-Torres, E.; Eliasson, N.; Sokołowski, K.; Wagner, A.; Dalle, K. E.; Huang, Z.; Scherman, O. A.; Hammarström, L.; García-Melchor, M.; Reisner, E.

Imidazolium-Modification Enhances Photocatalytic $CO_2$ reduction on ZnSe Quantum Dots. *Chem. Sci.* **2021**, *12*, 9078– 9087.

98) Sahm, C. D.; Ciotti, A.; Mates-Torres, E.; Badiani, V.; Sokołowski, K.; Neri, G.; Cowan, A. J.; García-Melchor, M.; Reisner, E. Tuning the Local Chemical Environment of ZnSe Quantum Dots with Dithiols Towards Photocatalytic $CO_2$ Reduction. *Chem. Sci.* **2022**, *13*, 5988– 5998.

99) Wei, Y.; Han, S.; Kim, J.; Soh, S.; Grzybowski, B. A. Photoswitchable Catalysis Mediated by Dynamic Aggregation of Nanoparticles. *J. Am. Chem. Soc.* **2010**, *132*, 11018-11020.

100) Zhuang, Q.; Yang, Z.; Sobolev, Y. I.; Beker, W.; Kong, J.; Grzybowski, B. A. Control and Switching of Charge-Selective Catalysis on Nanoparticles by Counterions. *ACS Catal.* **2018**, *8*, 7469-7474.

101) Arcudi, F.; Dordevic, L.; Nagasing, B.; Stupp, S. I.; Weiss, E. A. Quantum Dot-Sensitized Photoreduction of $CO_2$ in Water with Turnover Number > 80,000. *J. Am. Chem. Soc.* **2021**, *143*, 18131-18138.

102) Hernandez, F.; Yang, M.; Nagelj, N.; Lee, A. Y.; Noh, H.; Hur, K. P.; Fu, X.; Savoie, C. J.; Schwartzberg, A. M.; Olshansky, J. H. The Role of Surface Functionalization in Quantum Dot-Based Photocatalytic $CO_2$ Reduction: Balancing Efficiency and Stability. *Nanoscale* **2024**, *16*, 5624-5633.

103) Tsui, E. Y. Surface Considerations in Colloidal Semiconductor Nanocrystal Photocatalysis: A Mini Review. *Energy Fuels* **2025**, *39*, 7182–7195.

104) Brown, P. R.; Kim, D.; Lunt, R. R.; Zhao, N.; Bawendi, M. G.; Grossman, J. C.; Bulović, V. Energy Level Modification in Lead Sulfide Quantum Dot Thin Films through Ligand Exchange. *ACS Nano* **2014**, *8*, 5863-5872.

105) Kroupa, D. M.; Vörös, M.; Brawand, N. P.; McNichols, B. W.; Miller, E. M.; Gu, J.; Nozik, A. J.; Sellinger, A.; Galli, G.; Beard, M. C. Tuning colloidal quantum dot band edge positions through solution-phase surface chemistry modification. *Nat. Commun.* **2017**, *8*, 15257.

106) Carroll, G. M.; Tsui, E. Y.; Brozek, C. K.; Gamelin, D. R. Spectroelectrochemical Measurement of Surface Electrostatic Contributions to Colloidal CdSe Nanocrystal Redox Potentials. *Chem. Mater.* **2016**, *28*, 7912– 7918.

107) Hines, D. A.; Kamat, P. V. Quantum Dot Surface Chemistry: Ligand Effects and Electron Transfer Reactions. *J. Phys. Chem. C* **2013**, *117*, 14418-14426.

108) Sandeep, K.; Manoj, B.; Thomas, K. G. Gold Nanoparticle on Semiconductor Quantum Dot: Do Surface Ligands Influence Fermi Level Equilibration. *J. Chem. Phys.* **2020**, *152*, 044710.

109) Peterson, M. D.; Cass, L. C.; Harris, R. D.; Edme, K.; Sung, K.; Weiss, E. A. The Role of Ligands in Determining the Exciton Relaxation Dynamics in Semiconductor Quantum Dots. *Annu. Rev. Phys. Chem.* **2014**, *65*, 317-339.

110) Nakanishi, H.; Bishop, K. J. M.; Kowalczyk, B.; Nitzan, A.; Weiss, E. A.; Tretiakov, K. V.; Apodaca, M. M.; Klajn, R.; Stoddart, J. F.; Grzybowski, B. A. Photoconductance and Inverse Photoconductance in Films of Functionalized Metal Nanoparticles Nature **2009**, 460, 371-375.

111) Warren, S. C.; Walker, D. A.; Grzybowski, B. A. Plasmoelectronics: Coupling Plasmonic Excitation with Electron Flow. *Langmuir* **2012**, *28*, 9093-9102.

# Chapter – 2

## Materials, Methods, and Techniques

## 2.1. Materials and reagents

Tetrachloroaurate trihydrate ($HAuCl_4.3H_2O$), hexadecyltrimethylammonium bromide (CTAB), ascorbic acid, silver nitrate ($AgNO_3$) tetramethylammonium hydroxide (TMAOH) 25 % wt. in water, 11-mercaptoundecanoic acid (MUA), β-nicotinamide adenine dinucleotide sodium salt ($NAD^+$), β-nicotinamide adenine dinucleotide reduced disodium salt (NADH), rhodium chloride hydrate ($RhCl_3.H2O$), 1,2,3,4,5-pentamethylcyclopentadiene (Cp*), 2,2'-bipyridyl (bpy), tris-(dimethylamino)phosphine ($P(DMA)_3$), oleylamine (OAm), potassium nitrate ($KNO_3$), potassium nitrite ($KNO_2$), potassium nitrate-15N labeled ($K^{15}NO_3$), zinc stearate, 1-dodecanethiol (DDT), 1-octadecene (ODE), sulfur powder, trioctylphosphine (TOP), and glutamate dehydrogenase were purchased from Sigma-Aldrich. 1-Decanol, disodium 2-oxoglutarate, indium chloride ($InCl_3$), zinc chloride ($ZnCl_2$), indium bromide ($InBr_3$), and indium iodide ($InI_3$) were purchased from TCI Chemicals Pvt. Ltd. India. Triethanolamine (TEOA) was purchased from Avra Chemicals. Dimethylformamide (DMF) was purchased from Advent ChemBio. All the reagents were used as received without any further purification. *N, N, N*-Trimethyl(11-mercaptoundecyl) ammonium chloride (TMA) was synthesized according to the reported procedure.[1]

## 2.2. Synthesis of gold nanorods (AuNRs)

Gold nanorods (AuNRs) were synthesized following a modified literature procedure.[2] In a typical experiment, a solution of 50 mM CTAB/13.5 mM *n*-decanol was prepared by dissolving 9.111 g of CTAB and 1.068 g of *n*-decanol in 500 mL of Milli-Q water. This was followed by the preparation of small AuNP seeds (1–2 nm) by rapidly injecting 800 µL of $NaBH_4$ (20 mM) into 20 mL of a CTAB/*n*-decanol solution, 200 µL of $HAuCl_4$ (50 mM), and 100 µL of ascorbic acid (0.1 M). The seed solution turned yellowish-brown upon $NaBH_4$ addition and was kept for aging (at least 60 min) for complete consumption of excess $NaBH_4$. For the synthesis of small anisotropic AuNRs, 325 mL of a CTAB (50 mM)/*n*-decanol (13.5 mM) solution, 2.6 mL of $AgNO_3$ (10 mM), and 3.25 mL of $HAuCl_4$ (50 mM) were added. From this mixture, 25.45 mL of the solution was taken out in a different flask, and 325 µL of ascorbic acid (0.1 M) was added. The solution turned colorless and was

divided into five equal parts of 1.55 mL, followed by the addition of HCl (1 M) in increasing amounts, starting from 250 to 450 µL. The growth solution was left undisturbed for 3–4 h after adding 300 µL of the prepared AuNP seed solution. An appropriate amount of HCl was chosen for which the longitudinal SPR band lies at ~800 nm. Using the same reagent solutions, the same AuNP seeds, and an optimized HCl amount, the synthesis was scaled up to ~300 mL by keeping all ratios constant. The growth solution was left overnight to obtain a higher yield of NRs, followed by centrifugation at 10000 rpm for 30 min so as to obtain a concentrated colloidal solution. Scanning electron microscopy (SEM) images revealed uniform size distribution of AuNRs of an aspect ratio of ~4.

## 2.3. Synthesis of indium phosphide quantum dots (InP QDs)

### 2.3.1. Synthesis of core-only InP QDs

A modified literature procedure was used for the synthesis of red-emitting core-only InP QDs.[3,4] In a typical synthesis, indium(III) chloride (100 mg, 0.45 mmol), zinc chloride (300 mg, 2.2 mmol), and oleylamine (5.0 mL, 15 mmol) were placed in a 100 mL three-neck RB equipped with a stir bar. The mixture was heated to 120 °C under an Ar atmosphere with gentle stirring until a clear solution was obtained. The reaction mixture was degassed for ~60 min at 120 °C, followed by a rise in temperature to ~200 °C. Upon reaching ~200 °C, 350 µL of tris(dimethylamino)phosphine (1.93 mmol) in 1.0 mL of oleylamine was quickly injected into the reaction mixture. The temperature was maintained at ~200 °C for 60 min for the growth of the InP core QDs. In the end, the reaction mixture was quenched with a water bath, followed by the addition of 5.0 mL of hexane to arrest the growth of core-only QDs. The as-synthesized QD solution was centrifuged at 8000 rpm for 10 min to remove unreacted precursors. The resultant supernatant was purified by precipitation with ethanol and redispersed back in toluene for further use.

### 2.3.2. Synthesis of core/shell InP/ZnS QDs

For the synthesis of core/shell InP/ZnS QDs, firstly, core-only InP QDs were synthesized according to the procedure described in Section 2.3.1. After the complete growth of core-only InP QDs, the reaction mixture was cooled down to room temperature with a cold-water bath and further proceeded for ZnS shell growth. For the shell growth, zinc stearate (63 mg, 0.1 mmol ) and DDT (24 mL, 0.1 mmol) were dissolved in ODE and injected into the reaction mixture containing core-only InP QDs under inert conditions. The temperature was raised to 300 °C and kept for 20 min. Finally, the reaction mixture was quenched with a water bath, followed by the addition of 5 mL hexane to arrest the shell growth. As prepared, red-emitting InP/ZnS QDs were purified by precipitation with ethanol twice and redispersed in toluene for further use.

## 2.4. Ligand exchange reaction for AuNRs and InP QDs

### 2.4.1. Ligand exchange of AuNRs

CTAB/*n*-decanol-stabilized AuNRs, [+] AuNRs, were place-exchanged with negatively charged 11-mercaptoundecanoic acid (MUA, [−]) ligand to obtain [−] AuNRs (**Scheme 2.1**). In a typical place exchange, 1 mL of concentrated [+] AuNRs were precipitated by the addition of 25 mL of methanol, which yielded a black precipitate. The supernatant was carefully removed, and a 10 mM MUA ligand dissolved in methanol was added to the precipitated AuNRs. The solution was left undisturbed for 8 h to ensure complete place exchange with the MUA ligand. Next, the supernatant was decanted, and the precipitate was washed with 25 mL of methanol, followed by acetone. The precipitate was then dried and redispersed in Milli-Q water by adding 20 µL of tetramethylammonium hydroxide (25 % wt. in water) to deprotonate the carboxylic acid group. Zeta potential (ζ) measurements confirmed the successful ligand exchange, and the as-synthesized [−] AuNRs were used for further studies.

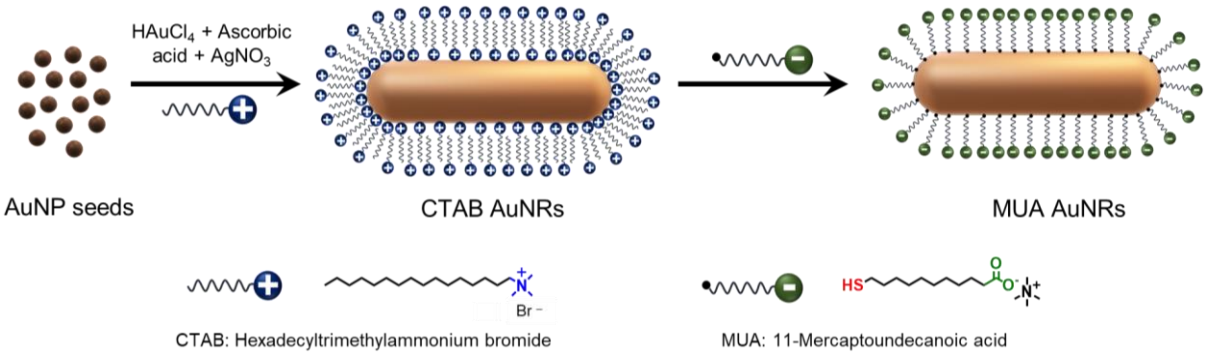


**Scheme 2.1.** Schematic illustration for the synthesis and place exchange of AuNRs. Positively-charged CTAB stabilized NRs, [+] AuNRs, were synthesized via the seed-mediated method and ligand exchanged with negatively charged MUA ligands to yield [-] AuNRs.

## 2.4.2. Ligand exchange of InP QDs

The parent OAm-capped InP QDs were subjected to ligand exchange with positively charged *N,N,N*-trimethyl(11-mercaptoundecyl) ammonium chloride (TMA, [+]) to achieve colloidal stability in an aqueous medium in accordance with the literature report (**Scheme 2.2**).[5] In a typical place exchange protocol, TMA (~50 mg) was dissolved in 2 mL of water, and 800 µL of parent OAm-capped InP QDs were added. The solution was vigorously shaken for ~5 min, followed by the addition of 1 mL of water and 10 mL of toluene. The solution was stirred overnight to facilitate a complete transfer of QDs from the organic phase to the aqueous phase. The aqueous phase was separated, precipitated with 2-propanol, and centrifuged to remove excess TMA ligands. Finally, [+] InP QDs were redispersed in water for photocatalytic studies.

Similarly, [−] InP QDs were prepared by a ligand exchange protocol using 11-mercaptoundecanoic acid (MUA, [−]) as the ligand (**Scheme 2.2**).[5] Here, MUA (~100 mg) was dissolved in a 1:4 ratio of water: methanol (0.3 and 1.2 mL, respectively), and the pH was adjusted to 10 using NaOH. To this, ~800 µL of parent QDs was added, followed by the addition of 2 mL of water and 10 mL of toluene. The solution was stirred overnight to facilitate a complete phase transfer of QDs from the organic phase to the aqueous phase. The aqueous phase was carefully transferred, precipitated with acetone, and centrifuged to remove the excess MUA ligands. The anionic [−] InP QDs were redispersed in water for further studies.

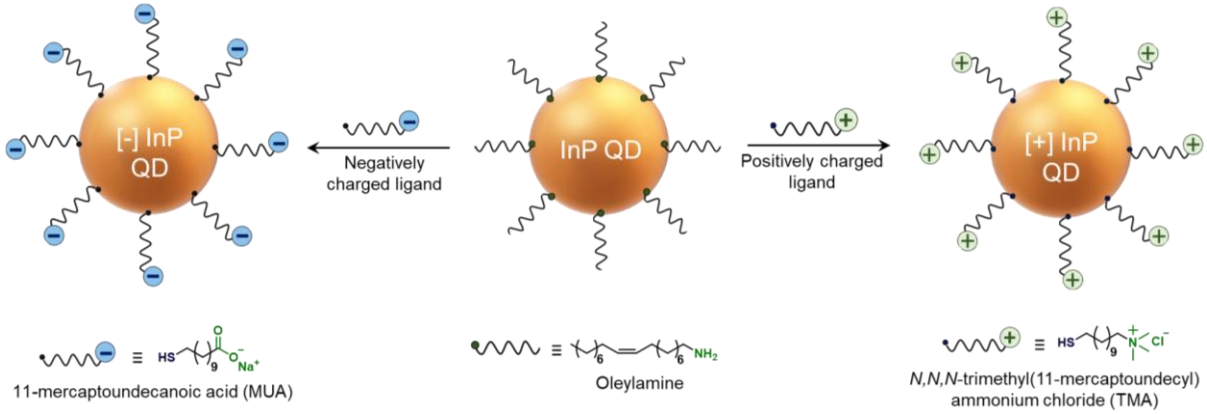


**Scheme 2.2.** Schematics showing the ligand exchange of oleylamine-capped InP QDs with positively charged *N,N,N*-trimethyl(11-mercaptoundecyl)ammonium chloride (TMA) and negatively charged 11-mercaptoundecanoic acid (MUA) thiolated ligands.

A modified literature protocol was used to functionalize a metal-solvent complex (MSC) on the InP QD surface.[6] Firstly, 50 mg $InCl_3$ was dissolved in 2 mL of DMF to form $[In(DMF)_6]^{3+}$ complex ([+] MSC). To this solution, 800 mL of parent OAm-capped InP QDs in hexane were added. The reaction mixture was stirred vigorously for 12 h to facilitate the transfer of InP QDs from hexane to DMF (**Scheme 2.3**). The place-exchanged QDs were purified twice with hexane, followed by precipitation using toluene, and redispersed in water for further photocatalytic reactions.

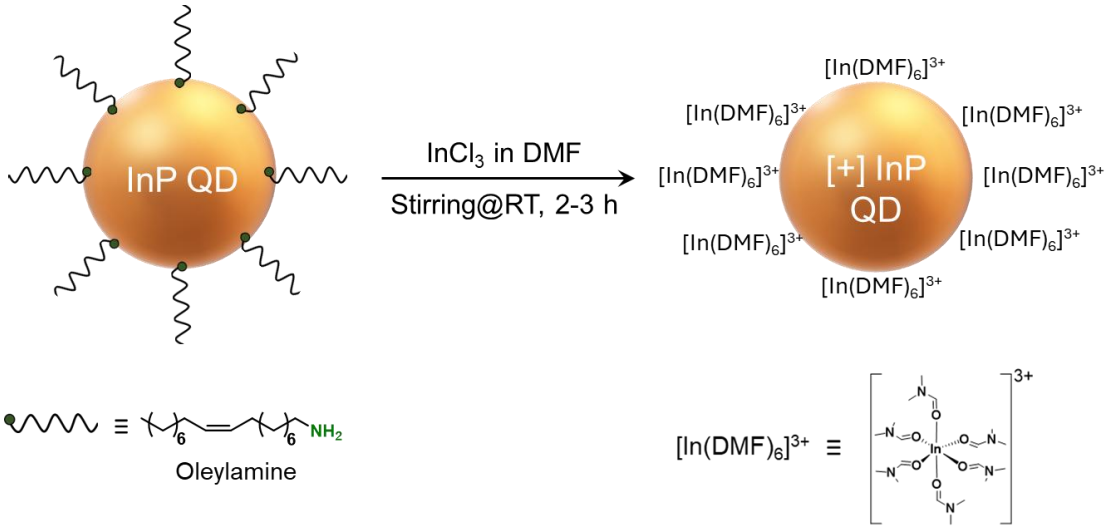


**Scheme 2.3.** Schematics of ligand exchange of InP QDs with positively charged metal-solvent coordination complex, $[In(DMF)_6]^{3+}$ ([+] MSC).

# 2.5. Instrumentation and techniques used

## 2.5.1. UV-vis absorption studies

All UV-vis absorbance data were recorded on a Shimadzu UV-3600 spectrophotometer and a quartz cuvette of path length 1 cm, over the range of 200-1200 nm. The concentration of AuNRs and InP QD solution was calculated using Beer-Lambert's law:

$$A = \varepsilon . c . l$$

where,

*A* is the absorbance

$\varepsilon$ is the molar extinction coefficient ($M^{-1}$ $cm^{-1}$)

*c* is the concentration of the solution (M)

*l* is the optical path length (cm).

Molar extinction coefficient for InP QDs was calculated using the following equations:[7]

$$D = (-3.7707 \times 10^{-12})\lambda^5 + (1.0262 \times 10^{-8})\lambda^4 - (1.0781 \times 10^{-5})\lambda^3 + (5.4550 \times 10^{-3})\lambda^2 - (1.3122)\lambda + 119.9$$

$$\varepsilon = 3046.1\ (D)^3 - 76532\ (D)^2 + (5.5137 \times 10^5)(D) - (8.9839 \times 10^5)$$

where D is the diameter of QDs in nm, and λ is the wavelength corresponding to the first excitonic peak of QDs in nm.

## 2.5.2. Zeta potential measurements

Zeta potential (ζ) measurements of the functionalized AuNRs and InP QDs were performed in Zetasizer Nano series, Nano-2590 (Malvern instruments, U.K.). The optical density of the solution was maintained ~0.05 during all the measurements. The ζ value was estimated from the electrophoretic mobility ($U_E$) (the velocity with which the charged particles are attracted to the oppositely charged electrodes) and is calculated using Henry's equation:[8]

$$U_E = \frac{2\varepsilon\zeta f(k_a)}{3\eta}$$

where,

$\varepsilon$ is the dielectric constant of the medium,

$\zeta$ is the zeta potential (mV)

$f(k_a)$ is Henry's function

$\eta$ is the viscosity of the medium (Pa s).

Smoluchowski's approximation was used to measure the zeta potential values.

### 2.5.3. Nuclear magnetic resonance (NMR) spectroscopy studies

$^1$H NMR data were recorded on a Bruker 400 MHz spectrometer.

### 2.5.4. Scanning electron microscopy (SEM) imaging

Field emission scanning electron microscopy (FESEM) studies were carried out using a Zeiss Ultra Plus FESEM instrument. The SEM sample was prepared by drop-casting a solution of AuNRs on a silicon wafer and dried under a vacuum. The SEM imaging for the paper-based dip catalyst system, loaded with [−] AuNRs, was carried out by taking a small portion of the paper film.

### 2.5.5. Transmission electron microscopy (TEM) imaging

NP and QD samples were drop-casted onto a 400-mesh copper grid (Ted Pella Inc.) and dried under vacuum. The high-resolution transmission electron microscopy (HRTEM) imaging was performed on Jeol JEM2200FS (200 kV) instrument.

### 2.5.6. Cyclic voltammetry (CV) studies

Metrohm DropSens μStat400 electrochemical workstation and Dropview 8400 software were used to carry out the CV experiments. Glassy carbon was used as the working electrode, non-aqueous $Ag/AgNO_3$ in acetonitrile as the reference electrode, and a Pt wire was used as the counter electrode. Ferrocene was used as the internal standard. The oxidation and reduction potential for QDs vs vacuum was determined using the following equations:

$$E_{VB} = -I_P = -(eE_{ox} + E_{ref})eV$$

$$E_{CB} = -E_A = -(eE_{red} + E_{ref})eV$$

where,

$E_{ox}$ and $E_{red}$ are the onset redox potentials with respect to the reference electrode,

$E_{ref}$ is the potential difference between the selected reference electrode and the vacuum energy level, and

$I_P$ and $I_A$ are the ionization potential and electron affinity.

### 2.5.7. Fourier-transform infrared spectroscopy (FTIR)

FTIR experiments were performed to confirm the presence of ligands on the surface of QDs. The measurements were performed on Bruker ALPHA II FTIR spectrometer.

### 2.5.8. Mass spectrometry

Qualitative gas analysis was performed with BELMASS II quadrupole mass spectrometer from Microtrac. Mass channels for the desired gases were selected, and the gases from the reactor's headspace were injected into the mass spectrometer using a gas-tight syringe.

### 2.5.9. X-ray photoelectron spectroscopy (XPS)

The XPS studies were performed on a Thermo Fisher Scientific Instrument, Leicestershire, UK (Model: K-Alpha+) using Al-Kα anode in a transmission lens mode and multi-channel plate (MCP) detector. OAm-InP QDs and [+] InP QDs before the reaction were drop-casted on a silicon wafer and dried completely in vacuum. To prepare the sample after the photocatalytic reaction, [+] InP QDs were precipitated from the reaction mixture by centrifugation and dried completely in vacuum. The dried [+] InP QD sample was dispersed in IPA and drop-cast on a silicon wafer. The binding energy scale was calibrated using the standard C 1s peak (284.6 eV), and the elemental peaks were analyzed using non-linear Shirley background correction. The peak position fittings were

carried out using XPSpeak41 software and optimized by a weight least-square fitting method using Gaussian and Lorentzian lineshape.

### 2.5.10. Ion chromatography

Dionex Aquion ion chromatography system from Thermo Fisher Scientific was used to quantify the concentration of different ions in the reaction. Cations and anions were analysed using CS16 column (5 x 250 mm) with CDRS 600 (4 mm) suppressor and AS23 column (4 x 250 mm) with ADRS 600 (4 mm) suppressor, respectively. Methanesulfonic acid (30 mM) and a mixture of sodium carbonate (4.5 mM) and sodium bicarbonate (0.8 mM) were used as the eluent for cation and anion analysis, respectively. The sample loop was kept constant at 25 μL for all studies. The concentrations of $NH_4^+$, $NO_3^-$, and $NO_2^-$ were deduced from the calibration curves plotted for the respective ions.

## 2.6. References

1) Tien, J.; Terfort, A.; Whitesides, G. M. Microfabrication Through Electrostatic Self-Assembly. *Langmuir* **1997**, 13, 5349-5355.

2) González-Rubio, G.; Kumar, V.; Llombart, P.; Díaz-Núñez, P.; Bladt, E.; Altantzis, T.; Bals, S.; Peña-Rodríguez, O.; Noya, E. G.; MacDowell, L. G.; Guerrero-Martínez, A.; Liz-Marzán, L. M. Disconnecting Symmetry Breaking from Seeded Growth for the Reproducible Synthesis of High Quality Gold Nanorods. *ACS Nano* **2019**, *13*, 4424-4435.

3) Tessier, M. D.; Dupont, D.; De Nolf, K.; De Roo, J.; Hens, Z. Economic and Size-Tunable Synthesis of InP/ZnE (E = S,Se) Colloidal Quantum Dots. *Chem. Mater.* **2015**, *27*, 4893-4898.

4) Tessier, M. D.; De Nolf, K.; Dupont, D.; Sinnaeve, D.; De Roo, J.; Hens, Z. Aminophosphines: A Double Role in the Synthesis of Colloidal Indium Phosphide Quantum Dots. *J. Am. Chem. Soc.* **2016**, *138*, 5923-5929.

5) Devatha, G.; Roy, S.; Rao, A.; Mallick, A.; Basu, S.; Pillai, P. P. Electrostatically Driven Resonance Energy Transfer in “Cationic” Biocompatible Indium Phosphide Quantum Dots. *Chem. Sci.* **2017**, *8*, 3879-3884.

6) Hai, Y.; Gahlot, K.; Tanchev, M.; Mutalik, S.; Tekelenburg, E. K.; Hong, J.; Ahmadi, M.; Piveteau, L.; Loi, M. A.; Protesescu, L. Metal-solvent Complex Formation at the Surface of InP Colloidal Quantum Dots. *J. Am. Chem. Soc.* **2024**, *146*, 12808-12818.

7) Reiss, P.; Protière, M.; Li, L. Core/Shell Semiconductor Nanocrystals. *Small* **2009**, 5, 154-168.

8) Henry, D. C. The Cataphoresis of Suspended Particles. Part I.—The Equation of Cataphoresis. *Proc. R. Soc. Lond.* **1931**, *A133*, 106-129.

# Chapter – 3

## Deciphering the Role of Light Excitation Attributes in Plasmonic Photocatalysis: The Case of Nicotinamide Cofactor Regeneration

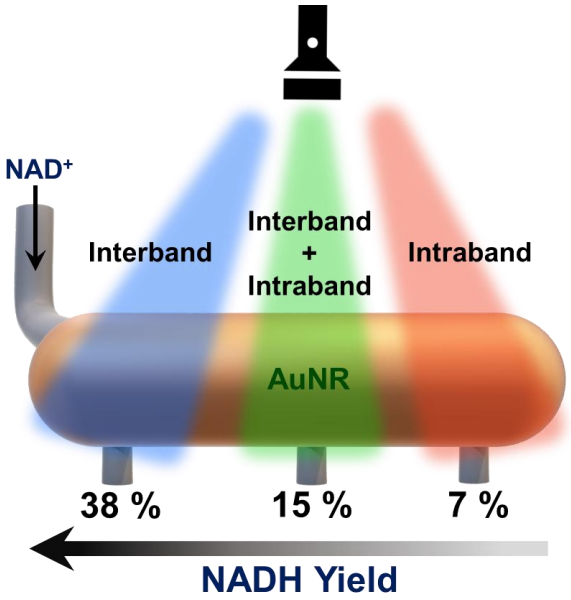


This Chapter has been adapted from the following paper with permission. Copyright 2023, American Chemical Society.

**Jain, V.**; Chakraborty, I. N.; Raj, R. B.; Pillai, P. P. Deciphering the Role of Light Excitation Attributes in Plasmonic Photocatalysis: The Case of Nicotinamide Cofactor Regeneration. *J. Phys. Chem. C* **2023**, *127*, 5153-5161.

## 3.1. Abstract

Photocatalysis with metal nanoparticles is attractive because of their unique plasmonic properties, such as large absorption cross-section, high charge density, spectral tunability, and photostability. As a result, plasmonic photocatalysis has emerged as a distinct area in catalysis for performing different classes of chemical transformations. However, disentangling the exact mechanism in plasmonic photocatalysis is often challenging because of the interference from different plasmon relaxation pathways, which in turn is highly dependent on the catalyst–reactant system. Presently, the field demands a detailed investigation into different factors involved in plasmonic chemistry to gain a better understanding of the complex reaction pathway. Herein, we reveal the critical role of light excitation attributes in the plasmon-driven photoregeneration of the nicotinamide (NADH) cofactor by gold nanorods (AuNRs). The two distinct surface plasmon bands in AuNRs allowed us to study the exclusive role of interband vs intraband transitions in NADH photoregeneration. Also, the choice of reaction is ideal for testing various hypotheses, as it proceeds only in the presence of both light and catalyst. Long-lived hot charge carriers generated through interband transition, in combination with a favorable catalyst–reactant interaction, drive the efficient photoregeneration of the NADH cofactor (~40 %). Our study emphasizes the need for an appropriately chosen catalyst–reactant system and reaction conditions to gain meaningful insights into various factors controlling the product yield and selectivity in plasmonic photocatalysis.

## 3.2. Introduction

Localized surface plasmon resonance (LSPR) in metal nanoparticles (NPs) offers a unique way for converting solar energy to chemical fuels, which forms the basis of the area of plasmonic photocatalysis.[1-3] Upon LSPR excitation, the plasmon can dephase via (i) radiative pathway by creating intense electric fields in the vicinity of the NP surface, or (ii) nonradiative pathways by forming highly energetic hot charge carriers, which eventually dissipate their excess energy to the surroundings in the form of heat.[2-6] Literature reports establish that both radiative (near-field enhancement) and nonradiative (hot charge carriers and local heating) processes can activate molecules and trigger useful chemical transformations in the presence of light (**Figure 3.1**).[7-19] As a result, the mechanism involved in a plasmon-driven chemical transformation is complex.[20,21] A better understanding, as well as control over the involvement of different relaxation pathways, is essential to overcome the existing challenges of low product yield and selectivity in plasmonic photocatalysis.[22-24]

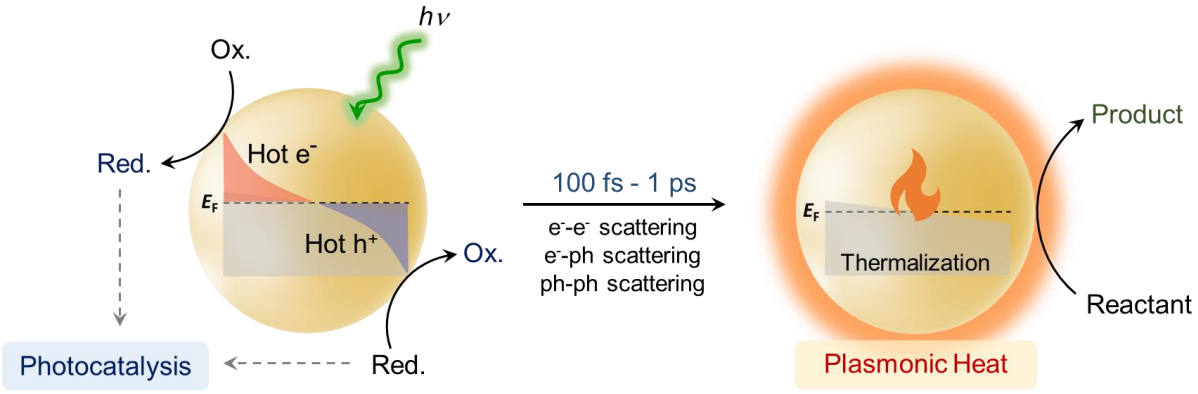


**Figure 3.1**. Schematics showing the feasibility of chemical transformations with plasmonic nanomaterials via different relaxation pathways. The non-radiative relaxation after plasmonic excitation results in generation of generation of hot charge carriers which can be extracted out to perform chemical reactions. The inefficient extraction of charge carriers results in dissipation of large amount of heat energy, which can also be utilized to do chemical transformations.

The contribution of different pathways will depend on the choice of chemical reaction, photocatalyst design, and reactor design (light excitation, volume, temperature, colloidal/solid phase, fluid flow, etc.).[20,21,24-26] For instance, Baldi and co-workers observed the change of dominant reaction mechanism from non-thermal to thermal,

depending on the fraction of NP volume under irradiation.[25] Herein, the authors investigated the contribution of different activation mechanisms by employing Au@Ag core@shell nanoparticles synthesis. The rate of Ag shell formation under different conditions was monitored through extinction spectroscopy as well as modelled to simulate light propagation and heat transfer dynamics. The local heating effects were completely overruled. However, a prominent participation of collective thermal effects was observed, accounting for 30 to 100 % of the total reaction rate when the volume of the reaction mixture was varied from 90 mL to 450 mL. Such a subtle change in the reaction volume leading to a complete change of reaction mechanism clearly shows the need to elucidate the role of vast reaction parameters for a holistic understanding of plasmon-powered processes.

In an interesting study by Un and Sivan, the impact of fluid flow on heat generation was elucidated in plasmon-mediated redox reactions (**Figure 3.2**).[26] The spatial distribution as well as temporal dynamics of temperature were analyzed in two exemplary experimental studies: a) plasmon-induced dithionite-mediated redox reactions (**Figures 3.2a,b**) and b) plasmon-mediated $CO_2$ reduction to $C_1$-$C_3$ hydrocarbons (**Figures 3.2c-e**), alongside the fluid convention dynamics. In the former case, the reaction was found to be driven via thermal effects, mainly because of the presence of a non-uniform temperature profile after light irradiation. Modeling studies revealed that the local temperature in the regions close to illuminated nanoparticles was higher, while no significant heating could be observed in the bulk. However, in the latter case, non-thermal effects dominated as forced convection by stirring reduced the temperature gradients. The convection dynamics (natural vs. forced) and the use of additional hole scavengers were responsible for such contrasting reaction mechanisms. This study demonstrates that minute differences in the experimental setup can turn out to be decisive in the elucidation of the underlying reaction mechanism in plasmon-powered processes.

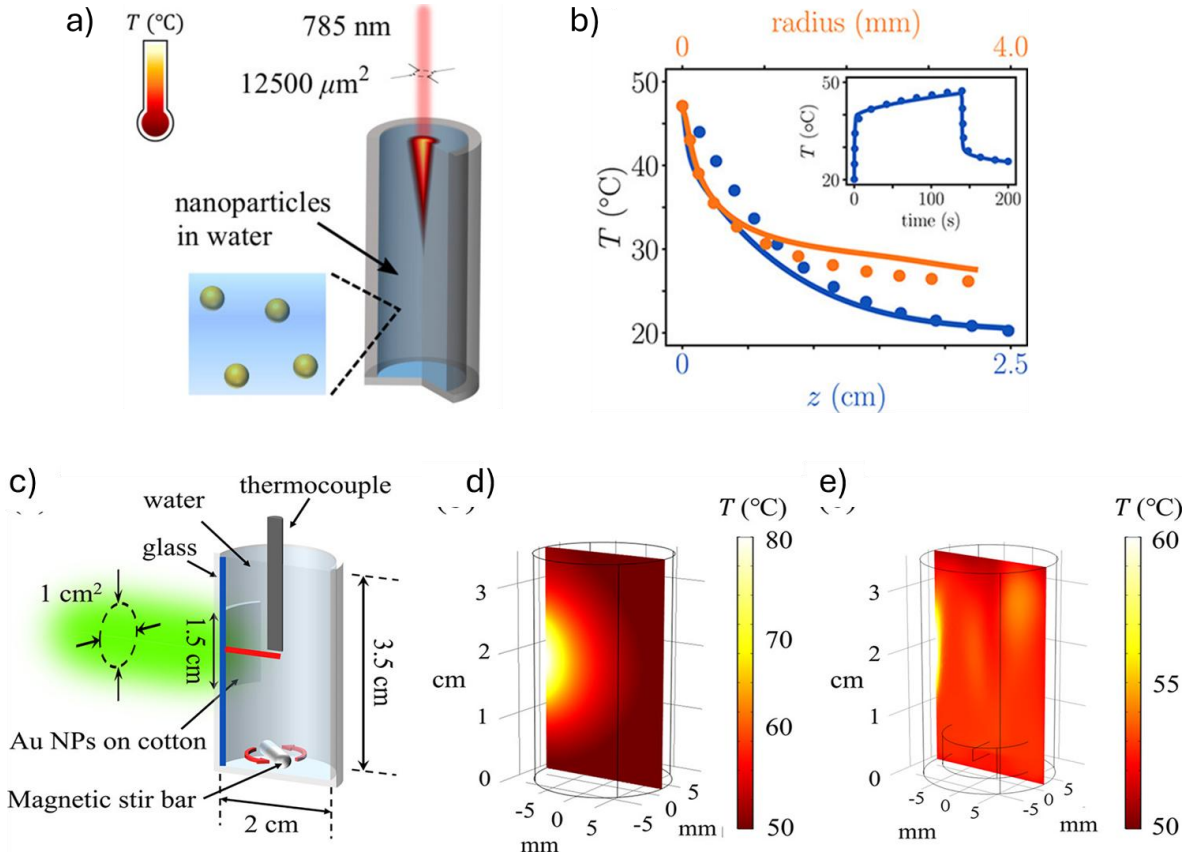


**Figure 3.2**. The role of fluid flow in plasmon-photocatalyzed chemical reactions. a) Schematics showing the simulation domain of the reactor used in plasmon-induced dithionite-mediated redox reactions. b) Temperature distribution as a function of distance from the center of the beam spot. The inset shows the temporal rise in temperature after light illumination. c) Schematics of the simulated reactor design used for plasmon-mediated $CO_2$ reduction to C1-C3 hydrocarbons. d) and e) are the temperature profiles after light irradiation in the absence and presence of forced convection by stirring, respectively. It can be clearly seen that the thermal gradients are significantly reduced when the reaction mixture is stirred. Reproduced with permission from reference 26. Copyright 2021 American Chemical Society.

Light excitation is one such parameter that is crucial for any photocatalytic reaction and can significantly impact the reaction rates and product selectivity. In the light of plasmonic photocatalysis, light excitation attributes play a crucial role in tuning the reaction parameters such as yield, rate, and selectivity. In a seminal work by Jain & coworkers, harvesting of multiple electrons becomes prevalent with continuous wave light excitation of moderate power after a threshold light intensity is achieved.[10] With the help of a hole scavenger and appropriate excitation wavelength, the reaction rate followed a superlinear trend as a function of photon flux. The authors strategically used this observation in another work to tune the selectivity in photocatalytic $CO_2$ reduction,

wherein the light intensity influenced the rate of formation of $C_1$ (methane) and $C_2$ (ethane) products.[9] Higher photon energy and flux favored $C_2$ products due to the simultaneous harvesting of multiple charge carriers. This study impressively utilizes light excitation as a tool to drive challenging multielectron chemical transformations with fine control over the reaction mechanism and selectivity. As the outcome of any plasmon-powered process is highly sensitive to the catalyst-reactant system as well as the experimental conditions, it cannot be generalized. Thus, given the diversity of parameters involved in the photocatalytic process, there is a need for catalyst and reaction-specific investigations to understand plasmon-powered chemical transformations.

In this direction, we report here the conclusive role of light excitation and hot charge carriers in dictating the outcome of a plasmon-catalyzed chemical transformation. Our study demands the appropriate choice of photocatalyst as well as a chemical reaction, to minimize the contribution from the other two relaxation processes (near field enhancement and thermal effects). Gold nanomaterial was our choice for the plasmonic photocatalyst because of its wide applicability in different classes of chemical transformations.[8-12,15,16] In the case of Au, plasmon is damped via excitation of interband *'d-sp'* and intraband *'sp-sp'* transitions (**Figure 3.3a**). [6,9,10,27-29] The threshold energy required for interband *'d-sp'* transitions is only 2.1 eV, which overlaps with the LSPR of spherical gold nanoparticles (AuNPs) at ~2.4 eV. [9,27-29] Therefore, interband transitions can significantly contribute to the observed reaction rate when LSPR (intra + interband transitions) is excited. This essentially suggests that AuNPs may not be the ideal choice of catalyst to study the role of light excitations in plasmonic photocatalysis. On the contrary, selective excitation of interband and intraband transitions is possible in anisotropic gold nanorods (AuNRs) because of the presence of two distinct LSPR bands - longitudinal and transverse bands (**Figure 3.3b**). Excitation at the longitudinal LSPR band results in the intraband transitions selectively; whereas excitation at the transverse LSPR band results in both interband and intraband transitions.[30,31] Further, the excitation with higher energy photons (>2.4 eV) will result in selective interband transitions.[9,27,28]

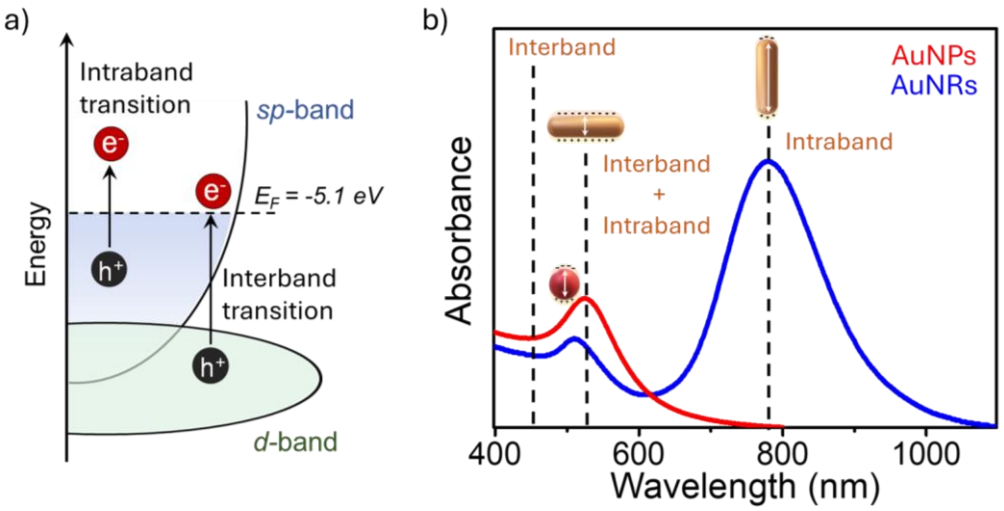


**Figure 3.3**. a) Representative band diagram of Au showing two different types of transitions that can occur upon plasmonic excitation. Intraband transition results in the formation of hot charge carriers in the sp band, whereas interband transition results in $e^-$–$h^+$ pair formation in the sp band and d band, respectively. b) Comparison of absorption profiles of spherical AuNPs and anisotropic AuNRs in the vis–NIR region. The presence of two distinct LSPR bands in AuNR allows the formation of hot charge carriers, selectively, via intraband or interband transitions.

As selective excitation pathways can be achieved, AuNRs have been used in recent studies as the catalyst for deconvoluting the role of different factors in plasmonic photocatalysis.[30,31] Somorjai, Alivisatos, and Toste investigated photoinduced etching of AuNRs with $FeCl_3$ to elucidate the effect of different excitations and implicated the dominating role of interband transitions in plasmonic photocatalysis (**Figure 3.4**).[30] The reaction rate under dark and different light excitation was monitored through changes in the absorption spectrum of AuNRs as $FeCl_3$ selectively etches the tip of AuNRs (**Figures 3.4a, b**). Kinetics studies revealed the highest etching rate with 450 nm light excitation, whereas the rate of etching was similar to dark when longitudinal LSPR excitation (650-850 nm) was used (**Figure 3.4b**). The rate constant under interband excitation was at least 3-4 orders of magnitude higher than selective intraband excitation at the longitudinal LSPR (**Figure 3.4c**). Furthermore, the rate of etching was significantly higher even at the transverse LSPR excitation (510 nm) because of the excellent overlap of interband and intraband transitions. A detailed reaction mechanism was proposed, which involved the reduction of $Fe^{3+}$ ions by hot electrons and holes accumulated in AuNRs to eventually form $Au^{3+}$, causing the etching of AuNRs (**Figure 3.4d**). The efficiency

of interband charge carriers was found to be better than the charge carriers generated upon plasmonic excitation.

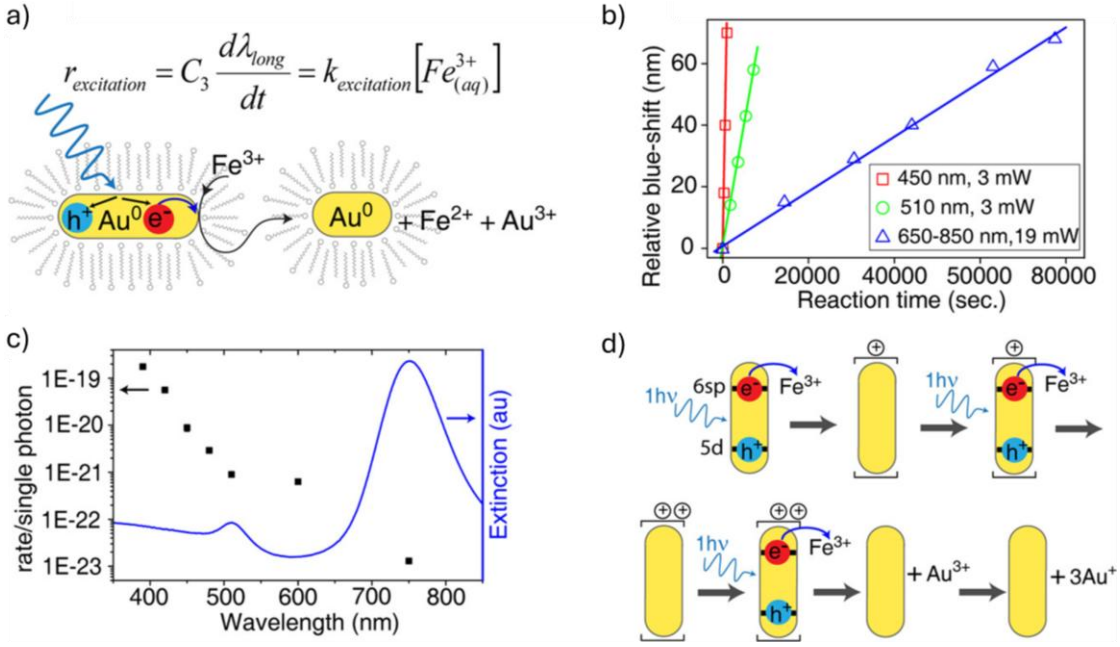


**Figure 3.4**. a) Schematic showing the photoinduced etching of AuNRs with $FeCl_3$. The blue shift in the longitudinal LSPR band of AuNRs served as a proxy to determine the reaction rate under different excitations. b) Rate of AuNR etching at different excitation wavelengths. c) Etching rate normalized with respect to each photon absorbed. d) Proposed reaction mechanism for AuNR etching under light illumination. Reproduced with permission from reference 30. Copyright 2017 American Chemical Society.

Along similar lines, Baldi and co-workers developed Au@Ag NR core@shell system to distinguish among different underlying plasmon activation mechanisms (**Figure 3.5a**).[31] The silver shell growth over AuNRs was monitored using TEM and in-situ extinction spectroscopy. The evolution of the extinction spectrum under 730 nm was similar to that of dark, suggesting the inefficiency of intraband hot charge carriers in enhancing the reaction kinetics (**Figure 3.5b**). In contrast, a similar spectral profile was observed with faster kinetics under 532 nm excitation with an initial 10-fold rate enhancement as compared to dark (**Figure 3.5c**). Using a combination of in-situ extinction spectroscopy, transmission electron microscopy, thermal characterization, and finite-difference time-domain simulations, the dominant role of hot charge carriers generated via interband charge carriers was established. This was further corroborated by single-particle studies, wherein shifts in the LSPR position were measured at polarizations parallel and orthogonal to laser polarizations. A clear lack of angular dependency was observed,

suggesting the isotropic distribution of charge carriers, which is characteristic of the interband hot charge carriers (**Figure 3.5d**). Though both studies suggest that interband transitions play a major role in carrying out photocatalytic conversions with Au as the plasmonic catalyst, the choice of reaction in these studies may not be ideal, as the reaction could proceed to some extent without the need for the catalyst and light.

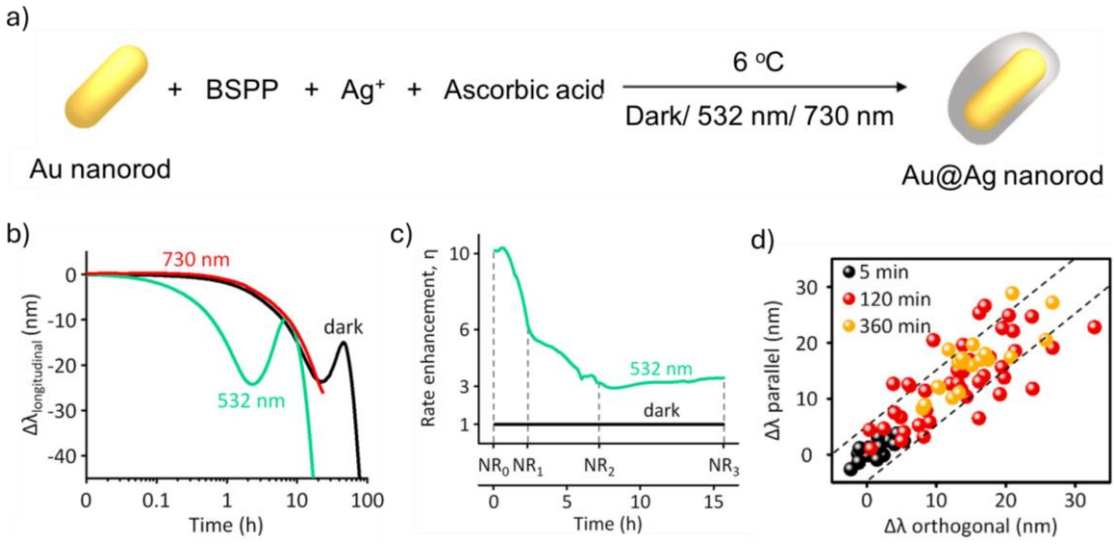


**Figure 3.5.** a) Schematics of the plasmon-driven Au@Ag core@shell NR synthesis. b) Evolution of longitudinal LSPR band of AuNRs under different light excitation conditions. Kinetics of Au@Ag core@shell NRs under longitudinal LSPR excitation at 730 nm were similar to the dark conditions, whereas a faster rate was observed under 532 nm excitation. c) Rate enhancement of Ag growth over AuNRs under 532 nm compared to dark as a function of time. A 10-fold enhancement was observed initially, which stabilizes to 3-fold over the course of reaction. d) Shifts in the LSPR position measured at single-particle level at polarizations parallel and orthogonal to laser polarization. A lack of angular dependency was clearly observed suggesting the isotropic distribution of charge carriers, characteristic of interband hot charge carriers. Reproduced with permission from reference 31. Copyright 2020 American Chemical Society.

The present work fills this gap by selecting the photoregeneration of nicotinamide cofactor (NADH) as the reaction of choice, which occurs only in the presence of both catalyst and light. Artificial regeneration of NADH from $NAD^+$ is a two electron-one proton transfer (or hydride ion transfer) process that is being used as a model reaction to test several hypotheses in plasmonic photocatalysis.[12,32-36] Along with this, NADH is a key cofactor required by a majority (~70 %) of oxidoreductase enzymes to carry out various biocatalytic reactions, thereby justifying the choice of the reaction from an applied perspective as well.[37,38] Our selection of AuNRs to photocatalyze the regeneration of NADH cofactor satisfies the fundamental requirements that a catalyst-reactant system

should possess, to gain conclusive insights into the role of light excitations in plasmonic photocatalysis. A widely used electron mediator, $[Cp^*Rh(bpy)(H_2O)]^{2+}$, was incorporated to enhance the charge transfer rate for a better comparison of the reaction yields under different excitations as well as to regenerate the enzymatically active 1,4-NADH (**Scheme 3.1**).[39-41] Moreover, the incorporation of a positively charged electron mediator allowed us to use electrostatic forces as a tool to install the concept of '*catalyst-reactant interaction*' in our study.[11,12,42] A favorable catalyst-reactant interaction will channelize the diffusion and increase the local concentration of the reactants close to the surface of the catalyst, thereby enhancing the possibility of the charge transfer process.[11,12,42] Accordingly, the surface of the AuNRs was appropriately functionalized with negatively charged ligands to achieve electrostatic attraction with the positively charged electron mediator (**Scheme 3.1**). Detailed wavelength-dependent experiments showed that hot charge carriers generated through selective interband transitions (via excitation at ~450 nm) yielded the best photocatalytic regeneration of NADH cofactor, compared to selective intraband (via excitation at ~808 nm) and inter + intraband transitions (via excitation at ~532 nm). The light intensity was tuned in such a way that the interference from the photothermal effects, *if any*, was similar under each excitation, thereby ruling out the thermal effects in this wavelength-dependent study. An attractive yield of ~40 % was obtained upon illumination of AuNRs with ~450 nm excitation for ~12 h, with a turnover frequency (TOF) of ~$16.8 \times 10^3$ $AuNR^{-1}$ $h^{-1}$. The incorporation of catalyst-reactant interaction, as well as the excitation of AuNR photocatalyst at a suitable wavelength, was the key to achieving a good conversion yield. In short, the appropriate selection of photocatalyst and reaction was crucial in conclusively proving the dominant role of charge carriers generated via interband transitions in photocatalyzing the NADH regeneration. Given the diversity of parameters involved in plasmonic photocatalysis, our study emphasizes the need for catalyst- and reaction-specific investigations to understand the role of each parameter in plasmon-powered processes. Such independent studies are essential for realizing the full potential of plasmonic materials in photocatalysis and other plasmon-powered processes.

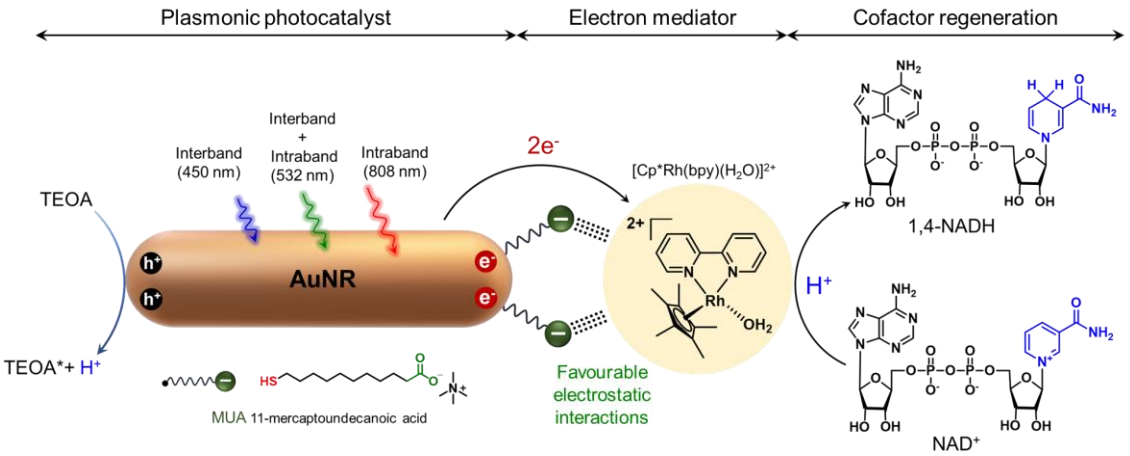


**Scheme 3.1.** Schematics showing the photocatalytic regeneration of the NADH cofactor with [−] AuNRs using $[Cp^*Rh(bpy)(H_2O)]^{2+}$ as an electron mediator and triethanolamine (TEOA) as a hole scavenger. The favorable electrostatic interaction between negatively charged AuNRs and a positively charged electron mediator facilitates an efficient electron transfer upon photoexcitation.

# 3.3. Experimental section

## 3.3.1. Synthesis of $[Cp^*Rh(bpy)(H_2O)]^{2+}$

$[Cp^*Rh(bpy)(H_2O)]^{2+}$ was synthesized using the literature procedure [41,43] as follows: In a 30 mL glass vial equipped with a stir bar, 0.55 mmol of RhCl3.H2O and 3 mL isopropanol (IPA) were added and stirred till the solution became deep red in color. Following this, 0.69 mmol of Cp* was added to the solution, and the vial was sealed with Teflon. The resulting mixture was heated at 85 °C for 1 h, resulting in the formation of a red-colored precipitate. The mixture was cooled down to room temperature and then kept at -20 °C for 5-6 h to allow complete precipitate formation. The precipitate was filtered and washed with cold IPA several times, followed by washing with *n*-pentane. The precipitate was dissolved in $CHCl_3$, and the solvent was evaporated under vacuum. This was followed by washing with diethyl ether, and finally, the solid was dried under vacuum to yield $[Cp^*RhCl_2]_2$ dimer. The dimer was suspended in 5 mL of methanol, and 2.5 equivalents of 2,2'-bipyridyl (bpy) were added to it. A clear orangish-yellow solution was obtained upon bpy addition. Methanol was evaporated under vacuum to concentrate the solution to 1 mL, and [Cp*Rh(bpy)Cl]Cl was precipitated by the addition of diethyl ether. The final product was dried for 12 h at 40 °C under vacuum. The product was

characterized by $^{1}$H-NMR spectroscopy (**Figure 3.12**). Since [Cp*Rh(bpy)Cl]Cl immediately hydrolyzes to form [Cp*Rh(bpy)(H2O)]2+, a stock solution of 10 mM was prepared in water and stored in the dark at 4 °C for further use.

### 3.3.2. Photocatalytic reduction of $NAD^+$ to NADH

The photocatalytic reduction of $NAD^+$ was carried out in a glass tube under continuous irradiation from tunable power CW diode lasers. The light intensity was measured with optical power meter from Newport (Model 842 PE) with a beam diameter of 1 cm for all different lasers. In a typical experiment, $NAD^+$ (1 mM), TEOA (1 M), and $[Cp^*Rh(bpy)(H_2O)]^{2+}$ (250 μM) were mixed in 50 mM phosphate buffer, and the pH of the solution was maintained at 8. AuNRs loaded paper-based catalyst strip was dipped in the reaction mixture, and purged with Ar for 30 min. The tube was sealed with Teflon, and the reaction mixture was kept under visible light irradiation for 12 h at room temperature. After 12 h, AuNRs-loaded paper strip was removed, and the photoregenerated NADH was quantified using UV-vis absorption spectroscopy.

### 3.3.3. Preparation of paper-based dip catalyst system

To prepare paper-based dip catalyst system, Whatman filter paper was cut into 2 cm x 1.2 cm strips. A mixture of [-] AuNRs ($O.D._{LSPR}$ ~ 2) was drop-casted in parts onto the paper strips, followed by drying with a dryer. The process was repeated thrice and kept for drying at 45 °C for at least 6 h before use. AuNRs loaded paper catalyst was characterized by UV-vis-NIR diffuse reflectance spectroscopy as well as scanning electron microscopy.

### 3.3.4. Yield calculation

Photocatalytic reduction of $NAD^+$ to NADH can be monitored by UV-visible absorption spectroscopy, wherein the emergence of peak at 340 nm can be used to quantify the yield of NADH.[37,40,41] Since $[Cp^*Rh(bpy)(H_2O)]^{2+}$ is present in the reaction mixture, the total absorbance at 340 nm cannot be taken into consideration for NADH quantification. Therefore, for all the experiments, a corrected spectrum was obtained by subtracting the absorption spectrum before light irradiation from the final absorption spectrum obtained

after 12 h light irradiation. Finally, the concentration of regenerated NADH was calculated using Beer-Lambert law:

$$C = \frac{A}{\varepsilon l} \qquad (1)$$

where C is the concentration of regenerated NADH, $A$ is the absorbance at 340 nm in the corrected spectrum obtained, ε is the molar extinction coefficient of NADH (6220 $M^{-1}$ $cm^{-1}$)[33] and $l$ is the optical path length of 1 cm. The percentage yield was calculated using the following equation:

$$Product\ yield(\%) = \frac{C_{NADH}}{C_{NAD^+}} \times 100 \qquad (2)$$

where $C_{NADH}$ is the concentration of regenerated NADH calculated from equation 1, $C_{NAD^+}$ is the initial concentration of $NAD^+$ (1 mM) in the reaction mixture.

### 3.3.5. Calculation of turnover number (TON) and turnover frequency (TOF)

The turnover number (TON) for the photocatalytic reaction was defined as the number of molecules of NADH regenerated per AuNR for the given irradiation time. The total number of AuNRs was calculated from Beer-Lambert's law. The absorbance of AuNRs at the longitudinal surface plasmon band was set to be ~2, and the extinction coefficient of $1.02\times10^9$ $M^{-1}$ $cm^{-1}$ was used for the calculation of the number of AuNRs.[44] Since the exact volume of AuNRs is drop-casted onto the paper strip, the number of AuNRs on the paper substrate can be considered the same as obtained by Beer-Lambert's law. From the above calculation, the total number of AuNRs was calculated to be $3.54\times10^{12}$. The turnover frequency (TOF) was defined as the number of molecules of NADH regenerated per AuNR per unit time of irradiation. The TOF was calculated by dividing TON by the total time of irradiation in h.

## 3.4. Results and discussion

### 3.4.1. AuNR photocatalyzed NADH photoregeneration

Gold nanorods functionalized with cetyltrimethylammonium bromide (CTAB, [+] AuNRs), having an aspect ratio of ~4, were prepared using a seed-mediated method.[45]

The CTAB ligands on [+] AuNRs were then place-exchanged with negatively charged MUA ligands to install the favorable electrostatic interaction between [-] AuNRs and $[Cp^*Rh(bpy)(H_2O)]^{2+}$ (**Scheme 3.1**). The UV-vis-NIR absorption characteristics of AuNRs were well-retained after the place-exchange with [-] ligands (**Figure 3.6a**). A shift in the zeta potential value from +40.9 ± 0.3 mV to -45.3 ± 0.2 mV confirms the successful functionalization of MUA ligands on the surface of [-] AuNRs (**Figure 3.6b**). SEM image proves the structural uniformity of AuNRs, with an average length of 43.2 ± 6.6 nm and width of 10.8 ± 1.8 nm (**Figures 3.6c, 3.13**). AuNRs with these dimensions were chosen in the present study to achieve a selective excitation of interband and intraband transitions. Specifically, the selective intraband transition can be achieved at the longitudinal LSPR band at ~795 nm by irradiating with an 808 nm laser, whereas the selective interband transition can be achieved with a 450 nm laser irradiation. It is to be noted that the threshold energy for the interband transitions in Au is ~ 2.1 eV (~590 nm),[10,27,28] which ensures a negligible interference between interband and intraband transitions at 808 nm laser irradiation. Further, the light illumination at the transverse LSPR band at ~510 nm with a 532 nm laser will result in both interband and intraband transitions.

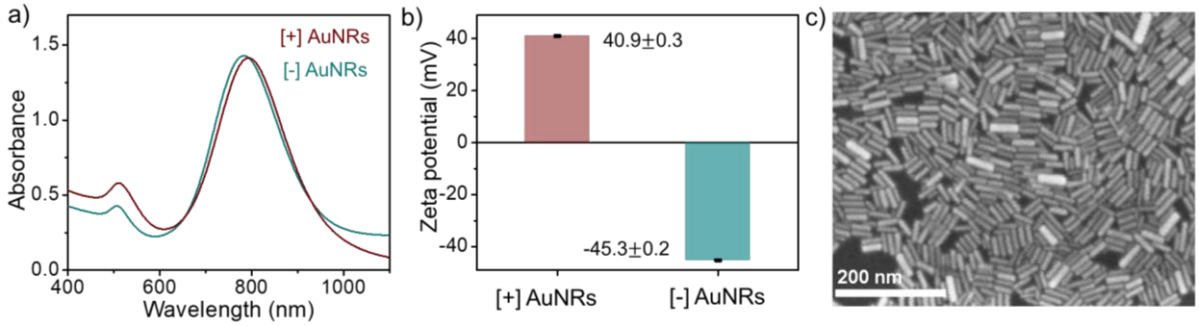


**Figure 3.6**. a) UV-Vis-NIR absorption, and b) zeta potential measurements of CTAB-stabilized [+] AuNRs and MUA functionalized [-] AuNRs. c) Representative SEM image proves the size and shape uniformity of [-] AuNRs.

To begin with, the role of hot charge carriers generated via the interband transition was tested in the photocatalytic regeneration of NADH cofactor. [-] AuNRs were used as the sole photocatalyst in the presence of $[Cp^*Rh(bpy)(H_2O)]^{2+}$ electron mediator, with triethanolamine (TEOA) as the hole scavenger, under continuous irradiation with 450 nm CW diode laser for 12 h (the total light intensity measured at the test tube wall was ~700

mW $cm^{-2}$, **Scheme 3.1**). The photocatalytic conversion of $NAD^+$ to NADH by [-] AuNRs was monitored through UV-vis spectroscopy, by following the absorption of NADH at ~340 nm.[12,37,41] A paper-based dip catalyst system was employed in the present study to overcome the issue of colloidal stability of [-] AuNRs in a photocatalytic reaction mixture (**Figure 3.14**). Here, [-] AuNRs were dropcast and dried on a Whatman filter paper substrate. [-] AuNRs loaded paper substrate was characterized with UV-Vis-NIR diffuse reflectance spectroscopy, where the presence of both transverse and longitudinal LSPR bands was observed (**Figure 3.7a**). Also, the optical photograph and SEM images confirm the successful adsorption of AuNRs on the paper substrate (**Figure 3.7b**). The adsorption of AuNRs on filter paper takes place through strong van der Waals and hydrophobic interactions between the metal nanoparticles and the cellulose fibers.[46]

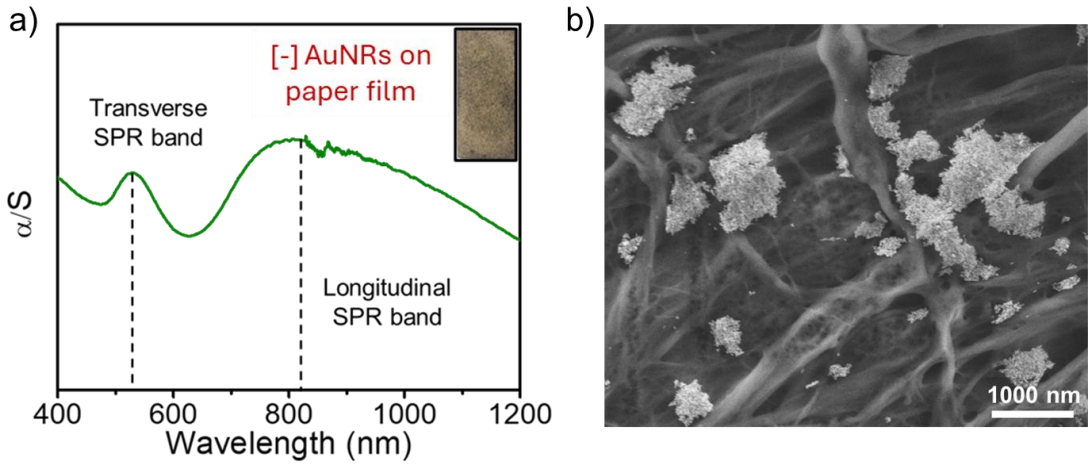


**Figure 3.7**. a) Vis-NIR diffuse reflectance spectrum of [-] AuNRs loaded on the filter paper, clearly showing the presence of both transverse and longitudinal LSPR bands. The inset shows the optical photograph of the [-] AuNRs loaded paper dip catalyst film. b) Representative SEM image of [-] AuNRs loaded on paper film.

Control experiments prove that both $NAD^+$ (reactant) and $[Cp^*Rh(bpy)(H_2O)]^{2+}$ were stable under prolonged light irradiation at 700 mW $cm^{-2}$ (**Figure 3.15**). No noticeable changes were observed in the UV-Vis absorption of the reaction mixture in the presence of [-] AuNRs, in the dark (**Figure 3.16**). Interestingly, a strong absorption at ~340 nm was observed upon 12 h irradiation with 450 nm CW laser in the presence of [-] AuNRs, confirming the photoregeneration of NADH (**Figures 3.8a,b**). The yield of the photoregenerated NADH was estimated to be ~38 %. It is worth mentioning that a poor to low yield is often reported in the literature during the plasmonically driven

photoregeneration of NADH cofactors by gold nanomaterials,[12,32,34,36] because of the poor charge separation and utilization steps. One of the main reasons for the decent yield obtained in the present study can be attributed to the favorable electrostatic interaction between the [-] AuNRs and [+] $[Cp^*Rh(bpy)(H_2O)]^{2+}$, leading to the channeling and increase in the local concentration of the electron mediators close to the surface of the catalyst. This, in turn, enhances the probability of the charge transfer process from the photocatalyst to the electron mediator. The exclusive role of this favorable electrostatic interaction was proved by performing the photocatalytic reaction with CTAB [+] AuNRs, under the same reaction conditions, wherein the yield of NADH photoregeneration was found to be merely ~12 % (**Figures 3.8c, 3.17**). An additional experiment was performed with AuNRs functionalized with N, N, N-trimethyl-(11-mercaptoundecyl)-ammonium chloride (TMA) ligand. It is to be noted that both TMA and MUA ligands are similar in length with thiol as the binding group, and differ only in the terminal head functional group ($-COO^-$ and $-NMe_3^+$ in MUA and TMA, respectively). The yield of NADH photoregeneration was only ~13 % (**Figure 3.18**) when positively charged TMA-AuNR was used as the photocatalyst. This again proves the dominant role of favorable electrostatic interaction between [-] AuNRs and $[Cp^*Rh(bpy)(H_2O)]^{2+}$. Thus, it can be concluded that ligands on AuNR surface mediate charge transfer by precisely regulating electrostatics between the catalyst and the reactants. The change in surface ligands predominantly affects the kinetics and not the reaction mechanism.

### 3.4.2. Confirming the role of hot charge carriers

A series of control experiments were performed to identify the dominant relaxation pathway in the photoregeneration of NADH cofactor by [-] AuNRs (**Figures 3.8c, 3.16**). Separate experiments performed in the absence of light, electron mediator, [-] AuNRs, and TEOA (hole scavenger) prove that the reaction follows the light-dependent pathway and proceeds via the participation of hot charge carriers. Moreover, the intensity dependence of NADH regeneration also validates the dominating role of hot-charge carriers under our reaction conditions (**Figures 3.8d, 3.19, 3.20**). A superlinear increase in NADH yield was observed as a function of light intensity, which is a characteristic of a multielectron transfer process (**Figure 3.8d**).[10,47] This was explained by constructing

*RT*lnTOF vs light intensity plot in accordance with the heuristic model developed by Jain and co-workers (**Figure 3. 21**).[47] According to this model, charge carriers generated upon plasmon excitation contribute to the free energy of the overall reaction rate, which in turn is dependent on light intensity as in **eq. 3.1**.

$$RTln\frac{R_f}{R_b} = -\Delta G_{dark} + \frac{z\,E_{ib}\,\sigma\,\eta_{ib}\,I}{h\nu\,k_{nr}} \qquad (\mathbf{3.1})$$

where, $\Delta G_{dark}$ is the free energy of the reaction under dark, where the probability of electron-hole generation will be negligible due to the high magnitude of interband energy gap ($E_{ib}$) compared to the thermal energy. $R_f$ and $R_b$ are the forward and backward reaction rates respectively, $z$ is the no. of $e^-$-$h^+$ pairs involved in the reaction, $E_{ib}$ is the interband energy gap, σ is the absorption cross-section of NP, $\eta_{ib}$ is the efficiency of conversion of plasmon excitation, $I$ is the intensity of light and $k_{nr}$ is the rate of recombination. According to **eq. 3.1**, the rate of a photochemical reaction is exponentially dependent on the intensity of light. The *RT*lnTOF vs. light intensity plot was constructed by calculating the TOF obtained from the intensity-dependent experiments, and T was the bulk temperature of the reaction mixture as measured to be 315, 314, 312, and 310 K at 700, 600, 500, and 400 mW $cm^{-2}$ light intensity, respectively. In our study, a linear dependence of *RT*lnTOF on light intensity confirms the active participation of photoexcited hot charge carriers in the regeneration of NADH (**Figure 3.21**).

As discussed earlier, irradiating the ensemble of plasmonic NPs can result in both localized and collective heating effects, which can also contribute to the observed reaction rate. Under the laser intensities used in our reaction, the calculated local increase in temperature at a single AuNR is negligible with $\Delta T_{local}$ of ~0.35 mK (see Appendix). Such a small increase in the local temperature of AuNRs is insufficient to drive the reduction of $NAD^+$ in a high yield of ~40 %. However, a large number of AuNRs under illumination can result in collective photothermal effects, which can increase the overall temperature by tens of Kelvin. It is worth mentioning that the temperature of the reaction medium rose to ~42 °C after 12 h of irradiation, in the presence of [-] AuNRs. To test the role of photothermal effects, a control experiment was performed in the dark at an elevated temperature of ~50 °C in the presence of [-] AuNRs. A low yield of ~7 %

confirmed that photothermal effects do not dominate the photoregeneration of NADH by [-] AuNRs (**Figures 3.8c, 3.22**). Thus, it can be confirmed that under our reaction conditions, the photoregeneration of the NADH cofactor is predominantly carried out by photoexcited charge carriers.

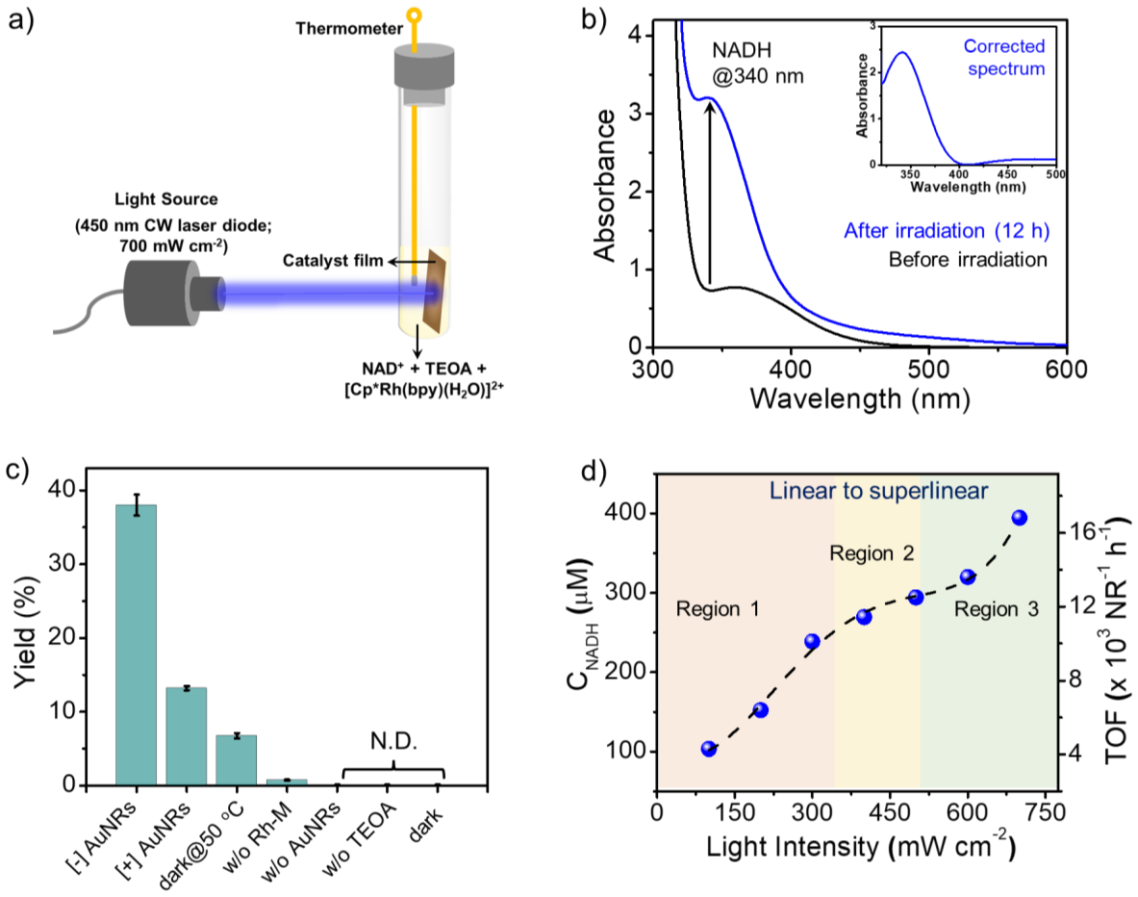


**Figure 3.8.** Photocatalytic regeneration of NADH cofactor with [-] AuNRs. a) A schematic representation of the photocatalytic reaction setup. b) UV-Vis absorption changes in the reaction mixture before and after 12 h light irradiation (450 nm, 700 mW $cm^{-2}$). The inset shows the corrected spectrum obtained after subtracting the initial absorption spectrum from the spectrum obtained after 12 h light irradiation. c) Bar diagram showing the photocatalytic activity of AuNRs under different control experiments obtained from the corrected spectrum, and d) variation in photoregenerated NADH as a function of light intensity. The dashed lines are in place to show the light intensity dependence of NADH regeneration. $C_{NADH}$ increases superlinearly from a threshold intensity of 400 mW $cm^{-2}$.

## 3.4.3. Role of light excitation attributes

The role of light excitation pathways in the photoregeneration of NADH was investigated by performing detailed wavelength-dependent studies. As mentioned earlier, the plasmon dephasing results in two types of electronic transitions in Au

nanomaterials - *'d-sp'* interband transitions, and *'sp-sp'* intraband transitions. Since the threshold energy for interband transition is ~2.1 eV (~590 nm), [9,27,28] irradiation at the longitudinal LSPR band of AuNRs (~795 nm) will selectively result in intraband transitions. Likewise, irradiating with higher energy photons of ~2.75 eV (~450 nm) will result in selective interband transitions. Therefore, a wavelength-dependent study should provide conclusive proof of the contribution of hot charge carriers generated under each excitation in the photoregeneration of NADH cofactor by [-] AuNRs. In one set of experiments, the power absorbed was normalized under different illumination wavelengths (450 nm, 532 nm, and 808 nm) at ~550 mW (**Table 3.1**). The photoregeneration of NADH was strongly dependent on the irradiation wavelength, where the absorbance at 340 nm increased with an increase in photon energy (**Figures 3.9a**, **3.23**). Irradiation with 450 nm resulted in ~38 % regeneration of NADH, followed by ~15 % with 532 nm, and ~8 % with 808 nm (**Figure 3.9b**). A similar trend was observed when the reaction was carried out by keeping the incident light intensity similar at ~700 mW $cm^{-2}$ (**Figures 3.9b**, **3.24**). Here again, the NADH yield was highest at 450 nm irradiation (~35 %), followed by 532 nm (~18 %) and 808 nm (~13 %).

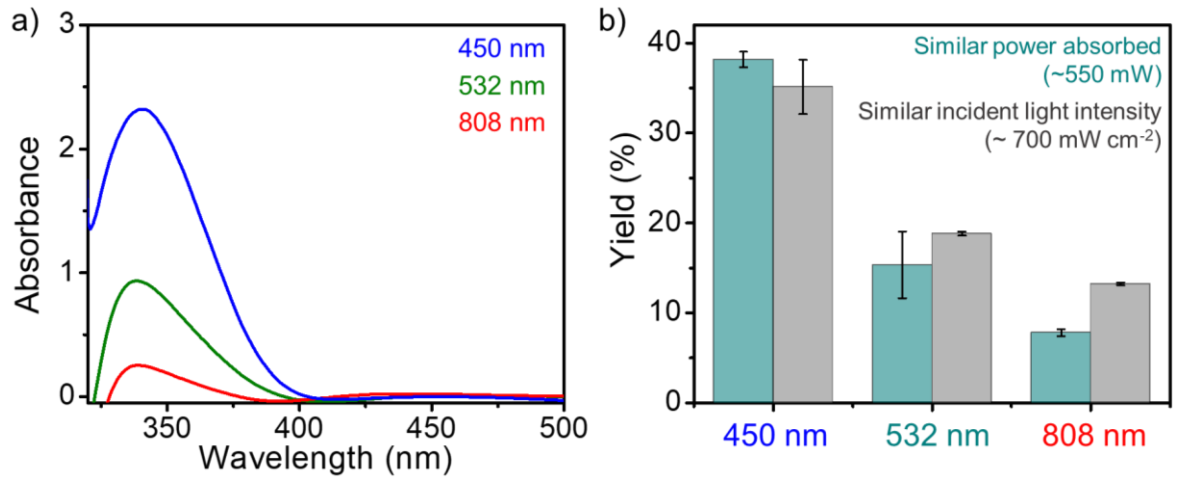


**Figure 3.9**. Wavelength-dependence of photoregenerated NADH with [-] AuNRs. a) Corrected absorption spectra of the reaction mixture irradiated for 12 h with different wavelengths, keeping the power absorbed by the reaction mixture similar (~550 mW). b) Bar diagram comparing the yield of photoregenerated NADH under different wavelengths, keeping the power absorbed similar (cyan-colored bars) and incident light intensity similar (grey-colored bars).

Another condition to perform the wavelength-dependent study involves keeping the photon flux (no. of photons falling per unit area per unit time) constant under all

irradiation wavelengths. In our study, the photon flux was different under both normalization conditions. However, the calculations reveal that the photon flux under 532 nm and 808 nm light irradiation is higher than at 450 nm under both the normalization conditions (**Table 3.2**); yet, the yield of NADH photoregeneration was highest under 450 nm excitation (**Figure 3.9b**). Thus, it can be concluded that the photoregeneration of NADH by [-] AuNRs is dominated by the hot charge carriers generated by interband transitions. This is further supported by the first-principles calculations performed by Atwater and coworkers, which predict that the generation of hot charge carriers via interband transitions will dominate over resistive losses in Au nanomaterials whenever the excitations above the threshold energy of 2.1 eV are possible.[28]

Apart from the involvement of interband charge carriers, the photothermal effects and plasmon-enhanced adsorbate excitation pathway can also contribute to the photoregeneration of NADH. The contribution from the photothermal effects will be predominant at the irradiation wavelengths close to the SPR bands of AuNRs (808 and 532 nm).[17,48] The superior photoregeneration of NADH at 450 nm excitation, along with the poor yield obtained in the thermal reaction under dark (**Figure 3.22**), clearly rules out the contribution from the photothermal effects. Plasmon-enhanced adsorbate excitation pathway is known to dominate when the plasmon resonance or excitation wavelength spectrally overlaps with the electronic transition energy of the molecules adsorbed on the NP photocatalyst.[18,19] As seen in **Figure 3.10**, there is a negligible spectral overlap between the electronic transition energy of $NAD^+$ and the plasmon resonances/ excitation wavelengths used in the study. It is possible that the modified energy levels of $NAD^+$, after adsorption, may have overlap with the excitation wavelengths used in the study (especially with 450 nm and 532 nm excitations). However, the NADH regeneration occurs by the interaction of $NAD^+$ with $[Cp^*Rh(bpy)(H_2O)]^{2+}$ and not directly with AuNRs (**Scheme 3.1**). Thus, $NAD^+$ is not directly adsorbed on the surface of AuNR photocatalysts, and the change in the electronic levels may not be significant. In this regard, the difference in the NADH yields obtained under 450 nm (~38 %) and 532 nm (~18 %) excitations cannot be attributed solely to the plasmon-enhanced adsorbate excitation pathway. Nevertheless, the contribution from

the plasmon-enhanced adsorbate electronic excitation pathway cannot be completely overruled. A separate study, presumably with adequate theoretical support, will be required to deconvolute the contributions of different pathways. Having said that, the experiments in the presence and absence of the hole scavenger, intensity-dependent studies, and thermal reaction under dark conclusively prove the dominant role of hot charge carriers in the photoregeneration of NADH cofactor.

**Table 3.1.** Total power absorbed in the reaction mixture at different illumination wavelengths.

| Excitation wavelength (nm) | Incident light power (mW) | Transmitted light power (mW) | Total power absorbed (mW) |
|---|---|---|---|
| 450 | 710 | 162 | 548 |
| 532 | 740 | 188 | 552 |
| 808 | 558 | 5 | 553 |

**Table 3.2.** Calculated photon flux under different irradiation conditions for NADH photoregeneration.

| Light excitation attributes | Photon Flux (no. of photons $cm^{-2}$ $s^{-1}$) | | |
|---|---|---|---|
| | 450 nm | 532 nm | 808 nm |
| Constant power absorbed (550 mW) | $1.6 \times 10^{18}$ | $2.0 \times 10^{18}$ | $2.3 \times 10^{18}$ |
| Constant light intensity (700 mW $cm^{-2}$) | $1.6 \times 10^{18}$ | $1.9 \times 10^{18}$ | $2.8 \times 10^{18}$ |

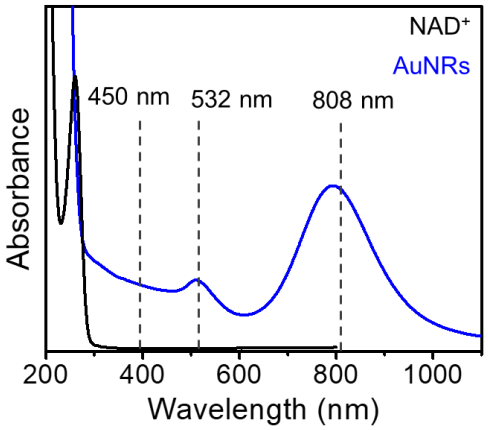


**Figure 3.10.** UV-Vis-NIR absorption spectra of AuNRs and $NAD^+$, showing negligible overlap between the electronic transition energy of $NAD^+$ and different excitation wavelengths used in the study (450 nm, 532 nm, and 808 nm).

Finally, a probable mechanism for the transfer of hot charge carriers generated via interband and intraband transitions is discussed. The photoregeneration of NADH by [-] AuNRs involves the oxidation of TEOA (by abstracting the holes from the photocatalyst) and reduction of $[Cp^*Rh(bpy)(H_2O)]^{2+}$ (by accepting the electrons from the photocatalyst). The electron mediator further takes up the $H^+$ ions from the oxidized TEOA to reduce $NAD^+$ to NADH. The energy and population of photogenerated charge carriers in [-] AuNRs will depend on the type of electronic transitions.[27,28,49] The dephasing of hot charge carriers in metal nanoparticles is completed within a time frame of ~100 fs - 1 ps,[2,5,6] resulting in the formation of thermalized charge carriers – referred to as the steady state condition. In the case of intraband transitions (at 808 nm excitation), photoexcited charge carriers reside close to the Fermi level of Au ($E_{F,\,Au}$ = -5.10 eV)[10] at the steady-state condition.[50,51] Now, the probability of hot electron transfer to the electron mediator will be limited because of the mismatch in the energy levels between the two (redox potential of $[Cp^*Rh(bpy)(H_2O)]^{2+}$ is -4.34 eV).[38] On the other hand, the TEOA has high oxidizing power (-3.40 eV)[38,52] to scavenge the holes generated in the *'sp'* band. This results in the accumulation of hot electrons above the Fermi energy level (photocharging),[29,53,54] which could attain sufficient energy to participate in an electron transfer process with the electron mediator. The outcome of the above two competing steps results in an inefficient transfer of hot electrons to the electron mediator, leading to the low yield of NADH regeneration at 808 nm excitation. On the contrary, the fate of

the photoexcited charge carriers is different when generated via the interband transitions (at 450 nm excitation). Here, the hot electrons and hot holes are formed in the *sp* and *d*-band, respectively, which increases the lifetime of the charge-separated pairs to ~1 ps.[10,29,55] This means that the hot holes have more energy than the hot electrons, as the former reside deep in the *d*-band. The highly energetic holes in the *d*-band are efficiently scavenged by the TEOA. This results in the higher accumulation of hot electrons at a steady state condition (photocharging), when compared to 808 nm excitation. Consequently, there is a buildup of excess potential that raises the Fermi energy level ($E_F$') and enhances the probability of electron transfer from AuNRs to $[Cp^*Rh(bpy)(H_2O)]^{2+}$ (**Figure 3.11**). Thus, it can be concluded that the photoregeneration of NADH by [-] AuNRs is limited by the hole scavenging step, which was further evident from the negligible progress of the reaction in the absence of a hole scavenger.

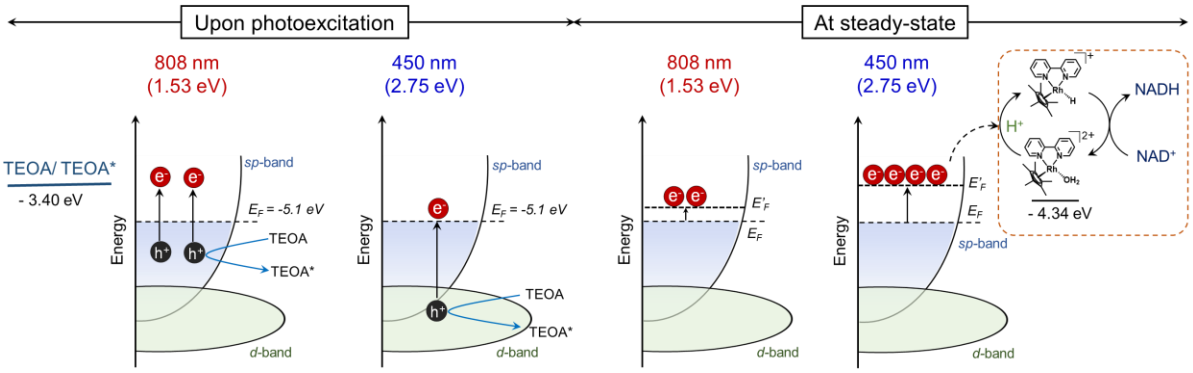


**Figure 3.11.** Energy level diagram and possible mechanism for the observed difference in the NADH regenerated under intraband and interband excitations, with AuNRs as the sole photocatalyst, TEOA as the hole scavenger, and $[Cp^*Rh(bpy)(H_2O)]^{2+}$ as the electron mediator. The higher oxidation potential of TEOA aids in faster hole extraction from AuNRs, resulting in the accumulation of electrons above the Fermi energy level (photocharging). The extent of electron accumulation depends on the energy as well as the lifetime of the photoexcited charge carriers.

## 3.5. Conclusions

The effect of different light excitations on plasmon-catalyzed photoregeneration of NADH cofactors was investigated. The choice of anisotropic AuNRs as the plasmonic photocatalyst allowed us to achieve the selective excitation of interband and intraband transitions in the present study. Detailed photocatalytic studies confirm the active role of hot charge carriers in the efficient photoregeneration of NADH by AuNRs. The hot

charge carriers generated through selective interband transitions (via excitation at ~450 nm) gave the maximum photocatalytic regeneration of NADH cofactor, compared to selective intraband (via excitation at ~808 nm) and inter + intraband transitions (via excitation at ~532 nm). Higher energy and longer lifetime of hot charge carriers generated from interband transitions were reasoned to the trend observed in the NADH yield during the wavelength-dependent study. Moreover, the hole scavenging process was identified as the limiting step in the photoregeneration of NADH by AuNRs. Light excitation is one of the main parameters that can influence the product yield, which should always be analyzed to get a better insight into the contribution of various relaxation pathways in plasmonic photocatalysis. Given the diversity of parameters involved in plasmonic photocatalysis, our study emphasizes the need for catalyst- and reactant-specific investigations for understanding the roles of each parameter in plasmon-powered processes.

## 3.6. References

1) Linic, S.; Christopher, P.; Ingram, D. B. Plasmonic-Metal Nanostructures for Efficient Conversion of Solar to Chemical Energy. *Nat. Mater.* **2011**, *10*, 911-921.

2) Brongersma, M. L.; Halas, N. J.; Nordlander, P. Plasmon-Induced Hot Carrier Science and Technology. *Nat. Nanotechnol.* **2015**, *10*, 25-34.

3) Jain, V.; Kashyap, R. K.; Pillai, P. P. Plasmonic Photocatalysis: Activating Chemical Bonds Through Light and Plasmon. *Adv. Opt. Mater.* **2022**, *10*, 2200463.

4) Hodak, J. H.; Martini, I.; Hartland, G. V. Spectroscopy and Dynamics of Nanometer-Sized Noble Metal Particles. *J. Phys. Chem. B* **1998**, *102*, 6958-6967.

5) Link, S.; El-Sayed, M. A. Spectral Properties and Relaxation Dynamics of Surface Plasmon Electronic Oscillations in Gold and Silver Nanodots and Nanorods. *J. Phys. Chem. B* **1999**, *103*, 8410-8426.

6) *Plasmonic Catalysis: From Fundamentals to Applications*; Camargo, P. H. C., Cortés, E., Eds.; Wiley-VCH: Weinheim, Germany, 2021.

7) Christopher, P.; Xin, H.; Linic, S. Visible-Light-Enhanced Catalytic Oxidation Reactions on Plasmonic Silver Nanostructures. *Nat. Chem.* **2011**, *3*, 462-472.

8) Mukherjee, S.; Libisch, F.; Large, N.; Neumann, O.; Brown, L. V.; Cheng, J.; Lassiter, J. B.; Carter, E. A.; Nordlander, P.; Halas, N. J. Hot Electrons Do the Impossible: Plasmon-Induced Dissociation of $H_2$ on Au. *Nano Lett.* **2013**, *13*, 240-247.

9) Yu, S.; Wilson, A. J.; Heo, J.; Jain, P. K. Plasmonic Control of Multi-Electron Transfer and C-C Coupling in Visible-Light-Driven $CO_2$ Reduction on Au Nanoparticles. *Nano Lett.* **2018**, *18*, 2189-2194.

10) Kim, Y.; Smith, J. G.; Jain, P. K. Harvesting Multiple Electron–Hole Pairs Generated Through Plasmonic Excitation of Au Nanoparticles. *Nat. Chem.* **2018**, *10*, 763-769.

11) Roy, S.; Roy, S.; Rao, A.; Devatha, G.; Pillai, P. P. Precise Nanoparticle-Reactant Interaction Outplays Ligand Poisoning in Visible-Light Photocatalysis. *ACS Catal.* **2018**, *30*, 8415-8419.

12) Roy, S.; Jain, V.; Kashyap, R. K.; Rao, A.; Pillai, P. P. Electrostatically Driven Multielectron Transfer for the Photocatalytic Regeneration of Nicotinamide Cofactor. *ACS Catal.* **2020**, *10*, 5522-5528.

13) Seemala, B.; Therrien, A. J.; Lou, M.; Li, K.; Finzel J. P.; Qi, J.; Nordlander, P.; Christopher, P. Plasmon-Mediated Catalytic $O_2$ Dissociation on Ag Nanostructures: Hot Electrons or Near Fields? *ACS Energy Lett.* **2019**, *4*, 1803-1809.

14) Qiu, J.; Wei, W. D. Surface Plasmon-Mediated Photothermal Chemistry. *J. Phys. Chem. C* **2014**, *118*, 20735-20749.

15) Dhiman, M.; Maity, A.; Das, A.; Belgamwar, R.; Chalke, B.; Lee, Y.; Sim, K.; Nam, J. -M.; Polshettiwar, V. Plasmonic Colloidosomes of Black Gold for Solar Energy Harvesting and Hotspots Directed Catalysis for $CO_2$ to Fuel Conversion. *Chem. Sci.* **2019**, *10*, 6594-6603.

16) Kashyap, R. K.; Dwivedi, I.; Roy, S.; Roy, S.; Rao, A.; Subramaniam, C.; Pillai, P. P. Insights into the Utilization and Quantification of Thermoplasmonic Properties in Gold Nanorod Arrays. *Chem. Mater.* **2022**, *34*, 7369-7378.

17) Kashyap, R. K.; Parammal, M. J.; Pillai, P. P. Effect of Nanoparticle Size on Plasmonic Heat-Driven Organic Transformation. *ChemNanoMat* **2022**, *8*, e202200252.

18) Kazuma, E.; Jung, J.; Ueba, H.; Trenary, M.; Kim, Y. Real-Space and Real-Time Observation of a Plasmon-Induced Chemical Reaction of a Single Molecule. *Science* **2018**, *360*, 521-526.

19) Tesema, T. E.; Kafle, B.; Habteyes, T. G. Plasmon-Driven Reaction Mechanisms: Hot Electron Transfer versus Plasmon-Pumped Adsorbate Excitation. *J. Phys. Chem. C* **2019**, *123*, 8469-8483.

20) Mascaretti, L.; Naldoni, A. Hot Electron and Thermal Effects in Plasmonic Photocatalysis. *J. Appl. Phys.* **2020**, *128*, 041101.

21) Jain, P. K. Taking the Heat Off of Plasmonic Chemistry. *J. Phys. Chem. C.* **2019**, *123*, 24347-24351.

22) Cortés, E.; Besteiro, L. V.; Alabastri, A.; Baldi, A.; Tagliabue, G.; Demetriadou, A.; Narang, P. Challenges in Plasmonic Catalysis. *ACS Nano* **2020**, *14*, 16202-16219.

23) Cortés, E. Efficiency and Bond Selectivity in Plasmon-Induced Photochemistry. *Adv. Opt. Mater.* **2017**, *5*, 1700191.

24) Elias, R. C.; Linic, S. Elucidating the Roles of Local and Nonlocal Rate Enhancement Mechanisms in Plasmonic Catalysis. *J. Am. Chem. Soc.* **2022**, *144*, 19990-19998.

25) Kamarudheen, R.; Castellanos, G. W.; Kamp, L. P. J.; Clercx, H. J. H.; Baldi, A. Quantifying Photothermal and Hot Charge Carrier Effects in Plasmon-Driven Nanoparticle Syntheses. *ACS Nano* **2018**, *12*, 8447-8455.

26) Un, I. -W.; Sivan, Y. The Role of Heat Generation and Fluid Flow in Plasmon-Enhanced Reduction–Oxidation Reactions. *ACS Photonics* **2021**, *8*, 1183-1190.

27) Bernardi, M.; Mustafa, J.; Neaton, J. B.; Louie, S. G. Theory and Computation of Hot Carriers Generated by Surface Plasmon Polaritons in Noble Metals. *Nat. Commun.* **2015**, *6*, 7044.

28) Brown, A. M.; Sundararaman, R.; Narang, P.; Goddard, W. A.; Atwater, H. A. Nonradiative Plasmon Decay and Hot Carrier Dynamics: Effects of Phonons, Surfaces, and Geometry. *ACS Nano* **2016**, *10*, 957-966.

29) Kim, Y.; Torres, D. D.; Jain, P. K. Activation Energies of Plasmonic Catalysts. *Nano Lett.* **2016**, *16*, 3399-3407.

30) Zhao, J.; Nguyen, S. C.; Ye, R.; Ye, B.; Weller, H.; Somorjai, G. A.; Alivisatos, A. P.; Toste, F. D. A Comparison of Photocatalytic Activities of Gold Nanoparticles Following Plasmonic and Interband Excitation and a Strategy for Harnessing Interband Hot Carriers for Solution Phase Photocatalysis. *ACS Cent. Sci.* **2017**, *3*, 482-488.

31) Kamarudheen, R.; Aalbers, G. J. W.; Hamans, R. F.; Kamp, L. P. J.; Baldi, A. Distinguishing Among All Possible Activation Mechanisms of a Plasmon-Driven Chemical Reaction. *ACS Energy Lett.* **2020**, *5*, 2605-2613.

32) Sánchez-Iglesias, A.; Chuvilin, A.; Grzelczak, M. Plasmon-Driven Photoregeneration of Cofactor Molecules. *Chem. Commun*. **2015**, *51*, 5330-5333.

33) Saba, T.; Li, J.; Burnett, J. W. H.; Howe, R. F.; Kechagiopoulos, P. N.; Wang, X. NADH Regeneration: A Case Study of Pt-Catalyzed $NAD^+$ Reduction with $H_2$. *ACS Catal.* **2021**, *11*, 283-289.

34) Sánchez-Iglesias, A.; Barroso, J.; Solís, D. M.; Taboada, J. M.; Obelleiro, F.; Pavlov, V.; Chuvilin, A.; Grzelczak, M. Plasmonic Substrates Comprising Gold Nanostars Efficiently Regenerate Cofactor Molecules. *J. Mater. Chem. A* **2016**, *4*, 7045-7052.

35) Tarnowicz-Staniak, N.; Vázquez-Díaz, S.; Pavlov, V.; Matczyszyn, K.; Grzelczak, M. Cellulose as an Inert Scaffold in Plasmon-Assisted Photoregeneration of Cofactor Molecules. *ACS Appl. Mater. Interfaces* **2020**, *12*, 19377-19383.

36) Rogolino, A.; Claes, N.; Cizaurre, J.; Marauri, A.; Jumbo-Nogales, A.; Lawera, Z.; Kruse, J.; Sanromán-Iglesias, M.; Zarketa, I.; Calvo, U.; et al. Metal-Polymer Heterojunction in Colloidal -Phase Plasmonic Catalysis. *J. Phys. Chem. Lett.* **2022**, *13*, 2264-2272.

37) Wang, X.; Saba, T.; Yiu, H. H. P.; Howe, R. F.; Anderson, J. A.; Shi, J. Cofactor NAD(P)H Regeneration Inspired by Heterogeneous Pathways. *Chem* **2017**, *2*, 621-654.

38) Lee, S. H.; Choi, D. S.; Kuk, S. K.; Park, C. B. Photobiocatalysis: Activating Redox Enzymes by Direct or Indirect Transfer of Photoinduced Electrons. *Angew. Chem., Int. Ed.* **2017**, *57*, 7958-7985.

39) Lo, H. C.; Buriez, O.; Kerr, J. B.; Fish, R. H. Regioselective Reduction of $NAD^+$ Models with $[Cp^*Rh(bpy)(H)]^+$: Structure-Activity Relationships and Mechanistic Aspects in the Formation of the 1,4-NADH Derivatives. *Angew. Chem., Int. Ed.* **1999**, *38*, 1429-1432.

40) Nam, D. H.; Lee, S. H.; Park, C. B. CdTe, CdSe, and CdS Nanocrystals for Highly Efficient Regeneration of Nicotinamide Cofactor Under Visible Light. *Small* **2010**, *6*, 922-926.

41) Liu, J.; Antonietti, M. Bio-Inspired NADH Regeneration by Carbon Nitride Photocatalysis Using Diatom Templates. *Energy Environ. Sci.* **2013**, *6*, 1486-1493.

42) Jain, V.; Roy, S.; Roy, P.; Pillai, P. P. When Design Meets Function: The Prodigious Role of Surface Ligands in Regulating Nanoparticle Chemistry. *Chem. Mater.* **2022**, *34*, 7579-7597.

43) Mantell, M. A.; Kampf, J. W.; Sanford, M. Improved Synthesis of $[Cp^RRhCl_2]_2$ Complexes. *Organometallics* **2018**, *37*, 3240-3242.

44) Jain, P. K.; Lee, K. S.; El-Sayed, I. H.; El-Sayed, M. A. Calculated Absorption and Scattering Properties of Gold Nanoparticles of Different Size, Shape, and Composition: Applications in Biological Imaging and Biomedicine. *J. Phys. Chem. B.* **2006**, *110*, 7238-7248.

45) González-Rubio, G.; Kumar, V.; Llombart, P.; Díaz-Núñez, P.; Bladt, E.; Altantzis, T.; Bals, S.; Peña-Rodríguez, O.; Noya, E. G.; MacDowell, L. G.; et al. Disconnecting Symmetry Breaking from Seeded Growth for the Reproducible Synthesis of High Quality Gold Nanorods. *ACS Nano* **2019**, *13*, 4424– 4435.

46) Zheng, G.; Polavarapu, L.; Liz-Marzán, L. M.; Pastoriza-Santos, I.; Pérez-Juste, J. Gold Nanoparticle-Loaded Filter Paper: A Recyclable Dip-Catalyst for Real-Time Reaction Monitoring by Surface Enhanced Raman Scattering. *Chem. Commun*. **2015**, *51*, 4572-4575.

47) Yu, S.; Jain, P. K. The Chemical Potential of Plasmonic Excitations. *Angew. Chem., Int. Ed*. **2019**, *59*, 2085-2088.

48) Govorov, A. O.; Richardson, H. H. Generating Heat with Metal Nanoparticles. *Nano Today* **2007**, *2*, 30-38.

49) Besteiro, L. V.; Kong, X. -T.; Wang, Z.; Hartland, G.; Govorov, A. O. Understanding Hot-Electron Generation and Plasmon Relaxation in Metal Nanocrystals: Quantum and Classical Mechanisms. *ACS Photonics* **2017**, *4*, 2759-2781.

50) Liu, Z.; Hou, W.; Pavaskar, P.; Aykol, M.; Cronin, S. B. Plasmon Resonant Enhancement of Photocatalytic Water Splitting Under Visible Light Illumination. *Nano Lett*. **2011**, *11*, 1111-1116.

51) Mubeen, S.; Lee, J.; Singh, N.; Krämer, S.; Stucky, G. D.; Moskovits, M. An Autonomous Photosynthetic Device in which All Charge Carriers Derive from Surface Plasmons. *Nat. Nanotechnol*. **2013**, *8*, 247-251.

52) Berr, M. J.; Wagner, P.; Fischbach, S.; Vaneski, A.; Schneider, J.; Susha, A. S.; Rogach, A. L.; Jäckel, F.; Feldmann, J. Hole Scavenger Redox Potentials Determine Quantum Efficiency and Stability of Pt-Decorated CdS Nanorods for Photocatalytic Hydrogen Generation. *Appl. Phys. Lett*. **2012**, *100*, 223903.

53) Wu, X.; Thrall, E. S.; Liu, H.; Steigerwald, M.; Brus, L. Plasmon Induced Photovoltage and Charge Separation in Citrate-Stabilized Gold Nanoparticles. *J. Phys. Chem. C* **2010**, *114*, 12896-12899.

54) Mao, Z.; Espinoza, R.; Garcia, A.; Enwright, A.; Vang, H.; Nguyen, S. C. Tuning Redox Potential of Gold Nanoparticle Photocatalysts with Light. *ACS Nano* **2020**, *14*, 7038-7045.

55) Guzelturk, B.; Utterback, J. K.; Coropceanu, I.; Kamysbayev, V.; Janke, E. M.; Zajac, M.; Yazdani, N.; Cotts, B. L.; Park, S.; Sood, A.; et al. Nonequilibrium Thermodynamics of Colloidal Gold Nanocrystals Monitored by Ultrafast Electron Diffraction and Optical Scattering Microscopy. *ACS Nano* **2020**, *14*, 4792-4808.

## 3.7. Appendix

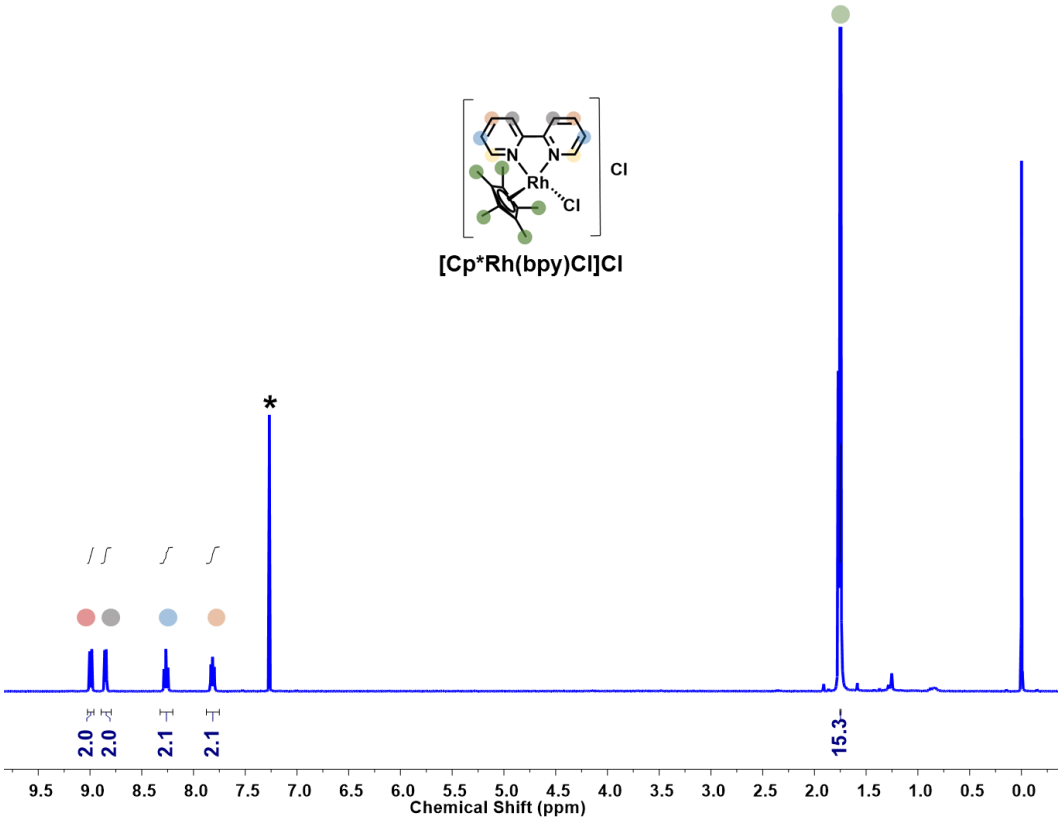


**Figure 3.12.** $^{1}$H-NMR spectrum of [Cp*Rh(bpy)Cl]Cl. $^{1}$H NMR (400 MHz, $CDCl_3$): δ (ppm) 8.9 (2H, d), 8.85 (2H, d), 8.26 (2H, t), 7.81 (2H,t), 1.75 (15H, s). Solvent peaks are marked with *.

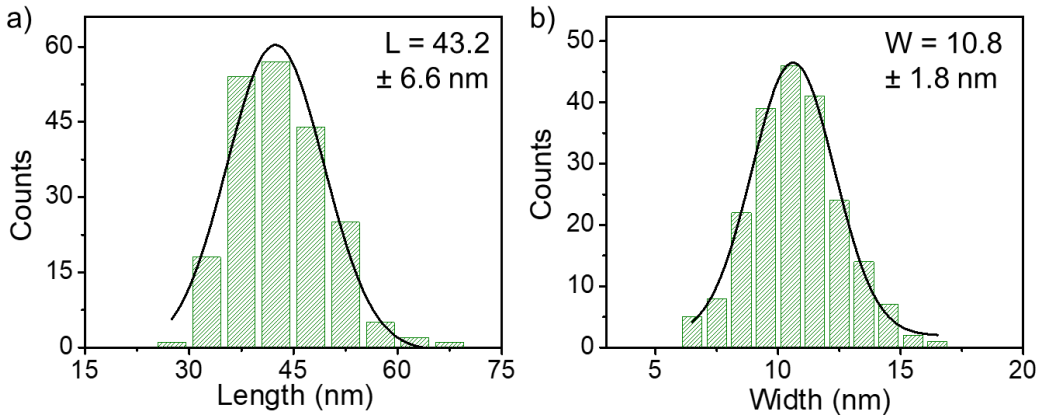


**Figure 3.13.** Size distribution histogram for a) lengths and b) widths of AuNRs calculated from scanning electron microscopy (SEM) images. The average length and width of AuNRs were calculated to be 43.2 ± 6.6 nm and 10.8 ± 1.8 nm, respectively, from ~200 NRs.

**Stability of colloidal [-] AuNRs in the photocatalytic reaction mixture**

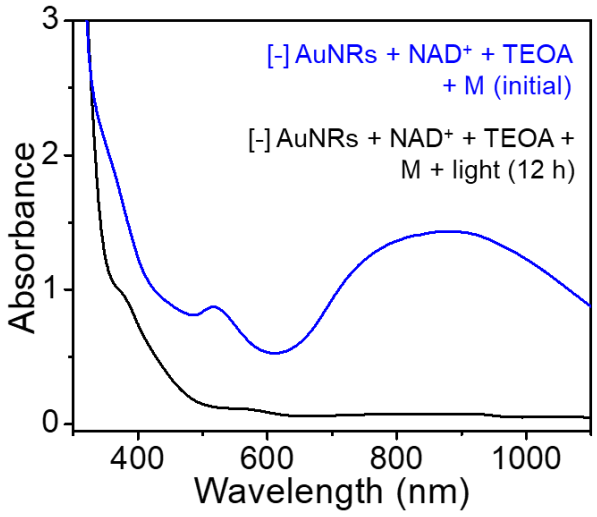


**Figure 3.14.** UV-Vis-NIR absorption of the reaction mixture consisting of [-] AuNRs in solution system before and after 450 nm light irradiation (laser power ~ 700 mW $cm^{-2}$) for 12 h. [-] AuNRs aggregated in the reaction mixture and a complete loss in colloidal stability was observed after prolonged light irradiation.

**Control experiments**

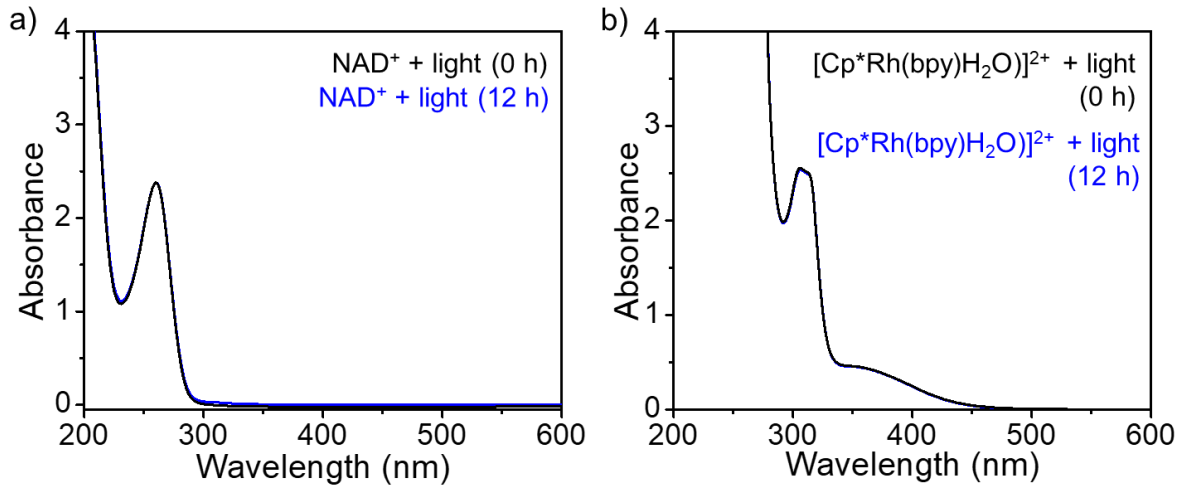


**Figure 3.15.** Photostability of a) $NAD^+$ and b) $[Cp^*Rh(bpy)(H_2O)]^{2+}$ under 450 nm light irradiation (laser power ~ 700 mW $cm^{-2}$) for 12 h.

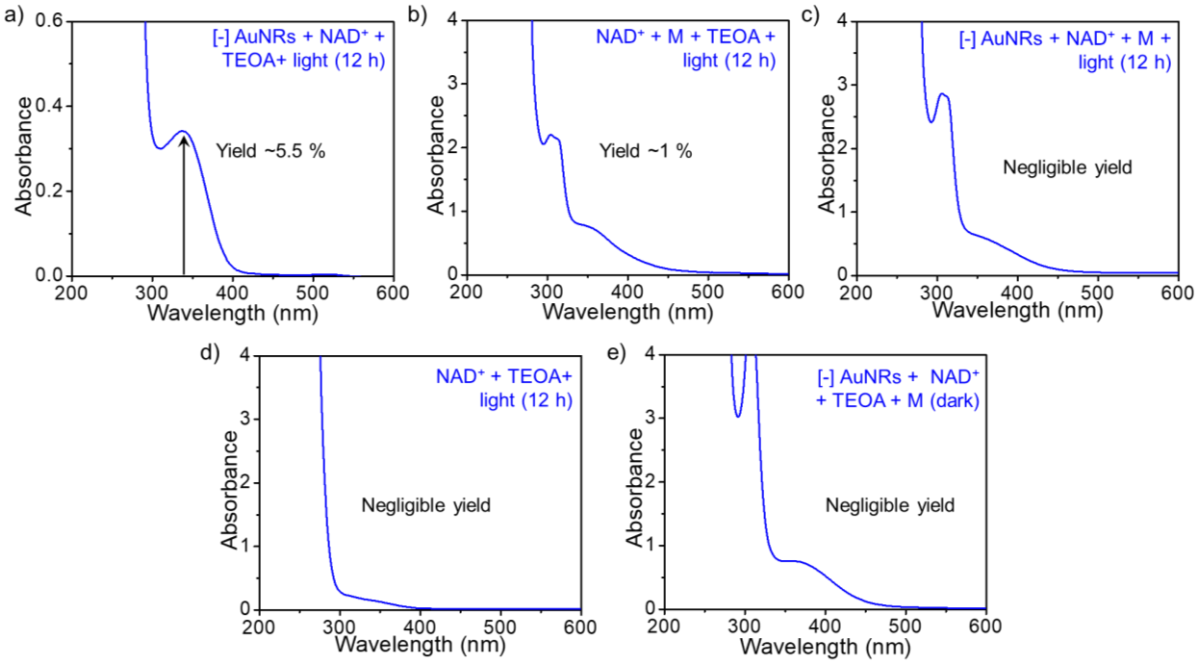


**Figure 3.16.** Photocatalytic reduction of $NAD^+$ under different control reaction conditions. UV-vis absorption of the reaction mixture in the absence of a) M = $[Cp^*Rh(bpy)(H_2O)]^{2+}$, b) [-] AuNRs, c) TEOA (hole scavenger), d) $[Cp^*Rh(bpy)(H_2O)]^{2+}$ and [-] AuNRs, and e) light for 12 h reaction time. All the light reactions were carried out with 450 nm CW laser diode at 700 mW $cm^{-2}$ intensity.

**Role of electrostatic interactions emanating from surface ligands on AuNRs**

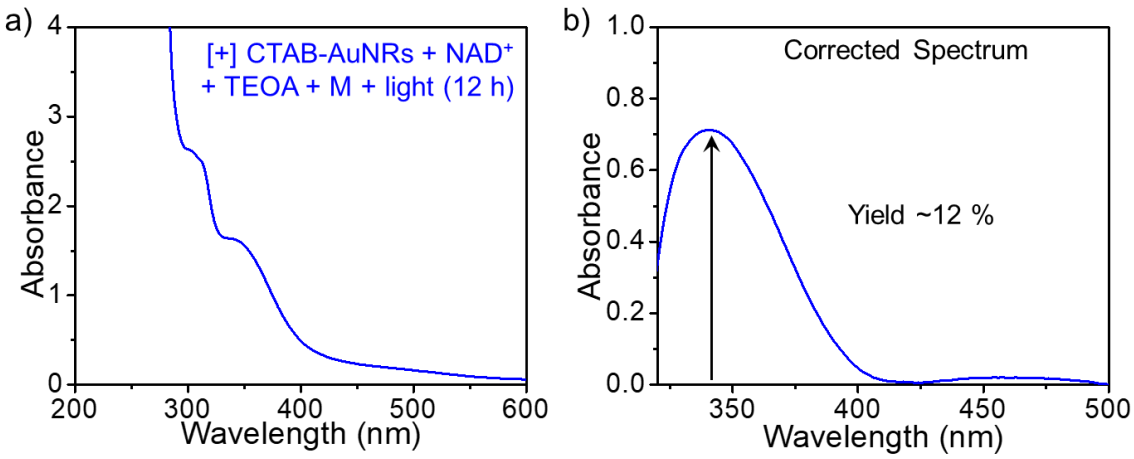


**Figure 3.17.** Effect of AuNR surface charge on photocatalytic NADH regeneration**.** UV-visible absorption of reaction mixture after 450 nm light irradiation (laser power ~ 700 mW $cm^{-2}$) for 12 h in presence of [+] CTAB-AuNRs (unfavorable interactions).

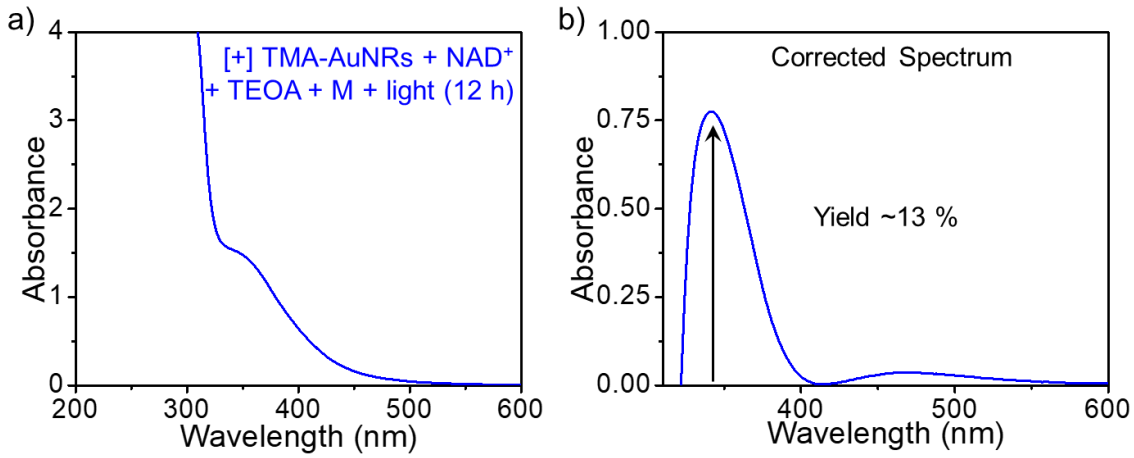


**Figure 3.18.** Effect of AuNR surface charge on photocatalytic NADH regeneration. UV-visible absorption of reaction mixture after 450 nm light irradiation (laser power ~ 700 mW $cm^{-2}$) for 12 h in presence of [+] TMA-AuNRs (unfavorable interactions).

**Intensity-dependent study**

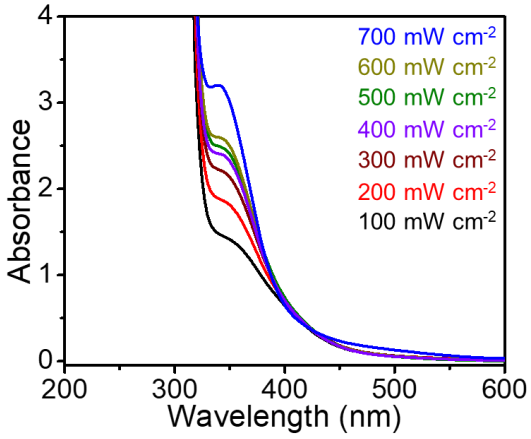


**Figure 3.19.** Intensity-dependent catalytic reduction of $NAD^+$ with [-] AuNRs. Progress of photocatalytic reduction of $NAD^+$ under 450 nm CW laser irradiation for 12 h, with [-] AuNRs at seven different illumination intensities.

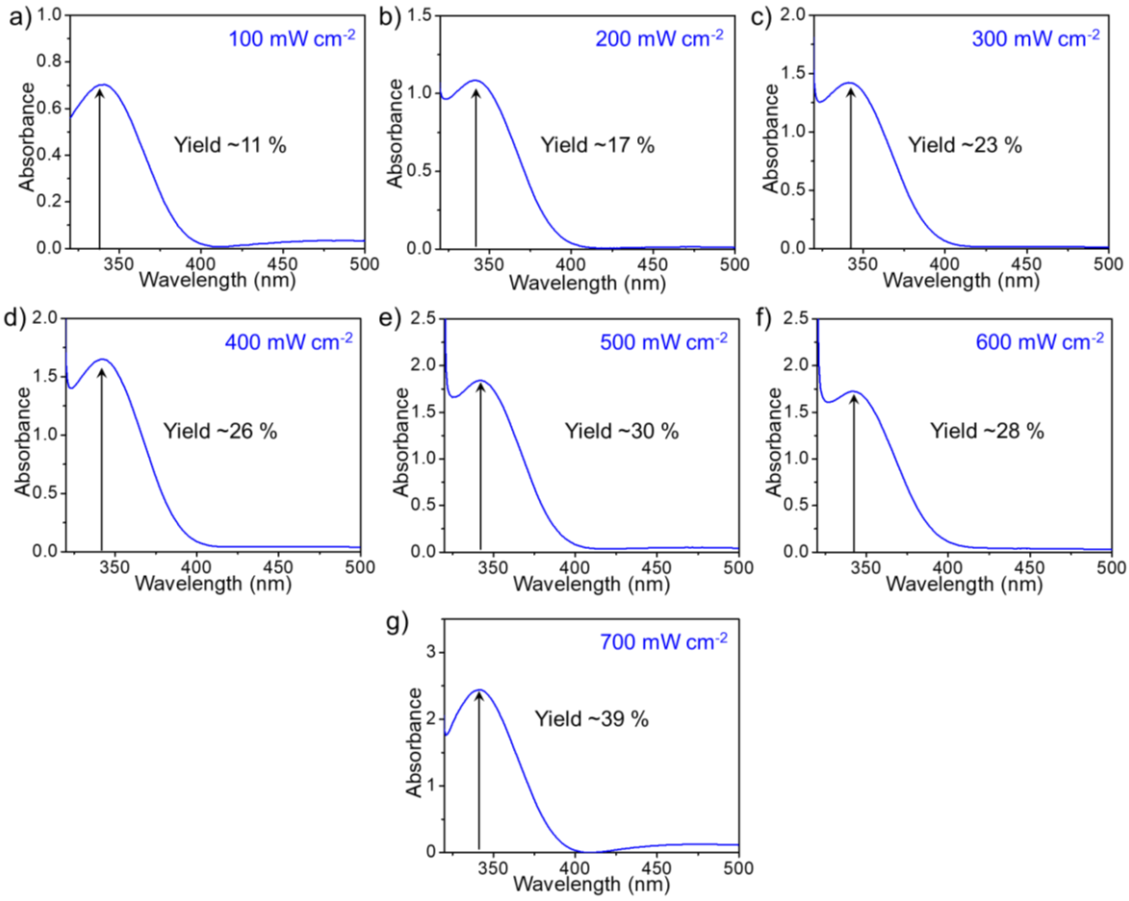


**Figure 3.20.** Corrected spectra of the reaction mixture after 12 h light irradiation with 450 nm CW laser at a) 100 mW $cm^{-2}$, b) 200 mW $cm^{-2}$, c) 300 mW $cm^{-2}$, d) 400 mW $cm^{-2}$, e) 500 mW $cm^{-2}$, f) 600 mW $cm^{-2}$, and g) 700 mW $cm^{-2}$.

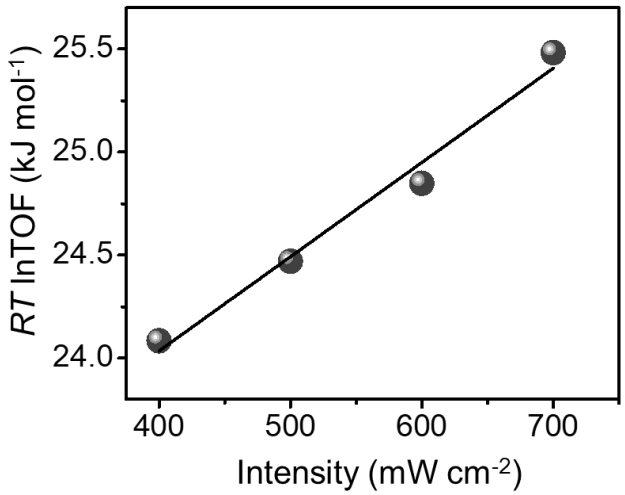


**Figure 3.21.** The linearized first-order fit for the variation in *RT* ln TOF, as a function of light intensity.

**Photocatalytic reaction at elevated temperature in dark**

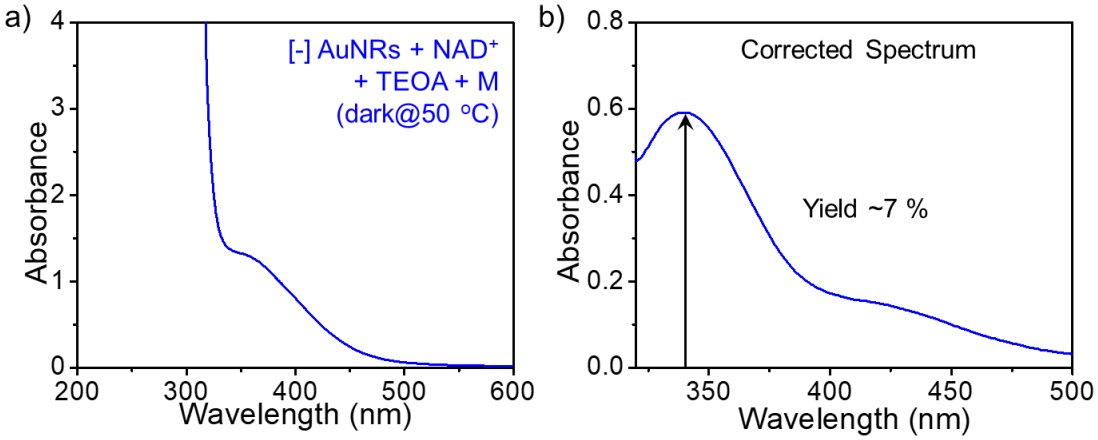


**Figure 3.22.** Photocatalytic reduction of $NAD^+$ under external heating condition at 50 °C. a) UV-visible absorption of reaction mixture heated at 50 °C in absence of light after 12 h, and b) the corresponding corrected absorption spectrum.

**Wavelength-dependent study**

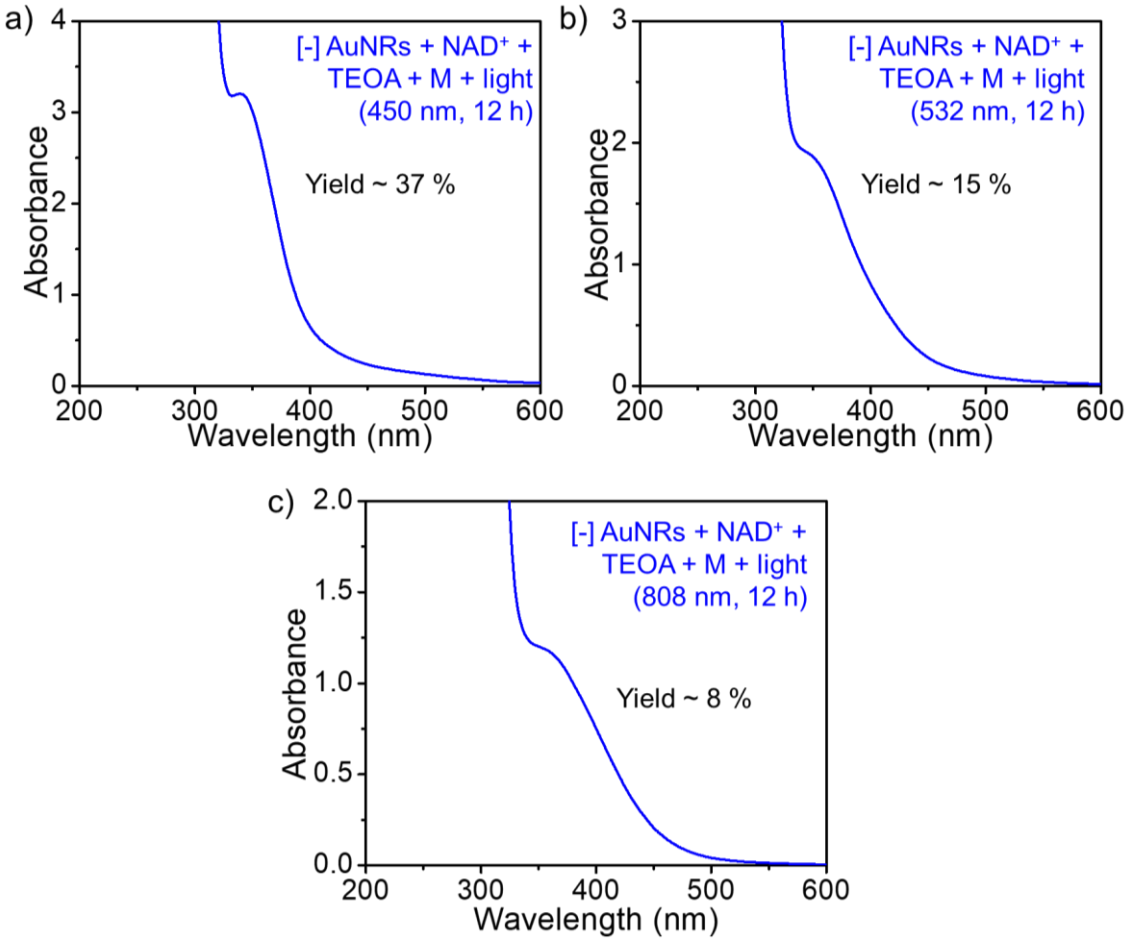


**Figure 3.23.** Photocatalytic reduction of $NAD^+$ under different excitation wavelengths with similar power absorbed (~ 550 mW) in the reaction mixture. Progress of the photocatalytic reduction of $NAD^+$ with [-] AuNRs under a) 450 nm, b) 532 nm, and c) 808 nm CW laser irradiation for 12 h.

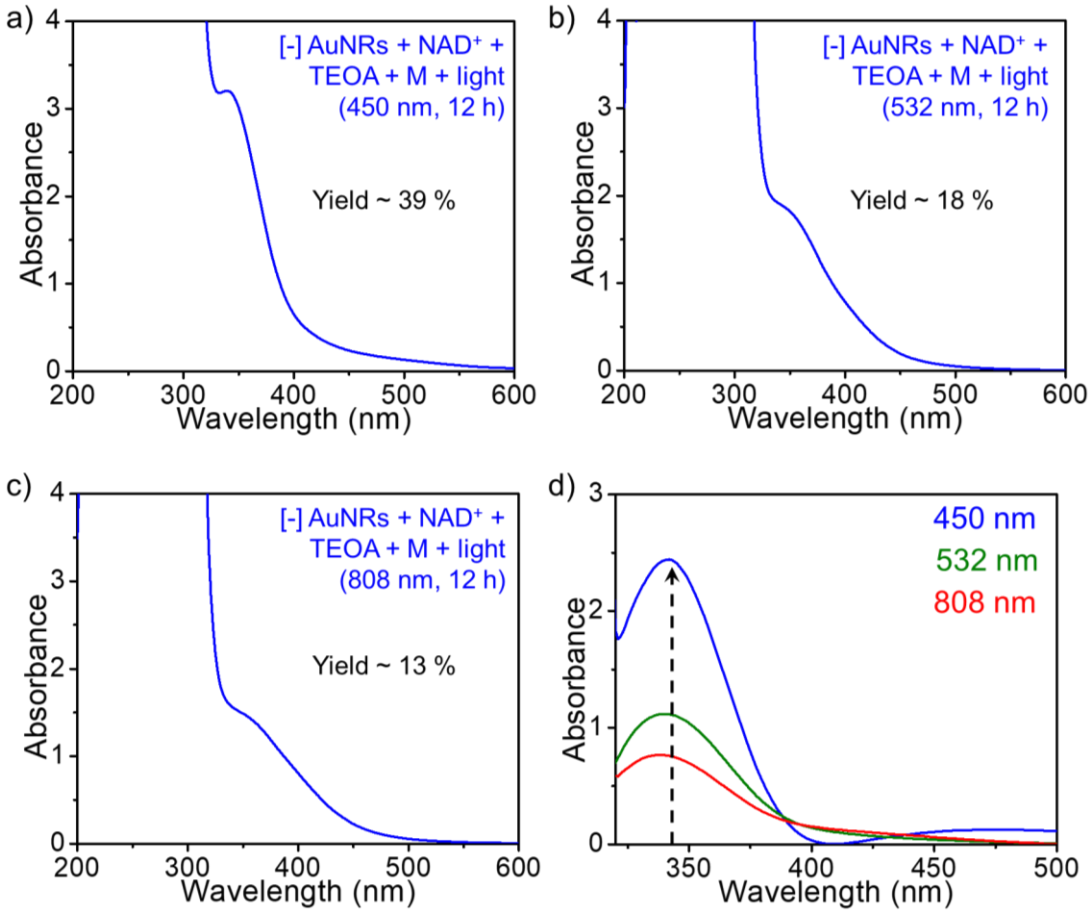


**Figure 3.24.** Photocatalytic reduction of $NAD^+$ under different excitation wavelengths with similar incident light intensity (~ 700 mW $cm^{-2}$). Progress of the photocatalytic reduction of $NAD^+$ with [-] AuNRs under a) 450 nm, b) 532 nm, and c) 808 nm CW laser irradiation for 12 h. d) The corresponding corrected spectra.

# Chapter – 4a

## Design Principles for the Development of Efficient Photocatalyst for Ammonia Synthesis

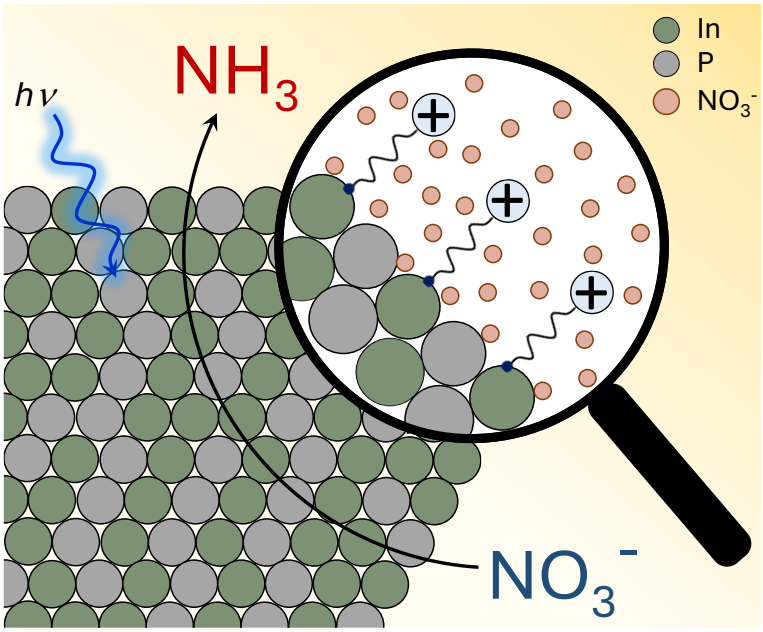


This Chapter has been adapted from the following paper with permission. Copyright 2024, American Chemical Society.

**Jain, V.**; Tyagi, S.; Roy, P.; Pillai, P. P. Ammonia Synthesis with Visible Light and Quantum Dots. *J. Am. Chem. Soc.* **2024**, *146*, 32356-32365.

## 4a.1. Abstract

Ammonia serves as a carbon-free energy source and a key ingredient of synthetic nitrogenous fertilizers, with a major proportion of it being produced via the industrial Haber-Bosch process. The large carbon footprint associated with the energy-intensive Haber-Bosch process calls for developing greener and sustainable alternatives for ammonia synthesis. Light-assisted synthesis of ammonia from nitrate and nitrite sources is a potential avenue for a sustainable ammonia economy. However, poor selectivity and the need for UV-active photocatalysts are the current bottlenecks in ammonia synthesis from nitrate and nitrite sources. Herein, we introduce a selective visible-light-driven ammonia production from nitrate and nitrite ions with indium phosphide quantum dots (InP QDs) as the photocatalyst. The presence of catalytic indium sites and microenvironment modulation through an interplay of catalyst-reactant interactions resulted in an efficient and selective ammonia formation under visible light. Ammonia was produced in an attractive yield of ~94 % in both aqueous and gaseous phases within 2 h of visible-light irradiation at room temperature. A decent formation of ammonia was observed under sunlight as well, strengthening the translational prospects of InP QD photocatalysts. Our study shows the impact of the rationally designed core and surface of InP QD-based photocatalysts in developing sustainable routes to produce ammonia *beyond the Haber-Bosch process*.

## 4a.2. Introduction

Ammonia ($NH_3$) is vital to life.[1-5] For the past century, $NH_3$ has been the major fertilizer feedstock and sustained life on this planet.[2,6] In the past decade, there has been a shift in the role of $NH_3$ from fertilizer feedstock to the liquid carrier of carbon-free energy.[4,5,7-9] A majority of current demands of $NH_3$ are met by a century-old industrial process known as the Haber-Bosch process.[10] While Fritz Haber created the breakthrough of $NH_3$ synthesis from its elements deploying high-pressure reactors, Carl Bosch developed the high-pressure chemistry on an industrial scale at BASF.[10-13] This translation to industrially relevant scale made $NH_3$ a top high-volume commodity chemical and facilitated the production of several chemical products, including hydrazine, nitric acid, urea, acrylonitrile, and phenol.[14,15] In a typical Haber-Bosch process, $N_2$ and $H_2$ react in the presence of Fe catalyst at an elevated temperature of 400-500 $^oC$ and pressures in the range of 100-200 bar to produce $NH_3$ with decent efficiency (energy efficiency ranges from 35-60 %).[10] However, the Haber-Bosch process comes with unintended environmental consequences because of energy-intensive $H_2$ production via methane reforming and extreme reaction conditions.[14-18] It is reported that this industrial $NH_3$ production consumes 1-2 % of the world's annual energy and is responsible for ~1 % of global greenhouse gas emissions.[14,15,18] The large carbon footprint associated with the energy-intensive Haber-Bosch process calls for developing greener and sustainable alternatives for $NH_3$ synthesis.[16-20] In this regard, utilizing the surplus energy dissipated from the Sun offers a promising approach for sustainable $NH_3$ synthesis.[16, 21-25]

Now, the main question is, what will the N-source be for green ammonia synthesis? Though $N_2$ present in the atmosphere is unequivocally the desired and abundant N-source, a careful look into the nitrogen cycle (N-cycle) reveals that all the forms of nitrogen are interconvertible, providing us the flexibility to choose any N-source to produce $NH_3$ ions (**Figure 4a.1a**).[26] According to the N-cycle, once $NH_3$ is oxidized back to nitrate/nitrite ions ($NO_3^-$/$NO_2^-$), some microorganisms can drive assimilatory/dissimilatory nitrate reduction to ammonium, resulting in N-recycling without any waste.[26-28] Inspired by this biological cycle, $NO_3^-$ and $NO_2^-$ ions have emerged

as alternate N-sources in artificial $NH_3$ synthesis.[29-34] Accordingly, nitrogen oxidation reactions (NOR) have been developed to increase the availability of $NO_3^-$ and $NO_2^-$ ions as a viable source for $NH_3$ synthesis.[35] Currently, the prospect of energy demands and efficiencies is being investigated for NOR. It has been theoretically predicted that the energy consumption for NOR via the non-thermal plasma process is comparable to or lower than the existing Haber-Bosch process,[35] with the added advantage of reduced greenhouse gas emission from the NOR process. Further, with the advent of industrial $NH_3$ production, there has been a disruption in the nitrogen cycle, resulting in excessive accumulation of $NO_3^-/NO_2^-$ in water bodies from industrial wastewater discharge and agricultural run-offs.[36-38] Motivated by assimilatory/dissimilatory ammonification in N-cycle, and the necessity to reduce the detrimental environmental effects of N-contamination in water bodies, the conversion of $NO_3^-$ and $NO_2^-$ ions to $NH_3$ offers a way for wastewater treatment while simultaneously generating a value-added commodity.[29-34, 37,38] Furthermore, $NO_3^-$ to $NH_3$ conversion from wastewater is attractive for niche applications such as delocalized production of fertilizers at agricultural locations with high levels of $NO_3^-$ pollution and on-site $NH_3$ demands.[39,40] Thus, the conversion of $NO_3^-$ and $NO_2^-$ ions to $NH_3$ has gained significant attention in recent years and emerged as a viable strategy for ammonia synthesis (**Figure 4a.1b**).[29-34]

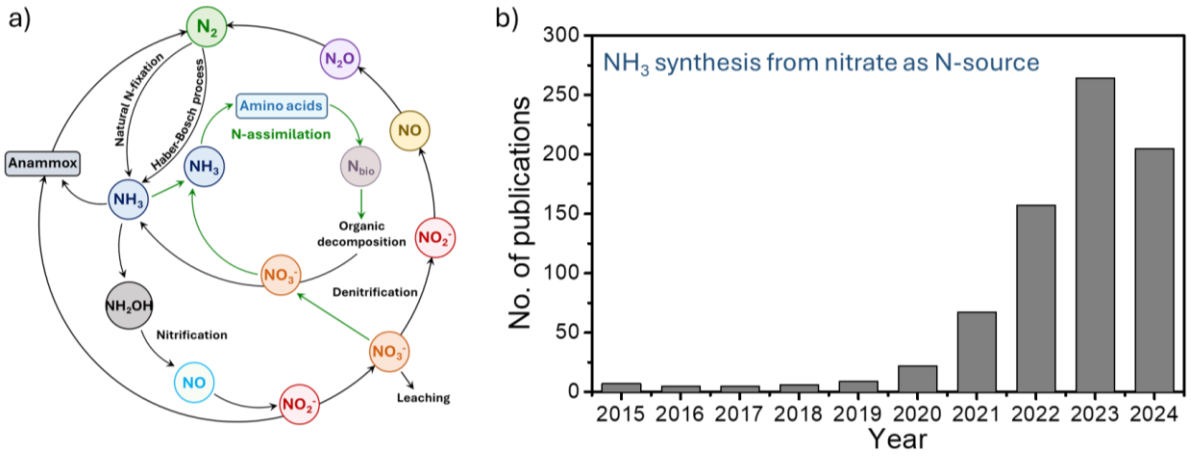


**Figure 4a.1**. a) The Nitrogen cycle shows major species and their interconversions. b) Bar diagram representing the number of annual publications related to ammonia synthesis from nitrate as the N-source in the past 10 years till August 2024. The statistics are based on Web of Science™ database with screening terms: 'Nitrate reduction to ammonia'. The results presented here depict publications only from 4 publishers (ACS, Wiley, RSC, and Springer Nature).

One of the earliest examples of photocatalytic $NH_3$ synthesis from $NO_3^-$/$NO_2^-$ as N-source dates to 1984 when Halmann and Zuckerman observed $NH_3$ synthesis in the presence of semiconductor powders suspended in aqueous alkaline sulfide solution under light illumination.[41] Various semiconductors such as $TiO_2$, $SrTiO_3$, CdS, and CdS-ZnS powders as the photocatalysts in the KOH-$Na_2S$ solution resulted in continuous ammonia production in the presence of $KNO_2$. Around a similar time, Onishi and coworkers explored $TiO_2$ supported metals (Pt, Rh, and Pd) as the photocatalyst for $NH_3$ synthesis from nitric acid and sodium nitrate solutions.[42] This was followed by a series of reports by Viswanathan and coworkers exploring various metals (Ru, Pd, Ir, Pt, Rh. etc.) and metal ions ($Fe^{3+}$, $Cr^{3+}$, $Co^{2+}$, $Mg^{2+}$, etc.)-loaded semiconductors such as CdS and $TiO_2$ for $NO_3^-$ and $NO_2^-$ reduction to $NH_3$.[43-46] While the focus shifted to $N_2$ as the N-source for green $NH_3$ production, there has been a huge surge again in the past 5 years for photocatalytic $NH_3$ generation from $NO_3^-$ and $NO_2^-$ ions (**Figure 4a.1b**). With the ever-expanding library of the designer photocatalysts, numerous reports on reduction of $NO_3^-$/$NO_2^-$ ions have emerged.[30-33, 47-50]

Photocatalytic reduction of $NO_3^-$ to $NH_3$ is a proton-coupled multielectron process ($8e^-/9H^+$), which has often been achieved with UV-active photocatalysts.[22,31-33,41-47,50] Additionally, the differences in kinetics and thermodynamics of multistep reaction pathways involved result in the accumulation of undesired by-products (majorly $N_2$ and $NO_x$ as the end-product).[32,33,51-54] For instance, Shiraishi and coworkers reported design principles to achieve selective reduction of $NO_3^-$ to $NH_3$ with $TiO_2$-based photocatalysts.[33] A series of commercially available $TiO_2$ particles such as JRC-TIO-1, ST-01, Aldrich anatase, P25, Wako rutile, JRC-TIO-6, Aldrich rutile, etc. were tested for photocatalytic $NO_3^-$ reduction. It was observed that most of the anatase and rutile TiO2 (JRC-TIO-1, ST-01, Aldrich anatase, P25, Wako rutile, Aldrich rutile) exhibited low selectivity for NH3 formation, except for the JRC-TIO-6 photocatalyst. For a better comparison, Japanese reference catalysts supplied from the Catalyst Society of Japan, JRC-TIO-1 and JRC-TIO-6, were investigated in detail. With an increase in the reaction time, JRC-TIO-1 produced both $N_2$ as well as $NH_3$ (31 % $NH_3$ selectivity) (**Figure 4a.2a**), whereas sole production of $NH_3$ was observed in the case of JRC-TIO-6 (97 % $NH_3$ selectivity) under similar reaction conditions (**Figure 4a.2b**). The difference in the behavior of $TiO_2$ based photocatalyst was

attributed to the presence of different reduction sites, surface defects or Lewis acid sites. Detailed studies revealed that the surface defects act as sites for selective $NO_3^-$ reduction to $NH_3$ while Lewis acid sites are non-selective (**Figures 4a.2c, 4a.2d**). The selectivity was altered because of the strong adsorption affinity of $NO_3^-$ ions on surface defects as compared to Lewis acid sites, which do not allow for liberation of $NO_2^-$ intermediates.

In another report by Han and coworkers, $Ag_2O$/P25 and Ag/P25 photocatalysts were used for $NO_3^-$ reduction using formic acid as the hole scavenger under UV irradiation (**Figures 4a.2e, 4a.2f**).[54] Even though a high $NO_3^-$ conversion of ~97 % was achieved, the major product was $N_2$ with ~83 % selectivity. It was reported that photoexcited electrons have weak $NO_3^-/NO_2^-$ reducing ability. Interestingly, in the presence of formic acid as hole scavenger, $CO_2^{\bullet-}$ species is generated after extraction of photogenerated holes. A strong reducing ability ($E^o$ ($CO_2/CO_2^{\bullet-}$) = -1.8 V) enables reduction of $NO_3^-$ to $NO_2^-$, $N_2$ or $NH_3$. Because of the involvement of $CO_2^{\bullet-}$, the most thermodynamically favourable product i.e., $N_2$ ($E^o$ ($NO_3^-/N_2$) = 1.25 V vs $E^o$ ($NO_3^-/NH_3$) = 1.20 V), was obtained under higher yields. In fact, the presence of ammonium ions inhibited $NO_3^-$ reduction. However, when $NO_3^-$ reduction was performed under visible light illumination instead of UV, negligible conversion was observed. Thus, a thorough literature search reveals only a few photocatalysts exhibiting selective $NH_3$ formation from $NO_3^-/NO_2^-$ ions under visible light irradiation. Hence, these limitations of existing approaches call for rationally designed visible-light photocatalysts for the efficient and selective $NH_3$ formation from $NO_3^-$ and $NO_2^-$ ions.

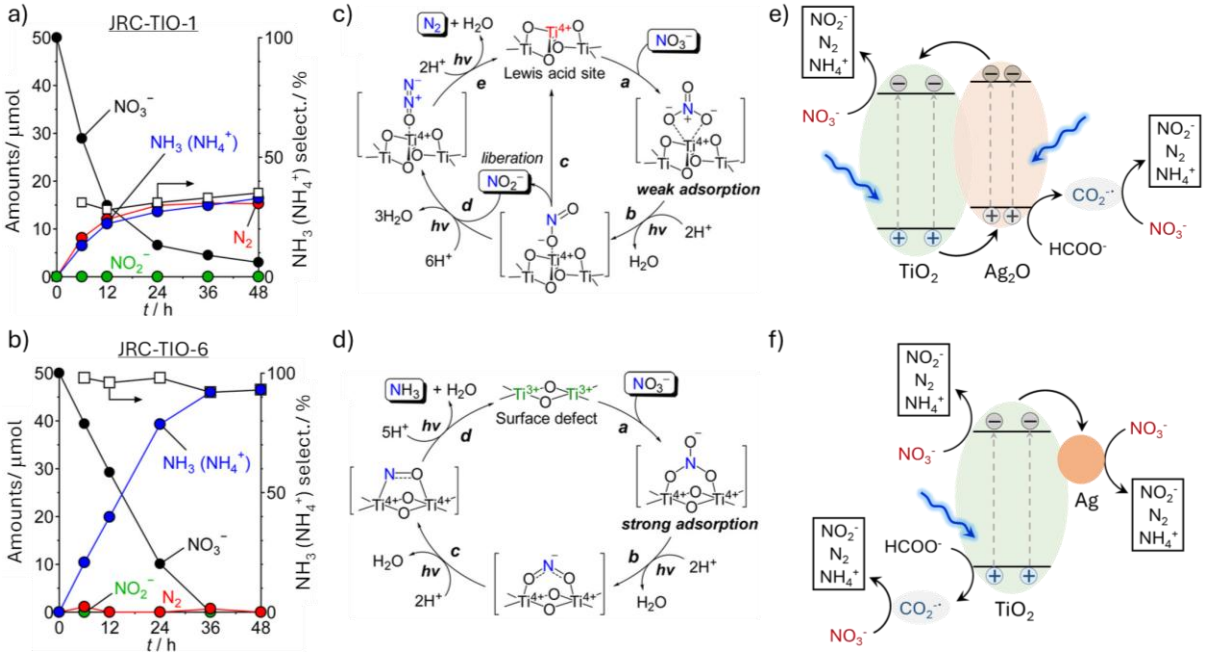


**Figure 4a.2**. Photocatalytic $NH_3$ formation from $NO_3^-$ as the N-source. Progress of photocatalytic $NO_3^-$ reduction under UV irradiation using commercially available $TiO_2$ photocatalysts, a) JRC-TIO-1 and b) JRC-TIO-6. Along with $NH_3$, $N_2$ was also produced in the presence of JRC-TIO-1 photocatalyst, whereas selective formation of $NH_3$ was observed with JRC-TIO-6. The difference in selectivity arises because of the presence of c) Lewis acid sites and d) surface defects mediated $NO_3^-$ reduction. $TiO_2$ with a greater proportion of surface defects results in better $NH_3$ selectivity by strongly adsorbing $NO_3^-$ ions. Reproduced with permission from reference 33. Copyright 2017 American Chemical Society. Photocatalytic $NO_3^-$ reduction in the presence of e) $Ag_2O/TiO_2$ and f) $Ag/TiO_2$ hybrid photocatalysts under UV light irradiation using HCOOH as the hole scavenger. With both photocatalysts, multiple $NO_3^-$ reduction products were obtained. The poor selectivity for $NH_3$ formation can be attributed to the presence of HCOOH as a hole scavenger, which results in $CO2^{\cdot-}$ radical formation. $CO_2^{\cdot-}$ radical is highly reducing and leads to non-selective $NO_3^-$ reduction to $NO_2^-$, $N_2$, and $NH_3$. Reproduced with permission from reference 54. Copyright 2015 Elsevier.

Converging $NO_3^-$ and $NO_2^-$ reduction to yield $NH_3$ demands photocatalysts that generate surplus charge carriers and allow optimum surface interaction with the N-sources. It was reported very recently by Wu and coworkers that II-VI cadmium selenide QDs and I-III-VI copper indium sulfide QDs are promising visible-light photocatalysts to reduce $NO_3^-$ and $NO_2^-$ to $NH_4^+$ ions.[30] This study calls for exploring the enormous potential hidden in QD-based photocatalysts for producing $NH_3$ beyond the Haber-Bosch process. In this Chapter, we introduce III-V indium phosphide (InP) QDs as the photocatalyst to drive the selective reduction of $NO_3^-$ and $NO_2^-$ to $NH_4^+$ under visible-light irradiation, at room temperature. Our choice of InP QD as the photocatalyst was based on its high molar extinction coefficient, tunable absorption profiles, high carrier mobility, long-lived

charge separation, and flexibility in tunability of the surface chemistry.[55-58] More importantly, III-V InP QDs exhibit distinct charge carrier dynamics from II-VI QDs because of the different nature of bonding.[59,60] While II-VI QDs are ionic in nature (Philips ionicity, $f$ = 0.685) because of the large electronegativity difference between the constituent elements, III-V InP QDs exhibit a more covalent nature (Philips ionicity, $f$ = 0.421) (**Figure 4a.3a**).[61] As a consequence of the covalent bonding nature, the effective mass of charge carriers becomes smaller for InP ($m^*/m_e$ = 0.13 for InP vs 0.20 for CdS) and the wavefunctions are more delocalized in III-V InP QDs (**Figure 4a.3b**) compared to II-VI QDs (**Figure 4a.3c**).[62] This implies a weaker coulombic interaction between electrons and holes in InP QDs compared to II-VI and I-III-VI QDs.[59-63] Along with a more delocalized wavefunction, a higher covalent bonding nature (**Figure 4a.3c**) results in the formation of deep trap states.[59-61] Heath and coworkers estimated that for similarly sized (~3.2 nm) InP and CdSe QDs, the depth of trap states below the conduction band is 25 times higher for InP QDs (6.3 kJ $mol^{-1}$) than CdSe QDs (0.25 kJ $mol^{-1}$).[59] In principle, the deep trap states can retard the charge recombination and enhance the carrier lifetime, which may turn beneficial for photocatalytic transformation. Moreover, in an interesting study by Cossairt and coworkers, InP QDs were reported to exhibit longest-lived charges (t = 25.5$\pm$0.4 min) after light illumination compared to CdSe (t = 11.1$\pm$0.5 min) and CdS (t = 7.2$\pm$0.4 min) QDs (**Figure 4a.3d**).[64] This was again attributed to the high covalency of the InP lattice, leading to less reversible redox changes on the QD surface and storing the charges for a longer time. Such prolonged charge storage is commensurate with the timescale at which photocatalytic reactions take place. Thus, the robust covalent framework of InP QDs enables the efficient charge separation, as well as the appropriate surface modification to enhance the charge extraction process.[59-63,65,66] As a result, InP QDs exhibit excellent visible-light harvesting properties,[66,67] which can find applications in photocatalysis as well.[63, 68-70] Furthermore, recent computational studies have proposed a promotional effect of In atoms in binding $NO_3^-$ via 2 oxygen atoms to form In-O bond, followed by the deoxygenation of $NO_3^-$ (**Figure 4a.3e**).[71] Additionally, the environmentally benign attributes, such as low intrinsic toxicity and biocompatibility, strengthen the translational prospects of InP QDs as an ideal visible-light photocatalyst for producing $NH_3$.[72-74]

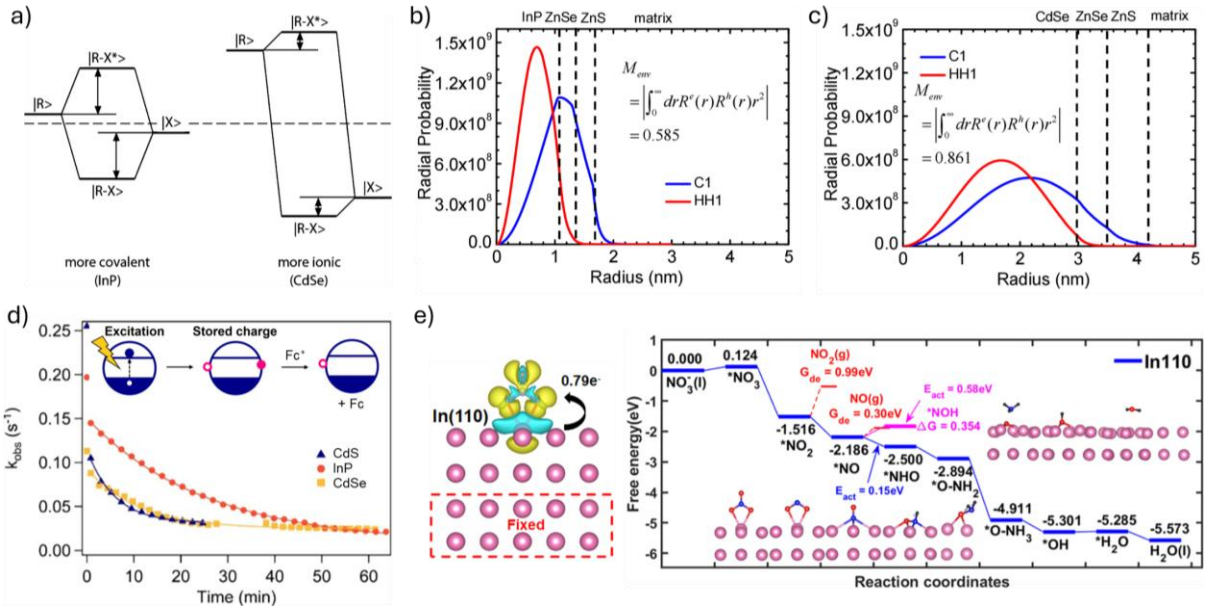


**Figure 4a.3**. Choice of InP QDs as the photocatalyst for $NO_3^-$ to $NH_3$ conversion. a) Schematics showing the diatomic molecular orbitals formed from atomic |R⟩ and |X⟩ of different electronegativities. In the case of III-V QDs, $e^-$ and $h^+$ trap states are formed in the middle of valence band and conduction band, while shallow trap states are formed close to valence and conduction band in case of II-VI QDs. Reproduced with permission from reference 61. Copyright 2021 American Chemical Society. Calculated radial probability of $e^-$ (blue) and $h^+$ (red) wavefunctions in the ground state of b) InP/ZnSe/ZnS and c) CdSe/ZnSe/ZnS. The wavefunctions are confined to the core with a large degree of overlap in CdSe as compared to InP QDs, where more delocalization is observed. Such a higher overlap between $e^-$ and $h^+$ wavefunctions results in higher confinement. Reproduced with permission from reference 62. Copyright 2019 Optica Publishing Group. d) Decay of electron transfer from QD to ferrocenium ion ($Fc^+$) extracted from cyclic voltammetry studies after QD illumination ends. All QDs (CdS, CdSe, and InP) were found to store charges after light irradiation, with InP having the longest-lived charges. Reproduced with permission from reference 64. Copyright 2024 American Chemical Society. e) Charge density difference plot showing the charge accumulation (yellow) on $NO_3^-$ adsorbed on In (110) surface. $NO_3^-$ binds to In atoms via two oxygen atoms. The free energy diagram shows the thermodynamically favorable reaction pathway of $NO_3^-$ reduction over In (110) surface. Reproduced with permission from reference 71. Copyright 2023 American Chemical Society.

In a step towards green $NH_3$ synthesis, the present work highlights a simple, yet efficient photocatalytic system based on InP QDs for the selective reduction $NO_3^-$ and $NO_2^-$ to $NH_4^+$ under visible-light irradiation at room temperature. A rational design of the core and appropriate surface chemistry of InP QDs were the key for the efficient $NH_3$ synthesis. The favorable catalyst-reactant interactions emanating from InP QD surface ligands accelerated the charge transfer and extraction steps, resulting in the efficient and selective formation of $NH_4^+$ in the aqueous phase within 2 h of visible-light irradiation (57.5±9.3% $NO_3^-$ to $NH_4^+$ and 42.9±8.9% $NO_2^-$ to $NH_4^+$ in aqueous phase). The sole

presence of $NH_3$ was detected in the gaseous phase as well, further adding to the total $NH_3$ yield of the photocatalytic reaction (430 μmol $g^{-1}$ and 6.8 ppm, accounting for ~94 % of the total $NO_3^-$ converted). The apparent quantum efficiency reached as high as 1.45 % and 3.7 % @450 nm for the photocatalytic ammonia synthesis using $NO_3^-$ and $NO_2^-$ ions as N-sources, respectively. In short, a preferential affinity of N-sources towards surface In atoms and ligands on InP QD photocatalysts led to the selective and efficient production of $NH_3$ under visible-light irradiation at room temperature. We anticipate that the excellent photocatalytic ability and environmentally benign attributes of InP QDs can complement existing methods of green $NH_3$ synthesis.

# 4a.3. Experimental section

## 4a.3.1. General procedure for the photocatalytic $NO_3^-$ to $NH_4^+$ conversion

All the photocatalytic experiments were performed in a 4 mL long-neck quartz cuvette. In a typical procedure, [+] InP QDs (2.5 μM, 0.5 mol %) and $KNO_3$ (0.5 mM) in water were mixed, purged with Ar, and irradiated with 2 x 10 W 450 nm LEDs for 2 h (total light intensity falling on wall of the cuvette was ~200 mW $cm^{-2}$). The total volume of the reaction mixture was maintained at 3 mL throughout the studies, and the pH was 5. Subsequently, the reaction mixture was analyzed for $NH_4^+$ formation using ion chromatography by injecting 500 μL of the reaction mixture. The area under the peak at retention time ~8.5 min was used to calculate the concentration of $NH_4^+$ formed from the calibration curve. A similar analysis was carried out for $NO_3^-$ and $NO_2^-$ conversion as well to calculate the total conversion yields.

## 4a.3.2. Photocatalytic experiments with isotope labelled $^{15}NO_3^-$

The proof for $NO_3^-$ as the sole N-source in the $NH_4^+$ formed was obtained from photocatalytic experiments performed with isotope labelled $^{15}NO_3^-$. After the photocatalytic experiment, the reaction mixture was acidified to a pH 1-2 with HCl. The reaction mixture was concentrated to half, from which 600 μL was mixed with 100 μL DMSO-$d_6$ and subjected to $^1$H-NMR spectroscopy. For comparison, the $^1$H-NMR

spectrum of $^{14}NO_3^-$ containing reaction mixture was also recorded. NMR signals between 6.5-7.5 ppm region were analyzed.

### 4a.3.3. Quantification of $NH_3$ in gas phase

The quantification of $NH_3$ in headspace was carried out using a BELMASS II quadrupole mass spectrometer from Microtrac. Firstly, a known amount of $NH_3$ gas (0.4 mL of 101141 ppm) was injected using a gas-tight syringe, and the area under the peak for m/z = 15 corresponding to the NH fragment, was analyzed. We chose m/z =15 of the NH fragment to avoid interference from $H_2O$ and its fragments (m/z = 18, 17, and 16). The standard $NH_3$ gas was injected thrice at different points in time, and the average area under the peak was calculated. The areas under the curves for m/z=15 were compared for standard and photocatalytic reactions to quantify the $NH_3$ amount in the gas phase.

Average area under the peak for m/z = 15 in standard $NH_3$ = $2.035 \times 10^{-9} \pm 6.3 \times 10^{-10}$

Average area under the peak for m/z = 15 after the photocatalytic reaction = $2.86 \times 10^{-11} \pm 3.7 \times 10^{-10}$

Moles of $NH_3$ in headspace = $0.37 \pm 0.11$ mmol

Total moles of $NH_3$ formed in photocatalytic reaction = $0.37 \pm 0.11$ mmol (in gas phase) + $0.43 \pm 0.08$ mmol (in aqueous phase) = $0.80 \pm 0.19$ mmol

Similarly, the amount of $NH_3$ present in the headspace was analyzed and calculated with $NO_2^-$ as the N-source.

### 4a.3.4. Apparent quantum yield calculations

The apparent quantum yield ($AQY$) of a photochemical process is calculated by dividing the number of photons utilized for $NH_4^+$ formation by the total number of incident photons. AQY was calculated using the following equation:

$$AQY\ (\%) = \frac{number\ of\ NH_4^+\ formed\ \times 8}{number\ of\ incident\ photons} \times 100 \qquad (\mathbf{4a.1})$$

Multiplication by 8 is to account for the total number of electrons required to form 1 molecule of $NH_4^+$ from $NO_3^-$ (photocatalytic reduction of $NO_3^-$ to $NH_4^+$ is an 8-electron process).

The total number of incident photons ($n_{photon}$) can be calculated as follows

$$n_{photon} = \frac{P_0 \times \lambda\,(m) \times t\,(s)}{hc} \qquad (\mathbf{4a.2})$$

$$n_{photon} = \frac{(0.2\,J/s) \times (450 \times 10^{-9}\,m) \times\ 7200\,s}{(3 \times 10^8\,m/s) \times (6.626 \times 10^{-34}\,J.s)} = 3.26 \times 10^{21}$$

The number of product molecules formed was calculated to be $5.90 \times 10^{18}$.

$$AQY_{450}(\%) = \frac{5.90 \times 10^{18}\ \times 8}{3.26 \times 10^{21}} \times 100 = 1.45\ \%$$

The AQY for $NO_3^-$ to $NH_4^+$ conversion with [+] InP QDs under 450 nm illumination was estimated to be 1.45%.

Likewise, the AQY for $NO_2^-$ to $NH_4^+$ conversion was calculated as follows:

$$n_{photon} = \frac{(0.2\,J/s) \times (450 \times 10^{-9}\,m) \times\ 3600\,s}{(3 \times 10^8\,m/s) \times (6.626 \times 10^{-34}\,J.s)} = 1.62 \times 10^{21}$$

The number of product molecules formed was calculated to be $9.99 \times 10^{18}$.

$$AQY\ _{450}(\%) = \frac{9.99 \times 10^{18}\ \times 6}{1.62 \times 10^{21}} \times 100 = 3.7\ \%$$

Similarly, AQY for $NO_3^-$ to $NH_4^+$ conversion performed under different irradiation wavelengths were estimated to be 0.146 % (@450 nm), 0.105 % (@532 nm), and 0.0335 % (@580 nm). It is to be noted that the wavelength-dependent experiments were performed at a lower scale (3 mL) while keeping the incident light intensity similar.

### 4a.3.5. Photocatalytic experiments in sunlight

Photocatalytic reactions in sunlight were performed by exposing the reaction mixture to direct sunlight. [+] InP QDs and $KNO_3$ were mixed in a long-neck quartz cuvette, and the reaction mixture was purged with Ar. The cuvette was exposed to natural sunlight for

2 h (light intensity was measured to be ~95 mW $cm^{-2}$). The reaction mixture was analyzed with IC to calculate the conversion yields.

# 4a.4. Results and discussion

## 4a.4.1. Preparation of InP QD-based visible-light photocatalysts

Red-emitting core-only InP QDs were prepared using modified literature protocols, involving the high-temperature organometallic reaction between indium(III) chloride and tris-(dimethylamino)phosphine in oleylamine (OAm).[75] Core-only InP QDs, without any shell, were our choice of photocatalyst to enhance the charge separation and extraction processes under light irradiation. Moreover, a recent theoretical study has predicted a favorable adsorption of $NO_3^-$ ions over In atoms via two oxygen atoms.[71] Appropriate choice and amounts of indium halide and phosphorus precursors were crucial for regulating nucleation and growth kinetics, and achieving high-quality core-only InP QDs.[75,76] The as-synthesized shows excellent light absorption in the visible region with a band gap of 2.02 eV as estimated from the Tauc plot (**Figure 4a.4a**). The core-only InP QDs possess appropriate band positions to facilitate photocatalytic reduction of $NO_3^-$ /$NO_2^-$ to $NH_4^+$ with visible-light irradiation. For as-synthesized OAm-InP QDs, only the peak corresponding to oxidation was observed in CV (black voltammogram) (**Figure 4a.4c**). This peak at 0.94 V vs. $Ag/AgNO_3$ corresponds to the valence band of OAm-InP QDs. Accordingly, the valence band position was estimated to be -5.59 eV with respect to vacuum. From the band gap value and the valence band position, the conduction band position was estimated to be -3.57 eV with respect to vacuum for OAm-InP QD. The native OAm ligands on InP QDs were place-exchanged with cationic *N,N,N*-trimethyl(11-mercaptoundecyl)ammonium chloride (TMA, [+]) ligand to achieve colloidal stability in aqueous medium as well as to install favourable catalyst-reactant interactions (**Figure 4a.5a**).[77,78] Negligible change in the band gap was observed after ligand exchange (**Figure 4a.4b**). However, it has been reported that ligands can significantly affect the QD band positions even up to 0.9 eV.[79] Therefore, we estimated the band positions for TMA-functionalized [+] InP QDs. For [+] InP QD, the peak corresponding to oxidation was observed at 0.92 V vs. $Ag/AgNO_3$ (blue voltammogram) (**Figure 4a.4c**). Accordingly, the

valence band position was estimated to be -5.57 eV with respect to vacuum. The valence and conduction bands of [+] InP QDs were positioned at -5.57 eV and -3.54 eV, respectively (**Figure 4a.4d**). The ligand exchange resulted in a negligible change on band edge positions for InP QDs, as confirmed by cyclic voltammetry and absorption studies.

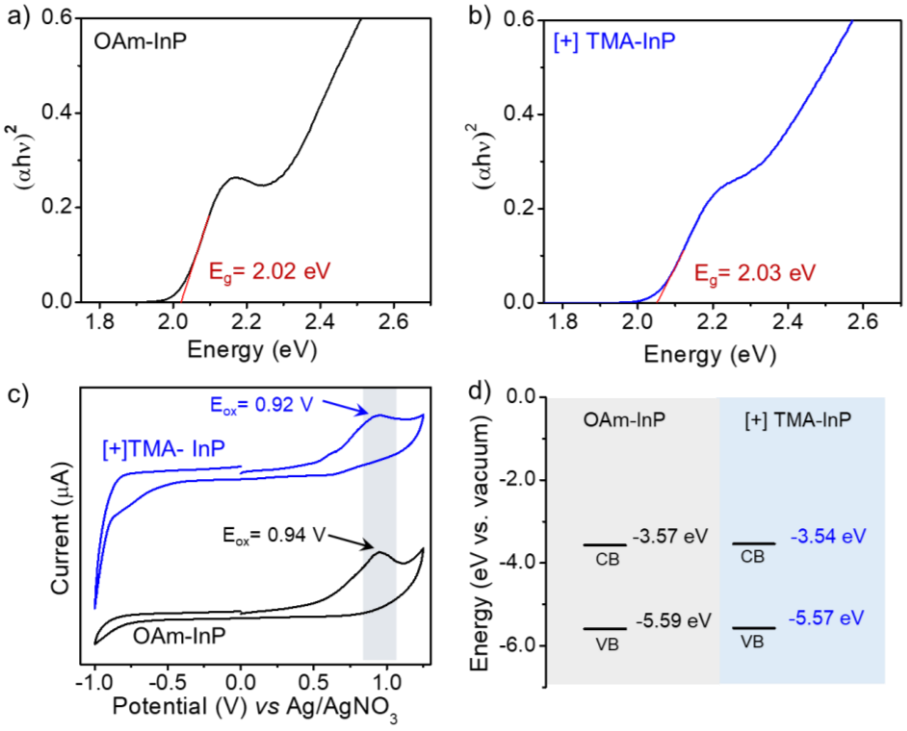


**Figure 4a.4**. Estimation of band positions for OAm-InP and [+] TMA-InP core-only QDs. Tauc plots of a) OAm-InP QDs and b) [+] InP QDs. c) Cyclic voltammograms (CV) of OAm-InP (black voltammogram) and [+] TMA-InP (blue voltammogram) core-only QDs. As the [+] InP QD film was made from an aqueous suspension, a water oxidation peak was also observed at 0.65 V in addition to the peak corresponding to the valence band of [+] InP. The water oxidation peak was validated by recording the CV of the electrolyte in the water-acetonitrile mixture (green voltammogram). d) Plot showing the band positions of OAm-InP and [+] TMA-InP QDs calculated from Tauc and CV plots.

The absence of S-H stretching frequency peak in Fourier transform infrared spectroscopy (FTIR) analysis revealed that TMA ligands bind to core-only InP QDs predominantly as X-type thiolates (**Figure 4a.5b**). To prove the role of electrostatic interactions emanating from the surface ligands of InP QDs, negatively charged ([-]) InP QDs were prepared by ligand place exchanging the native OAm ligands with 11-mercaptoundecanoic acid (MUA) ligands (**Figure 4a.5a**). The complete transfer of InP QDs from toluene to the aqueous phase indicates the successful ligand exchange with TMA and MUA ligands, respectively. The thiol groups of TMA and MUA bind to the QD

surface, while the terminal positively charged quaternary ammonium group in TMA and negatively charged carboxylic acid group in MUA provide dispersion in the aqueous medium. The zeta potential values of +24.0±8.5 mV and -37.0±6.9 mV confirm the successful functionalization of TMA and MUA ligands on the surface of InP QDs, respectively (**Figure 4a.5c**). There was a negligible change in the zeta potential of [+] InP QDs across a wide pH range (3-10) (**Figure 4a.10**). Transmission electron microscopy (TEM) studies confirm the formation of uniform-sized [+] InP QDs having an average diameter of 3.5 ± 0.4 nm (**Figures 4a.5d, 4a.11**). After the successful synthesis, characterization, and ligand exchange, the core-only InP QDs were employed for photocatalytic ammonia synthesis with visible light.

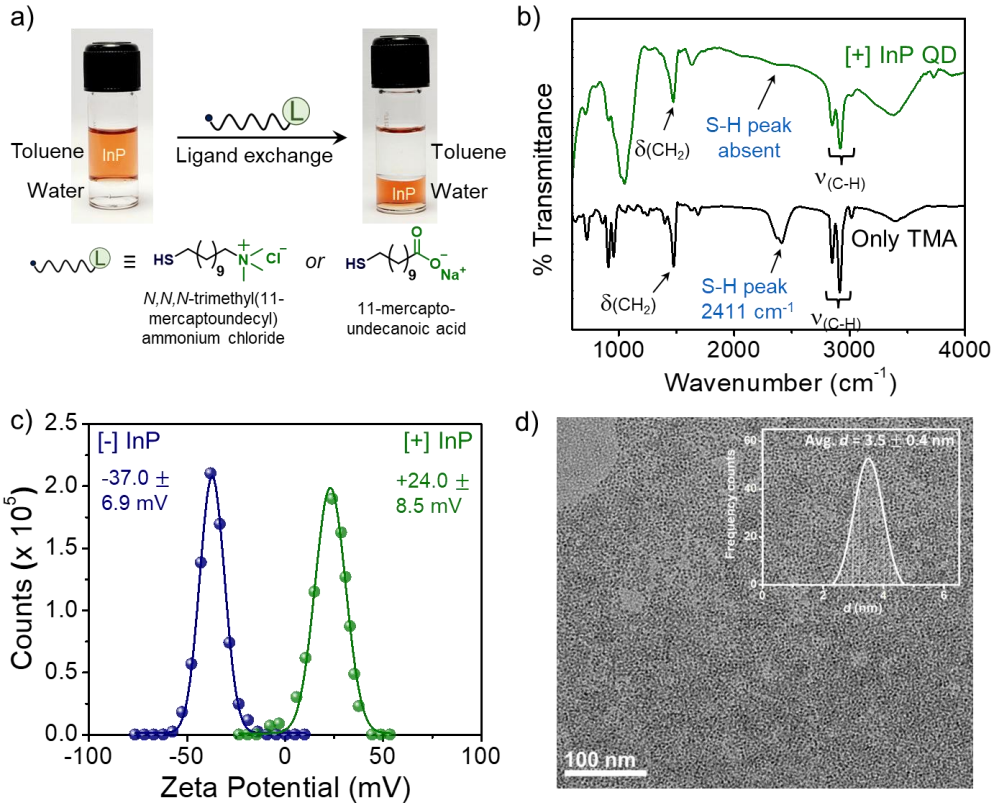


**Figure 4a.5**. Characterization of core-only InP QDs. a) Schematics showing the ligand exchange of oleylamine-capped InP QDs with positively charged *N,N,N*-trimethyl(11-mercaptoundecyl)ammonium chloride (TMA) and negatively charged 11-mercaptoundecanoic acid (MUA) thiolated ligands. b)FTIR spectra of [+] TMA ligand (black) and [+] TMA capped [+] InP QDs (green). c) Zeta potential plot confirming the successful functionalization of InP QDs with [+] and [-] thiolated ligands. Zeta potential was measured at the pH of the reaction mixture (pH ~5 and ~10 for [+] and [-] InP QDs, respectively). d) A representative TEM image of core-only [+] InP QDs. Inset shows the corresponding size distribution histogram (collected from ~ 300 QDs).

## 4a.4.2. Photocatalytic reduction of nitrate and nitrite ions to ammonia

The permanent positive charge of the quaternary ammonium group modifies the local environment of [+] InP QD by electrostatically channeling $NO_3^-$ and $NO_2^-$ reactants towards the QD photocatalysts (**Figure 4a.6a**).[77,78] The concentration profiles as a function of distance were computed which clearly show the channeling effect in [+] InP QDs due to favourable electrostatic interaction between [+] InP QD and [-] $NO_3^-$ ions (**Figure 4a.6b**; See Appendix for details, **Figure 4a.12**). The enhanced local concentration of [-] $NO_3^-$ ions enhances the probability of charge transfer step from photoexcited [+] InP QDs. The electron transfer can happen from photoexcited [+] InP QDs directly to the adsorbed $NO_3^-$ ions, as well as through the TMA ligands.[80,81] A typical photocatalytic reaction consists of an Ar-purged [+] InP QDs (2.5 μM, 0.5 mol %) and $KNO_3$/$KNO_2$ (0.5 mM) reaction mixture in water, (the total volume of the reaction mixture was 3 mL and pH was maintained at 5), which was irradiated for 2 h with visible light (2 x 10 W 450 nm LEDs. The total light intensity falling on cuvette walls was ~200 mW $cm^{-2}$). Subsequently, the amounts of $NO_3^-$ converted and $NH_4^+$ formed were analyzed with ion chromatography (IC) and $^1$H-NMR techniques (**Figures 4a.13, 4a.14**). It must be noted that IC and $^1$H-NMR have been proposed to be the most reliable methods to quantify $NH_4^+$ with negligible interference from the reaction mixture constituents.[82,83]

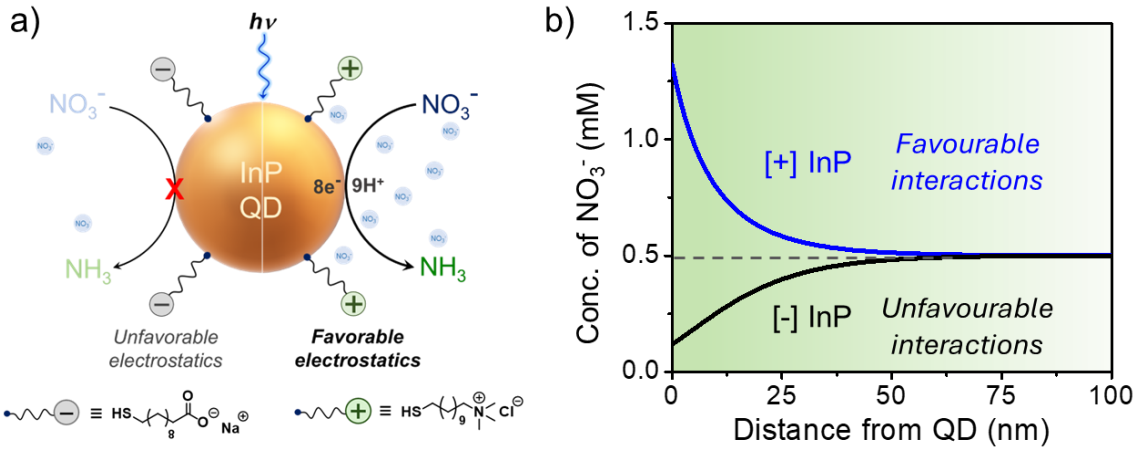


**Figure 4a.6**. a) Schematics showing the regulation of catalyst (InP QD)-reactant ($NO_3^-$) interactions through electrostatic forces emanating from QD surface ligands. A favorable catalyst-reactant interaction between [+] InP and [-] $NO_3^-$ ions enables efficient and selective $NH_4^+$ formation. b) Variation in concentration of $NO_3^-$ calculated as a function of distance from the surface of [+] InP QD and [-] InP QD. The local concentration of $NO_3^-$ was ~2.5 times higher for [+] InP compared to [-] InP QDs.

A series of experiments were performed to optimize the reaction conditions with respect to [+] InP QD photocatalyst, reactant, and time of irradiation. With the increase in the concentration of [+] InP QDs, there was a gradual increase in the $NO_3^-$ conversion as well as $NH_4^+$ formation within 2 h of visible-light irradiation (**Figures 4a.7a, 4a.15**). Even though the maximum $NH_4^+$ formation was obtained with 5.0 μM (1.0 mol %) [+] InP QDs, 2.5 μM (0.5 mol %) of photocatalyst was used in further studies to avoid the excessive use of QDs. The $NH_4^+$ production increased by ~48 %, with an increase in $KNO_3$ from 0.25 mM to 0.5 mM (**Figures 4a.7b, 4a.16, 4a.17**). A further increase in $KNO_3$ concentration did not increase $NH_4^+$ production, which may be due to the saturation of all active sites on [+] InP QD photocatalyst. Likewise, the $NH_4^+$ production saturated after 2 h of visible-light irradiation of the reaction mixture containing of 2.5 μM [+] InP QDs and 0.5 mM $KNO_3$ (**Figures 4a.7c, 4a.18**).

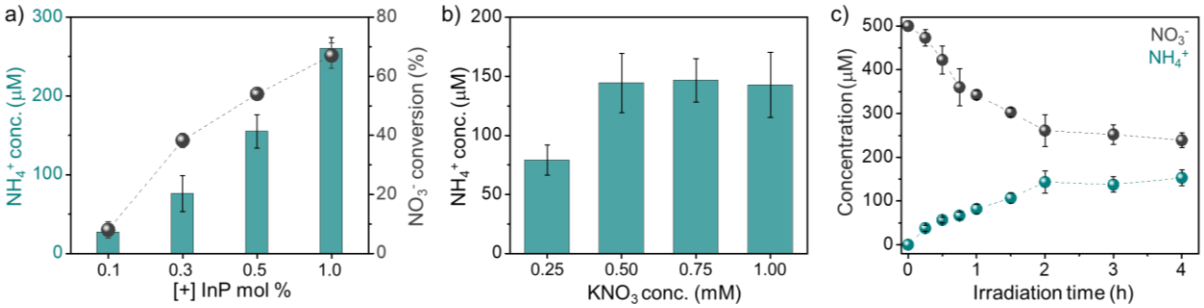


**Figure 4a.7**. Optimization of reaction parameters for photocatalytic reduction of $NO_3^-$ to $NH_4^+$ with visible light. a) Variation in $NH_4^+$ concentration and total $NO_3^-$ conversion as a function of [+] InP amount. [$KNO_3$] = 0.5 mM, t = 2 h. b) Bar diagram summarizing the effect of $KNO_3$ (reactant) concentration on $NH_4^+$ with 0.5 mol % [+] InP QDs under 2 h visible-light irradiation. c) Progress of [+] InP QD photocatalysed reduction of $NO_3^-$ to $NH_4^+$ monitored through IC. $NH_4^+$ concentration increases gradually and attains saturation after 2 h of visible-light irradiation with 0.5 mol % [+] InP QDs and 0.5 mM $KNO_3$. The dotted lines are only to guide the eyes.

Under the optimized condition (2.5 μM, 0.5 mol % [+] InP QDs, 0.5 mM $KNO_3$, and 2 h visible light irradiation), the formation of $NH_4^+$ reached 143±25 μM (~2.5 ppm, ~160 μmol $g^{-1}$) in the aqueous phase (**Figure 4a.8a**). It was observed that only 52.2±7.4 % (261.2±3.7 μM) of $NO_3^-$ has reacted, which could be attributed to the incomplete extraction of photoexcited charge carriers from [+] InP QD photocatalyst, as well as the involvement of other competing reactions, such as hydrogen evolution, as reported in the literature [22,29,30] (**Figure 4a.7c**). The yield of $NH_4^+$ was estimated to be 57.5±9.3 % in

aqueous phase with respect to $NO_3^-$ conversion. A series of control experiments revealed that a negligible amount of $NH_4^+$ was formed in the absence of either light or [+] InP QDs, confirming their necessity for the photocatalytic reduction of $NO_3^-$ to $NH_4^+$ (**Figure 4a.8a, 4a.19**). Further, a characteristic triplet ($J$ = 52 Hz) corresponding to $NH_4^+$ was observed in the $^1$H-NMR study (**Figure 4a.8b**). More importantly, the isotope studies with $^{15}NO_3^-$ provided the ultimate proof for $NO_3^-$ as the sole N-source in the [+] InP QD photocatalysed synthesis of $NH_4^+$ (a characteristic doublet, $J$ = 73 Hz, corresponding to $^{15}NH_4^+$ was observed in the $^1$H-NMR spectrum. **Figure 4a.8b**). Quantitatively similar amounts of $^{14}NH_4^+$ and $^{15}NH_4^+$ were formed from $^{14}NO_3^-$ and $^{15}NO_3^-$ reactants, respectively, which further validates the claim of $NO_3^-$ as the sole N-source for $NH_4^+$ synthesis (**Figures 4a.8c, 4a.20**). Interestingly, the gas phase mass analysis revealed the sole presence of $NH_3$ in the headspace as well (**Figure 4a.8d**). The amount of $NH_3$ in the gas phase was estimated to be 0.37$\pm$0.11 μmoles, resulting in a total 0.80$\pm$0.19 μmol (~6.8 ppm, ~430 μmol $g^{-1}$) of $NH_3$ in aqueous and gas phases (**Figure 4a.21**). This accounts for ~94 % of the total $NO_3^-$ converted, proving the excellent selectivity of [+] InP QD towards $NH_3$ production. The presence of $NH_3$ in the headspace was further validated by performing isotope studies with labeled $^{15}NO_3^-$, where mass signals corresponding to $^{15}NH_3$ were observed (**Figure 4a.8e**).

Interestingly, a mere change of the surface ligands from positively charged [+] TMA to negatively charged [-] 11-mercaptoundecanoic acid ([-] MUA) completely *switched off* the photocatalytic conversion (**Figures 4a.8f, 4a.22**). This is attributed to the strong electrostatic repulsion between similarly charged $NO_3^-$ ions and [-] MUA ligands, which restricts the substrate access to the [-] InP QD photocatalyst surface. As a result, the local concentration of $NO_3^-$ ions will be less near the [-] InP QD surface (**Figure 4a.12**), eventually lowering the probability of the photoexcited electron transfer process. Thus, ligands play a crucial role as gatekeepers in regulating the photocatalytic property of InP QDs towards the reduction of $NO_3^-$/$NO_2^-$ to $NH_3$.

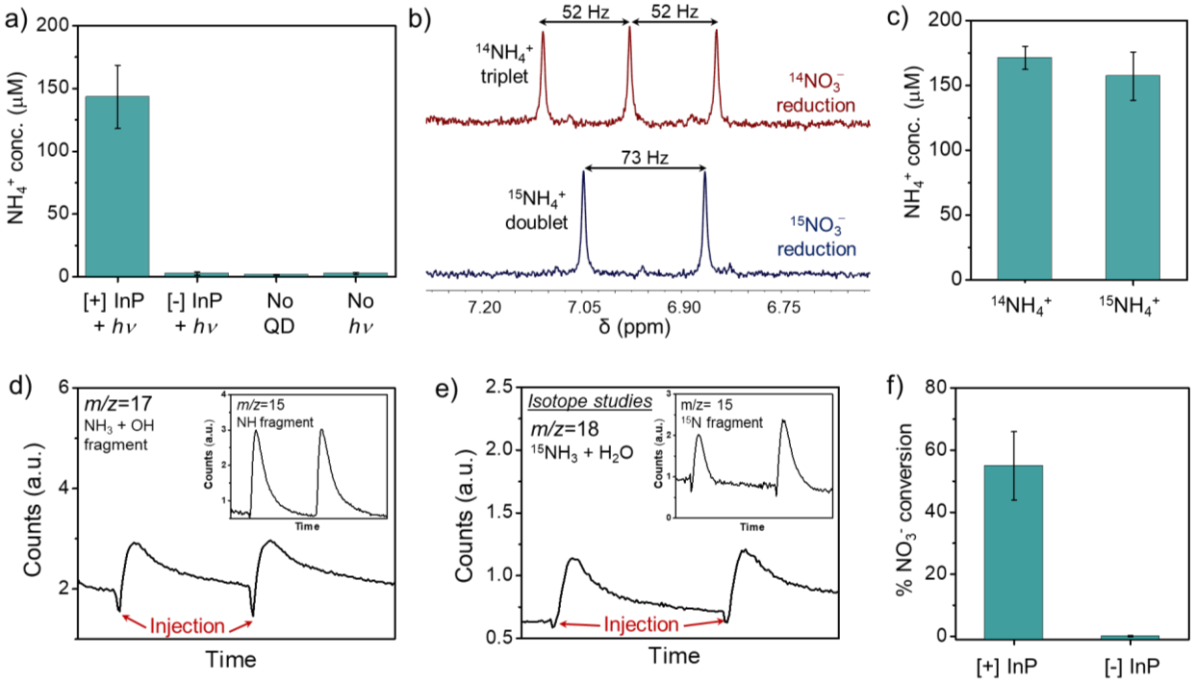


**Figure 4a.8**. InP QDs photocatalysed synthesis of $NH_4^+$ under visible-light irradiation. a) Comparison of $NH_4^+$ formed under different control experiments, clearly confirming the need for both light and [+] InP QDs for the ammonia synthesis. b) $^1$H-NMR spectra of $^{14}NH_4^+$ and $^{15}NH_4^+$ formed after the photocatalytic reduction of $^{14}NO_3^-$ and $^{15}NO_3^-$ by [+] InP QDs, respectively. c) Bar diagram comparing $^{14}NH_4^+$ and $^{15}NH_4^+$ formed from $^{14}NO_3^-$ and $^{15}NO_3^-$, respectively, confirming $NO_3^-$ to be the sole N-source. Mass analysis of the gases in the headspace after photocatalytic reaction performed with d) $^{14}NO_3^-$ and e) $^{15}NO_3^-$ as the N-source, respectively. *m/z* =17 and *m/z* =18 indicate the presence of $^{14}NH_3$ and $^{15}NH_3$ in the gaseous phase from $^{14}NO_3^-$ and $^{15}NO_3^-$, respectively. Inset of d) and e) shows characteristic $^{14}NH$ and $^{15}N$ fragments of $^{14}NH_3$ and $^{15}NH_3$, respectively, with no interference from $H_2O$, confirming the presence of gaseous $NH_3$ in reactor's headspace. f) Proof of favorable catalyst-reactant interactions through a change of QD surface ligands. Bar diagram showing the % $NO_3^-$ conversion with [+] and [-] InP QDs (0.5 mol %) under visible-light illumination (450 nm) for 2 h.

As InP QDs exhibited a broad absorption in the visible region with significant overlap with the solar spectrum (**Figure 4a.9a**), we first tested the photocatalytic activity under different excitation wavelengths. The action spectrum constructed using the apparent quantum yield (AQY) at different excitation wavelengths (580 nm, 532 nm, and 450 nm) followed the ground state absorption profile of [+] InP QDs **(Figures 4a.9b, 4a.23)**, which again confirmed the active participation of InP QDs in the photocatalytic $NH_4^+$ synthesis.[84,85] A decent $NH_4^+$ production across broad visible-light spectrum motivated us to perform the photocatalytic reaction under direct sunlight (**Figure 4a.24**). Notably, we observed 91±30 μM of $NH_4^+$ ($NO_3^-$ conversion = 26.5±7.7 %) within 2 h of exposure of reaction mixture to natural sunlight **(Inset to Figure 4a.9b)**. It must be noted that the

photocatalytic performance under sunlight and LED irradiations cannot be compared, because of the variations associated with the flux, power, chromaticity, and coherence of the two light excitation sources. The sole purpose of performing the photocatalytic reduction under sunlight was to showcase the feasibility in real-world conditions and strengthen the translational aspect of [+] InP QD-based $NH_3$ synthesis. All these experiments conclusively prove the excellent potential of [+] InP QDs for efficient and sustainable $NH_3$ synthesis with visible light. Based on the photocatalysis parameters such as light excitation, reaction time, selectivity, AQY, etc., our photocatalytic system comprising simple [+] InP QDs stands out when compared with the limited literature reports available for the photocatalytic reduction of $NO_3^-$ to $NH_4^+$ (**Table 4a.1**).

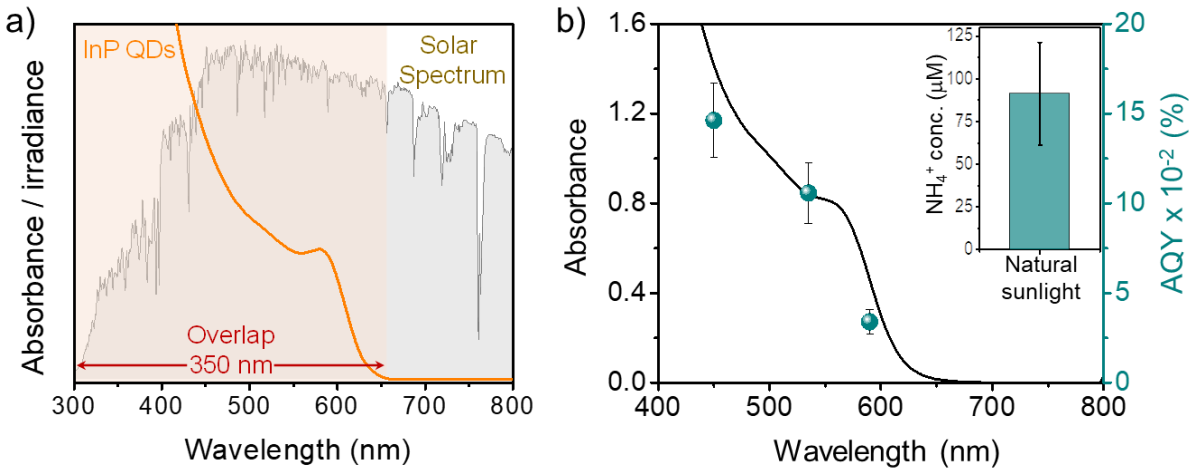


**Figure 4a.9**. a) Spectral overlap between the absorption of [+] InP QDs and the solar spectrum. The reference solar spectrum was adapted from SMARTS v. 2.9.2 (AM 1.5) for the comparison. b) Action spectra showing the variation in the $NH_4^+$ formation with [+] InP QDs as a function of different wavelengths. Inset shows the feasibility of ammonia production with [+] InP QDs in sunlight.

**Comparison with state-of-the-art photocatalyst for $NO_3^-$ to $NH_4^+$ conversion**

**Table 4a.1**: Summary of state-of-the-art photocatalysts available for $NO_3^-$ to $NH_4^+$.

| Photocatalyst | $NH_4^+$ conc. | Catalyst amount | Time | Light source | Hole scavenger | AQY |
|---|---|---|---|---|---|---|
| [+] InP QD *(this work)* | 490 μmol $g^{-1}$ ($NO_3^-$ to $NH_3$) | 19.6 mg | 2 h | Visible light 450 nm | No hole scavengers added | 1.45 % @450 nm |
| | 830 μmol $g^{-1}$ ($NO_2^-$ to $NH_3$) | 19.6 mg | 1 h | | | 3.7 % @450 nm |
| CuPd/$TiO_2$ [22] | 893 μmol $g^{-1}$ | 100 mg | 5 h | UV | MeOH | 0.22 % @365nm |
| JRC-TiO-6 [33] | 384 μmol $g^{-1}$ | 100 mg | 24 h | UV | HCOOH | - |
| BaO-TNS [31] | 89.8 mmol $g^{-1}$ | 1 mg | 1 h | UV | Ethylene glycol | 0.53 % @524.5 nm |
| | 3.1 mmol $g^{-1}$ | | | Simulated solar light | | |
| $Cu_2O$ sub-nanoclusters [47] | 73.8 μmol $h^{-1}$ | 20 mg | 2 h | Full spectrum | HCHO | - |
| CdSe QD [30] | 47 mmol $g^{-1}$ | 2.35 mg | 2 h | Visible light 440 nm | Ascorbic acid + sodium ascorbate | 5.45 % @440 nm |
| $CuInS_2$ QD [30] | 40 mmol $g^{-1}$ | 34 mg | 60 h | Simulated solar light | | - |

## 4a.5. Conclusions

In a step towards green $NH_3$ synthesis, the present work highlights a simple yet efficient photocatalytic system based on InP QDs for the selective reduction of $NO_3^-$ and $NO_2^-$ to $NH_4^+$ under visible-light irradiation at room temperature. A rational design of the core and appropriate surface chemistry of InP QDs was the key to efficient $NH_3$ synthesis. A preferential affinity of N-sources towards surface In atoms and ligands on InP QD

photocatalysts led to the selective and efficient ammonia production under visible-light irradiation at room temperature. We anticipate that the excellent photocatalytic ability and environmentally benign attributes of InP QDs can complement existing methods of green $NH_3$ synthesis. Because there is always a room for improvement, consistent efforts are needed to outcompete the efficiency of the conventional Haber-Bosch process for $NH_3$ synthesis through better design of the photocatalyst as well as in-depth understanding of the parameters dominating the reaction coordinate for the scalable green $NH_3$ production.

## 4a.6. References


1) Green, L. Jr. An Ammonia Energy Vector for the Hydrogen Economy. *Int. J. Hydrogen Energy* **1982**, *7*, 355-359.

2) Erisman, J. W.; Sutton, M. A.; Galloway, J.; Klimont, Z.; Winiwarter, W. How a Century of Ammonia Synthesis Changed the World. *Nat. Geosci.* **2008**, *1*, 636-639.

3) Lim, J.; Fernández, C. A.; Lee, S. W.; Hatzell, M. C. Ammonia and Nitric Acid Demands for Fertilizer Use in 2050. *ACS Energy Lett.* **2021**, *6*, 3676-3685.

4) Guo, J.; Chen. P. Catalyst: $NH_3$ as an Energy Carrier. *Chem* **2017**, *3*, 709-712.

5) MacFarlane, D. R.; Cherepanov, P. V.; Choi, J.; Suryanto, B. H. R.; Hodgetts, R. Y.; Bakker, J. M.; Vallana, F. M. F.; Simonov, A. N. A Roadmap to the Ammonia Economy. *Joule* **2020**, *4*, 1186-1205.

6) Smil, V. Detonator of the Population Explosion. *Nature* **1999**, *400*, 415.

7) Giddey, S.; Badwal, S. P. S.; Munnings, C.; Dolan, M. Ammonia as a Renewable Energy Transportation Media. *ACS Sustainable Chem. Eng.* **2017**, *5*, 10231-10239.

8) Zhao, Y.; Setzler, B. P.; Wang, J.; Nash, J.; Wang, T.; Xu, B.; Yan, Y. An Efficient Direct Ammonia Fuel Cell for Affordable Carbon-Neutral Transportation. *Joule* **2019**, *3*, 2472-2484.

9) David, W. I. F.; Agnew, G. D.; Bañares-Alcántara, R.; Barth, J.; Hansen, J. B.; Bréquigny, P.; de Joannon, M.; Stott, S. F.; Stott, C. F.; Guati-Rojo, A.; Hatzell, M.;

MacFarlane, D. R.; Makepeace, J. W.; Mastorakos, E.; Mauss, F.; Medford, A.; Mounaïm-Rousselle, C.; Nowicki, D. A.; Picciani, M. A.; Postma, R. S.; Rouwenhorst, K. H. R.; Sabia, P.; Salmon, N.; Simonov, A. N.; Smith, C.; Torrente-Murciano, L.; Valera-Medina, A. 2023 Roadmap on Ammonia as a Carbon-Free Fuel. *J. Phys. Energy* **2024**, *6*, 021501.

10) Appl, M. Ammonia. In Ullmann's Encyclopedia of Industrial Chemistry; Wiley-VCH Verlag GmbH & Co. KGaA: Weinheim, 2006 DOI: 10.1002/14356007.a02_143.pub2

11) Haber, F. in *Nobel Lectures in Chemistry 1901-1921*. Amsterdam: Elsevier, 1966

12) Haber, F.; Le Rossignol, R. Production of Ammonia. US1202995A, **1909**

13) Bosch, C.; Mittasch, A.; Wolf, H.; Stern, G. Catalytic Agent for Use in Producing Ammonia. US1148570A, **1910**.

14) International Energy Agency. Technology Roadmap: Energy and GHG Reductions in the Chemical Industry via Catalytic Processes. *International Energy Agency (IEA)* **2013**. https://www.iea.org/reports/technology-roadmap-energy-and-ghg-reductions-in-the-chemical-industry-via-catalytic-processes

15) International Energy Agency. Ammonia Technology Roadmap: Towards More Sustainable Nitrogen Fertiliser Production. *International Energy Agency (IEA)* **2021**. https://www.iea.org/reports/ammonia-technology-roadmap

16) Medford, A. J.; Hatzell, M. C. Photon-Driven Nitrogen Fixation: Current Progress, Thermodynamic Considerations, and Future Outlook. *ACS Catal.* **2017**, *7*, 2624-2643.

17) Chen, J. G.; Crooks, R. M.; Seefeldt, L. C.; Bren, K. L.; Bullock, R. M.; Darensbourg, M. Y.; Holland, P. L.; Hoffman, B.; Janik, M. J.; Jones, A. K.; Kanatzidis, M. G.; King, P.; Lancaster, K. M.; Lymar, S. V.; Pfromm, P.; Schneider, W. F.; Schrock, R. R. Beyond Fossil Fuel–Driven Nitrogen Transformations. *Science* **2018**, *360*, eaar6611.

18) Hatzell, M. C. The Colors of Ammonia. *ACS Energy Lett.* **2024**, *9*, 2920-2921.

19) Wang, L.; Xia, M.; Wang, H.; Huang, K.; Qian, C.; Maravelias, C. T.; Ozin, G. A. Greening Ammonia Toward the Solar Ammonia Refinery. *Joule* **2018**, *2*, 1055-1074.

20) Lee, B.; Winter, L. R.; Lee, H.; Lim, D.; Lim, H.; Elimelech, M. Pathways to a Green Ammonia Future. *ACS Energy Lett.* **2022**, *7*, 3031-3038.

21) Oshikiri, T.; Ueno, K.; Misawa, H. Selective Dinitrogen Conversion to Ammonia Using Water and Visible Light through Plasmon-induced Charge Separation. *Angew. Chem., Int. Ed.* **2016**, *55*, 3942-3946.

22) Yamauchi, M.; Abe, R.; Tsukuda, T.; Kato, K.; Takata, M. Highly Selective Ammonia Synthesis from Nitrate with Photocatalytically Generated Hydrogen on CuPd/$TiO_2$. *J. Am. Chem. Soc.* **2011**, *133*, 1150-1152.

23) Brown, K. A.; Harris, D. F.; Wilker, M. B.; Rasmussen, A.; Khadka, N.; Hamby, H.; Keable, S.; Dukovic, G.; Peters, J. W.; Seefeldt, L. C.; King, P. W. Light-Driven Dinitrogen Reduction Catalyzed by a CdS:Nitrogenase MoFe Protein Biohybrid. *Science* **2016**, *352*, 448-450.

24) Shi, R.; Zhao, Y.; Waterhouse, G. I. N.; Zhang, S.; Zhang, T. Defect Engineering in Photocatalytic Nitrogen Fixation. *ACS Catal.* **2019**, *9*, 9739-9750.

25) Hu, C.; Chen, X.; Jin, J.; Han, Y.; Chen, S.; Ju, H.; Cai, J.; Qiu, Y.; Gao, C.; Wang, C.; Qi, Z.; Long, R.; Song, L.; Liu, Z.; Xiong, Y. Surface Plasmon Enabling Nitrogen Fixation in Pure Water through a Dissociative Mechanism under Mild Conditions. *J. Am. Chem. Soc.* **2019**, *141*, 7807-7814.

26) Grant, W. D.; Long, P. E. The Nitrogen Cycle. *In Environmental Microbiology. Tertiary Level Biology*, Springer, Boston, MA. Ch. 6, **1981**.

27) Brittain, T.; Blackmore, R.; Greenwood, C.; Thomson, A. J. Bacterial Nitrite-Reducing Enzymes. *Eur. J. Biochem.* **1992**, *209*, 793-802.

28) Maia, L. B.; Moura, J. J. G. How Biology Handles Nitrite. *Chem. Rev.* **2014**, *114*, 5273-5357.

29) Contreras, E.; Nixon, R.; Litts, C.; Zhang, W.; Alcorn, F. M.; Jain, P. K. Plasmon-Assisted Ammonia Electrosynthesis. *J. Am. Chem. Soc.* **2022**, *144*, 10743-10751.

30) Meng, S. -L.; Li, J. -H.; Ye, C.; Yin, Y. -L.; Zhang, X. -L; Zhang, C.; Li, X. -B.; Tung, C. -H.; Wu, L. -Z. Concurrent Ammonia Synthesis and Alcohol Oxidation Boosted by Glutathione-Capped Quantum Dots Under Visible Light. *Adv. Mater.* **2024**, *36*, 2311982.

31) Li, J.; Chen, R.; Wang, J.; Zhou, Y.; Yang, G.; Dong, F. Subnanometric Alkaline-Earth Oxide Clusters for Sustainable Nitrate to Ammonia Photosynthesis. *Nat. Commun.* **2022**, *13*, 1098.

32) Doudrick, K.; Yang, T.; Hristovski, K.; Westerhoff, P. Photocatalytic Nitrate Reduction in Water: Managing the Hole Scavenger and Reaction By-Product Selectivity. *Appl. Catal., B* **2013**, *136*, 40-47.

33) Hirakawa, H.; Hashimoto, M.; Shiraishi, Y.; Hirai, T. Selective Nitrate-to-Ammonia Transformation on Surface Defects of Titanium Dioxide Photocatalysts. *ACS Catal.* **2017**, *7*, 3713-3720.

34) Yang, W.; Wang, J.; Chen, R.; Xiao, L.; Shen, S.; Li, J.; Dong, F. Reaction Mechanism and Selectivity Regulation of Photocatalytic Nitrate Reduction for Wastewater Purification: Progress and Challenges. *J. Mater. Chem. A* **2022**, *10*, 17357-17376.

35) Bogaerts, A.; Neyts, E. C. Plasma Technology: An Emerging Technology for Energy Storage. *ACS Energy Lett.* **2018**, *3*, 1013-1027.

36) Wakida, F. T.; Lerner, D. N. Non-Agricultural Sources of Groundwater Nitrate: A Review and Case Study. *Water Res.* **2005**, *39*, 3-16.

37) Heck, K. N.; Garcia-Segura, S.; Westerhoff, P.; Wong, M. S. Catalytic Converters for Water Treatment. *Acc. Chem. Res.* **2019**, *52*, 906-915.

38) Wei, L.; Liu, D. -J.; Rosales, B. A.; Evans, J. W.; Vela, J. Mild and Selective Hydrogenation of Nitrate to Ammonia in the Absence of Noble Metals. *ACS Catal.* **2020**, *10*, 3618-3628.

39) Comer, B. M.; Fuentes, P.; Dimkpa, C. O.; Liu, Y.-H.; Fernandez, C. A.; Arora, P.; Realff, M.; Singh, U.; Hatzell, M. C.; Medford, A. J. Prospects and Challenges for Solar Fertilizers. *Joule* **2019**, *3*, 1578-1605.

40) Favero, S.; Titirici, M.; Stephens, I. E. L. Toward Photovalorization of Waste at Scale? *Joule* **2024**, *8*, 1880-1883.

41) Halmann, M.; Zuckerman, K. Nitrite Ion Reduction to Ammonia in Illuminated Aqueous Suspensions of Powdered Semiconductors in Alkaline Sulphide Solutions. *J. Chem. Soc., Chem. Commun.* **1986**, *6*, 455-457.

42) Kudo, A.; Domen, K.; Maruya, K.; Onishi, T. Photocatalytic Reduction of $NO_3^-$ to form $NH_3$ over Pt-$TiO_2$. *Chem. Lett.* **1987**, *16*, 1019-1022.

43) Ranjit, K. T.; Krishnamoorthy, R.; Viswanathan B. Photocatalytic Reduction of Nitrite and Nitrate on ZnS. *J. Photochem. Photobio. A- Chemistry* **1994**, *81*, 55-58.

44) Ranjit, K. T.; Krishnamoorthy, R.; Varadarajan, T. K.; Viswanathan B. Photocatalytic Reduction of Nitrite on CdS. *J. Photochem. Photobio. A- Chemistry* **1995**, *86*, 185-189.

45) Ranjit, K. T.; Varadarajan, T. K.; Viswanathan B. Photocatalytic Reduction of Nitrite and Nitrate Ions to Ammonia on Ru/$TiO_2$ Catalysts. *J. Photochem. Photobio. A- Chemistry* **1995**, *89*, 67-68.

46) Ranjit, K. T.; Viswanathan B. Photocatalytic Reduction of Nitrite and Nitrate Ions Over Doped $TiO_2$ Catalysts. *J. Photochem. Photobio. A- Chemistry* **1997**, *107*, 215-220.

47) Li, J.; Chen, R.; Wang, J.; Wang, K.; Zhou, Y.; Xing, M.; Dong, F. Dynamic In Situ Formation of $Cu_2O$ Sub-Nanoclusters Through Photoinduced Pseudo-Fehling's Reaction for Selective and Efficient Nitrate-to-Ammonia Photosynthesis. *Angew. Chem., Int. Ed.* **2024**, *63*, e202317575.

48) Shiraishi, Y.; Akiyama, S.; Hiramatsu, W.; Adachi, K.; Ichikawa, S.; Hirai, T. Sunlight-Driven Nitrate-to-Ammonia Reduction with Water by Iron Oxyhydroxide Photocatalysts. *JACS Au* **2024**, *4*, 1863-1874.

49) Zhang, C.; Li, J.; Chen, R.; Shen, S.; Wang, J.; Sun, Y.; Dong, F. $NH_3$ Synthesis from $N_1$ Compounds by Photocatalytic Technology: Promotion Mechanism, Reaction Pathways, and Efficiency Evaluation Criteria. *ACS Catal.* **2024**, *14*, 15721-15742.

50) Hiramatsu, W.; Shiraishi, Y.; Ichikawa, S.; Tanaka, S.; Kawada, Y.; Hiraiwa, C.; Hirai, T. Surface Oxygen Vacancies on Copper-Doped Titanium Dioxide for Photocatalytic Nitrate-to-Ammonia Reduction. *J. Am. Chem. Soc.* **2025**, *147*, 1968-1979.

51) Sá, J.; Agüera, C. A.; Gross, S.; Anderson, J. A. Photocatalytic Nitrate Reduction over Metal Modified $TiO_2$. *Appl. Catal. B: Environmental* **2009**, *85*, 192-200.

52) Anderson, J. A. Photocatalytic Nitrate Reduction Over Au/$TiO_2$. *Catal. Today* **2011**, *175*, 316-321.

53) Yue, M.; Wang, R.; Ma, B.; Cong, R.; Gao, W.; Yang, T. Superior Performance of $CuInS_2$ for Photocatalytic Water Treatment: Full Conversion of Highly Stable Nitrate Ions into Harmless $N_2$ Under Visible Light. *Catal. Sci. Technol.* **2016**, *6*, 8300-8308.

54) Ren, H. -T.; Jia, S. -Y.; Zou, J. -J.; Wu, S. -H.; Han, X.; A Facile Preparation of $Ag_2O$/P25 Photocatalyst for Selective Reduction of Nitrate. *Appl. Catal. B: Environmental* **2015**, 176, 53-61.

55) Nirmal, M.; Brus, L. Luminescence Photophysics in Semiconductor Nanocrystals. *Acc. Chem. Res.* **1999**, *32*, 407-414.

56) Alivisatos, A. P. Perspectives on the Physical Chemistry of Semiconductor Nanocrystals. *J. Phys. Chem.* **1996**, *100*, 13226-13239.

57) Dolzhnikov, D. S.; Zhang, H.; Jang, J.; Son, J. S.; Panthani, M. G.; Shibata, T.; Chattopadhyay, S.; Talapin, D. V. Composition-Matched Molecular "Solders" for Semiconductors. *Science* **2015**, *347*, 425- 428.

58) Weiss, E. A. Designing the Surfaces of Semiconductor Quantum Dots for Colloidal Photocatalysis. *ACS Energy Lett.* **2017**, *2*, 1005-1013.

59) Heath, J. R. Covalency in Semiconductor Quantum Dots. *Chem. Soc. Rev.* **1998**, *27*, 65-71.

60) Thomas, A.; Sandeep, K.; Somasundaran, S. M.; Thomas, K. G. How Trap States Affect Charge Carrier Dynamics of CdSe and InP Quantum Dots: Visualization through Complexation with Viologen. *ACS Energy Lett.* **2018**, *3*, 2368-2375.

61) Dümbgen, K. C.; Zito, J.; Infante, I.; Hens, Z. Shape, Electronic Structure, and Trap States in Indium Phosphide Quantum Dots. *Chem. Mater.* **2021**, *33*, 6885-6896.

62) Jang, D.; Han, Y.; Baek, S.; Kim, J. Theoretical Comparison of The Energies and Wave Functions of the Electron and Hole States Between CdSe- and InP-Based Core/Shell/Shell Quantum Dots: Effect of the Bandgap Energy of the Core Material on the Emission Spectrum. *Opt. Mater. Express* **2019**, *9*, 1257-1270.

63) Yu, S.; Fan, X.-B.; Wang, X.; Li, J.; Zhang, Q.; Xia, A.; Wei, S.; Wu, L.-Z.; Zhou, Y.; Patzke, G. R. Efficient Photocatalytic Hydrogen Evolution with Ligand Engineered All-Inorganic InP and InP/ZnS Colloidal Quantum Dots. *Nat. Commun.* **2018**, *9*, 4009.

64) Homer, M. K.; Larson, H. C.; Dixon, G. J.; Miura-Stempel, E.; Armstong, N. R.; Cossairt, B. M. Extremely Long-Lived Charge Donor States Formed by Visible Irradiation of Quantum Dots. *ACS Nano* **2024**, *18*, 24591-24602.

65) Dümbgen, K. C.; Leemans, J.; De Roo, V.; Minjauw, M.; Detavernier, C.; Hens, Z. Surface Chemistry of InP Quantum Dots, Amine–Halide Co-Passivation, and Binding of Z-Type Ligands. *Chem. Mater.* **2023**, *35*, 1037-1046.

66) Devatha, G.; Rao, A.; Roy, S.; Pillai, P. P. Förster Resonance Energy Transfer Regulated Multicolor Photopatterning from Single Quantum Dot Nanohybrid Films. *ACS Energy Lett.* **2019**, *4*, 1710-1716.

67) Chakraborty, I. N.; Roy, P.; Rao, A.; Devatha, G.; Roy, S.; Pillai, P. P. The Unconventional Role of Surface Ligands in Dictating the Light Harvesting Properties of Quantum Dots. *J. Mater. Chem. A* **2021**, *9*, 7422-7457.

68) Guo, J.; Suástegui, M.; Sakimoto, K. K.; Moody, V. M.; Xiao, G.; Nocera, D. G.; Joshi, N. S. Light-Driven Fine Chemical Production in Yeast Biohybrids. *Science* **2018**, *362*, 813-816.

69) Chakraborty, I. N.; Roy, S.; Devatha, G.; Rao, A.; Pillai, P. P. InP/ZnS Quantum Dots as Efficient Visible-Light Photocatalysts for Redox and Carbon-Carbon Coupling Reactions. *Chem. Mater.* **2019**, *31*, 2258-2262.

70) Chakraborty, I. N.; Roy, P.; Pillai, P. P. Visible Light-Mediated Quantum Dot Photocatalysis Enables Olefination Reactions at Room Temperature. *ACS Catal.* **2023**, *13*, 7331-7338.

71) Yin, H.; Mao, X.; Bell, S.; Golberg, D.; Du, A. Transition-Metal-Free, Pure p-Block Alloy Electrocatalysts for the Highly Efficient Nitrate Reduction to Ammonia. *Chem. Mater.* **2023**, *35*, 2884-2891.

72) Bharali, D. J.; Lucey, D. W.; Jayakumar, H.; Pudavar, H. E.; Prasad, P. N. Folate-Receptor-Mediated Delivery of InP Quantum Dots for Bioimaging Using Confocal and Two-Photon Microscopy. *J. Am. Chem. Soc.* **2005**, *127*, 11364-11371.

73) Devatha, G.; Roy, S.; Rao, A.; Mallick, A.; Basu, S.; Pillai, P. P. Electrostatically Driven Resonance Energy Transfer in "Cationic" Biocompatible Indium Phosphide Quantum Dots. *Chem. Sci.* **2017**, *8*, 3879-3884.

74) Roy, P.; Virmani, M.; Pillai, P. P. Blue-Emitting InP Quantum Dots Participate in an Efficient Resonance Energy Transfer Process in Water. *Chem. Sci.* **2023**, *14*, 5167-5176.

75) Tessier, M. D.; Dupont, D.; De Nolf, K.; De Roo, J.; Hens, Z. Economic and Size-Tunable Synthesis of InP/ZnE (E = S,Se) Colloidal Quantum Dots. *Chem. Mater.* **2015**, *27*, 4893-4898.

76) Tessier, M. D.; De Nolf, K.; Dupont, D.; Sinnaeve, D.; De Roo, J.; Hens, Z. Aminophosphines: A Double Role in the Synthesis of Colloidal Indium Phosphide Quantum Dots. *J. Am. Chem. Soc.* **2016**, *138*, 5923-5929.

77) Roy, S.; Rao, A.; Devatha, G.; Pillai, P. P. Revealing the Role of Electrostatics in Gold-Nanoparticle-Catalyzed Reduction of Charged Substrates. *ACS Catal.* **2017**, *7*, 7141-7145.

78) Roy, S.; Jain, V.; Kashyap, R. K.; Rao, A.; Pillai, P. P. Electrostatically Driven Multielectron Transfer for the Photocatalytic Regeneration of Nicotinamide Cofactor. *ACS Catal.* **2020**, *10*, 5522-5528.

79) Brown, P. R.; Kim, D.; Lunt, R. R.; Zhao, N.; Bawendi, M. G.; Grossman, J. C.; Bulović, V. Energy Level Modification in Lead Sulfide Quantum Dot Thin Films through Ligand Exchange. *ACS Nano* **2014**, *8*, 5863-5872.

80) Kim, Y.; Wilson, A. J.; Jain, P. K. The Nature of Plasmonically Assisted Hot-Electron Transfer in a Donor–Bridge–Acceptor Complex. *ACS Catal.* **2017**, *7*, 4360-4365.

81) Roy, S.; Roy, S.; Rao, A.; Devatha, G.; Pillai, P. P. Precise Nanoparticle–Reactant Interaction Outplays Ligand Poisoning in Visible-Light Photocatalysis. *Chem. Mater.* **2018**, *30*, 8415-8419.

82) Zhao, Y.; Shi, R.; Bian, X.; Zhou, C.; Zhao, Y.; Zhang, S.; Wu, F.; Waterhouse, G. I. N.; Wu, L. -Z.; Tung, C. -H.; Zhang, T. Ammonia Detection Methods in Photocatalytic and Electrocatalytic Experiments: How to Improve the Reliability of $NH_3$ Production Rates? *Adv. Sci*. **2019**, *6*, 1802109.

83) Huang, P. -W.; Hatzell, M. C. Prospects and Good Experimental Practices for Photocatalytic Ammonia Synthesis. *Nat. Commun.* **2022**, *13*, 7908.

84) Tian, Y.; Tatsuma, T. Mechanisms and Applications of Plasmon-Induced Charge Separation at $TiO_2$ Films Loaded with Gold Nanoparticles. *J. Am. Chem. Soc.* **2005**, *127*, 7632-7637.

85) Robel, I.; Subramanian, V.; Kuno, M.; Kamat, P. V. Quantum Dot Solar Cells. Harvesting Light Energy with CdSe Nanocrystals Molecularly Linked to Mesoscopic $TiO_2$ Films. *J. Am. Chem. Soc.* **2006**, *128*, 2385-2393.

86) Israelachvili, J. N. *Intermolecular and Surface Forces (Third Edition)*; Academic Press: Amsterdam, **2011**.

87) Tabeling, P. *Introduction to Microfluidics*; Oxford University Press: Oxford, **2005**.

# 4a.7. Appendix

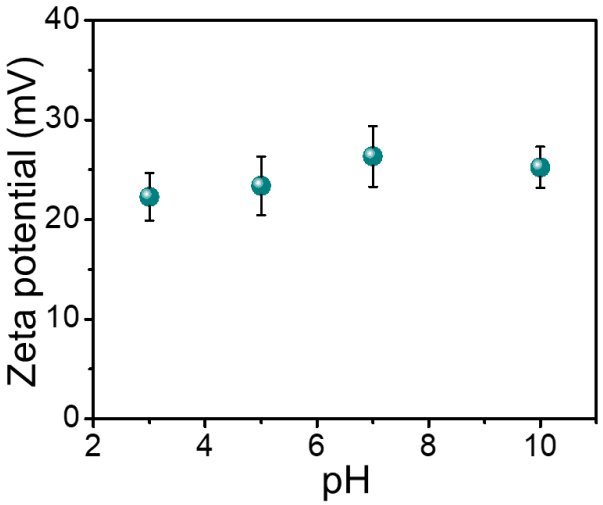


**Figure 4a.10**. Zeta potential of [+] InP QDs as a function of pH. A negligible change in zeta potential was observed for a wide pH range (3-10).

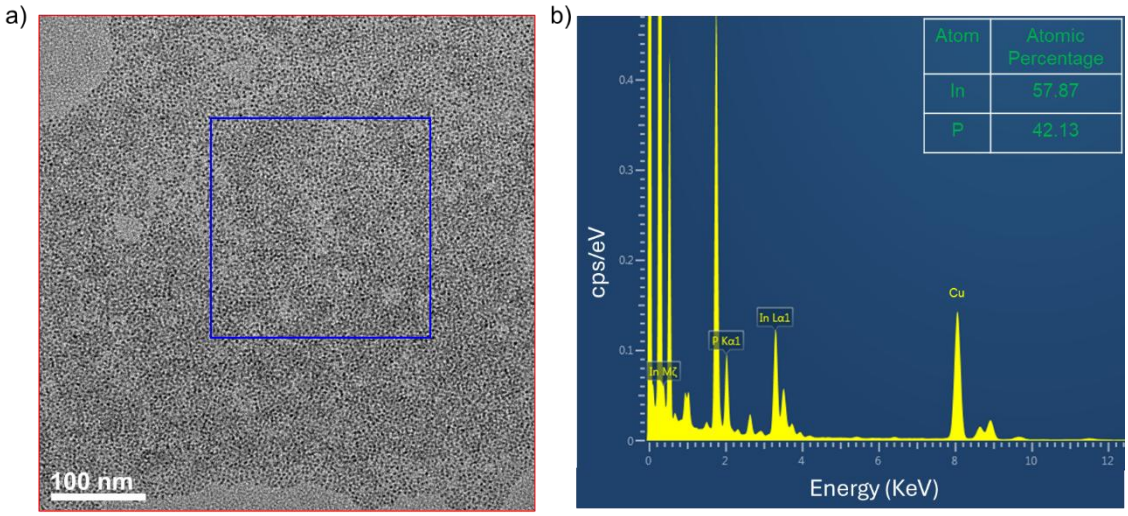


**Figure 4a.11.** a) Representative TEM image used for EDAX analysis. The area enclosed in blue box was analyzed to record EDAX spectrum. b) Corresponding EDAX spectrum of [+] InP QD. Inset shows the atomic percentages for In and P.

**Microenvironment modulation through surface ligands of InP QD**

**Concentration profiles of $K^+$ and $NO_3^-$ ions**

The concentrations of $K^+$ and $NO_3^-$ in the diffused layer of [+] InP and [-] InP QDs will follow the Boltzmann distribution, and is given by the following equation:[86,87]

$$c_{\pm} = c_0 \exp\left(\mp \frac{ze\varphi}{k_B T}\right) \qquad (\mathbf{4a.3})$$

where,

$c_+$ and $c_-$ are the concentrations of $K^+$ and $NO_3^-$ respectively,

$c_0$ is the concentration of $KNO_3$ in the bulk, 0.5 mM,

$z$ is the valency of the ions,

$\phi$ is the surface potential at a given point, and

$k_B T$ is the thermal energy

To find out the concentration profile as a function of distance from charged InP QD surface, we need the variation in $\phi$ as a function of distance. The variation in $\phi$ as a function of distance (x) in the diffused layer is given by the Poisson Boltzmann equation as follows: [86,87]

$$\nabla^2 \varphi = -\frac{\rho}{\epsilon} \qquad (\mathbf{4a.4})$$

Here, ρ is the charge density, and ε is the dielectric constant of the medium.

To compute variation of $\phi$ in x-direction, the above equation transforms into:

$$\frac{d^2\varphi}{dx^2} = -\frac{\rho}{\epsilon} = -\frac{zF(c_+ - c_-)}{\epsilon} \qquad (\mathbf{4a.5})$$

Upon substituting the value of $c_+$ and $c_-$ from (4a.1) into (4a.3), we get

$$\frac{d^2\varphi}{dx^2} = c_0 zF\epsilon\left[\exp\left(\frac{ze\varphi}{k_B T}\right) - exp\left(-\frac{ze\varphi}{k_B T}\right)\right] = \frac{2c_0 zF}{\epsilon} sinh\left(\frac{ze\varphi}{k_B T}\right) \qquad (\mathbf{4a.6})$$

Applying the boundary conditions, we get

$\varphi\ (x = 0) = \zeta$ and $\varphi\ (x = \infty) = 0$

Here, $\zeta$ is the zeta potential which is equal to + 25 mV and -37 mV for [+] InP and [-] InP QDs, respectively.

Applying Debye-Huckel approximation for dilute solution, $\left(\frac{ze\varphi}{k_B T}\right) \ll 1$, **eq. 4a.6** can be rewritten as:

$$\frac{d^2\varphi}{dx^2} = \frac{c_0 zF}{\epsilon}\left[\left(1 + \frac{ze\varphi}{k_B T}\right) - \left(1 - \frac{ze\varphi}{k_B T}\right)\right]$$

$$= \frac{c_0 zF}{\epsilon}\left[\frac{2ze\varphi}{k_B T}\right]$$

$$= \frac{2(ze)^2 N_a c_0 \varphi}{\epsilon k_B T}$$

$$= \frac{\varphi}{\kappa^2} \qquad (\mathbf{4a.7})$$

where, κ is the Debye length.

Solving (4a.5) yields the final **eq. 4a.8**,

$$\varphi = \zeta\ exp\left(-\frac{x}{\kappa}\right) \qquad (\mathbf{4a.8})$$

The concentration profiles as a function of distance were computed using **eq. 4a.3** and **eq. 4a.8**. The computed graphs are shown in **Figure 4a.12**. The concentration profiles clearly show the channeling effect in [+] InP QDs due to favourable electrostatic interaction between [+] InP QD and [-] $NO_3^-$ ions. The enhanced local concentration of [-] $NO_3^-$ ions enhances the probability of the charge transfer step from photoexcited [+] InP QDs.

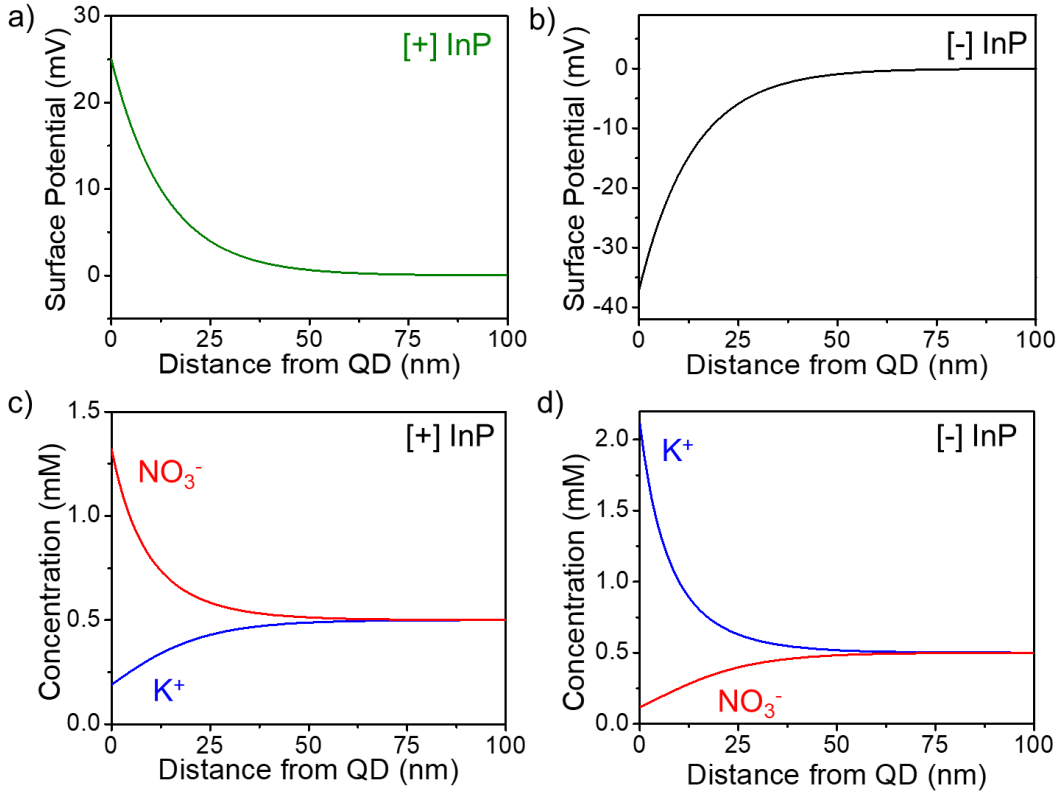


**Figure 4a.12.** Variation in the surface potential as a function of distance from the surface of a) [+] InP QD and b) [-] InP QD. Variation in concentration of $NO_3^-$ and $K^+$ as a function of distance from the surface of c) [+] InP QD and d) [-] InP QD.

### Calibration curves for estimation of reaction yield

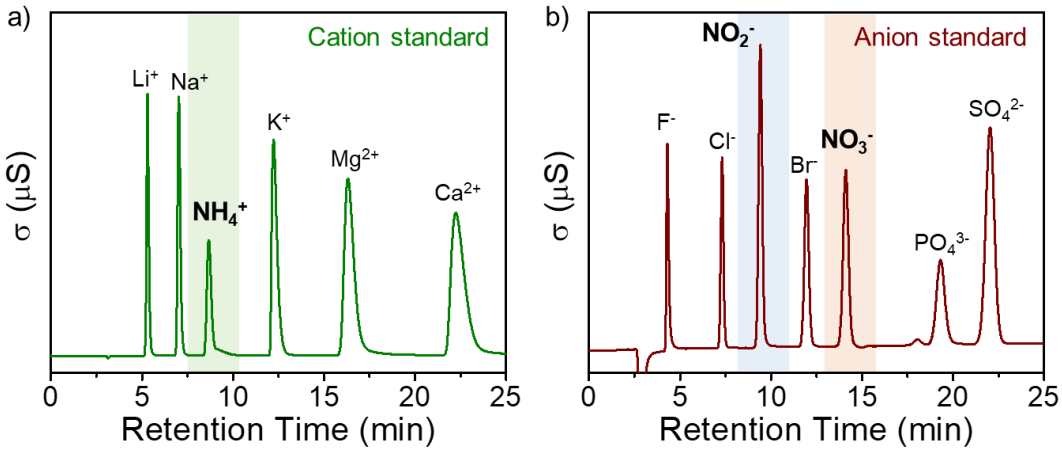


**Figure 4a.13**. Representative chromatograms of a) Dionex six cation standard and b) Dionex seven anion standard solution. Signals at ~8.5 min in the cation chromatogram and at ~9.5 min and ~14.5 min in the anion chromatogram correspond to $NH_4^+$, $NO_2^-$, and $NO_3^-$, respectively.

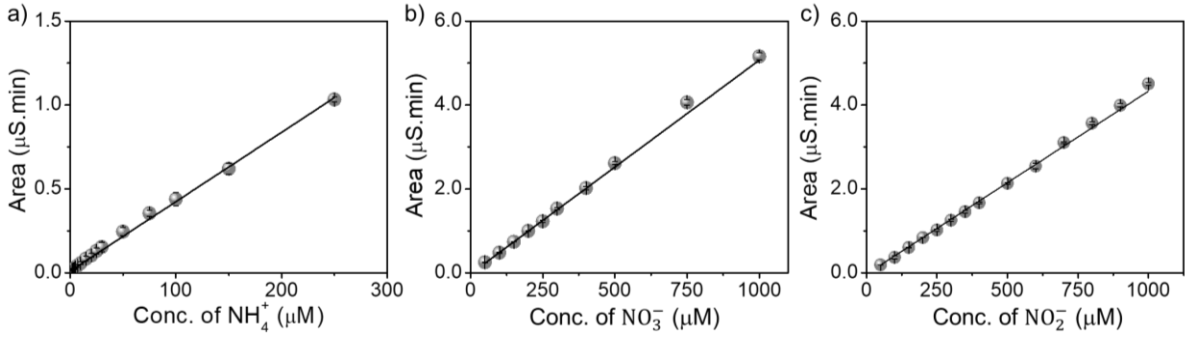


**Figure 4a.14**. Standard curves for a) $NH_4^+$, b) $NO_3^-$, and c) $NO_2^-$ detection with ion chromatography, prepared with different concentrations of $NH_4Cl$ (0-250 μM), $KNO_3$ (0-1000 μM), and $KNO_2$ (0-1000 μM), respectively.

## Optimization of reaction parameters

Concentration of [+] InP

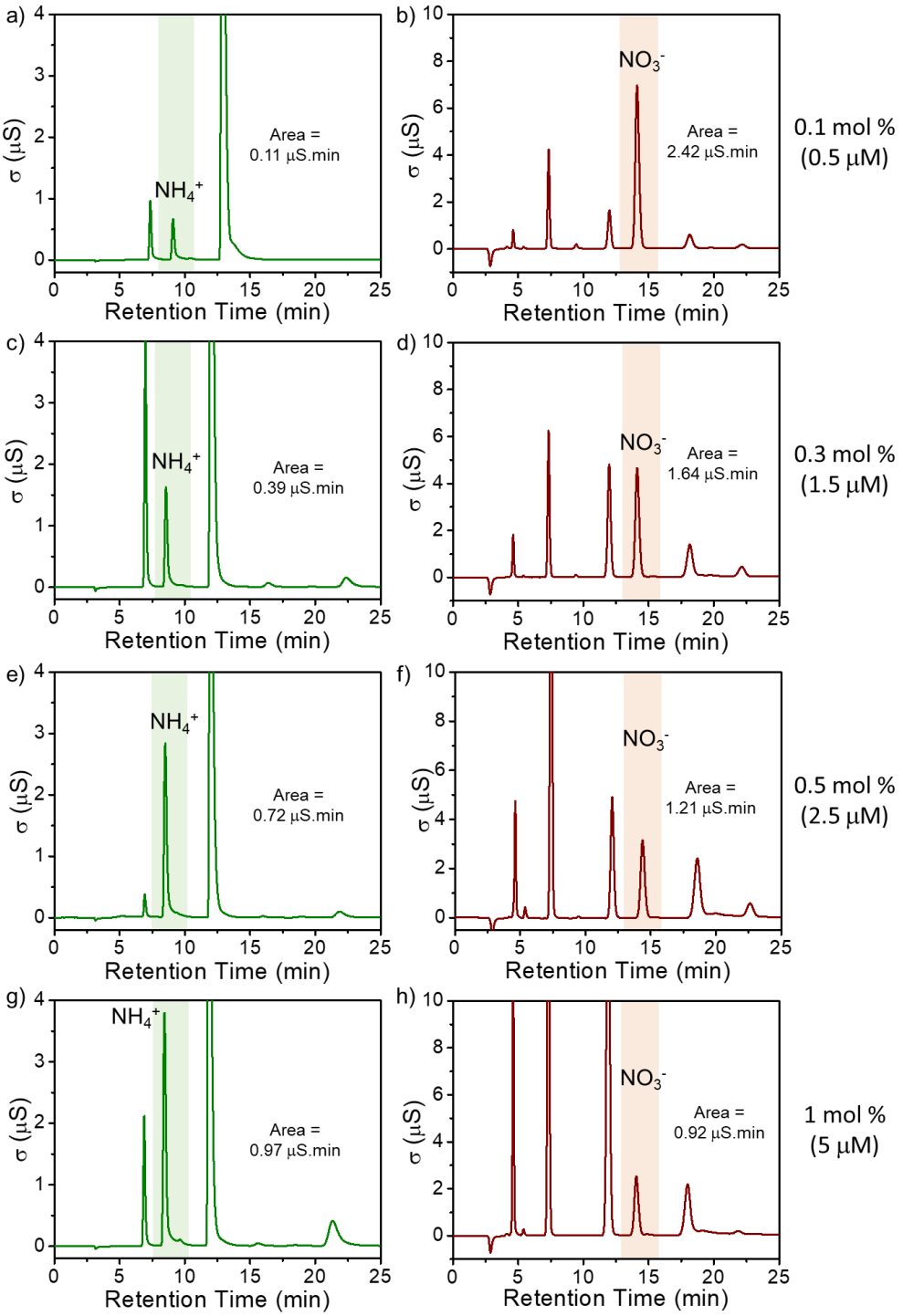


**Figure 4a.15**. Cation (a,c,e,g) and anion (b,d,f,h) chromatograms for photocatalytic reactions performed with different concentrations of [+] InP QDs. a,b) 0.1 mol %, c,d) 0.3 mol %, e,f) 0.5 mol %, and g,h) 1 mol % of [+] InP QDs.

KNO$_3$ concentration

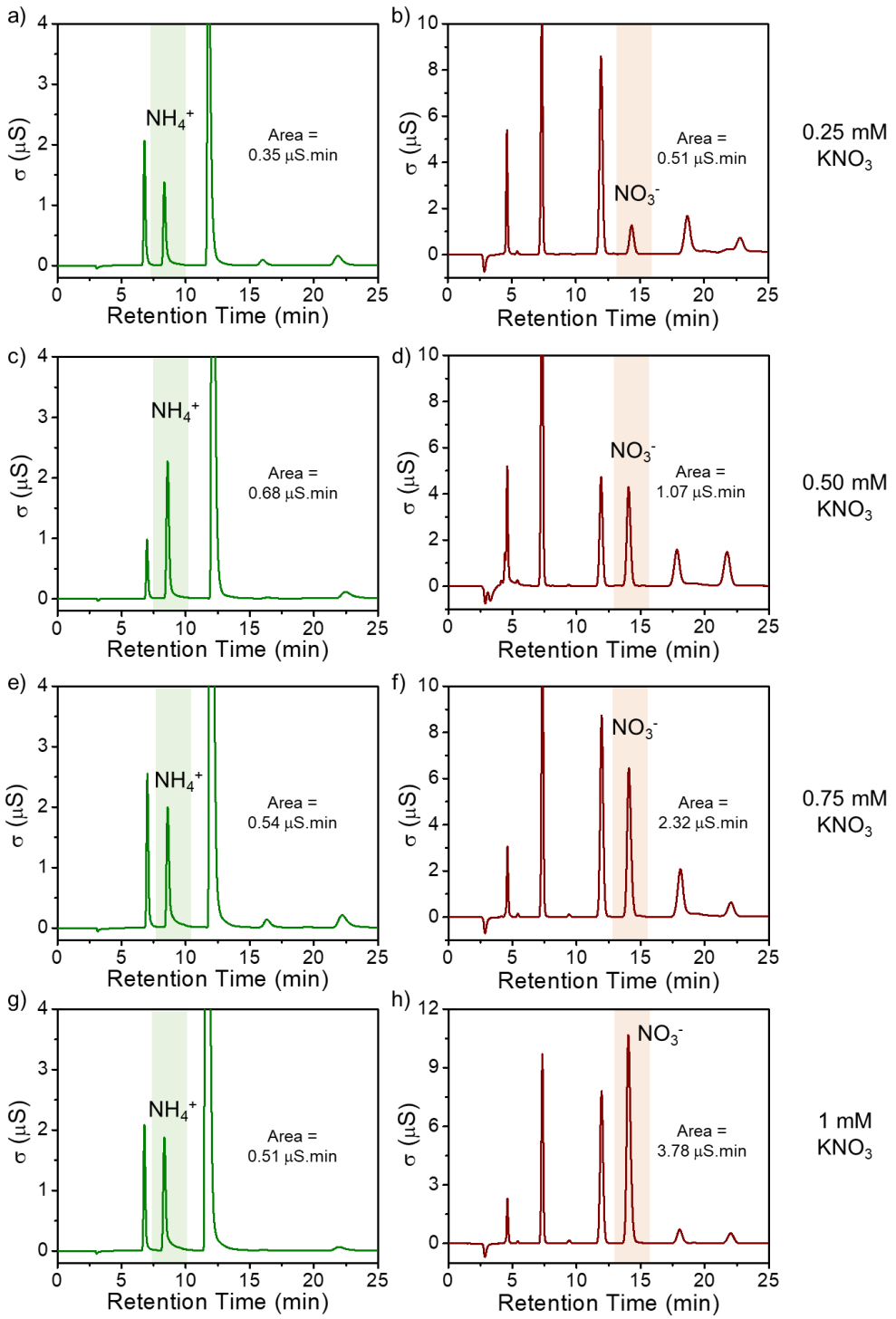


**Figure 4a.16**. Cation (a,c,e,g) and anion (b,d,f,h) chromatograms for photocatalytic reactions performed with different substrate concentrations. a,b) 0.25 mM, c,d) 0.50 mM, e,f) 0.75 mM, and g,h) 1.00 mM KNO$_3$.

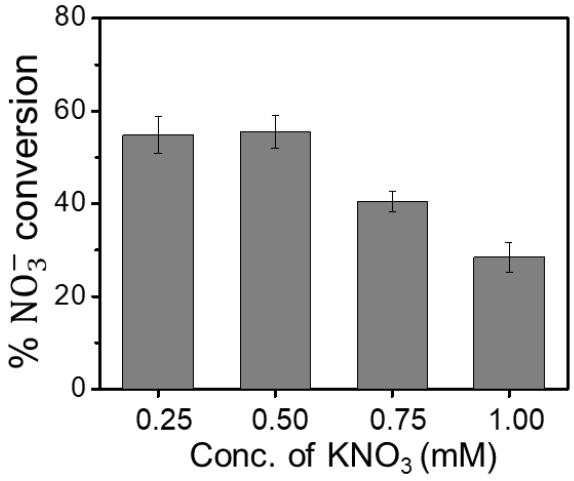


**Figure 4a.17**. Bar diagrams summarizing total $NO_3^-$ conversion as a function of $KNO_3$ concentration with 0.5 mol % [+] InP QDs. With the increase in substrate concentration, there was an increase in $NH_4^+$ concentration and eventually attains saturation. Consequently, we chose 0.5 mM $KNO_3$ and 0.5 mol % [+] InP QDs for further studies.

Time-dependent studies through ion chromatography

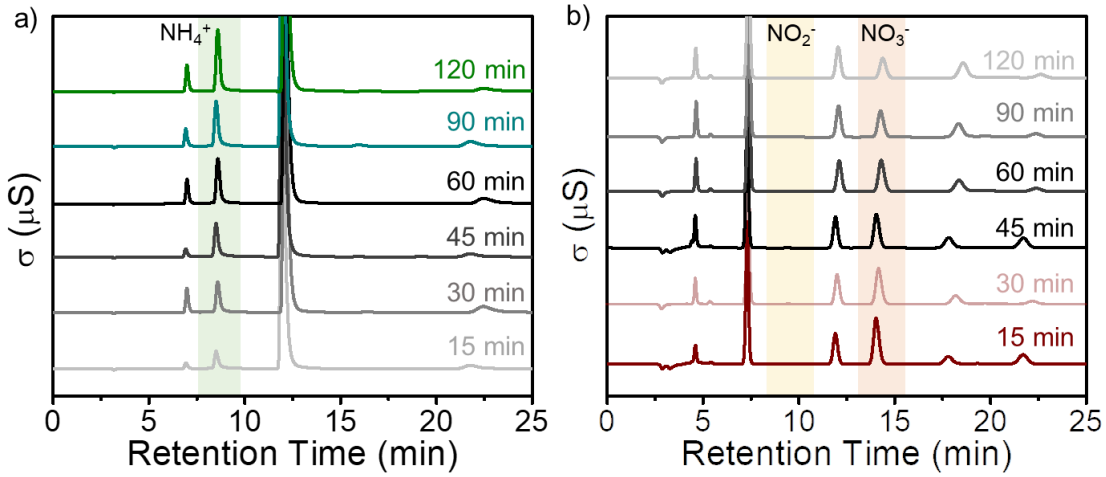


**Figure 4a.18**. Progress of the reaction monitored through ion chromatography. With increasing reaction time, a) the amount of $NH_4^+$ increases with b) a gradual decrease in $NO_3^-$ concentration, as can be seen from variation in peak intensities. No traces of $NO_2^-$ were observed during the photocatalytic reaction.

### Control experiments

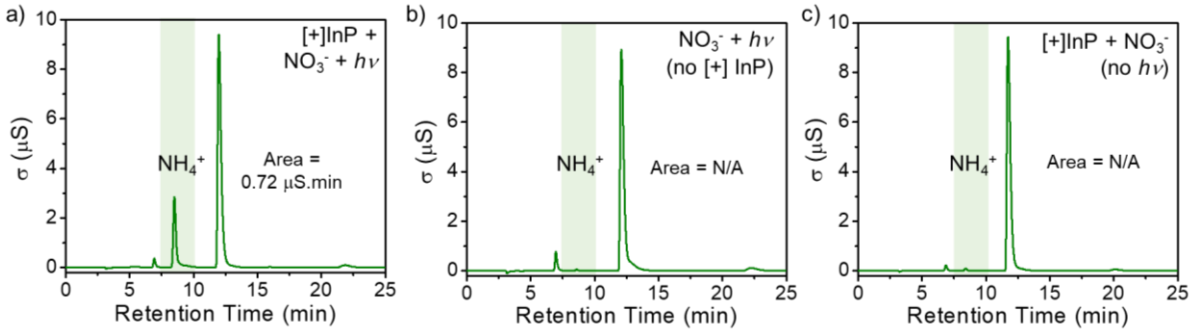


**Figure 4a.19**. Cation chromatograms for the quantification of $NH_3$ in aqueous phase for different control experiments. The appearance of signal at ~8.5 min in a) optimized reaction conditions corresponds to the formation of $NH_4^+$, whereas negligible amounts of $NH_4^+$ were formed in the absence of b) [+] InP QDs and c) light. Control experiments clearly confirm the necessity of both the photocatalyst and light for the conversion of $NO_3^-$ to $NH_4^+$.

### Photocatalytic experiments with isotope labelled $^{15}NO_3^-$

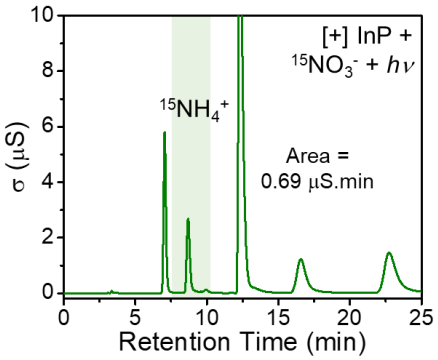


**Figure 4a.20**. Ion chromatogram showing the formation of $^{15}NH_4^+$ obtained from isotope-labelled $^{15}NO_3^-$.

### Quantification of $NH_3$ in the gas phase

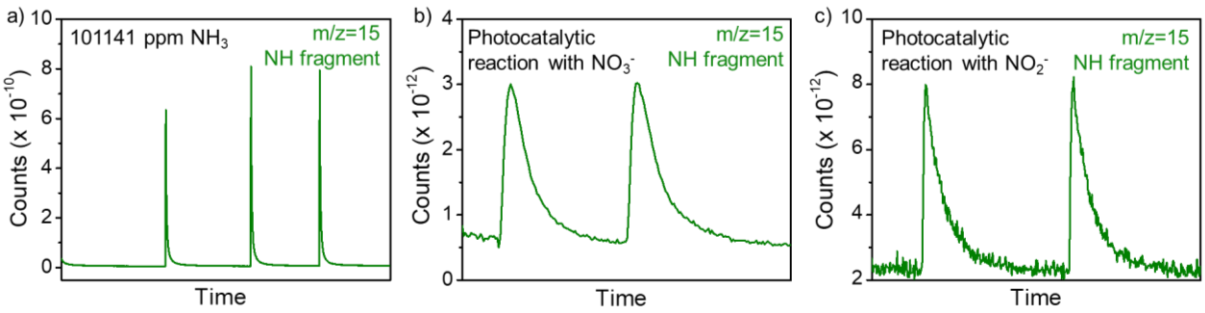


**Figure 4a.21.** Gas-phase mass analysis of a) standard $NH_3$ gas (conc.= 101141 ppm) and photocatalytic reaction performed with [+] InP QDs with b) $NO_3^-$ and c) $NO_2^-$ as N-source.

### Proof of electrostatics

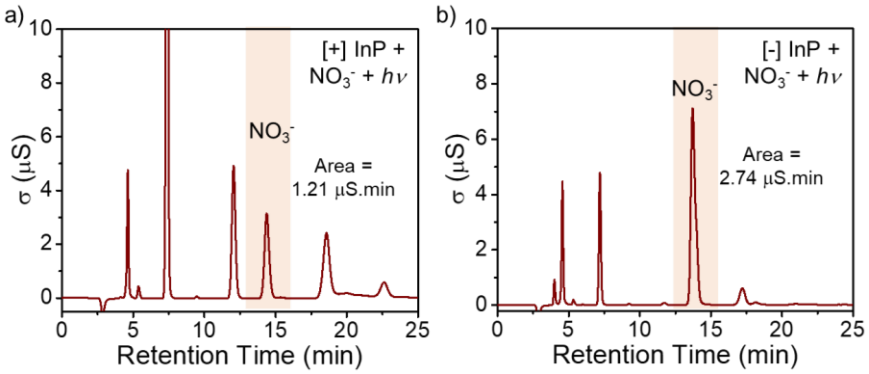


**Figure 4a.22**. Proof of favourable catalyst-reactant interactions through change of QD surface ligands. Anion chromatograms for the quantification of $NO_3^-$ conversion with a) [+] InP and b) [-] InP. The area under signal ~14.5 min was lower for photocatalytic reaction performed with TMA-capped [+] InP QDs, compared to MUA-capped [-] InP QDs.

### Constitution of action spectra

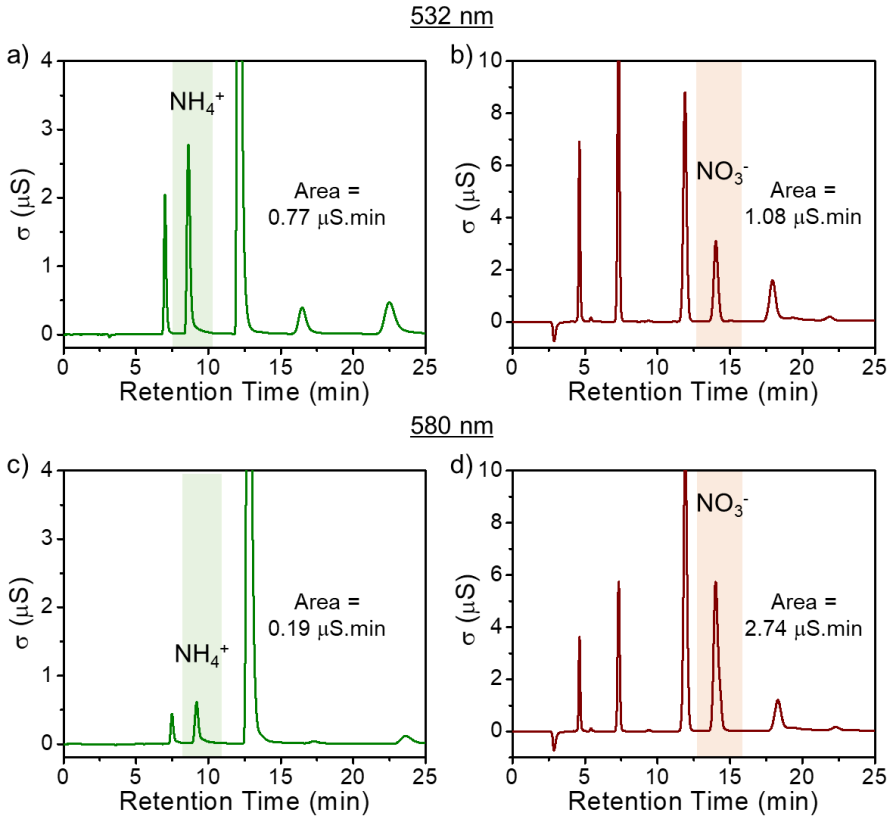


**Figure 4a.23**. Wavelength-dependent photocatalytic $NH_4^+$ synthesis with [+] InP QDs. Cation (a,c) and anion (b,d) chromatograms for photocatalytic experiment performed under a, b) 532 nm and c, d) 580 nm irradiation using 2 x 10 W LEDs (incident light intensity was kept similar ~200 mW $cm^{-2}$).

**Photocatalytic experiments in sunlight**

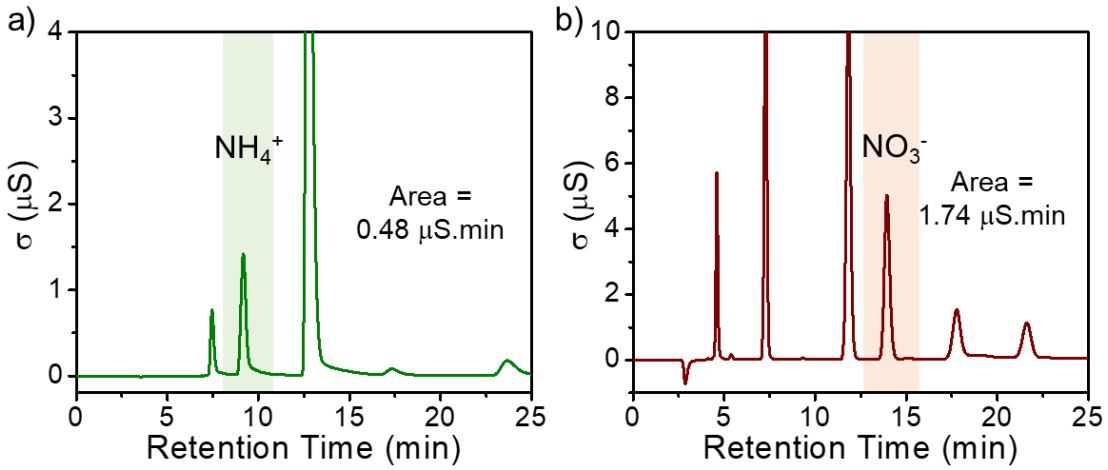


**Figure 4a.24.** Representative chromatograms for a) $NH_4^+$ and b) $NO_3^-$ quantification after the photocatalytic reaction performed with [+] InP QDs under natural sunlight for 2 h.

# Chapter – 4b

## Insights into Photocatalytic Ammonia Synthesis with InP Quantum Dots

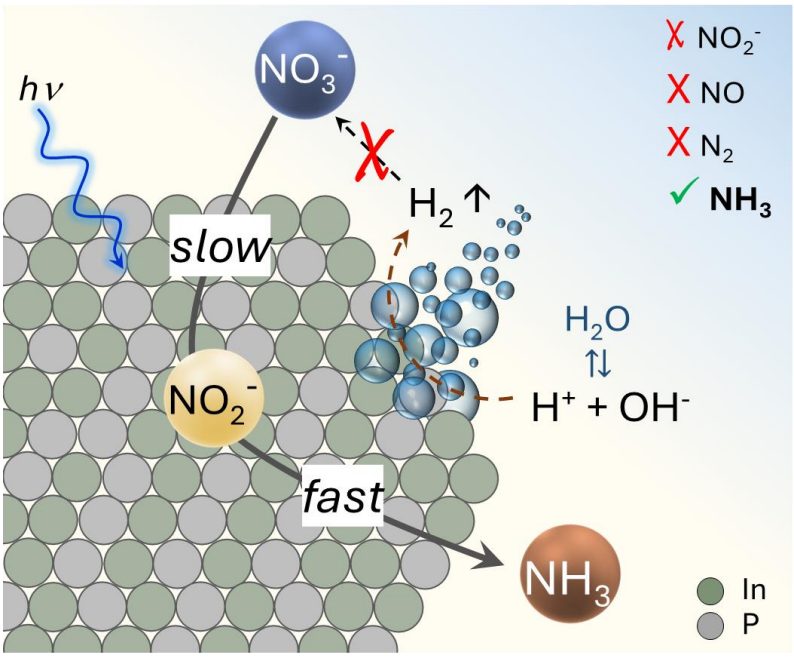


This Chapter has been adapted from the following paper with permission. Copyright 2024, American Chemical Society.

**Jain, V.**; Tyagi, S.; Roy, P.; Pillai, P. P. Ammonia Synthesis with Visible Light and Quantum Dots. *J. Am. Chem. Soc.* **2024**, *146*, 32356-32365.

## 4b.1. Abstract

Light-driven ammonia synthesis from nitrate/nitrite ions has emerged as a viable strategy to complement the existing methods of green ammonia synthesis. In this direction, we designed a simple yet efficient, III-V indium phosphide (InP) quantum dots (QDs) based photocatalytic system to produce ammonia under visible light irradiation at room temperature. The presence of catalytic indium sites and microenvironment modulation through precise regulation of catalyst-reactant interactions in InP QDs were the keys to achieving excellent photocatalytic activity. As nitrate-to-ammonia conversion is a multielectron and multiproton coupled process, we attempt to gain an in-depth understanding of important pathways involved in the InP QDs photocatalysed synthesis of ammonia. Kinetic studies revealed the energetically challenging nitrate-to-nitrite conversion as the rate-determining step, with subsequent reactions proceeding with ~100 % conversion to yield ammonia. The sole presence of ammonia in both the aqueous and gaseous phases, along with negligible accumulation of any byproducts, confirms the excellent selectivity of InP QDs. Further mechanistic investigations ascertained a negligible role of competing hydrogen evolution in the direct nitrate reduction, confirming the active participation of photoexcited charge carriers from InP QDs in the ammonia synthesis. A series of experiments concluded that water is the proton source in InP QD photocatalysed ammonia synthesis. Finally, optimizing the photocatalytic reaction system by using core/shell InP/ZnS QDs and an additional hole scavenger enabled long-term photocatalytic experiments, with complete retention of the photocatalytic activity up to 4 cycles and 75 % retention in the subsequent cycles. In short, the present study provides important mechanistic insights into establishing InP QD as a potential visible-light photocatalyst for ammonia synthesis.

## 4b.2. Introduction

Ammonia ($NH_3$) synthesis from nitrate ($NO_3^-$) and nitrite ($NO_2^-$) ions as the N-source emerges as a viable route to reduce the burden on the existing Haber-Bosch process while simultaneously offering water remediation opportunities.[1-5] The reduction of $NO_3^-$ to $NH_3$ is a multiproton ($9H^+$) coupled multielectron ($8e^-$) transfer transformation, which proceeds via multiple deoxygenation and protonation steps.[4,5] For the deep reduction of $NO_3^-$ (oxidation state = +5) to form $NH_3$ (oxidation state = -3), multiple electrons ($8e^-$) must be transferred, which necessitates the stabilization of $1e^-$ intermediates long enough till the successive electron transfer process can take place.[6] Further, the transformation is accompanied by elementary multiple proton transfer steps. Since there exists a mass difference between electrons and protons, the latter being heavier, the coordination between electron and proton delivery is inherently challenging.[6] Because of the difference in thermodynamics, kinetics, and reactivities of the electron and protons, photocatalytic $NO_3^-$ to $NH_3$ conversion suffers from low quantum efficiencies, accumulation of side reactions, and coexistence of competing $2e^-/2H^+$ proton reduction to $H_2$.[1-5,7-9] The standard reduction potential of different steps involved in $NO_3^-$ reduction, as shown in **Table 4b.1.**, clearly shows that $N_2$ and $NH_3$ are the most thermodynamically stable products.[4,10] As multiple steps are involved in $NO_3^-$ reduction, several reaction paths exist that branch out to yield $N_2$, $N_2H_4$, or $NH_3$, which makes the elucidation of the exact reduction pathway challenging (**Figure 4b.1**).[4,10]

**Table 4b.1.** Standard redox potentials for different $NO_3^-$ reduction products

| Reduction reaction | Standard redox potential |
|---|---|
| $NO_3^- + 2H^+ + 2e^- \rightleftharpoons NO_2^- + H_2O$ | $E^o = 0.49$ V |
| $NO_3^- + 4H^+ + 3e^- \rightleftharpoons NO + 2H_2O$ | $E^o = 0.96$ V |
| $NO_3^- + 7H^+ + 6e^- \rightleftharpoons NH_2OH + 2H_2O$ | $E^o = 0.67$ V |
| $NO_3^- + 10H^+ + 8e^- \rightleftharpoons NH_4^+ + 3H_2O$ | $E^o = 1.20$ V |
| $2NO_3^- + 10H^+ + 8e^- \rightleftharpoons N_2O + 5H_2O$ | $E^o = 1.12$ V |
| $2NO_3^- + 12H^+ + 10e^- \rightleftharpoons N_2 + 6H_2O$ | $E^o = 1.25$ V |
| $2NO_2^- + 8H^+ + 6e^- \rightleftharpoons NH_4^+ + 2H_2O$ | $E^o = 0.90$ V |

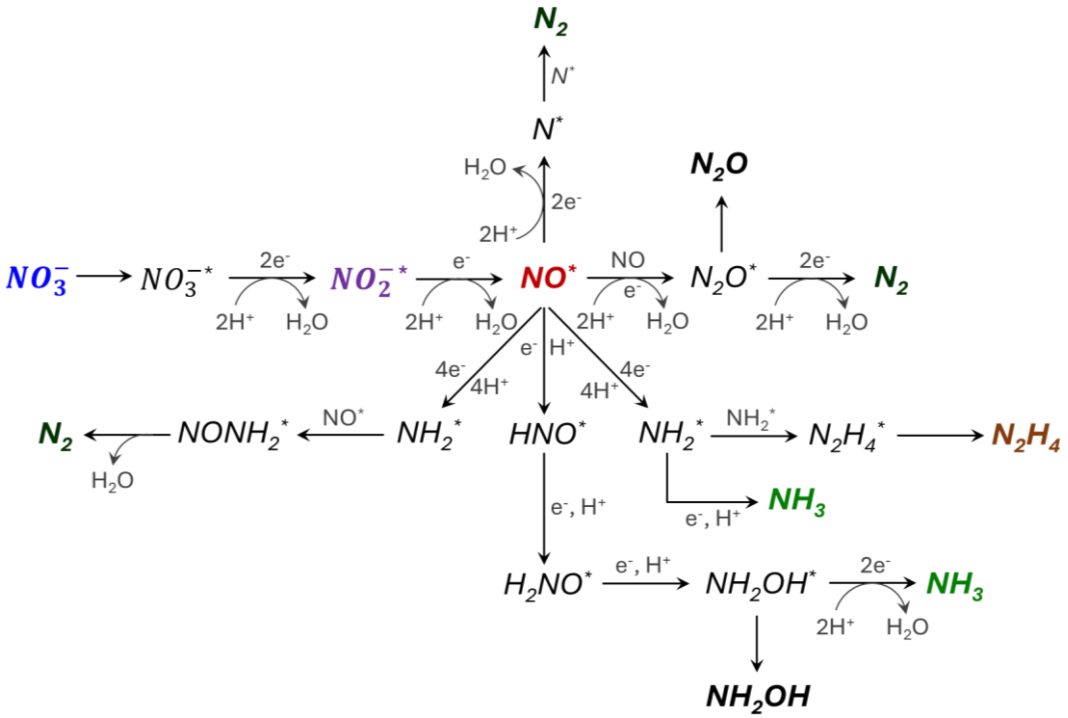


**Figure 4b.1**. Schematics showing the proposed reaction mechanism for $NO_3^-$ reduction. Redrawn with permission from references 4 and 10. Copyright 2022 The Royal Society of Chemistry and Copyright 2020 American Chemical Society. * refers to adsorbed molecule.

Given the limited literature reports on photocatalytic $NO_3^-$ reduction to $NH_3$, there is only a limited understanding of the exact mechanistic pathways. In most cases, there is a heavy reliance on theoretical support to gain an in-depth understanding of the pathway involved.[2,11-14] However, attempts have been made recently to elucidate the reaction mechanisms using in-situ techniques.[15,16] For instance, in an interesting work by Shiraishi and coworkers, $Cu^{2+}$ doped $TiO_2$ was explored for $NO_3^-$ reduction to ammonia using water as an electron donor.[16] Here, $Cu^{2+}$ doping eliminates lattice O from $TiO_2$ and produces vacancies, which play a crucial role in $NO_3^-$ adsorption and subsequent reduction. The photocatalytic $NO_3^-$ reduction yielded $NH_4^+$ and $NO_2^-$ as the major products along with $H_2$ (**Figure 4b.2a**). While the rate of $NO_2^-$ generation decreases with time, a gradual increase in $NH_3$ formation indicated simultaneous $8e^-$ and $2e^-$ reduction of $NO_3^-$ to $NH_3$ and $NO_2^-$, respectively. In-situ diffuse reflectance infrared Fourier transform spectroscopy (DRIFTS) was employed to study the role of O-vacancies in $NO_3^-$ reduction. In-situ DRIFTS spectrum revealed the emergence of negative peaks in the 3100-3600 $cm^{-1}$ and ~1620 $cm^{-1}$ region, corresponding to stretching band of adsorbed water molecules ($\nu$(O-H)) and $NO_3^-$ ions ($\nu(NO_3^-)$), respectively (**Figure 4b.2b**). Upon light

irradiation, a broad band appeared at ~2080 $cm^{-1}$ which was attributed to the stretching band of nitrosyl intermediates (ν(N=O)) (**Figure 4b.2b**). As the reaction progressed, stretching and bending bands at 2970 $cm^{-1}$ and 1690 $cm^{-1}$ intensified, suggesting the formation of N-H bonds (**Figure 4b.2b**). No such bands appeared when Cu(0) was doped into $TiO_2$, indicating the active participation of O-vacancies created by $Cu^{2+}$ in $NO_3^-$ reduction (**Figure 4b.2b**). The overall reaction was proposed by combining in-situ DRIFTS data with DFT calculations. The Lewis-base $NO_3^-$ adsorbs onto $Ti^{3+}$ and $Cu^{2+}$ sites of O-vacant $Cu^{2+}$-doped $TiO_2$, and undergoes N-O cleavage by photoexcited electrons localized on $Ti^{3+}$ sites. This results in $NO_2^-$ intermediate adsorbed and $Cu^{2+}$ sites via N-Cu bond and removal of one water molecule. Further N-O bond cleavage results in a bridging NO intermediate, which further undergoes a deoxygenation step to form a secondary amine intermediate, ultimately forming $NH_3$. Finally, adsorbed $NH_3$ is desorbed from the surface (**Figure 4b.c**). DFT calculations also revealed that the N-O cleavage of $NO_3^-$ is the rate-determining step, whereas the other three steps proceed with negligible activation energies. Moreover, it was proposed that the accumulation of $NO_2^-$ occurs due to the involvement of indirect $NO_3^-$ reduction pathways where weakly absorbed $NO_2^-$ intermediate desorbs from O-vacancies. The promotion of a direct pathway instead of this indirect pathway was found to be dependent on photon flux, with higher $NH_3$ formation with higher light intensities.

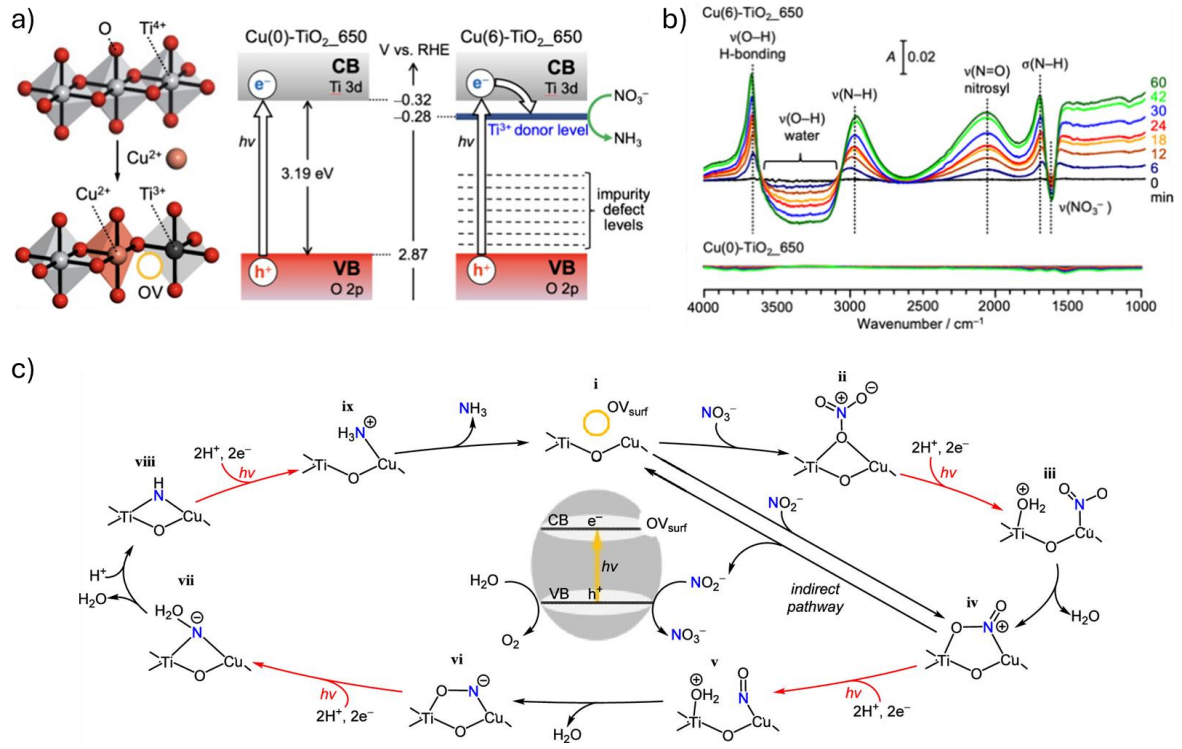


**Figure 4b.2**. Photocatalytic $NO_3^-$ reduction with $Cu^{2+}$-doped $TiO_2$. a) Schematics of the $Cu^{2+}$ doping into $TiO_2$ and its effect on the electronic structure. b) In-situ DRIFTS spectra of $NO_3^-$ reduction over $Cu^{2+}$-$TiO_2$ and Cu(0)-$TiO_2$ under continuous light irradiation at -173 °C in vacuum. c) Proposed reaction mechanism for $NO_3^-$ reduction to $NH_3$ based on in-situ DRFITS and DFT calculations. Reproduced with permission from reference 16. Copyright 2025 American Chemical Society.

It is widely known that the majority of proton-coupled multielectron reactions are accompanied by kinetically facile $2H^+/2e^-$ reduction reactions, evolving $H_2$.[6] In the case of $NO_3^-$ reduction, $H_2$ evolution is not just a competing reaction but is proven to be non-innocent in some cases.[8,9,17-19] In an early example, Yamauchi and coworkers observed that selective $NH_3$ was produced from $NO_3^-$ ions with photocatalytically generated $H_2$ over CuPd/$TiO_2$.[8] The excellent hydrogenation over CuPd nanoalloys to form $NH_3$ was attributed to the high ratio of reductant H species to the surface coverage of N species, H/N (**Figure 4b.3a**). As $H_2$ evolution was higher in the case of CuPd/$TiO_2$ than Pd/$TiO_2$, the adsorbed N species are continuously in proximity with nascent H atoms, resulting in complete hydrogenation of $NO_3^-$ to form $NH_3$. In another instance, Kamiya and coworkers coupled Pt/$TiO_2$ photocatalysts and SnPd/$Al_2O_3$ non-photocatalyst for photocatalytic $NO_3^-$ reduction to $N_2$ in water.[18] Here, $H_2$ was photocatalytically generated by Pt/$TiO_2$, which was then utilized as a reductant by SnPd/$Al_2O_3$ to convert $NO_3^-$ to $N_2$. Negligible

$NO_3^-$ conversion occurred in the presence of only $Pt/TiO_2$ or $SnPd/Al_2O_3$, suggesting the need for a coupled system. Control experiments revealed that the amount of $N_2$ formed corroborates well with the amount of $H_2$ generated in the absence of $NO_3^-$ under similar reaction conditions. An excellent catalytic hydrogenation of $NO_3^-$ over $SnPd/Al_2O_3$ with $H_2$ gas under dark conditions confirmed the active participation of photocatalytically generated $H_2$ evolution from $Pt/TiO_2$ in reducing $NO_3^-$ over $SnPd/Al_2O_3$. Recently, some transition metal phosphides have also showcased hydrogenation ability for nitrate reduction.[19,20] The rationale behind the participation of H-atoms in direct hydrogenation of $NO_3^-$ usually stems from the H-adsorption capability and the proximal presence of diverse surface sites for the adsorption of different intermediates on transition metal phosphides (**Figure 4b.3b**).[19] Such proximity between H-adsorption sites and local active sites allows ready reaction between the two, resulting in a dominant role of the hydrogenation pathway rather than the charge transfer one.

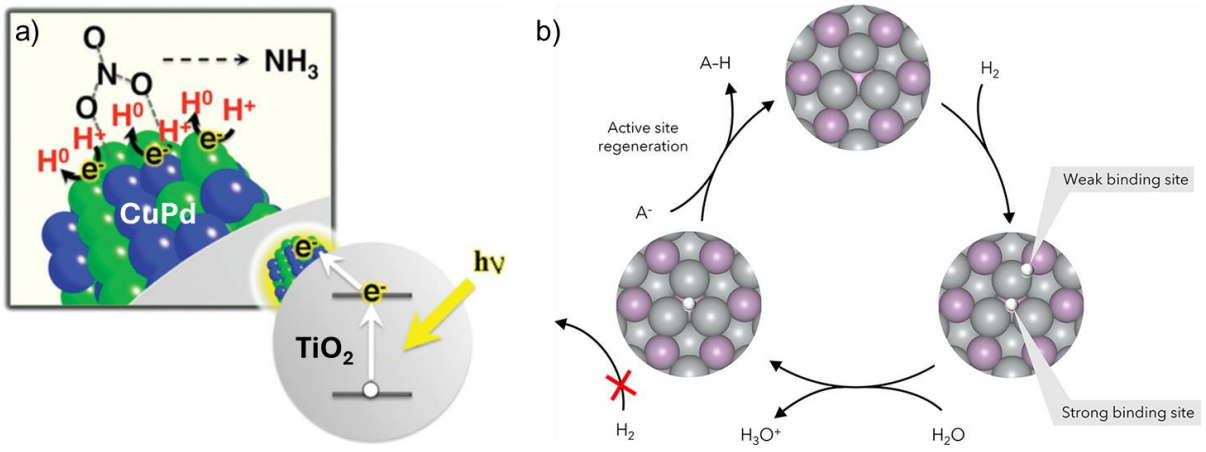


**Figure 4b.3**. Role of competing $H_2$ evolution in nitrate reduction. a) Schematics of nitrate reduction with photocatalytically generated hydrogen over PdCu-$TiO_2$ under UV excitation. Reproduced with permission from reference 8. Copyright 2011 American Chemical Society. b) Schematics showing the role of adsorbed H atoms in facilitating hydrogenation of $A^-$ over transition metal phosphides. Here, white, grey, and purple spheres represent H, Ni, and P atoms. Reproduced with permission from reference 19. Copyright 2023 American Chemical Society.

Herein, we attempt to gain an in-depth understanding of the important pathways involved in the InP QDs photocatalysed $NH_3$ synthesis from $NO_3^-/NO_2^-$ ions. The sole formation of $NH_3$ in the aqueous and gaseous phases, without accumulation of any of the side products, confirmed the selective $NH_3$ synthesis with InP QDs. Detailed kinetics

and isotope-labeled studies suggested the first $2e^-$ transfer step involving $NO_3^-$ to $NO_2^-$ conversion as the rate-determining step. The absence of any side product except $NH_3$ clearly rules out several pathways for $NO_3^-$ reduction, yielding $N_2$ as the final product. However, the fast kinetics associated with $NO_2^-$ to $NH_3$ conversion make it challenging to decipher the exact reaction pathway for $NH_3$ synthesis, as shown in **Figure 4b.1**. Along with $NO_3^-$ reduction, InP QDs also photocatalyzed $H_2$ evolution. The interference from the competing $H_2$ evolution reaction was overruled in the direct photoreduction of $NO_3^-$, proving that the photoexcited charge carriers formed in InP QDs mediate photocatalytic $NH_3$ synthesis. Finally, water was identified as the proton source in the photocatalytic $NH_3$ synthesis with [+] InP QDs. Further, optimizing the photocatalytic reaction system by using core/shell InP/ZnS QDs and an additional hole scavenger enabled long-term photocatalytic experiments, with complete retention of the photocatalytic activity up to 4 cycles and 75 % retention in the subsequent cycles. Given the limited literature available on photocatalytic $NO_3^-$ to $NH_3$ conversion, we provide key mechanistic details related to the kinetics, competing reactions, proton source, and the fate of photoexcited holes in the multielectron transformation of $NO_3^-$ to $NH_3$.

# 4b.3. Experimental section

## 4b.3.1. Identification of side products

As $NO_3^-$ reduction to $NH_4^+$ involves multiple electrons and protons, various side products tend to accumulate during the reaction. Most commonly observed products include $NO_2^-$, $NH_2OH$, $N_2H_4$, $N_2$, and $NO_x$ (g).[4,5] We analyzed the formation of these products in our photocatalytic reduction reaction through chromatographic and spectroscopic techniques. In our study, $NO_2^-$ ions were analyzed using ion chromatography, $NH_2OH$ and $N_2H_4$ were analyzed with colorimetry assays, and $N_2$ and $NO_x$ in the headspace were analyzed with mass spectrometry.

### 4b.3.1a. Identification of hydroxylamine ($NH_2OH$)

The presence of $NH_2OH$ was determined from 8-hydroxyquinoline-based colorimetric method.[21] A typical analysis consists of mixing 1 mL of analyte solution, 1 mL of PBS, and

1 mL of 1 % 8-hydroxyquinoline. To this mixture, 1 mL of 0.1 M $Na_2CO_3$ was added under vigorous shaking, followed by heating at 100 °C. The development of bright bluish green color with absorption peak at ~706 nm confirms the presence of $NH_2OH$. A calibration curve was plotted with 0-250 μM $NH_2OH$ solutions from the absorption spectra.

4b.3.1b. Identification of hydrazine ($N_2H_4$)

The amount of $N_2H_4$ was determined by standard Watt-Chrisp method.[22] In a typical procedure, the coloring agent was prepared by dissolving 4-(dimethylamino)benzaldehyde in conc. $H_2SO_4$ and ethanol. Equal volumes of $N_2H_4$ containing solution and coloring agent were mixed and left for 20 min for the color to develop. In the presence of hydrazine, the solution turns yellow with a characteristic absorption peak at 458 nm. A calibration curve was plotted from standard $N_2H_4$ solutions (0-3 ppm), and the amount of $N_2H_4$ formed during the photocatalytic reduction of $NO_3^-$ was obtained from this.

## 4b.3.2. Glutamate dehydrogenase (GLDH) assay

GLDH assay[23] was used to derivatize $^{15}ND_4^+$ formed after the photocatalytic reaction performed in $D_2O$ with [+] InP QDs to prove the role of water as the proton source. In a typical procedure, [+] InP QDs were removed after the photocatalytic reaction, and to this reaction mixture, NADH (6 μM), α-ketoglutarate (20 μM), and GLDH enzyme (1.2 units) were added. The reaction mixture was incubated at 25 °C for 6 h for the formation of glutamate. The progress of glutamate formation was monitored using UV-vis absorption, where the peak at 340 nm corresponding to NADH was monitored. After the enzyme assay, the reaction mixture was analyzed using high-resolution mass spectrometry (HRMS). A similar procedure was adopted for the analysis of isotope-labelled glutamate formed via reaction between $^{15}ND_4^+$ (formed in the photocatalytic reaction carried out in $D_2O$ with $^{15}NO_3^-$ as N-source) and α-ketoglutarate in the presence of NADH and GLDH.

### 4b.3.3. Recyclability study and long-term experiments

#### 4b.3.3a. With core-only InP QDs

The recyclability experiments were performed using a dip-catalyst system, which was prepared by the drop-cast of oleylamine (OAm)-capped InP QDs on Whatman filter paper film (2 cm x 1 cm), followed by drying. This paper film was dipped in the aqueous reaction mixture containing $KNO_2$ (0.5 mM) and irradiated for 6 h. After each photocatalytic cycle, the film was removed, washed, and dried for the next cycle, and the reaction mixture was analyzed using IC.

#### 4b.3.3b. With core-shell InP/ZnS QDs

The challenge associated with the etching of core-only QDs was overcome by performing recyclability studies with InP/ZnS core/shell QDs, which is a well-known type-I core/shell material.[24] A paper-based dip catalyst system was prepared by drop-casting OAm-capped InP/ZnS QDs on Whatman filter paper film (2 cm x 1 cm), followed by drying. This paper film was dipped in the aqueous reaction mixture containing $KNO_2$ (0.5 mM) and 10 % ethanol and irradiated for 6 h. Because type I core/shell QDs have a higher degree of confinement of the excitons within the core material, which reduces the charge transfer efficiency, ethanol was introduced as the hole scavenger to enhance the conversion yield. After each photocatalytic cycle, the film was removed, washed, and dried for the next cycle, and the reaction mixture was analyzed using IC.

## 4b.4. Results and discussion

### 4b.4.1. Identification of side products

As $NO_3^-$ reduction to $NH_4^+$ involves multiple electrons ($8e^-$) and protons ($10H^+$), various side products tend to accumulate during the reaction, which can impact the product selectivity.[4,5] As time progressed, a gradual decrease in $NO_3^-$ concentration from 500 μM to 260±36 μM was observed with a concomitant increase in $NH_4^+$ in the aqueous phase (**Figure 4b.4a**). However, the $NH_4^+$ concentration in the aqueous phase did not corroborate well with the total $NO_3^-$ conversion, suggesting the formation of other

reduction products. Thus, detailed studies were performed to detect the presence of side-products formed during the [+] InP QD photocatalyzed synthesis of $NH_4^+$. Most commonly observed $NO_3^-$ reduction products include $NO_2^-$ (aq.), $NH_2OH$ (aq.), $N_2H_4$ (aq.), $N_2$ (g), and NO (g).[4,5,10] Ion-chromatography studies revealed a negligible accumulation of $NO_2^-$ ions during the course of the photocatalytic reaction (**Figure 4b.4b**). Furthermore, gas-phase mass analysis and spectroscopic studies show a negligible formation of gaseous ($N_2$ and NO) and aqueous phase products ($NH_2OH$ and $N_2H_4$), respectively (**Figures 4b.4c-f, 4b.12, 4b.13**). As gas phase analysis revealed the presence of $NH_3$ in the reactor's headspace, we calculated the amount of $NH_3$ present in the gaseous phase. The cumulative $NH_3$ production in both aqueous and gaseous phases reached $0.80 \pm 0.19$ µmoles (~6.8 ppm, ~430 µmol $g^{-1}$), which accounts for ~94 % of the total $NO_3^-$ converted. In essence, it can be concluded that [+] InP QDs selectively reduce $NO_3^-$ to $NH_3$ under visible-light illumination.

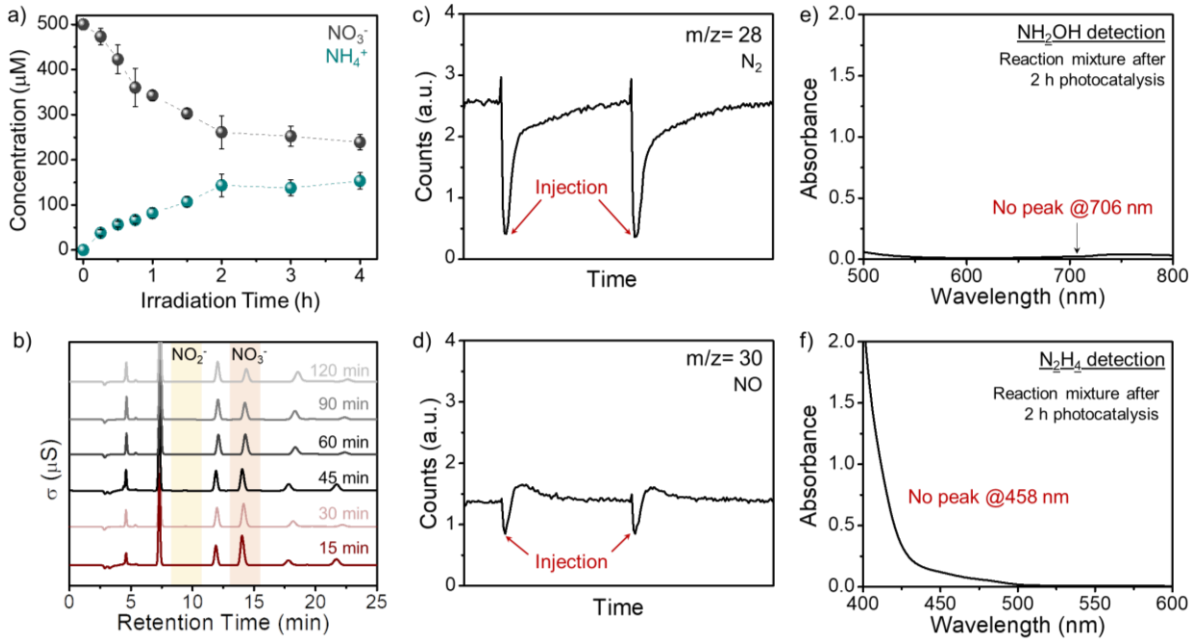


**Figure 4b.4**. Identification of side products in InP QDs photocatalyzed ammonia synthesis. a) Progress of [+] InP QD photocatalysed reduction of $NO_3^-$ to $NH_4^+$ monitored through IC. The dotted lines are only to guide the eyes. b) Progress of the reaction monitored through ion chromatography. With increasing reaction time, a gradual decrease in $NO_3^-$ concentration can be seen from variation in peak intensities. No traces of $NO_2^-$ were observed during the photocatalytic reaction. Analysis of common gaseous side products c) $N_2$ and d) NO through mass spectrometry. Negligible traces of $N_2$ and NO were observed in the reactor's headspace. Absorption spectrum of the reaction mixture after photocatalytic reduction of $NO_3^-$ to $NH_4^+$ with [+] InP QDs for identification of e) hydroxylamine ($NH_2OH$) and f) hydrazine ($N_2H_4$). Absence of

absorption peak @706 nm and @458 nm confirm negligible formation of $NH_2OH$ and $N_2H_4$, respectively, in our study.

## 4b.4.2. Elucidation of rate-determining step

As per the electrochemical potentials, the initial two-electron reduction of $NO_3^-$ to $NO_2^-$ is the most energetically challenging step ($E^o$ = 0.49 V vs SHE) in the $NH_4^+$ synthesis from $NO_3^-$(**Figure 4b.5a**).[25,26] Accordingly, $NO_2^-$ was chosen as the N-source to evaluate the impact of reactant on [+] InP QD photocatalysed synthesis of $NH_4^+$. Strikingly, a complete conversion of $NO_2^-$ was observed within 1 h of visible-light illumination, along with an increase in $NH_4^+$ concentration in the aqueous phase to 280±25 μM (~5.5 ppm, ~320 μmol $g^{-1}$) (**Figures 4b.5b, 4b.14**). The total $NH_3$ formed in the aqueous and gas phases was found to be 1.36 μmoles, which amounts to ~91 % of the total $NO_2^-$ converted. The faster kinetics associated with $NO_2^-$ to $NH_4^+$ conversion, corroborates well with the negligible accumulation of $NO_2^-$ during the [+] InP QD photocatalysed reduction of $NO_3^-$ (**Figure 4b.4b**). Further insights were obtained from competitive photocatalytic experiment performed with an equimolar mixture of $^{14}NO_3^-$ + $^{14}NO_2^-$, as the N-source. IC analysis reveals ~100 % conversion for $NO_2^-$, while ~50 % $NO_3^-$ remained unreacted after 2 h of photocatalysis (**Figure 4b.5c, 4b.15**). This confirms a greater preference of [+] InP QDs towards $NO_2^-$ reduction over $NO_3^-$ reduction. An isotopic competition experiment between $^{14}NO_2^-$ and $^{15}NO_3^-$ further validated the greater affinity of nitrite reduction with [+] InP QD photocatalyst. $^1$H-NMR studies explicitly show that the formation of $^{14}NH_4^+$ from $^{14}NO_2^-$ source was remarkably higher than the formation of $^{15}NH_4^+$ from $^{15}NO_3^-$ source (**Figure 4b.5d**). All these experiments suggest that $NO_3^-$ to $NO_2^-$ conversion is the probable rate-limiting step controlling the overall $NH_3$ synthesis when $NO_3^-$ is used as the N-source.

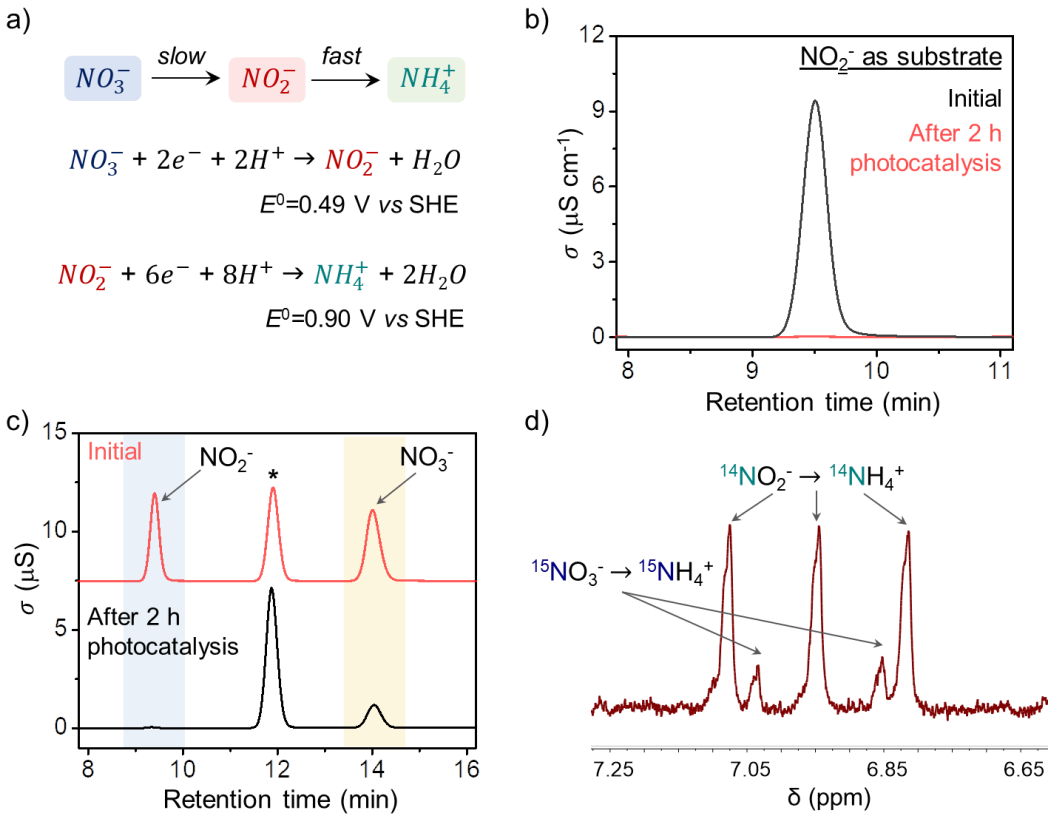


**Figure 4b.5**. a) A reaction scheme suggesting $NO_3^-$ to $NO_2^-$ conversion to be the probable rate-limiting step controlling the overall $NH_3$ synthesis, when $NO_3^-$ is used as the N-source. b) Ion chromatograph for the photocatalytic experiment performed with $NO_2^-$ as the N-source. c) Ion chromatograms and d) $^1$H-NMR spectra for competitive photocatalytic experiments performed with equimolar mixture of $^{14}NO_2^-$ + $^{14}NO_3^-$ and $^{14}NO_2^-$ + $^{15}NO_3^-$ as the N-source, respectively. *represents $Cl^-$ ion present in the reaction mixture. A clear preference for nitrite reduction over nitrate reduction was observed with [+] InP QDs.

## 4b.4.3. Effect of competing hydrogen evolution reaction

Proton-coupled multielectron reactions are often challenged by the kinetically facile $H_2$ evolution reaction.[6] From the band positions of InP QD, it is clear that both $H_2$ evolution as well $NO_3^-/NO_2^-$ reduction reactions are thermodynamically feasible (**Figure 4b.6**). Indeed, we observed $H_2$ evolution along with $NH_4^+$ production from $NO_3^-$ as well as $NO_2^-$ under our reaction conditions (**Table 4b.2**). Previous literature reports suggest that photocatalytic $H_2$ evolution is not only a competing reaction but is a potent reductant for $NO_3^-$ ions as well.[8,16-19] This motivated us to delve into the role of $H_2$ in $NO_3^-$ reduction in our system. The active role of photocatalytically generated $H_2$ in the direct reduction of $NO_3^-/NO_2^-$ was evaluated through a series of control experiments (**Table 4b.2**). Firstly, the reaction mixture containing only [+] InP QDs was irradiated to produce $H_2$. To this

preirradiated reaction mixture, $KNO_3$/$KNO_2$ was added under inert conditions and left for incubation for 2 h in the dark. IC analysis revealed negligible production of $NH_4^+$ for samples incubated in dark, whereas a strong signal corresponding to $NH_4^+$ appeared only after the light illumination of the above incubated sample (**Table 4b.2, Figures 4b.16, 4b.17**). Likewise, no noticeable $NH_4^+$ was formed by directly purging $H_2$ gas into the reaction mixture containing [+] InP QDs and $KNO_3$ in dark (**Table 4b.2, Figure 4b.18**), confirming the negligible interference of $H_2$ in the present study. Thus, all the control experiments confirm the active role of photoexcited charge carriers from [+] InP QDs for $NO_3^-$/$NO_2^-$ reduction to $NH_4^+$ under visible-light illumination. Here, $H_2$ evolution is an inherent side reaction and does not affect the kinetics of $NH_4^+$ formation from $NO_3^-$ as well as $NO_2^-$. However, it does influence the percentage conversion of $NO_3^-$, as a portion of the photoexcited charge carries generated in [+] InP QDs are used for the $H_2$ evolution reaction as well (17.5 % of photoexcited charge carries is used for $H_2$ vs 82.5 % for $NO_3^-$ reduction to $NH_4^+$, details are provided in the Appendix). In the future, it would be interesting to adapt existing strategies from electrocatalysis to suppress the $H_2$ evolution reaction and improve the absolute amount of $NH_4^+$ formation. One such strategy could be to use ligand head groups with higher pKa values, so as to break the H-bonding that is a crucial aspect for $H_2$ evolution.[27] Another approach would be to add surface modifier ions such as $Sr^{2+}$, $Mg^{2+}$ or $Al^{3+}$, which are non-catalytic for proton reduction and possess high negative reduction potentials.[28]

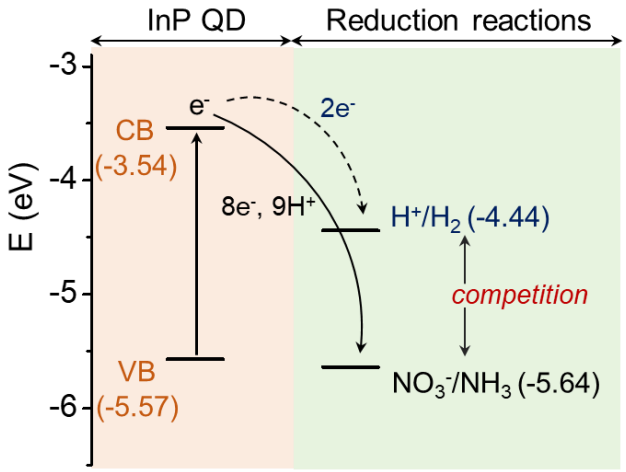


**Figure 4b.6**. Schematics of energy level diagram representing the thermodynamic feasibility of possible reduction reactions with [+] InP QDs. Under our reaction condition, photocatalytic $NO_3^-$ to $NH_3$ transformation was accompanied by $H_2$ evolution reaction.

**Table 4b.2.** Table summarizing the effect of photocatalytically generated $H_2$ in the direct reduction of $NO_3^-$ to $NH_4^+$.

| Reaction Condition | $NO_3^-$ conversion (%) | $NH_{3\,(aq.)}$ (%) | $H_2$ evolved (nmol) |
|---|---|---|---|
| Pre-irradiated [+] InP + $KNO_3$ (incubated in dark) | Negligible | Not formed | 742 ± 52 |
| Pre-irradiated [+] InP + $KNO_3$ + *hn* | 52.2 ± 7.4 | 28.6 ± 5.0 | 678 ± 101 |
| Pre-irradiated [+] InP + $NO_2^-$ (incubated in dark) | Negligible | Not formed | 632 ± 168 |
| [+] InP + $H_2$ + $NO_3^-$ (dark) | Negligible | Not formed | - |
| [+] InP + $H_2$ + $NO_3^-$ (*hn*) | 48.5 ± 4.6 | 25.7 ± 2.3 | - |

## 4b.4.4. Proton source and hole scavenger

Since photocatalytic $NO_3^-$ reduction to $NH_4^+$ requires $10H^+$, we probed into the possible sources of protons in our reaction conditions. There are two possible proton sources in our system: (i) water and (ii) thiol group on TMA ligands present on the surface of [+] InP QDs. A series of experiments were performed to confirm the identity of the proton source. First, FTIR studies confirmed that TMA ligands bind as X-type ligands in the form of thiolates and, therefore, are devoid of any ionizable protons (**Figure 4a.5b**). This was further validated in a recent study by Hens and co-workers, where the native oleylamine ligands participated in acid-base reaction to form oleylammonium chloride leaving thiolates to bind on InP QDs.[29] Next, appreciable $NH_3$ formation was observed when InP QDs functionalized with non-thiolate quaternary ammonium ligands ($^-$OOC-$CH_2$-$NMe_3^+$, Betaine-InP QDs) were used as the photocatalyst (~45 % $NO_3^-$ conversion, 2.16 ppm of $NH_4^+$ formed in the aqueous phase. **Figure 4b.7a, Scheme 4b.1**). This was further confirmed by performing photocatalytic experiments with the isotope-labeled $^{15}NO_3^-$. A clear emergence of characteristic doublet in $^1$H-NMR ($J$= 72 Hz) corresponding to isotope labelled $^{15}NH_4^+$, confirming $NO_3^-$ to be the N-source (**Figure 4b.7b**). It is to be

noted that betaine, again, is devoid of any ionizable protons and cannot act as a proton source. All these experiments rule out the possibility of TMA ligands as a proton source.

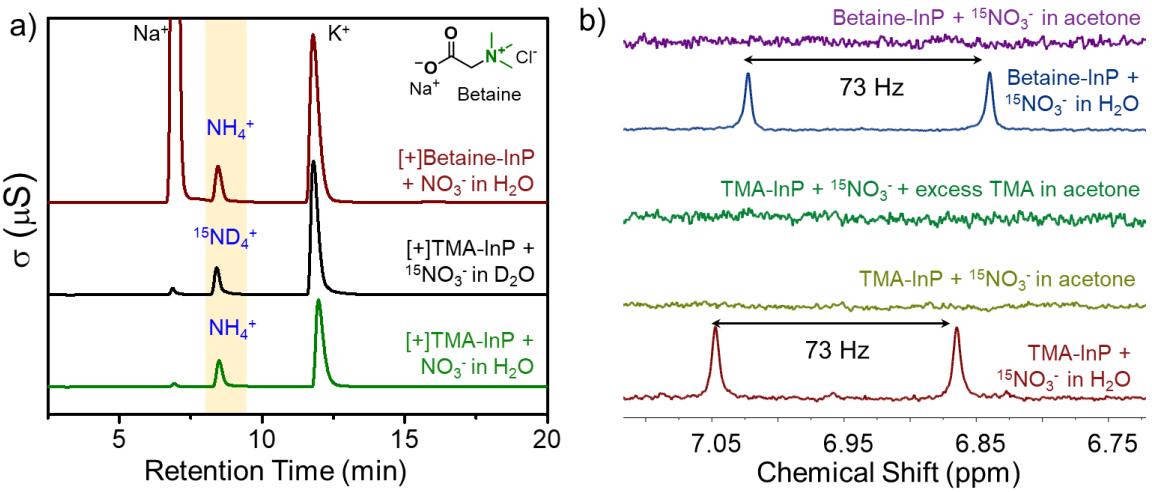


**Figure 4b.7.** Identification of proton source in photocatalytic $NH_3$ synthesis with [+] InP QDs. a) Cation chromatograms of photocatalytic reactions performed in [+]-InP QDs in $D_2O$ and non-thiolated betaine ligand capped InP QDs, in comparison with [+]-InP QDs in $H_2O$ (the optimized condition). A clear formation of ammonium ion shows a prominent role of water as the proton source. b) Comparison of $^1$H-NMR under different reaction conditions performed with $^{15}NO_3^-$ as the N-source.

Further, the photocatalytic reduction of $NO_3^-$ by [+] InP QD was performed in a polar aprotic medium. Some of the most used polar aprotic solvents are acetone, acetonitrile, DMF and DMSO.[30] Here, we chose acetone as the polar aprotic solvent based on a prior literature report in QD photocatalysis by Wu and coworkers,[31] where water was discovered as the sole proton source for $H_2$ evolution. In our study, no signs of $NH_3$ formation were observed when the reaction was performed in acetone (**Figure 4b.7b, Table 4b.3**). This indicates that water could probably be the proton source. An additional experiment performed in the presence of excess TMA-thiol ligands in acetone also resulted in negligible formation of $NH_3$ (**Figure 4b.7b, Table 4b.3**). In another control experiment, the photocatalytic reduction was performed in deuterated water ($D_2O$), which yielded a similar amount of ammonium ions as in the case of $H_2O$ (125.5±2 μM and 143±25 μM of ammonium ions in $D_2O$ and $H_2O$, respectively in the aqueous phase. **Figure 4b.7a**).

The proof for water as the proton source came from glutamate dehydrogenase (GLDH) assay-based ammonia derivatization study, wherein $^{15}ND_4^+$ produced during the photocatalytic reaction forms isotope-labeled glutamate (**Figures 4b.8a, 4b.19-4b.21, Scheme 4b.2**). Further, the ultimate validation comes from the gas phase mass signals for m/z=21 and m/z=19 corresponding to $^{15}ND_3$ and $^{15}ND_2$ fragments, respectively (**Figures 4b.8b, 4b.22**). The evolution of $H_2$ in addition to $NH_4^+$ synthesis under photocatalytic conditions, also supports our claim of water as the proton source. From all the possible experiments performed, it can be concluded that water is surely acting as the sole proton source in the photocatalytic $NH_3$ synthesis with [+] InP QDs (**Table 4b.3**).

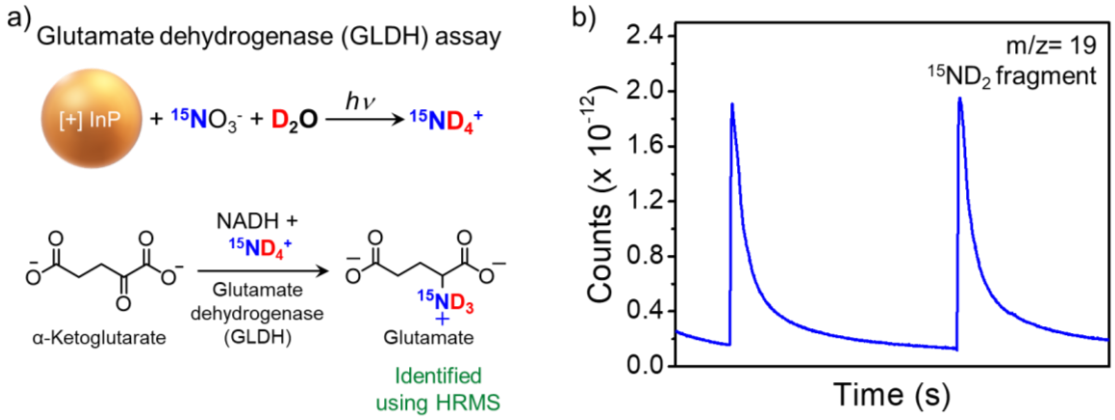


**Figure 4b.8.** Proof of water as the proton source in InP photocatalyzed ammonia synthesis from $NO_3^-$. a) Schematics showing the photocatalytic reduction of $^{15}NO_3^-$ to $^{15}ND_4^+$ with [+] InP QDs in $D_2O$. The bottom panel shows the glutamate dehydrogenase assay which converts a-ketoglutarate to isotope labelled-glutamate in presence of NADH, GLDH enzyme, and $^{15}ND_4^+$ (formed during photocatalysis). The identification of isotope-labelled glutamate using HRMS unambiguously confirmed that water is the sole proton source in the present study (**Figure 4b.21**). b) Gas phase mass analysis of the photocatalytic reaction performed with $^{15}NO_3^-$ in $D_2O$. Signals for m/z =19, corresponding to $^{15}ND_2$ fragment confirm water as the proton source.

Next, probable processes dictating the fate of photoexcited holes are discussed. Intuitively, TMA-thiolate ligand and water could be the probable species that can act as hole scavengers. However, we failed to observe any oxidized products of TMA-thiolate as well as water, overruling their participation as the hole scavenger in our system. Literature reports reveal the presence of deep hole trap states in InP QDs, which in principle, can trap photoexcited holes from the valence band.[29,32,33] Another possibility is the hole transfer-mediated dissociation of ligands from the QD surface, which was

reported in the case of CdS QDs.[34] All these possibilities can affect the photostability as well as the recyclability of the photocatalyst. In our study, a visual color change was observed for [+] InP QDs during the photocatalytic reaction (the deep orange color of [+] InP QDs faded with time). A time-dependent absorption study revealed a gradual blue shift of the first excitonic peak along with a decrease in the absorbance under light irradiation, confirming the etching of QDs during the photocatalytic process (**Figure 4b.9a**). The etching of InP was accompanied with surface oxidation of QD as evident from XPS studies (**Figures 4b.9b, 4b.23**). After the photocatalytic reaction, oxidation features were prominent for both In 3d and P 2p peaks (**Figure 4b.23**). In particular, the In 3d peak broadened, and a significant enhancement in P 2p peaks corresponding to $InPO_x$ was observed, which confirms the oxidation process of core-only [+] InP QDs after the photocatalytic reaction (**Figures 4b.9b, 4b.23**). Consequently, the photocatalytic activity of InP QDs gradually decreased in each cycle, thereby impeding the recyclability beyond three cycles (**Figure 4b.24**). It is well known that InP QDs are prone to oxidation as oxygen and water can dissociatively adsorb on the InP surface.[35-37] In a recent report by Jeong and coworkers, photoassisted surface oxidation of InP tetrahedrons was observed, which led to the blue shift in the absorption spectrum.[38] This was explained as follows:[38]

$$InP + h\nu \rightarrow e^- + h^+$$

$$InP + e^-/h^+ + O_2 \rightarrow (InP + h^+) + O_2^{\cdot-}$$

$$(InP + 2h^+) + 2O_2^{\cdot-} \rightarrow InP + InPO_4$$

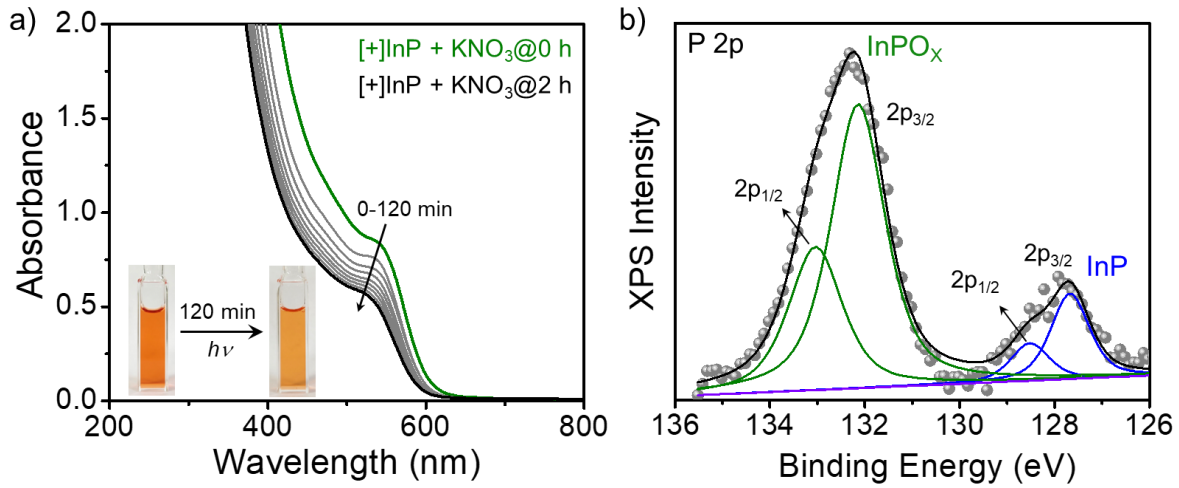


**Figure 4b.9.** Stability of InP QDs during the photocatalytic ammonia synthesis. a) Time-dependent absorption profile of [+] InP QDs in the photocatalytic reaction mixture. Inset shows the optical photograph of the reaction mixture before and after the photocatalytic reaction. A visual color change was observed for [+] InP QDs during the photocatalytic reaction (the deep orange color of [+] InP QDs faded with time), indicating the etching of QDs. b) Analysis of XPS spectra for [+] InP QDs after the photocatalytic reaction.

To gain better insight into the hole-scavenging step and improve the recyclability, we introduced InP/ZnS core/shell QDs and ethanol (EtOH) as the photocatalyst and external hole scavenger, respectively. EtOH provides a better driving force ($E^o$ = −4.66 eV) than water ($E^o$ = −5.67 eV) for the extraction of holes from the valence band of QDs. Moreover, employing EtOH as an additional hole scavenger aligns well with the current focus of producing more useful products in the oxidation half-cycle in photocatalysis.[39,40] Interestingly, the use of EtOH allowed us to retain excellent photocatalytic efficiency with InP/ZnS core/shell QDs which was comparable to core-only InP QDs for ammonia synthesis (**Figures 4b.10a, 4b.10b**). The presence of acetaldehyde, an oxidized product of EtOH, was also observed during the gas-phase mass analysis (**Figure 4b.10c**). Along with the complete retention of their photocatalytic activity, InP/ZnS QDs exhibited excellent stability under prolonged irradiation for 36 h without any visual color change or etching (**Figures 4b.10d, 4b.25**). This enabled long-term photocatalytic experiments with complete retention of the photocatalytic activity up to 4 cycles, followed by 75 % retention in the subsequent cycles (**Figure 4b.10e**). It is to be noted that recyclability is an untouched aspect of QD photocatalysis, and we achieved this feat through the rational design of our photocatalytic system.

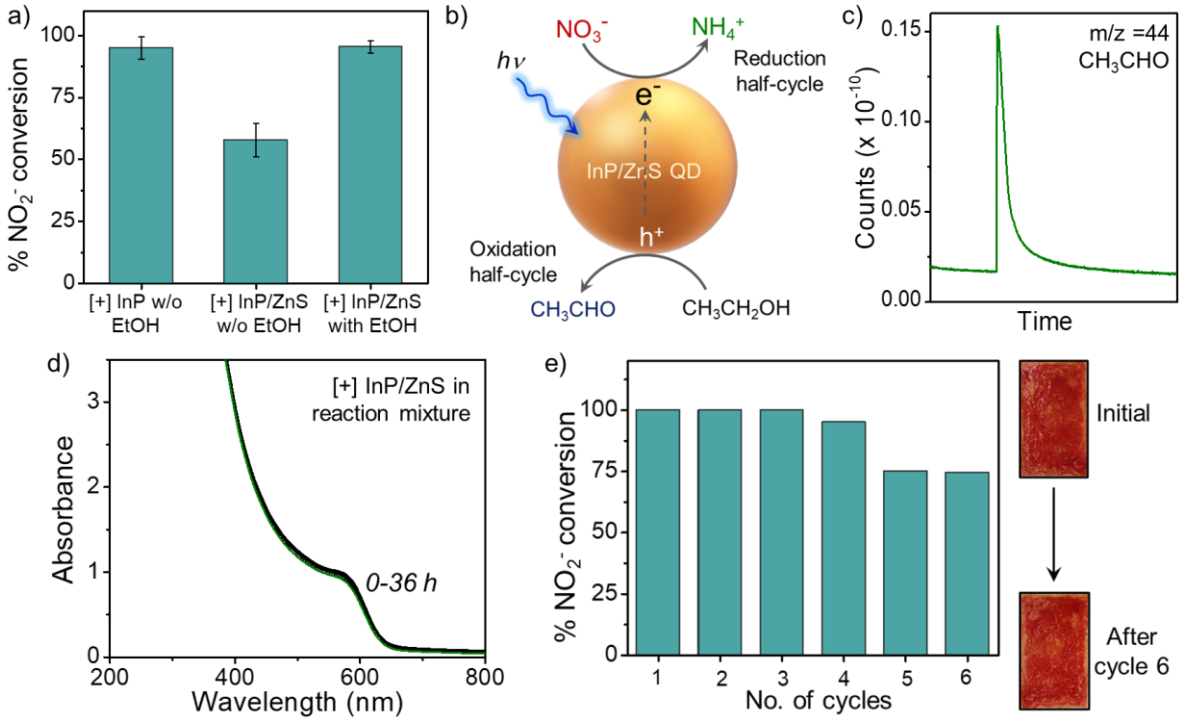


**Figure 4b.10.** a) Effect of ethanol (additional hole scavenger) on the photocatalytic activity. Bar diagram showing the efficiency of core-only InP vs core/shell InP/ZnS QDs in the presence and absence of ethanol as a hole scavenger. b) Schematics showing the photocatalytic processes in reduction and oxidation half-cycles with InP/ZnS QDs in presence of external hole scavenger (ethanol). c) Gas phase mass analysis of the photocatalytic reaction performed in the presence of ethanol ($CH_3CH_2OH$). The mass signal at m/z=44, corresponding to acetaldehyde ($CH_3CHO$), which is the oxidized product of ethanol, was observed. d) Time-dependent absorption spectra of the reaction mixture consisting of [+] InP/ZnS, $KNO_2$, and ethanol (EtOH) show negligible change in the optical properties upon continuous light irradiation for 36 h with 2 X 10W 450 nm LEDs. e) Recyclability studies performed with a paper-based dip-catalyst system show excellent retention of photocatalytic activity with InP/ZnS core/shell QDs in the presence of ethanol as an additional hole scavenger. Optical photographs of paper-based dip catalyst film show excellent stability of InP/ZnS QDs even after ~36 h of continuous irradiation.

## 4b.4.5. Probable mechanism

Based on the accumulated experimental evidence and prior literature, we propose an overall mechanism for $NO_3^-$ reduction to $NH_3$ with [+] InP QDs (**Figure 4b.11a**). Favourable electrostatic attraction between [+] InP QD and [-] $NO_3^-$ modifies the microenvironment of QD photocatalyst by increasing the local concentration of $NO_3^-$, which enhances the probability of the charge transfer process. The photoexcited electrons are utilized for $NO_3^-$ reduction, where $NO_3^-$ to $NO_2^-$ reduction step is slow and determines the overall rate of the reaction (**Figure 4b.11a**). The subsequent reduction of $NO_2^-$ to $NH_3$ takes place rapidly with ~100 % conversion. A series of control experiments

with deuterated water ($D_2O$), non-thiolated ligands, and in polar aprotic medium, with additional support from FTIR studies, confirm that water is the proton source in our study. A part of photoexcited electrons drive the competing $H_2$ evolution reaction, which does not interfere with the reduction of $NO_3^-$ as well as $NO_2^-$ to $NH_3$ by [+] InP QDs (**Figure 4b.11a**). Now, the reduction of $NO_3^-$ is reported to follow three main pathways: one resulting in $N_2$ as the end-product, whereas $NH_3$ is the end-product in remaining two pathways (**Figure 4b.11b**).[4,5,41,42] Absence of $N_2$ formation, along with the selective formation of $NH_3$ with [+] InP QDs rules out one of the three major pathways (**Figure 4b.11b**). Separate experiments were performed to identify the exact pathway involved in the present study (**Figure 4b.26**). However, the fast kinetics of $NO_2^-$ to $NH_4^+$ formation inhibits the accumulation of any intermediates to be detected, which made the elucidation of the exact reaction pathway challenging. Appropriate in-situ experiments must be designed to detect the crucial short-lived intermediates and elucidate the exact pathway involved, which demands for a separate study.[43] Despite this, the present study provides important mechanistic insights in establishing InP QD as a potential visible-light photocatalyst for the synthesis of ammonia.

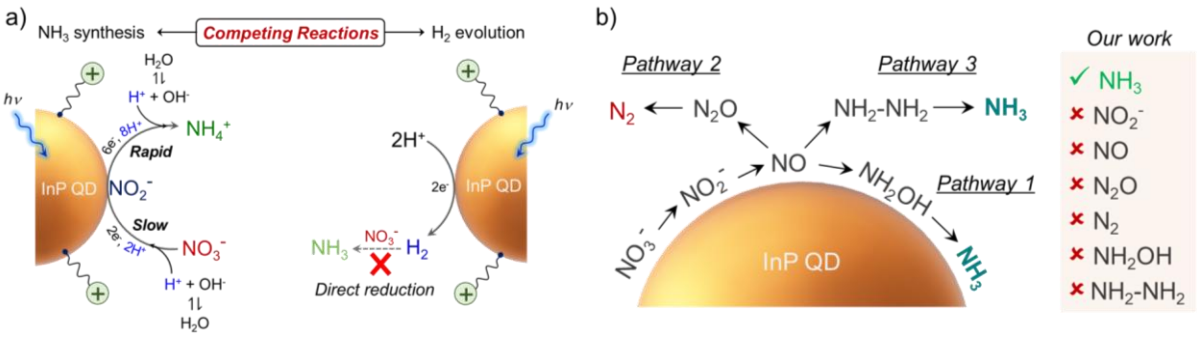


**Figure 4b.11.** a) Schematics of the proposed reaction mechanism for the visible-light photocatalysed reduction of $NO_3^-$ to $NH_4^+$ by [+] InP QDs. b) Schematic representation of the three major pathways involved in photocatalytic reduction of $NO_3^-$. Appropriate experiments were performed to identify different intermediates formed during the ammonia synthesis with [+] InP QDs. However, the fast kinetics of $NO_2^-$ to $NH_4^+$ formation inhibits the accumulation of any intermediates to be detected. A selective formation of $NH_3$ in aqueous and gaseous phases was achieved with [+] InP QD as the photocatalyst.

## 4b.5. Conclusions

In light of establishing III-V InP QDs as visible-light photocatalysts for nitrate-to-ammonia conversion, a detailed mechanistic investigation was carried out in the present study. Kinetic analysis, in combination with isotope-labeled studies, revealed that the first two electron transfer steps for conversion of $NO_3^-$ to $NO_2^-$ determine the overall efficiency of ammonia synthesis with InP QDs. Negligible accumulation of any of the nitrate reduction products in the aqueous as well as the gas phase confirmed excellent selectivity of InP QDs for ammonia production under visible light irradiation. Along with ammonia formation, a part of the photoexcited charge carriers was involved in a kinetically facile $H_2$ evolution reaction, which proved innocent in the direct nitrate reduction. A series of control experiments ascertained water as the sole proton source in ammonia formation. We also gained insights into the hole scavenging step, which turned out to be crucial in achieving enhanced recyclability and enabled long-term photocatalytic experiments. In short, we listed key findings associated with reaction rate, competing reactions, proton source, and the fate of photoexcited holes in the multielectron transformation of nitrate to ammonia. With the insufficient research on reaction pathways for nitrate reduction, we strongly believe that our findings would serve as the blueprint for understanding a broad landscape of photocatalytic elements involved across different classes of materials. As visible-light photocatalytic reduction of nitrate to ammonia is still in the nascent stage, we envision that experimental data, in combination with appropriate in-situ studies and theoretical simulations, will build a strong foundation for scalable and sustainable $NH_3$ formation.

## 4b.6. References

1) Contreras, E.; Nixon, R.; Litts, C.; Zhang, W.; Alcorn, F. M.; Jain, P. K. Plasmon-Assisted Ammonia Electrosynthesis. *J. Am. Chem. Soc.* **2022**, *144*, 10743-10751.

2) Li, J.; Chen, R.; Wang, J.; Zhou, Y.; Yang, G.; Dong, F. Subnanometric Alkaline-Earth Oxide Clusters for Sustainable Nitrate to Ammonia Photosynthesis. *Nat. Commun.* **2022**, *13*, 1098.

3) Meng, S.-L.; Li, J.-H.; Ye, C.; Yin, Y.-L.; Zhang, X. -L; Zhang, C.; Li, X.-B.; Tung, C.-H.; Wu, L.-Z. Concurrent Ammonia Synthesis and Alcohol Oxidation Boosted by Glutathione-Capped Quantum Dots Under Visible Light. *Adv. Mater.* **2024**, *36*, 2311982.

4) Yang, W.; Wang, J.; Chen, R.; Xiao, L.; Shen, S.; Li, J.; Dong, F. Reaction Mechanism and Selectivity Regulation of Photocatalytic Nitrate Reduction for Wastewater Purification: Progress and Challenges. *J. Mater. Chem. A* **2022**, *10*, 17357-17376.

5) Zhang, C.; Li, J.; Chen, R.; Shen, S.; Wang, J.; Sun, Y.; Dong, F. $NH_3$ Synthesis from $N_1$ Compounds by Photocatalytic Technology: Promotion Mechanism, Reaction Pathways, and Efficiency Evaluation Criteria. *ACS Catal.* **2024**, *14*, 15721-15742.

6) Meng, S.-L.; Ye, C.; Li, X.-B.; Tung, C.-H.; Wu, L.-Z. Photochemistry Journey to Multielectron and Multiproton Chemical Transformation. *J. Am. Chem. Soc.* **2022**, *144*, 16219-16231.

7) Hirakawa, H.; Hashimoto, M.; Shiraishi, Y.; Hirai, T. Selective Nitrate-to-Ammonia Transformation on Surface Defects of Titanium Dioxide Photocatalysts. *ACS Catal.* **2017**, *7*, 3713-3720.

8) Yamauchi, M.; Abe, R.; Tsukuda, T.; Kato, K.; Takata, M. Highly Selective Ammonia Synthesis from Nitrate with Photocatalytically Generated Hydrogen on CuPd/$TiO_2$. *J. Am. Chem. Soc.* **2011**, *133*, 1150-1152.

9) Challagulla, S.; Tarafder, K.; Ganesan, R.; Roy, S. All That Glitters Is Not Gold: A Probe into Photocatalytic Nitrate Reduction Mechanism over Noble Metal Doped and Undoped $TiO_2$. *J. Phys. Chem. C* **2017**, *121*, 27406-27416.

10) Clark, C. A.; Reddy, C. P.; Xu, H.; Heck, K. N.; Luo, G.; Senftle, T. P.; Wong, M. S. Mechanistic Insights into pH-Controlled Nitrite Reduction to Ammonia and Hydrazine over Rhodium. *ACS Catal.* **2020**, *10*, 494-509.

11) Wang, Y.; Zhou, W.; Jia, R.; Yu, Y.; Zhang, B. Unveiling the Activity Origin of a Copper-based Electrocatalyst for Selective Nitrate Reduction to Ammonia. *Angew. Chem. Int. Ed.* **2020**, *59*, 5350-5354.

12) Zhang, S.; Wu, J.; Zheng, M.; Jin, X.; Shen, Z.; Li, Z.; Wang, Y.; Wang, Q.; Wang, X.; Wei, H.; Zhang, J.; Wang, P.; Zhang, S.; Yu, L.; Dong, L.; Zhu, Q.; Zhang, H.; Lu, J. Fe/Cu Diatomic Catalysts for Electrochemical Nitrate Reduction to Ammonia. *Nat. Commun.* **2023**, *14*, 3634.

13) Shiraishi, Y.; Akiyama, S.; Hiramatsu, W.; Adachi, K.; Ichikawa, S.; Hirai, T. Sunlight-Driven Nitrate-to-Ammonia Reduction with Water by Iron Oxyhydroxide Photocatalysts. *JACS Au* **2024**, *4*, 1863-1874.

14) Zhao, Y.; Shen, J.; Yuan, J.; Mao, H.; Cheng, X.; Xu, Z.; Bian, Z. Modulating Electronic Structures of MOF Through Orbital Rehybridization by Cu Doping Promotes Photocatalytic Reduction of Nitrate to Produce Ammonia. *Nano Energy* **2024**, **124**, 109499

15) Bai, L.; Franco, F.; Timoshenko, J.; Rettenmaier, C.; Scholten, F.; Jeon, H. S.; Yoon, A.; Rüscher, M.; Herzog, A.; Haase, F. T.; Kühl, S.; Chee, S. W.; Bergmann, A.; Beatriz, R. C. Electrocatalytic Nitrate and Nitrite Reduction toward Ammonia Using $Cu_2O$ Nanocubes: Active Species and Reaction Mechanisms. *J. Am. Chem. Soc.* **2024**, *146*, 9665-9678.

16) Hiramatsu, W.; Shiraishi, Y.; Ichikawa, S.; Tanaka, S.; Kawada, Y.; Hiraiwa, C.; Hirai, T. Surface Oxygen Vacancies on Copper-Doped Titanium Dioxide for Photocatalytic Nitrate-to-Ammonia Reduction. *J. Am. Chem. Soc.* **2025**, *147*, 1968-1979.

17) Hirayama, J.; Kondo, H.; Miura, Y.-k.; Abe, R.; Kamiya, Y. Highly Effective Photocatalytic System Comprising Semiconductor Photocatalyst and Supported Bimetallic Non-Photocatalyst for Selective Reduction of Nitrate to Nitrogen in Water. *Catal. Commun.* **2012**, *20*, 99-102.

18) Hirayama, J.; Kamiya, Y. Combining the Photocatalyst $Pt/TiO_2$ and the Nonphotocatalyst $SnPd/Al_2O_3$ for Effective Photocatalytic Purification of Groundwater Polluted with Nitrate. *ACS Catal.* **2014**, *4*, 2207-2215.

19) Kuo, D.-Y.; Nishiwaki, E.; Rivera-Maldonado, R. A.; Cossairt, B. M. The Role of Hydrogen Adsorption Site Diversity in Catalysis on Transition-Metal Phosphide Surfaces. *ACS Catal.* **2023**, *13*, 287-295.

20) Wei, L.; Liu, D.-J.; Rosales, B. A.; Evans, J. W.; Vela, J. Mild and Selective Hydrogenation of Nitrate to Ammonia in the Absence of Noble Metals. *ACS Catal.* **2020**, *10*, 3618-3628.

21) Frear, D. S.; Burrell, R.C. Spectrophotometric Method for Determining Hydroxylamine Reductase Activity in Higher Plants. *Anal. Chem.* **1955**, *27*, 1664-1665.

22) Watt, G. W.; Chrisp, J. D. A Spectrophotometric Method for the Determination of Hydrazine. *Anal. Chem.* **1952**, *24*, 2006-2008.

23) Lin, H.; Liu, Y.; Yang, C.; Zhao, G.; Song, J.; Zhang, T.; Huang, X. Microfluidic Artificial Photosynthetic System for Continuous NADH Regeneration and L-glutamate Synthesis. *Catal. Sci. Technol.* **2022**, *12*, 4057-4065.

24) Reiss, P.; Protière, M.; Li, L. Core/Shell Semiconductor Nanocrystals. *Small* **2009**, *5*, 154-168.

25) Li, P.; Li, R.; Liu, Y.; Xie, M.; Jin, Z.; Yu, G. Pulsed Nitrate-to-Ammonia Electroreduction Facilitated by Tandem Catalysis of Nitrite Intermediates. *J. Am. Chem. Soc.* **2023**, *145*, 6471-6479.

26) Kim, H. E.; Kim, J.; Ra, E. C.; Zhang, H.; Jang, Y. J.; Lee, J. S. Photoelectrochemical Nitrate Reduction to Ammonia on Ordered Silicon Nanowire Array Photocathodes. *Angew. Chem., Int. Ed.* **2022**, *61*, e202204117.

27) Fang, Y.; Flake, J. C. Electrochemical Reduction of $CO_2$ at Functionalized Au Electrodes. *J. Am. Chem. Soc.* **2017**, *139*, 3399-3405.

28) Chamousis, R. L.; Osterloh, F. E. Use of Potential Determining Ions to Control Energetics and Photochemical Charge Transfer of a Nanoscale Water Splitting Photocatalyst. *Energy Environ. Sci.* **2014**, *7*, 736-743.

29) Dümbgen, K. C.; Leemans, J.; De Roo, V.; Minjauw, M.; Detavernier, C.; Hens, Z. Surface Chemistry of InP Quantum Dots, Amine–Halide Co-Passivation, and Binding of Z-Type Ligands. *Chem. Mater.* **2023**, *35*, 1037-1046.

30) Bryden, M. A.; Zysman-Colman, E. Organic Thermally Activated Delayed Fluorescence (TADF) Compounds used in Photocatalysis. *Chem. Soc. Rev.* **2021**, *50*, 7587-7680.

31) Li, X.-B.; Li, Z.-J.; Gao, Y.-J.; Meng, Q.-Y.; Yu, S.; Weiss, R. G.; Tung, C.-H.; Wu, L.-Z. Mechanistic Insights into the Interface-Directed Transformation of Thiols into Disulfides and Molecular Hydrogen by Visible-Light Irradiation of Quantum Dots. *Angew. Chem., Int. Ed.* **2014**, *53*, 2085-2089.

32) Mićić, O. I.; Nozik, A. J.; Lifshitz, E.; Rajh, T.; Poluektov, O. G.; Thurnauer, M. C. Electron and Hole Adducts Formed in Illuminated InP Colloidal Quantum Dots Studied by Electron Paramagnetic Resonance. *J. Phys. Chem. B* **2002**, *106*, 4390-4395.

33) Thomas, A.; Sandeep, K.; Somasundaran, S. M.; Thomas, K. G. How Trap States Affect Charge Carrier Dynamics of CdSe and InP Quantum Dots: Visualization through Complexation with Viologen. *ACS Energy Lett.* **2018**, *3*, 2368-2375.

34) Shulenberger, K. E.; Keller, H. R.; Pellows, L. M.; Brown, N. L.; Dukovic, G. Photocharging of Colloidal CdS Nanocrystals. *J. Phys. Chem. C* **2021**, *125*, 22650-22659.

35) Chen, G.; Visbeck, S. B.; Law, D. C.; Hicks, R. F. Structure-Sensitive Oxidation of the Indium Phosphide (001) Surface. *J. Appl. Phys.* **2002**, *91*, 9362-9367.

36) May, M. M.; Lewerenz, H.-J.; Hannappel, T. Optical In Situ Study of InP (100) Surface Chemistry: Dissociative Adsorption of Water and Oxygen. *J. Phys. Chem. C* **2014**, *118*, 19032-19041.

37) Almeida, G.; Ubbink, R. F.; Stam, M.; du Fosse, I.; Houtepen, A. J. InP Colloidal Quantum Dots for Visible and Near-Infrared Photonics. *Nat. Rev. Chem.* **2023**, *8*, 742-758.

38) Cho, E.; Kim, M.; Ouyang, L.; Kim, H.; Bonifas, F.; Coppel, Y.; Nayral, C.; Delpech, F.; Jeong, S. Unraveling the Facet-Dependent Surface Chemistry at Molecular Scale:

Photoassisted Oxidation of InP Nanocrystals. *J. Am. Chem. Soc.* **2024**, *146*, 31691-31701.

39) Kim, J.; Lin, J.-A.; Kim, J.; Roh, I.; Lee, S.; Yang, P. A Red-light-powered Silicon Nanowire Biophotochemical Diode for Simultaneous $CO_2$ Reduction and Glycerol Valorization. *Nat. Catal.* **2024**, *7*, 977-986.

40) Teng, J.; Li, W.; Wei, Z.; Hao, D.; Jing, L.; Liu, Y.; Dai, H.; Zhu, Y.; Ma, T.; Deng, J. Coupling Photocatalytic Hydrogen Production with Key Oxidation Reactions. *Angew. Chem., Int. Ed.* **2024**, e202416039.

41) Guo, Y.; Stroka, J. R.; Kandemir, B.; Dickerson, C. E.; Bren, K. L. Cobalt Metallopeptide Electrocatalyst for the Selective Reduction of Nitrite to Ammonium. *J. Am. Chem. Soc.* **2018**, *140*, 16888-16892.

42) Wang, Z.; Richards, D.; Singh, N. Recent Discoveries in the Reaction Mechanism of Heterogeneous Electrocatalytic Nitrate Reduction. *Catal. Sci. Technol.* **2021**, *11*, 705-725.

43) Wang, H.; Huang, J.; Cai, J.; Wei, Y.; Cao, A.; Liu, B.; Lu, S. In Situ/Operando Methods for Understanding Electrocatalytic Nitrate Reduction Reaction. *Small Methods* **2023**, *7*, 2300169

44) Virieux, H.; Le Troedec, M.; Cros-Gagneux, A.; Ojo, W. S.; Delpech, F.; Nayral, C.; Martinez, H.; Chaudret, B. InP/ZnS Nanocrystals: Coupling NMR and XPS for Fine Surface and Interface Description. *J. Am. Chem. Soc.* **2012**, *134*, 19701-19708.

45) Eren, G. O.; Sadeghi, S.; Jalali, H. B.; Ritter, M.; Han, M.; Baylam, I.; Melikov, R.; Onal, A.; Oz, F.; Sahin, M.; Ow-Yang, C. W.; Sennaroglu, A.; Lechner, R. T.; Nizamoglu, S. Cadmium-Free and Efficient Type-II InP/ZnO/ZnS Quantum Dots and Their Application for LEDs. *ACS Appl. Mater. Interfaces* **2021**, *13*, 32022-32030.

46) Roy, P.; Virmani, M.; Pillai, P. P. Blue-Emitting InP Quantum Dots Participate in an Efficient Resonance Energy Transfer Process in Water. *Chem. Sci.* **2023**, *14*, 5167-5176.

47) Weng, B.; Qi, M.-Y.; Han, C.; Tang, Z.-R.; Xu, Y.-J. Photocorrosion Inhibition of Semiconductor-Based Photocatalysts: Basic Principle, Current Development, and Future Perspective. *ACS Catal.* **2019**, *9*, 4642-4687.

48) Dou, F. Y.; Nishiwaki, E.; Larson, H.; Homer, M. K.; Zion, T.; Nguyen, H. A.; Cossairt, B. M. Pathways of CdS Quantum Dot Degradation During Photocatalysis: Implications for Enhancing Stability and Efficiency for Organic Synthesis. *ACS Appl. Nano Mater.* **2024**, *7*, 15781-15785.

# 4b.7. Appendix

**Identification of side products**

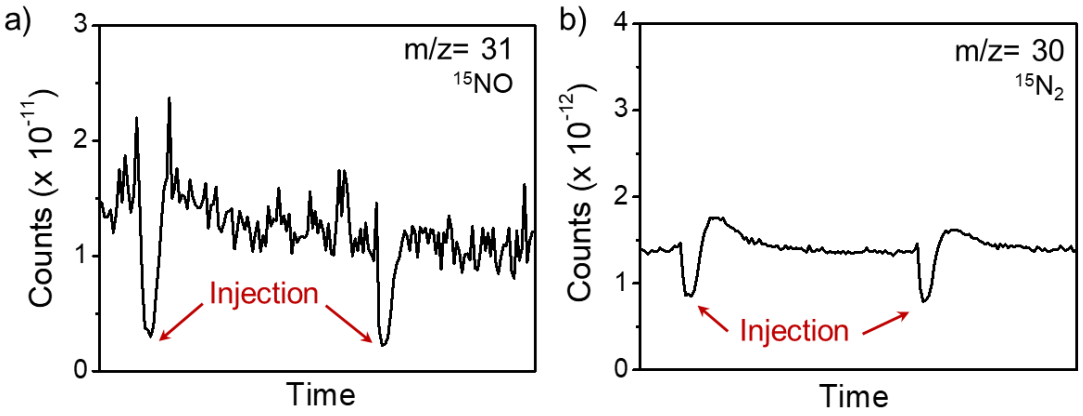


**Figure 4b.12**. Headspace analysis of the photocatalytic reaction performed with isotope labelled $^{15}NO_3^-$. Signals for a) m/z =31 and b) m/z = 30 corresponds to $^{15}NO$ and $^{15}N_2$, respectively. A negligible amount of these gaseous products was observed in the headspace, confirming the selective formation of $NH_3$.

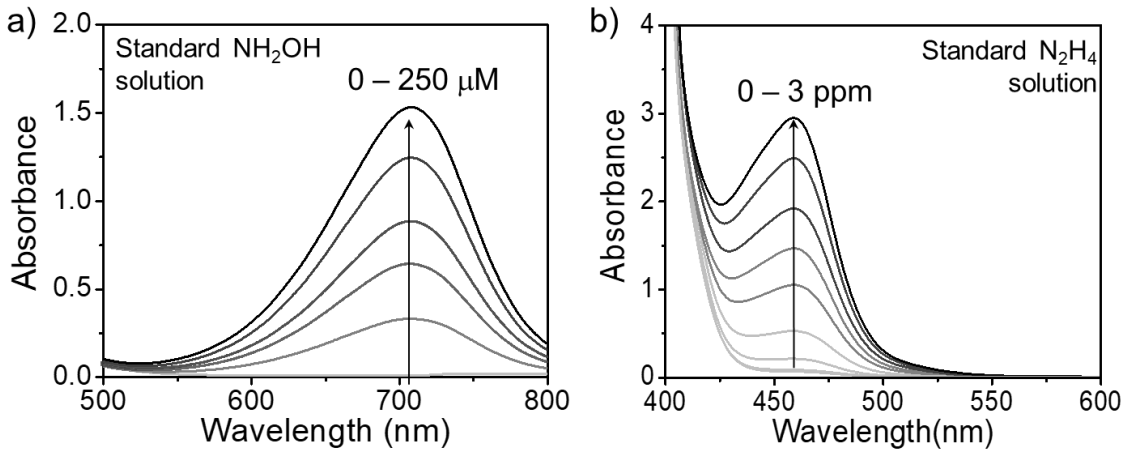


**Figure 4b.13.** a) Identification of $NH_2OH$ in photocatalytic $NO_3^-$ reduction to $NH_4^+$ using 8-hydroxyquinoline based colorimetry assay. Absorption spectra of the reaction mixture with a known concentration (0-250 μM) of $NH_2OH$. b) Identification of $N_2H_4$ in photocatalytic $NO_3^-$ reduction to $NH_4^+$ using spectrophotometric Watt-Chrisp method. Absorption spectra of the reaction mixture with a known concentration (0-3 ppm) of $N_2H_4$.

### Elucidation of rate-determining step

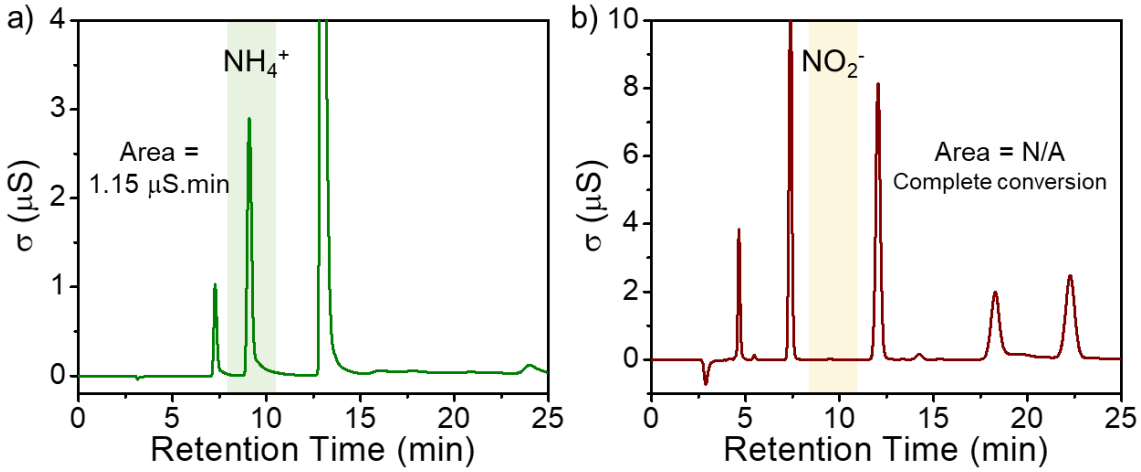


**Figure 4b.14**. Photocatalytic reaction with $NO_2^-$ as the substrate. a) Cation and b) anion ion chromatograms for the reaction mixture, clearly showing the formation of $NH_4^+$ along with complete reduction of $NO_2^-$ (retention time ~ 9.5 min).

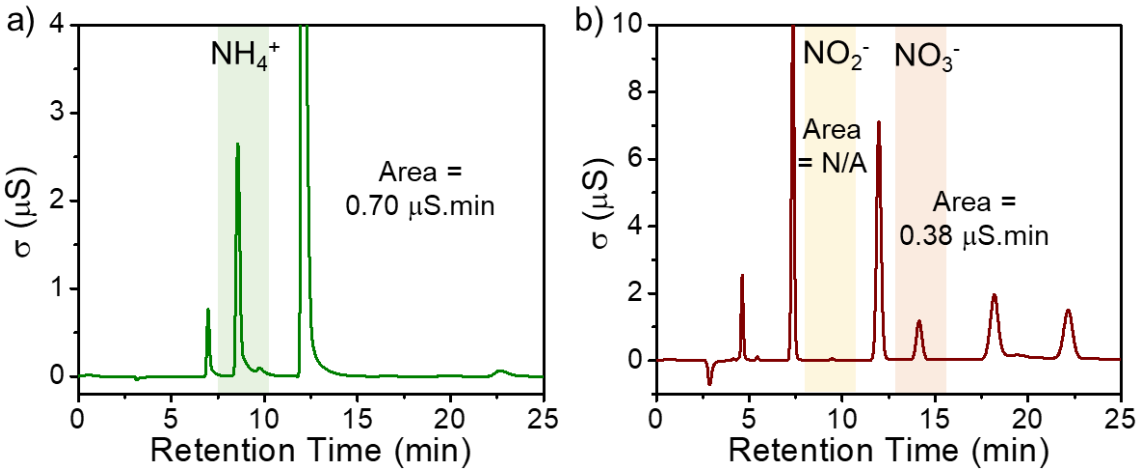


**Figure 4b.15**. Competing photocatalytic experiment performed with a mixture of $NO_3^-$ and $NO_2^-$. a) Cation and b) anion ion chromatograms depicting the formation of $NH_4^+$ and conversion of $NO_3^-$ and $NO_2^-$. Anion chromatograms show complete conversion of $NO_2^-$, whereas $NO_3^-$ still remained unreacted, suggesting $NO_3^-$ to $NO_2^-$ a probable rate determining step.

### Role of $H_2$ in reduction of $NO_3^-$/$NO_2^-$ ions

$H_2$ evolution is a commonly observed competing reaction in photocatalytic reactions involving multiple electrons and protons. To evaluate its impact on photocatalytic nitrate reduction with InP QDs, we performed a series of control experiments. In one set of experiments, we irradiated [+] InP QDs in water for 2 h with 2 x 10 W 450 nm LEDs. This resulted in generation of $H_2$ which was analyzed using Agilent 7890 GC. To this pre-irradiated reaction mixture, we added 0.5 mM $KNO_3$ to evaluate whether $H_2$ can reduce $NO_3^-$ or not. The reaction mixture was incubated in dark as well as light for next 2 h and analyzed using ion chromatography (**Figure 4b.16**). $NH_3$ formation was observed only under light illumination with little-to-no impact on reaction efficiency. Similarly, $H_2$ evolution did not impact $NH_3$ formation with $NO_2^-$ as the substrate as well (**Figure 4b.17**). We further validated the negligible role of $H_2$ by directly purging $H_2$ gas in the reaction mixture and incubated for 2 h in light as well as dark conditions. Again, reaction was found to proceed only in the presence of light with no activity at all in the dark conditions (**Figure 4b.18**). All these experiments confirm that $H_2$ evolution is merely a competing reaction and does not participate in reduction of $NO_3^-$ and $NO_2^-$ to form $NH_3$.

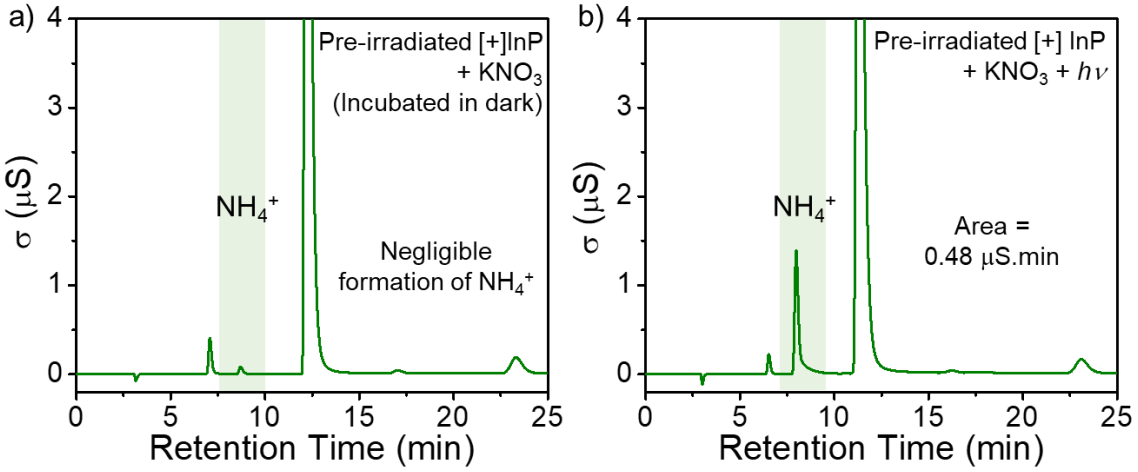


**Figure 4b.16**. Role of photocatalytic $H_2$ evolution in nitrate reduction. Cation ion chromatograms a) in absence of light and b) in presence of light after addition of $KNO_3$ in the preirradiated reaction mixture containing [+] InP QDs. Irradiation of [+] InP QDs in water results in $H_2$ evolution. However, no $NH_4^+$ formation took place after addition of $NO_3^-$ to this irradiated reaction mixture when incubated in dark upto 2 h. $NH_4^+$ forms only in the presence of light, confirming the photocatalytic pathway for $NO_3^-$ to $NH_3$ production.

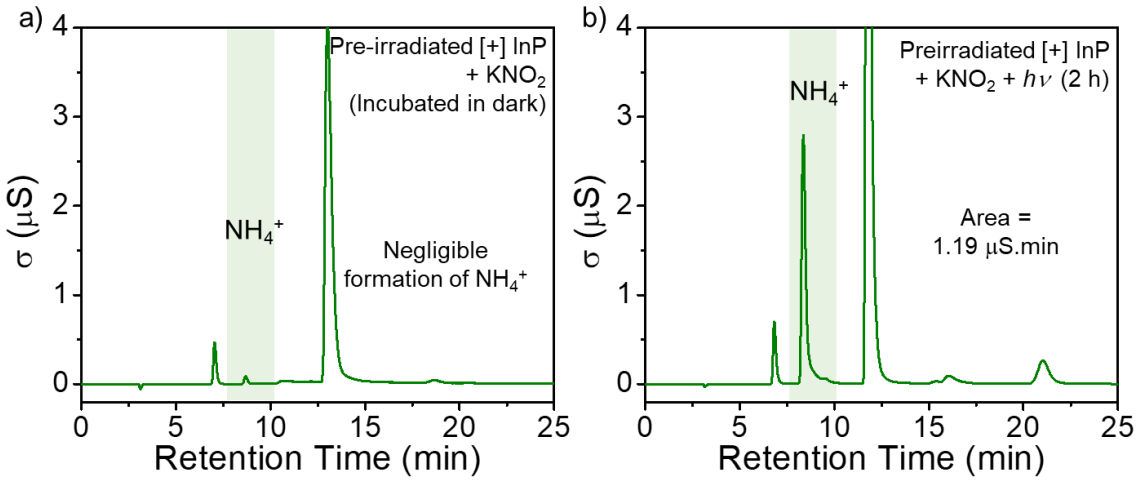


**Figure 4b.17**. Effect of photocatalytic $H_2$ evolution on $KNO_2$ reduction with [+] InP QDs. Cation ion chromatograms a) in absence of light and b) in presence of light after addition of $KNO_2$ in the preirradiated reaction mixture containing [+] InP QDs. Photocatalytic hydrogen evolution does not inhibit photocatalytic $NH_4^+$ formation.

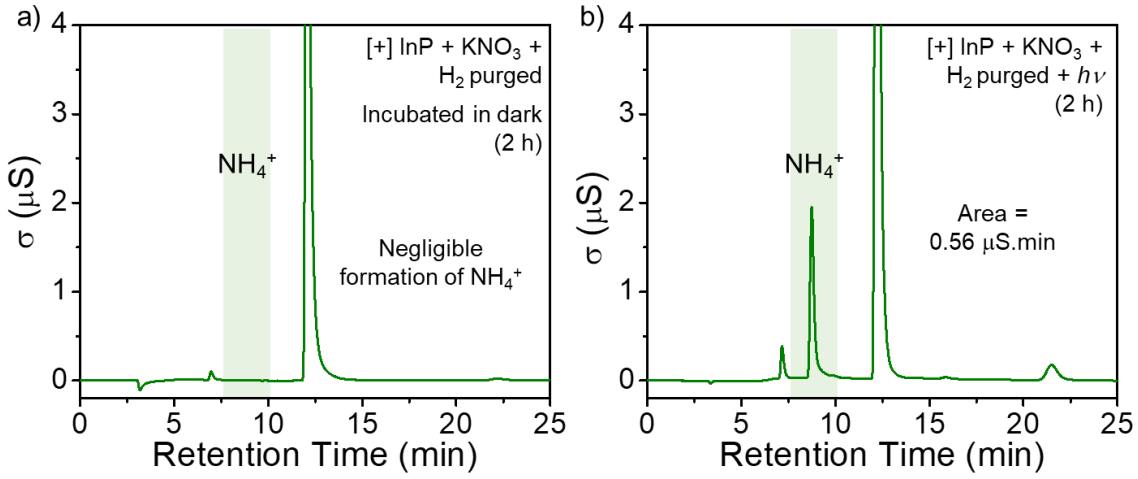


**Figure 4b.18**. Proof for active participation of photoexcited charge carriers in nitrate reduction. Ion chromatograms of reaction mixture purged with $H_2$ gas a) in absence of light, and b) in presence of light. A negligible formation of $NH_4^+$ was observed in presence of $H_2$ without light illumination, confirming negligible role of $H_2$ in direct reduction of $NO_3^-$ to $NH_3$.

**Utilization of photoexcited charge electrons**

Assuming that each absorbed photon generates one $e^-$-$h^+$ pair, the total number of photoexcited electrons will be 3.13 x $10^{21}$ at 450 nm excitation, as per the following equation:

$$number\ \ of\ e^- - h^+\ pairs\ generated = \frac{P_0 \times \lambda\ (m) \times t\ (s)}{hc} \times \%\ incident\ light\ absorbed$$

where, $P_0$(J $s^{-1}$) is the power of incident light, $\lambda\ (m)$ is the wavelength (in meters) of LED light source, $t\ (s)$ is the total irradiation time (in seconds), *h* is the Plank's constant (J.s), and *c* is the speed of light (m $s^{-1}$).

The number of electrons extracted to form $NH_4^+$ and $H_2$ was calculated to be 4.82 x $10^{18}$ using the following equation:

$$number\ \ of\ e^- extracted = (8 \times no.of\ moles\ of\ NH_4^+ \times N_A) + (2 \times no.of\ moles\ of\ H_2 \times N_A)$$

Here, 8 and 2 correspond to the number of electrons required for the reduction of nitrate to ammonium ions and proton to hydrogen, respectively. Moles of $NH_4^+$ and $H_2$ formed were estimated from ion chromatography and gas chromatography experiments, respectively. $N_A$ is the Avogadro number.

As can be seen, ~$10^3$ electrons are lost without participating in the desired reaction. This inefficiency in extracting all the photoexcited charge carriers is well reflected in the low internal quantum yield (IQY), as reported in our study.

The complex interplay of exciton dynamics and interfacial catalytic events across different scales accounts for these losses. Upon light irradiation, excitons are generated in QDs within fs timescale. These photogenerated excitons in QDs can undergo band-edge recombination in the ns timescale, be trapped at the defect sites in QD crystal, or undergo interfacial charge transfer to the reactant molecules. The trapped charge carriers can also undergo recombination from respective sites or transfer to reactant molecules. In short, the transfer of charge carriers always competes with various radiative or non-radiative processes. For chemical transformations involving multielectron reactions such as $NO_3^-$ reduction to $NH_4^+$, multiple electrons (8 $e^-$) must be transferred, which necessitates the stabilization of 1e- intermediates long enough till the next electron transfer process can take place. Additionally, most of the multielectron reactions (in our case, $NO_3^-$ reduction to $NH_4^+$) are accompanied by the proton transfer as well, which makes each proton-coupled electron transfer step challenging, impacting the overall efficiency of photocatalytic reactions.

As $H_2$ evolution reaction was observed alongside photocatalytic reduction of $NO_3^-$ to $NH_4^+$, we calculated the effective photoexcited electron utilization for the competing reactions. As $H_2$ evolution involves 2 electrons and $NO_3^-$ to $NH_4^+$ conversion requires 8 electrons, the fraction of electrons utilized for these two reactions was calculated as follows:

<u>For $H_2$ evolution reaction:</u>

Moles of $H_2$ generated = 678$\pm$101 nmol

Moles of electrons = 2 (moles of $H_2$) = ~1400 nmol

<u>For $NO_3^-$ to $NH_4^+$ conversion:</u>

Moles of $NH_4^+$ generated = 783$\pm$111 nmol

Moles of electrons = 8 (moles of $NH_4^+$) = ~6600 nmol

Therefore, total electrons involved in photocatalytic reactions = ~8000 nmoles

Thus,

The fraction of electrons used for $H_2$ evolution = 1400/8000 = ~0.175 = ~17.5 %

The fraction of electrons used for $H_2$ evolution = 6600/8000 = ~0.825 = ~82.5 %

**Identification of proton source and hole scavenger**

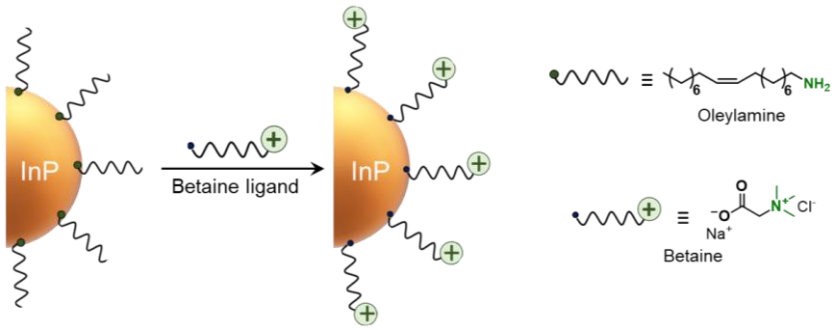


**Scheme 4b.1**. Schematics showing the ligand exchange of InP QDs with non-thiolated betaine ligand.

<u>Glutamate dehydrogenase (GLDH) assay</u>

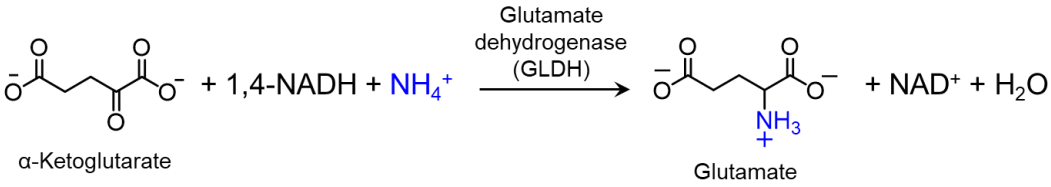


**Scheme 4b.2**. Schematics of glutamate dehydrogenase assay to form glutamate from a-ketoglutarate in the presence of NADH and $NH_4^+$.

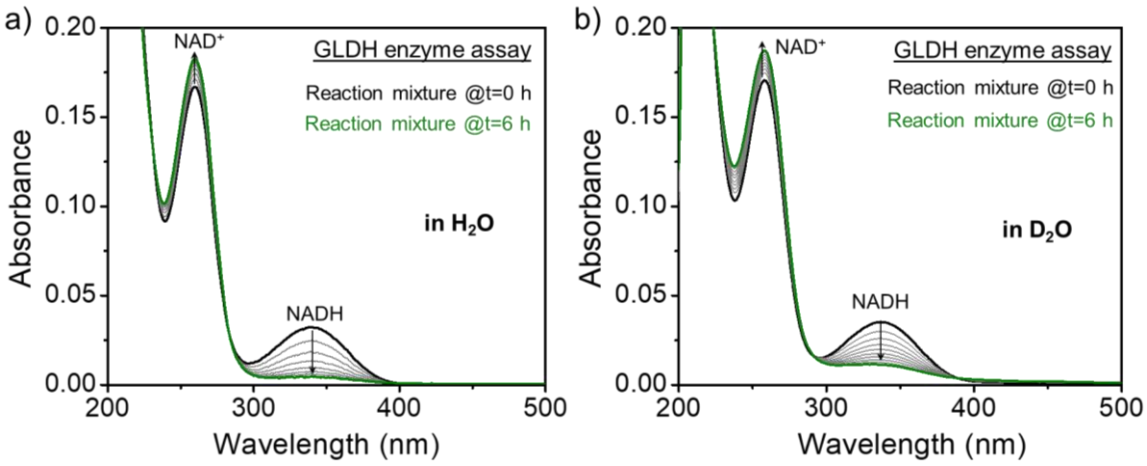


**Figure 4b.19**. UV-vis absorption spectra of GLDH assay proving the formation of glutamate in the presence of a) $NH_4^+$ (in $H_2O$) and b) isotope-labelled $^{15}ND_4^+$ (in $D_2O$) produced during the photocatalytic reaction.

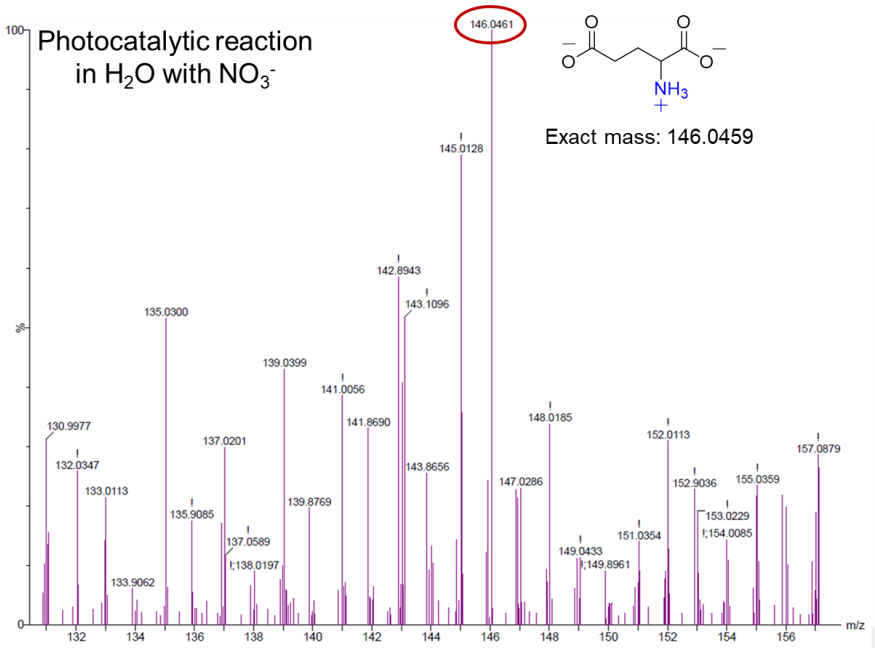


**Figure 4b.20.** High-resolution mass spectrum (HRMS) of glutamate formed from photocatalytically generated $NH_4^+$ with [+] InP QDs as photocatalyst and $NO_3^-$ as N-source, in water.

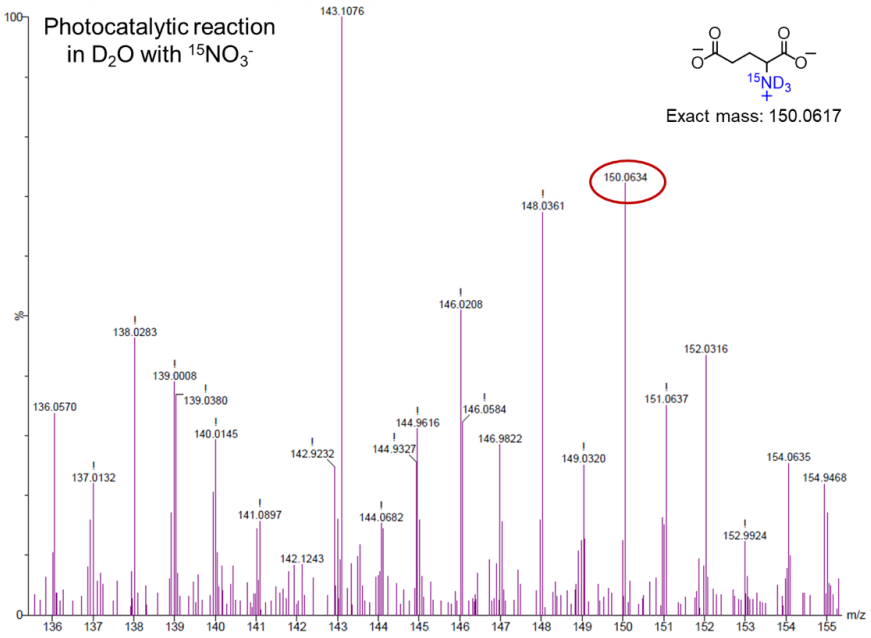


**Figure 4b.21.** High-resolution mass spectrum (HRMS) of isotope-labelled glutamate formed from photocatalytically generated $^{15}ND_4^+$ by performing reaction in $D_2O$ with $^{15}NO_3^-$ as N-source, confirming water as the proton source.

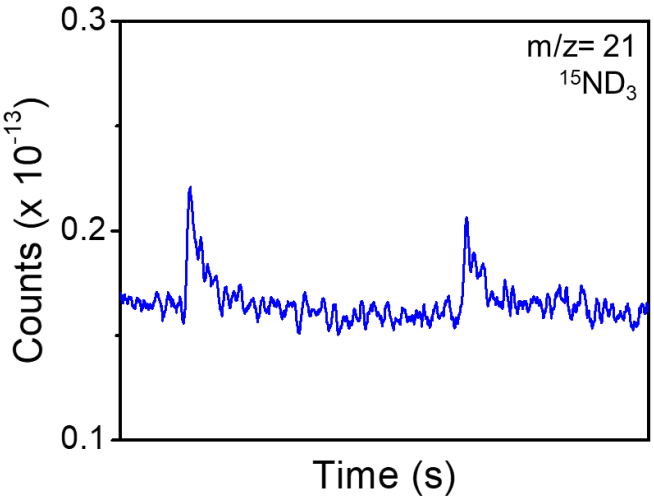


**Figure 4b.22.** Gas phase mass analysis of the photocatalytic reaction performed with $^{15}NO_3^-$ in $D_2O$. Signals for m/z =21, corresponding to $^{15}ND_3$, confirm water as the proton source.

**Table 4b.3.** Table summarizing the reactions performed to identify the probable proton source and hole scavenger in the photocatalytic $NO_3^-$ reduction to $NH_3$ by [+] InP QDs.

| Reactions | $NH_3$ formation | Remarks |
|---|---|---|
| [+] InP QD + $^{15}NO_3^-$ in water | ✓ | [+] InP QD is photocatalysing the reduction of nitrate to ammonia. |
| [+] InP QD + $^{15}NO_3^-$ in acetone* | × | Water ***surely*** plays an active role. ***May*** act as a proton source. |
| [+] InP QD + $^{14}NO_3^-$ + excess [+] TMA in water | ✓ | Enhanced stability of InP QD photocatalysts in the presence of excess TMA ligands. |
| [+] InP QD+ $^{15}NO_3^-$ + excess [+] TMA in acetone* | × | Overrules the possibility of [+] TMA ligand acting as a proton source. |
| Betaine-InP QD + $^{14}NO_3^-$ in water | ✓ | |
| Betaine-InP QD + $^{15}NO_3^-$ in water | ✓ | |
| Betaine-InP QD + $^{15}NO_3^-$ in acetone* | × | Water ***surely*** plays an active role.<br><br>Overrules the possibility of [+] TMA ligand acting as a proton source. |
| [+] InP QD + $^{15}NO_3^-$ in $D_2O$ | ✓ | Water is ***surely*** the proton source. |

*All the reactions in acetone (polar aprotic solvent) were performed using the Whatman filter paper based-dip-catalyst system. Concentrations of [+] InP and $NO_3^-$ were maintained at 0.5 mol % and 0.5 mM, respectively. It is to be noted that the paper substrate does not affect the photocatalytic activity of [+] InP QDs when the reaction was performed in water under similar conditions (as seen in the recyclability studies).

**Stability of [+] InP QDs in photocatalytic conditions**

X-ray photoelectron spectroscopy (XPS)

X-ray photoelectron spectroscopy (XPS) studies were carried out before and after the photocatalytic reaction to verify the change in the chemical composition of [+] InP QDs. Pristine [+] InP QDs (before irradiation) showed doublet for In 3d and P 2p spectra, which are characteristic of the In-P bond (**Figure 4b.23**). The In 3d doublet was located at 443.62 eV and 451.22 eV, corresponding to $3d_{5/2}$ and $3d_{3/2}$, respectively (spin-orbit splitting energy = 7.6 eV). The doublet for P 2p appears at 127.54 eV and 128.44 eV, corresponding to $2p_{3/2}$ and $2p_{1/2}$, respectively (spin-orbit splitting energy = 0.9 eV).[44-46] In addition to the P 2p doublet, we also observed a new P 2p peak in the range of 131.94-132.84 eV, which corroborates with the formation of $InPO_x$. The formation of $InPO_x$ stems from the presence of oxidative environments such as water and oxygen (the XPS sample was prepared from an aqueous solution of [+] InP), and is commonly observed by other groups as well.[44,45] It must be noted that as-synthesized oleylamine-capped InP QDs (OAm-InP) displayed no such oxidation features (**Figures 4b.23a, 4b.23b**). After the photocatalytic reaction, oxidation features were prominent for both In 3d and P 2p peaks (**Figure 4b.23d**). In particular, the In 3d peak broadened, and a significant enhancement in P 2p peaks corresponding to $InPO_x$ was observed, which confirms the oxidation process of core-only [+] InP QDs after the photocatalytic reaction. We believe that the oxidation of [+] InP QDs could be the probable reason for the etching of QDs during the photocatalytic process. It is well-known in the literature that core-only QDs can undergo chemical changes under photocatalytic conditions because of the presence of chemical reactants, reagents, and the charge transfer process.[47,48] Even though core-only [+] InP QDs undergo oxidation during the photocatalytic process, the colloidal stability was maintained throughout the reaction timescale, as can be seen from the optical photographs (**4b.9a**).

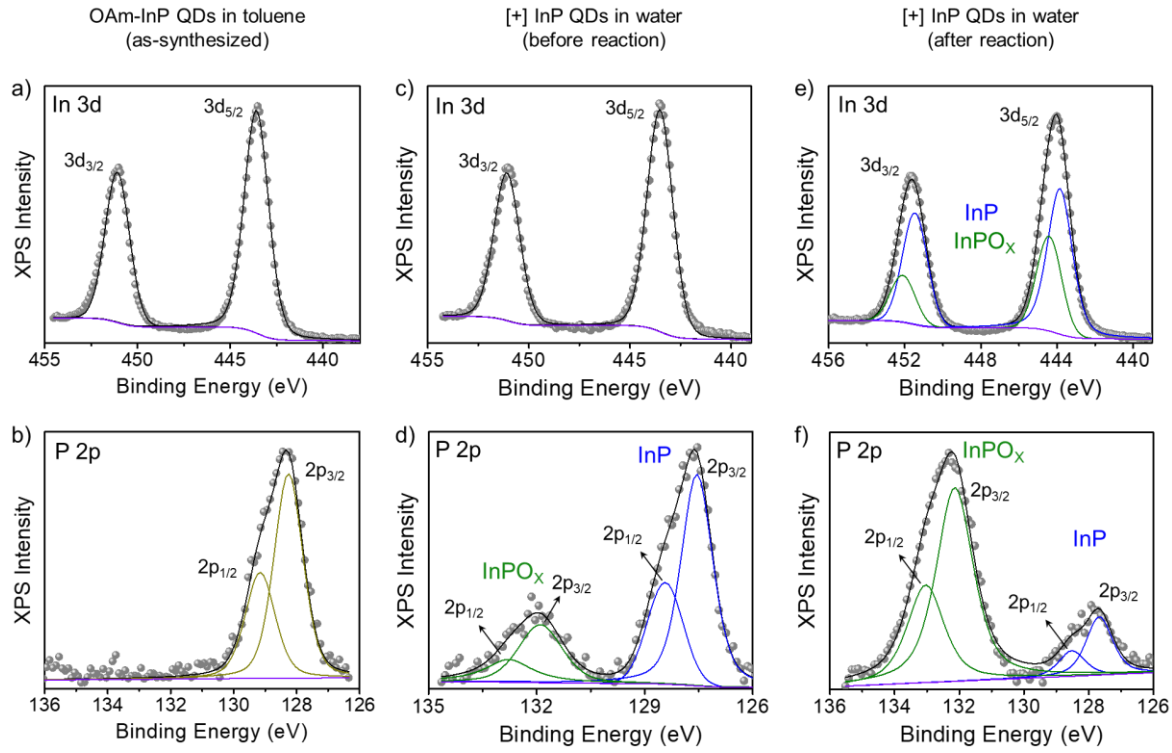


**Figure 4b.23**: Analysis of XPS spectra for a,b) as-synthesized OAm-InP QDs before, c,d) [+] InP QDs before the reaction and e,f) [+] InP QDs after the photocatalytic reaction. For the analysis, the charge correction for all the spectral peaks was performed according to the carbon-1s standard peak (284.6 eV).

**Recyclability study and long-term stability experiments**

With core-only InP QDs

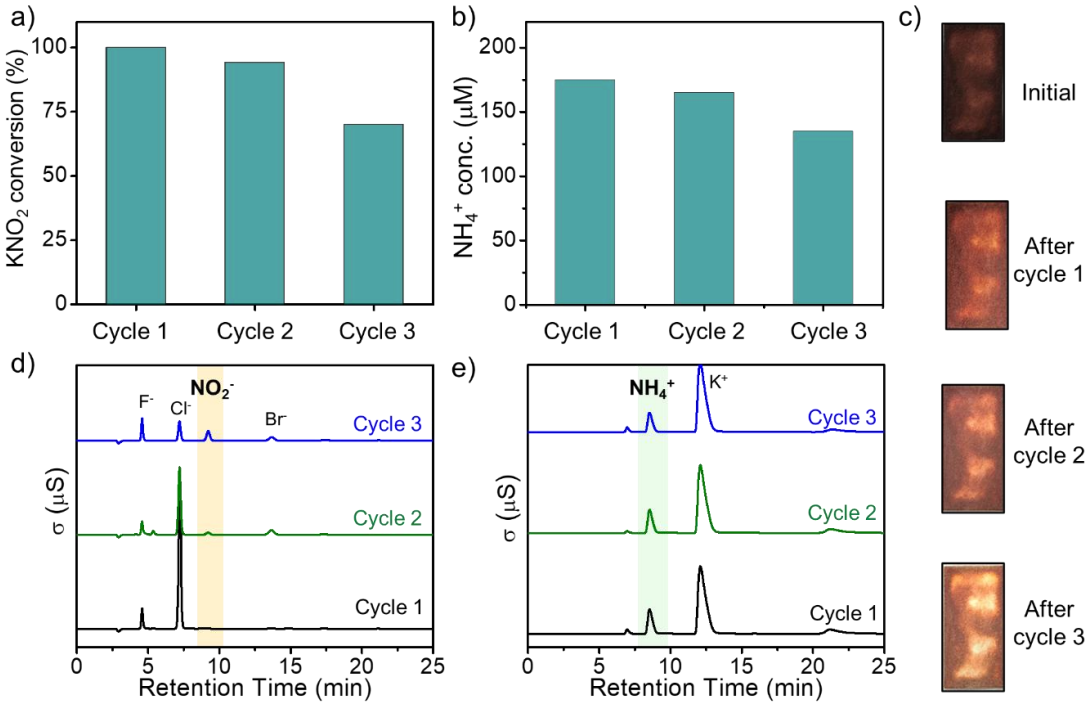


**Figure 4b.24**. Recyclability studies performed with paper-based dip-catalyst system show decent retention of photocatalytic activity a) for $NO_2^-$ conversion and b) $NH_4^+$ production up to three cycles. c) Optical photographs of the InP QD loaded paper-film after each cycle. A significant etching of QDs was observed after 3 cycles. d) Anion and e) cation chromatograms of the reaction mixture after each cycle.

With core/shell InP/ZnS QDs

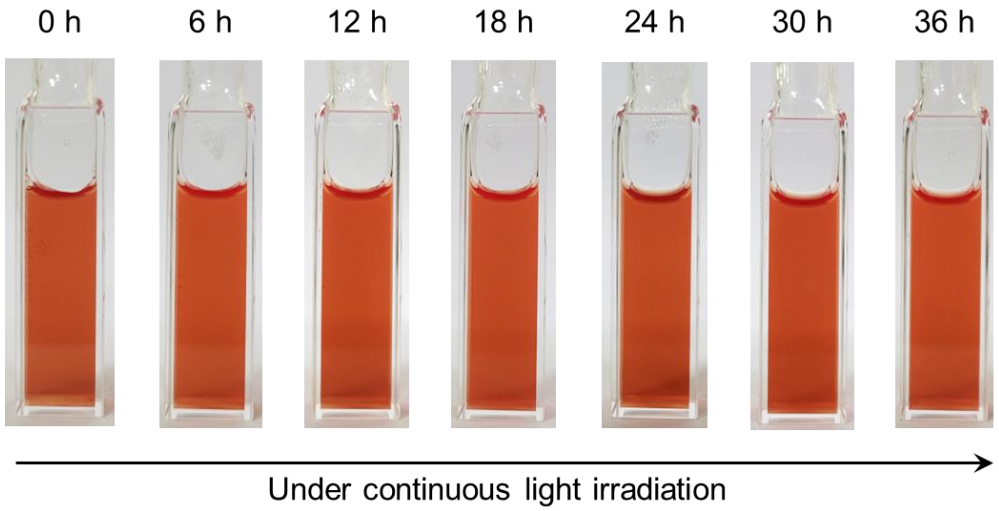


**Figure 4b.25**. Time-dependent optical photographs of the reaction mixture consisting of [+] InP/ZnS, $KNO_2$, and ethanol (EtOH), captured at different times, clearly show negligible color

change upon continuous light irradiation for 36 h with 2 X 10W 450 nm LEDs. This clearly confirms the excellent colloidal and photostability of [+] InP/ZnS QD photocatalyst.

**Identification of reaction pathway**

From the literature reports, reduction of $NO_3^-$ is found to proceed through three main pathways (**Figure 4b.1**).[4,5] In our study, the absence of $N_2$ formation with [+] InP QDs rules out one of the three major pathways. The other two pathways result in $NH_4^+$ as the end-product and proceeds through $N_2H_4$ or $NH_2OH$ as intermediates. As a selective $NH_4^+$ formation was achieved with [+] InP as the photocatalyst, we checked the feasibility of [+] InP QDs to produce $NH_4^+$ from $N_2H_4$ and $NH_2OH$ as the starting reactants, respectively. However, both $N_2H_4$ and $NH_2OH$ were photocatalytically reduced to $NH_4^+$ under similar reaction conditions (**Figure 4b.26**). This made the elucidation of the exact reaction pathway challenging.

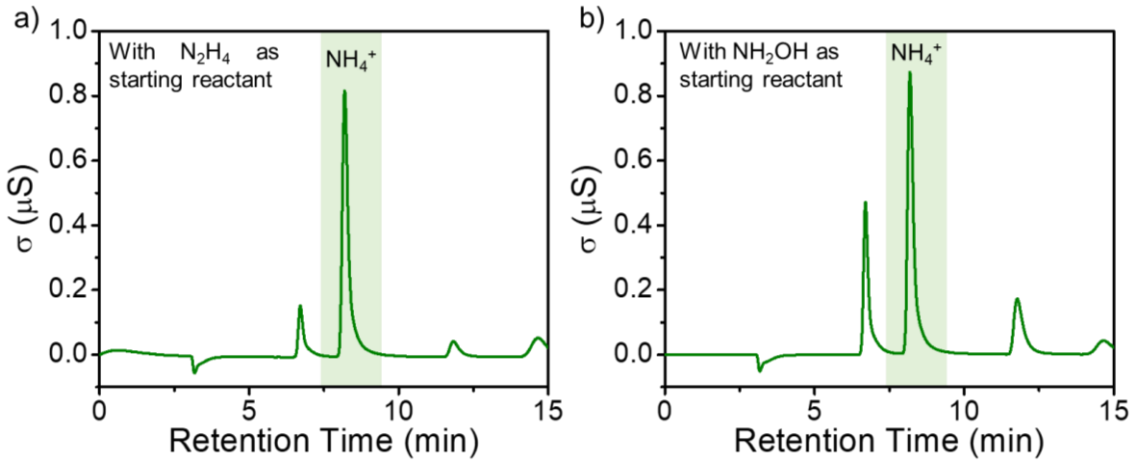


**Figure 4b.26**. Cation chromatograms showing the [+] InP QD photocatalysed formation of $NH_4^+$ from a) $N_2H_4$ and b) $NH_2OH$ as the starting reactants.

# Chapter – 5

## Metal-Solvent Complex on Quantum Dot Surface Enhances Ammonia Formation with Visible Light

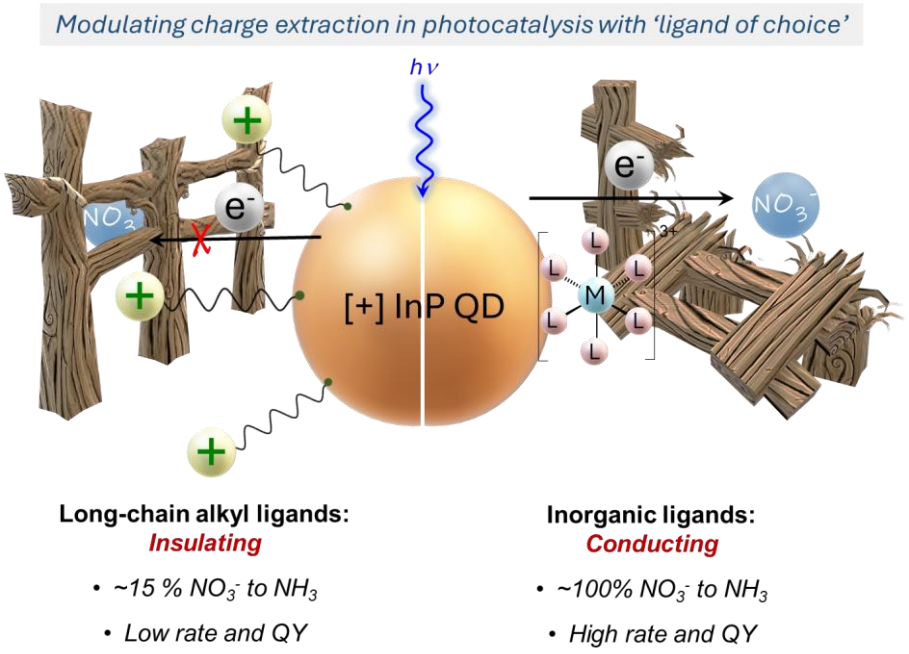


**Jain, V.**; Pillai, P. P. Metal-Solvent Complex on Quantum Dot Surface Enhances Ammonia Formation with Visible Light. *Manuscript Submitted*

## 5.1. Abstract

Achieving high photocatalytic efficiency in multielectron and multiproton chemical transformations is a fundamental challenge in the development of photocatalytic platforms. While traditional approaches rely on developing novel photocatalysts, fine-tuning the catalyst-reactant interactions via ligand chemistry is an emerging route. In this work, we opted for a less-explored route of attaching the *"ligand of choice"* to the indium phosphide quantum dot (InP QD) photocatalyst for enhanced ammonia production under visible light. Herein, instead of conventional long-chain alkyl ligands, a positively charged Lewis acid metal-solvent complex was employed as the surface ligand on InP QD to improve the charge extraction process. The facile charge transport with inorganic surface ligands leads to ~16-fold and 8-fold enhancement in the reaction rate and apparent quantum efficiency, respectively, compared to organic alkyl ligands. Nitrate conversion to ammonia reached ~100 % within 30 min of visible light illumination, with the sole formation of ammonia in the aqueous as well as gaseous phases. Further, we tested the applicability of other Lewis acid metal halide complexes as surface ligands on InP QDs for photocatalytic ammonia synthesis. Overall, our study shows the significance of the appropriate choice of surface ligands and the need for establishing new surface chemistries in regulating the photocatalytic activity of QDs in multielectron/multiproton reactions.

## 5.2. Introduction

Ligands are ubiquitous in colloidal nanocrystals (NCs), often acting as stabilizing agents to provide stable dispersions in different media.[1-3] However, the surface ligands on NCs play a far more significant role in dictating the outcome of the photophysical event under study.[3-9] As seen from the basic NC anatomy, surface ligands have three sub-parts: binding group, spacer, and terminal/headgroup. In principle, all the sub-parts of surface ligands can influence the photophysical properties of NCs.[1,9] From the lens of photocatalysis, electron transfer is one of the major fundamental processes, and manipulating surface ligands strongly influences its efficiency by changing the chemical and electronic environment around the NC.[3-5, 9-15]

For instance, Kamat and coworkers reported the effects of surface chemistry on electron transfer from CdSe QDs to $TiO_2$.[10] The native trioctylphosphine oxide (TOPO) capped CdSe QDs were functionalized with 3-mercaptopropionic acid (3-MPA) and β-alanine (β-Ala). Compared to TOPO-CdSe QDs, 3-MPA-CdSe results in the formation of Se vacancies (electron traps), which results in the delocalization of the electron wavefunction (**Figure 5.1a**). On the other hand, binding of β-Ala on CdSe QD via -$NH_2$ group confines the electron wavefunction to the core of QD by remediation of electron trap states (**Figure 5.1a**). The presence of the -COOH group in both 3-MPA and β-Ala ligands helps in the binding of CdSe QDs to $TiO_2$. While the presence of ligands results in higher CdSe loading, the electron transfer rates become extremely slow compared to the direct deposition of CdSe onto $TiO_2$ (**Figure 5.1b**). Between the two ligands, the electron transfer rate was ~ 3 times higher for β-Ala CdSe than 3-MPA CdSe QD (**Figure 5.1b**). This was attributed to the ability of the -$NH_2$ group to fill surface trap states, which then facilitates the charge transfer. In another elegant study by Thomas and coworkers, the role of binding groups was explored for regulating energy level equilibration in CdSe-Au hetero-nanostructures.[11] Herein, commonly used capping ligands, dodecylthiol (DDT) and dodecylamine (DDA), were chosen to study their impact on charge transfer properties of the CdSe-Au hetero-nanostructures (**Figure 5.1c**). Transient absorption studies revealed a slower bleach recovery for CdSe-Au@DDT and a faster one for CdSe-

Au@DDA heterostructure. This suggests a long-lived excited state for CdSe–Au@DDT, which can be attributed to the energetically facile hole transfer from CdSe to DDT (**Figure 5.1d**). Such a hole transfer event results in electron transfer to AuNP, leading to a rise in the Fermi level and achieving better Fermi level equilibration (**Figure 5.1d**). On the contrary, the relative energy level of DDT lies below the valence band of CdSe QD and hence cannot abstract photoexcited holes (**Figure 5.1d**). As a result, Au-mediated charge recombination becomes prominent and restricts the charge transport to the electron acceptor (**Figure 5.1d**).

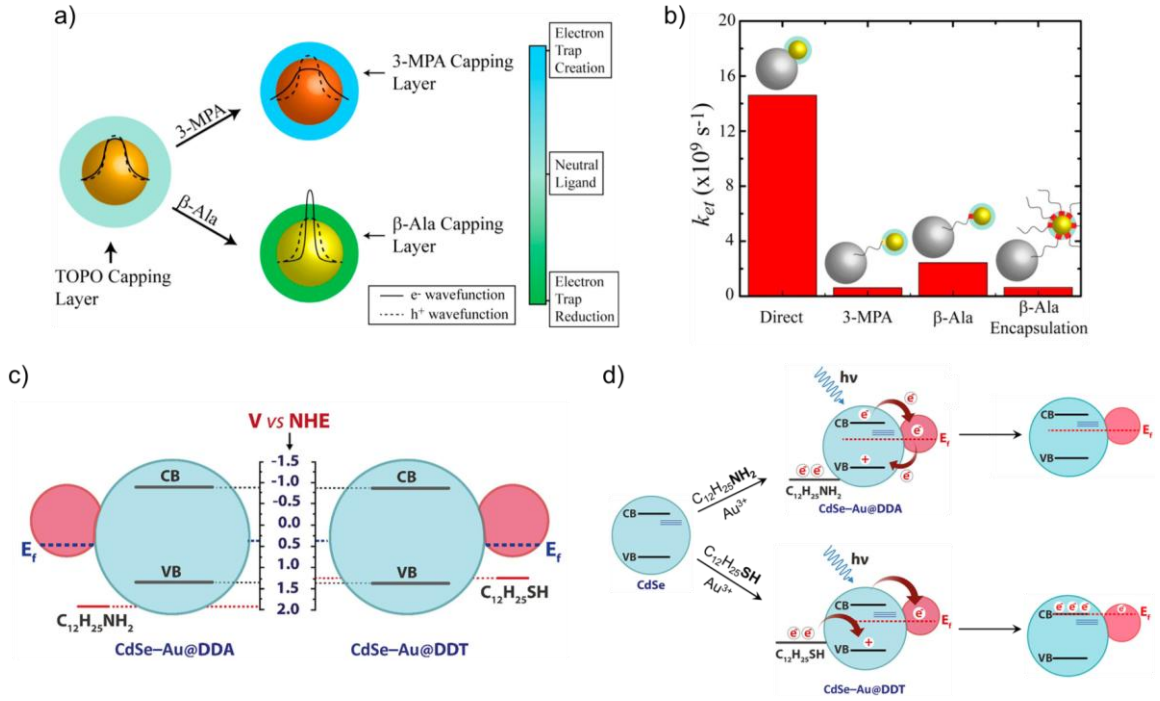


**Figure 5.1**. Effect of ligand anchoring group on charge transfer dynamics. a) Scheme showing the effect of different ligands on the electron wavefunctions of CdSe QD. 3-MPA ligands result in the delocalization of the electron wavefunction due to the creation of electron traps, whereas β-Ala confines the electron wavefunction to the CdSe core by removing the surface trap states. b) Rate of electron transfer from CdSe QD to $TiO_2$. Reproduced with permission from reference 10. Copyright 2013 American Chemical Society. c) Schematics showing the energy levels of CdSe QD, Au, DDT, and DDA. d) Scheme showing the various charge transfer processes in ligand-modified CdSe-Au hetero-nanostructures. The hole-accepting DDT ligand results in Fermi-level equilibration, whereas the non-hole-accepting DDA ligand promotes exciton recombination. Reproduced with permission from reference 11. Copyright 2020 AIP Publishing.

While the anchoring group of ligands significantly affects the electronic structure of NC, the nature and length of the spacer are also known to impact the charge transfer dynamics.[16-19] Generally, the Marcus equation for non-adiabatic charge transfer (**eq. 5.1**)

is employed to analyze the charge transfer from NC to acceptors.[20] In this equation, $|V_{a,b}|^2$ is the electronic coupling between the donor and acceptor, which varies with the distance between the two and results in a distance-dependent charge transfer rate. Such variation can be observed by changing the spacer length of the ligand.[21]

$$k_{CT} = \frac{2\pi}{\hbar}|V_{a,b}|^2 \frac{1}{\sqrt{4\pi\lambda k_B T}} \exp\left(\frac{(-\lambda + \Delta G_o)^2}{4\lambda k_B T}\right) \qquad (\mathbf{5.1})$$

In an interesting study by Kinge, Cánovas, and coworkers, electron transfer rates were controlled by tuning the coupling between CdSe QDs and mesoporous $SnO_2$ through *n*-methylene (SH–$[CH_2]_n$–COOH) and *n*-phenylene (SH–$[C_6H_4]_n$–COOH) molecular bridges.[17] These molecular bridges impose a barrier potential to electron transfer, and the electron transfer rate decreases exponentially with barrier height and barrier length (**Figure 5.2a**). **Figure 5.2b** clearly shows the change in electron transfer rate as a function of molecule length. In the case of alkyl n-methylene molecular bridges, an exponential decrease in electron transfer rate was observed with an increase in bridge length. Moreover, for a given molecular bridge distance, it was observed that aromatic n-phenylene bridges allow faster electron transfer than their alkyl counterparts because of higher delocalized molecular orbitals (**Figure 5.2b**). This clearly suggests that, along with the length, the nature of the spacer on NC also has a strong influence on charge transfer properties.

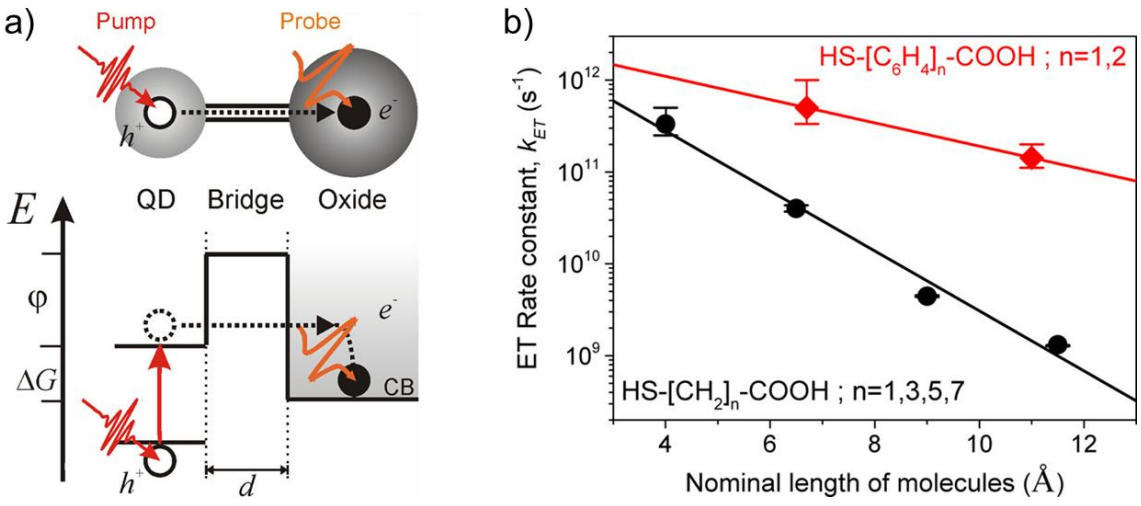


**Figure 5.2.** Influence of spacer on charge transfer. a) Schematics showing photoinduced electron transfer from CdSe QD to mesoporous $SnO_2$ through molecular bridges. The molecular

bridges impose a barrier of height $\phi$ and width $d$ for electron transfer, which in turn depends on the length and nature of molecules. b) Plot showing the variation in electron transfer rate as a function of spacer length for *n*-methylene-based alkyl (HS–$[CH_2]_n$–COOH, black) and *n*-phenylene-based aromatic bridges (HS–$[C_6H_4]_n$–COOH, red). Reproduced with permission from reference 17. Copyright 2013 American Chemical Society.

It is clear from the above discussion that ligands are not merely stabilizing agents, but all the parts of ligands significantly impact the charge transfer dynamics and, in principle, can significantly affect the photocatalytic activity of NCs. However, the ligand shell on the NC surface acts as a physical barrier primarily because of the use of alkyl ligands, which restricts the movement of photoexcited charge carriers.[21,22] As a result, the photocatalytic reaction parameters such as reaction yield, rate, and quantum efficiencies are significantly compromised.[3-5,22] A way out is to adopt the '*ligand of choice'* approach to overcome existing challenges of ligand poisoning in photocatalysis. Herein, an ideal *ligand of choice* must allow for enhanced charge extraction and install favourable catalyst-reactant interactions while retaining the colloidal stability of the QDs.

In light of enhancing the charge transport, Talapin and coworkers explored new surface chemistries and introduced inorganic molecular metal chalcogenides and metal-free inorganic ligands (**Figure 5.3**).[23,24] In the first report by Talapin and coworkers, molecular metal chalcogenide complexes (MCCs) were used for surface functionalization for various colloidal nanostructures, including CdSe NCs, CdTe NCs, CdS NRs, $Bi_2S_3$ NRs, Au NCs, and Pd NCs (**Figure 5.3a**).[23] A diverse range of MCCs, such as $Sn_2Se_6^{4-}$, $In_2Se_4^{2-}$, $In_2Te_3$, $Ga_2Se_3$, ZnTe, $HgSe_2^{2-}$, etc., were tested for stabilizing NCs in polar solvents (**Figure 5.3b**). MCC-capped NCs displayed strong electron delocalization when assembled in thin films. The charge transport properties of MCC-stabilized NCs were studied through conductivity and field-effect transistor (FET) measurements. While the organic ligands were highly insulating, MCC-capped NCs showed ~11 orders higher conductivity. In another report, Talapin and coworkers replaced organic capping ligands with metal-free inorganic ions such as $S^{2-}$, $HS^-$, $Se^{2-}$, $OH^-$, $NH_2^-$, etc. (**Figure 5.3c**).[24] The characteristic photophysical properties of NCs were well retained even after the ligand exchange process (**Figure 5.3c**), clearly suggesting negligible change in size, shape, and

ensemble distribution. Furthermore, the stabilization was not just restricted to CdSe NCs but could easily be extended to other NC cores such as InP, Au, ZnSe NCs, etc. The electron mobility in inorganic ligands stabilized NC arrays was measured from field-effect transistor studies (**Figure 5.3d**). The drain current ($I_D$) increased with increasing drain-source voltage ($V_{DS}$), which is characteristic of n-type transport and suggests excellent electron mobility in the array of inorganic ligands functionalized NCs.

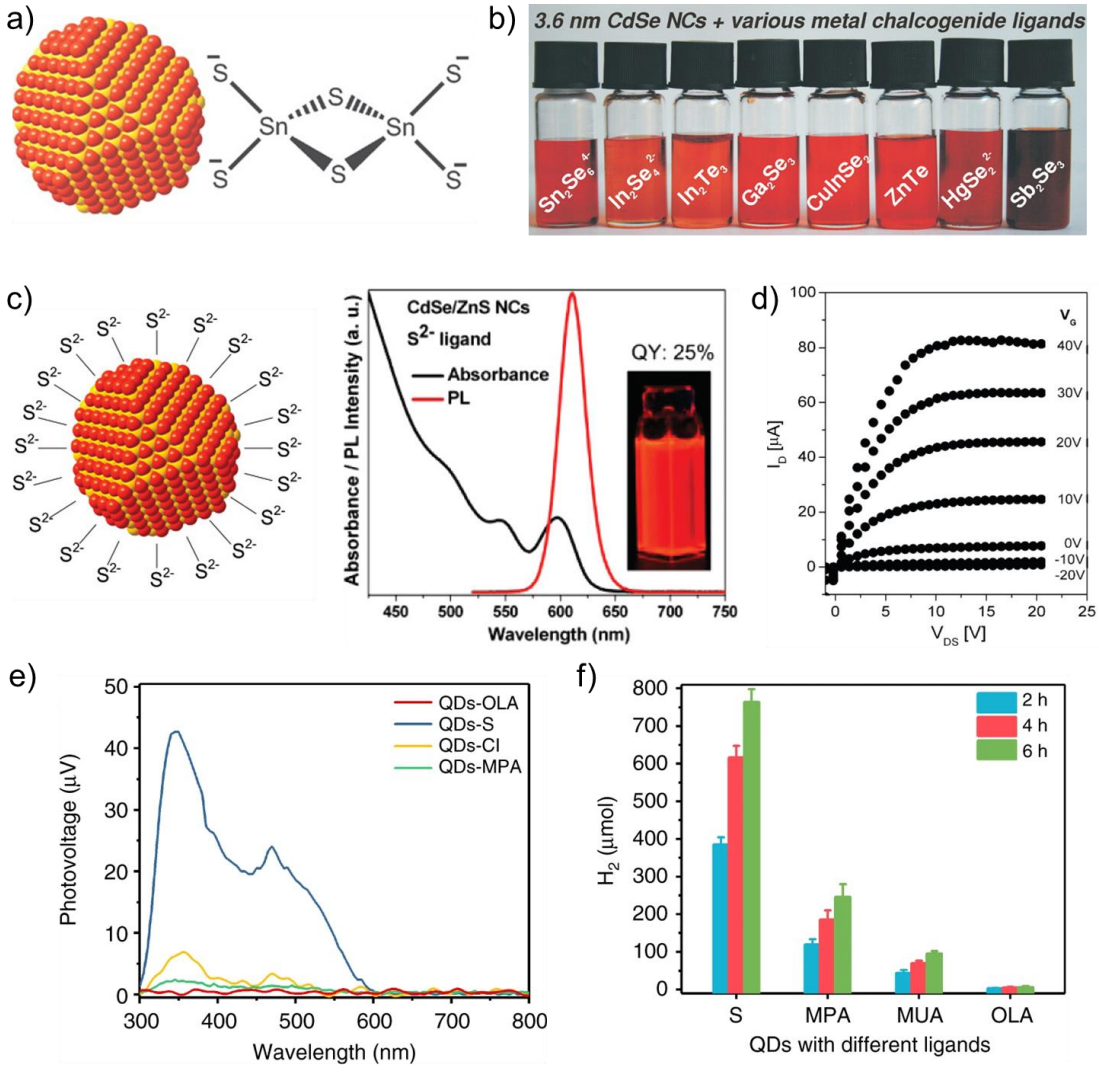


**Figure 5.3**. Use of inorganic ligands to modulate charge transport properties of NCs. a) Schematics showing NC capped with metal molecular chalcogenide (MCC), $Sn_2S_6^{4-}$. b) Photographs clearly showing colloidal stability of CdSe QDs functionalized with various MCCs. Reproduced with permission from reference 23. Copyright 2009 American Association for the Advancement of Science. c) Schematics of NC functionalized with metal-free inorganic $S_2^-$ ion. $S^{2-}$ ligand functionalized CdSe QDs retained the key photophysical features. d) Plot of drain current as a function of drain-source voltage at different potentials, revealing the excellent electron mobility. Reproduced with permission from reference 24. Copyright 2011 American Chemical Society. e) Photovoltage of InP QDs functionalized with various ligands. The highest

photovoltage was observed for InP QD functionalized with inorganic $S^{2-}$ ions. f) Comparison of the photocatalytic $H_2$ evolution activity of InP QDs with varied surface chemistry, clearly showing that inorganic surface ligands outperform alkyl ligands. Reproduced with permission from reference 25. Copyright 2018 Springer Nature.

Even though such MCC and metal-free inorganic ligands capped NCs exhibit excellent charge transport behavior, their utility in photocatalysis is scarce. In an interesting study by Wu, Zhou, Patzke, and coworkers, all-inorganic $S^{2-}$-capped InP QDs photocatalyzed $H_2$ evolution reaction.[25] The use of small $S^{2-}$ ions as ligands exhibited a dual role: 1) decrease the photoexcited charge transfer barrier between the QD and acceptors, and 2) facilitate extraction of photoexcited holes from the valence band. The surface photovoltage spectra were obtained for InP QD functionalized with different ligands to gain information about charge separation and extraction process. A large photovoltage was recorded for $S^{2-}$-InP QDs compared to oleylamine (OAm), $Cl^-$, and 3-MPA functionalized InP QDs (**Figure 5.3e**). The large photovoltage indicates the accumulation of positive charge at the QDs surface, which was attributed to the hole transfer to $S^{2-}$ ligands. This was further verified by transient absorption and EPR studies. The effect of inorganic $S^{2-}$ ligands was clearly visible in excellent $H_2$ evolution activity compared to alkyl ligand capped-InP QDs (**Figure 5.3f**).

With this motivation, we studied the effect of unconventional inorganic ligands in enhancing the efficiency of multielectron/multiproton ($8e^-/9H^+$) photocatalytic nitrate ($NO_3^-$) conversion to ammonia ($NH_3$) with QDs. In the previous Chapter, we established III-V indium phosphide (InP) QDs to synthesize $NH_3$ with visible light, wherein the favorable electrostatic interaction emanating from the positively charged surface ligands on InP QDs and negatively charged $NO_3^-$ ions was found to be the key driving force (**Scheme 5.1**).[26] This necessitates the presence of positively charged inorganic ligands, which are rarely reported in the literature.[24,27] This is because NCs typically have electrophilic metal-rich surfaces with preferential affinity toward nucleophilic ligands.[24] A recent report emerged wherein Protesescu and coworkers explored group 3 Lewis acid metal salts as surface ligands for InP QDs in polar solvents (**Figure 5.4a**).[28] The Lewis acid metal salts were found to form cationic coordination complexes in polar solvents like *N*-dimethylformamide (NMF), *N,N*-dimethylformamide (DMF), dimethylsulphoxide

(DMSO), etc., and passivate QD surface to provide colloidally stable dispersions (**Figure 5.4 b**).

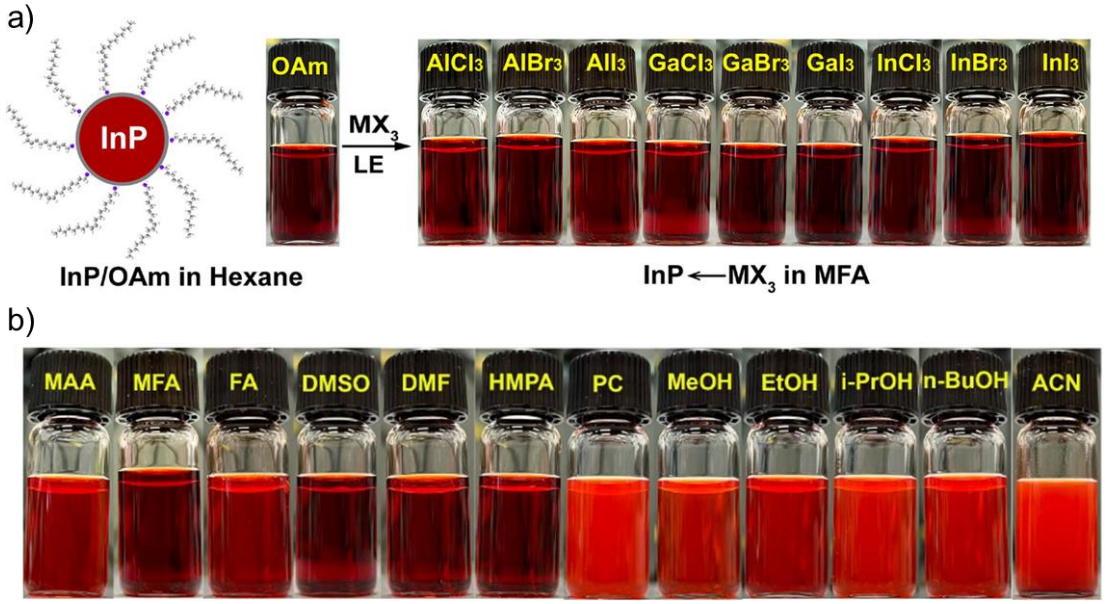


**Figure 5.4**. Metal-solvent complex as surface ligands for InP QDs. a) Schematics showing the ligand place exchange of oleylamine-capped InP with Lewis acid metal salts in *N*-methylformamide. b) Photographs of metal-solvent complex functionalized InP QDs in different polar solvents show excellent colloidal stability. Reproduced with permission from reference 28. Copyright 2024 American Chemical Society.

We took this opportunity to employ metal-solvent complex (MSC) stabilized InP QDs for photocatalytic $NO_3^-$ to $NH_3$ production under visible-light irradiation (**Scheme 5.1**). We chose $InCl_3$ as a Lewis acid metal halide, forming a hexacoordinated complex in DMF, $[In(DMF)_6]^{3+}$ ([+] MSC). An appropriate place exchange protocol was developed to disperse MSC-capped InP QDs ([+] MSC-InP QD) in the aqueous medium. A ~3.75-fold enhancement in photocurrent was observed for inorganic [+] MSC-InP QDs compared to long-chain alkyl [+] TMA-InP QDs, clearly suggesting enhanced photoexcited charge separation and transfer. Consequently, a complete conversion of $NO_3^-$ was achieved within 30 min of visible light illumination, along with complete retention of selectivity for $NH_3$ formation. Interestingly, [+] MSC-InP QDs exhibited ~16 times enhancement in the reaction rate (~45 μM $min^{-1}$) compared to [+] TMA-InP QDs (~3 μM $min^{-1}$). Consequently, the apparent quantum yield (AQY) reached 1.17 % @450 nm, which is ~8 times higher than [+] TMA-InP QDs (0.146 % @450 nm). Photocatalytic experiments performed with isotope-labeled $^{15}NO_3^-$ confirmed that $NO_3^-$ ion is the sole N-source for $NH_3$ formation.

The enhanced charge transfer with metal-solvent complex ligand also accelerated the competing proton reduction reaction to produce $H_2$. Finally, we showcase the use of other Lewis acid metal halides capped InP QDs for photocatalytic $NH_3$ synthesis. In short, our work highlights the impact of rationally chosen surface ligands and their nature in regulating the efficiencies of InP QD photocatalysts in challenging multielectron/multiproton reactions.

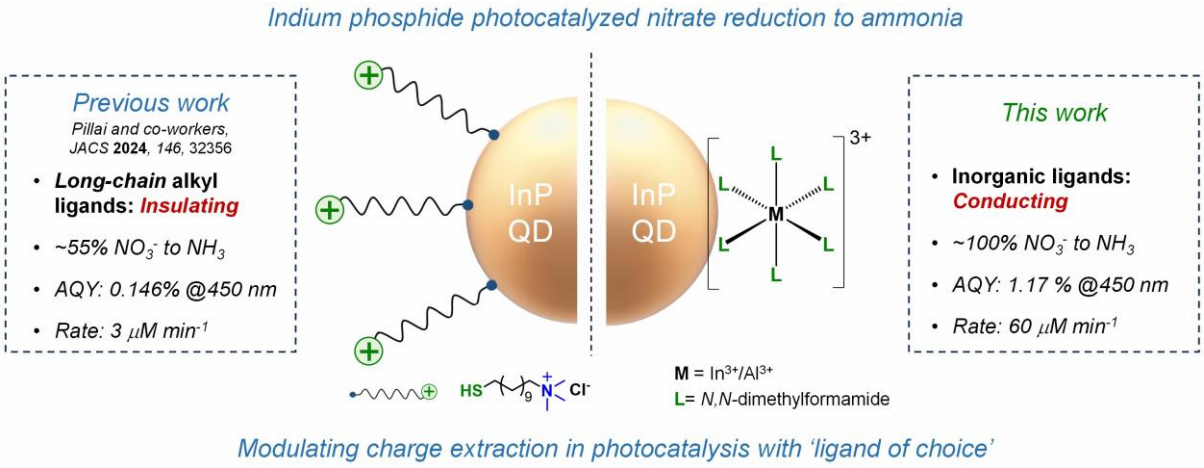


**Scheme 5.1.** Maximizing charge extraction in QD photocatalysis by appropriate use of inorganic surface ligands. Replacing long-chain alkyl ligands with inorganic ligands improves charge transfer in photocatalysis, leading to high reaction rates and quantum efficiencies.

## 5.3. Experimental section

### 5.3.1. General procedure for the photocatalytic $NO_3^-$ to $NH_4^+$ conversion

All the reaction conditions were kept similar to that of [+] TMA-InP QDs for a fair comparison. In a typical procedure, [+] MSC-InP QDs (2.5 μM, 0.5 mol %) and $KNO_3$ (0.5 mM) in water were mixed, purged with Ar, and irradiated with 2 x 10 W 450 nm LEDs for 2 h. The total volume of the reaction mixture was maintained at 3 mL throughout the studies, and the pH was 5. The light intensity falling on the reaction cuvette was measured to be ~200 mW $cm^{-2}$. Subsequently, the reaction mixture was analyzed for $NH_4^+$ formation using ion chromatography by injecting 500 μL of the reaction mixture. The area under the peak at retention time ~9 min was used to calculate the concentration of

$NH_4^+$ formed from the calibration curve. A similar analysis was carried out for $NO_3^-$ conversion as well to calculate the total conversion yields.

### 5.3.2. Preparation of $S^{2-}$ functionalized InP QDs

A reported protocol was adopted to prepare negatively charged $S^{2-}$-functionalized InP QDs.[25] Firstly, 0.05 M of $Na_2S$ solution was prepared in NMF, and 1.5 mL of this solution was mixed with 800 μL of as-synthesized OAm-InP QDs in hexane. The biphasic mixture was stirred for 30 min, and the success of the place exchange could be observed by the complete transfer of InP QDs from hexane to NMF. The place exchanged QDs were purified twice with hexane to remove free OAm ligands, followed by purification with acetone. Finally, the precipitated $S^{2-}$-InP QDs were dispersed in water by ultrasonication and stored in the dark for further use.

## 5.4. Results and discussion

### 5.4.1. Preparation and characterization of [+] MSC-InP QDs

A modified literature procedure involving a high-temperature organometallic reaction was used to prepare oleylamine (OAm) stabilized InP QDs.[29,30] In a typical reaction, indium (III) chloride ($InCl_3$) reacts with tris(dimethylamino)phosphine ($P(DMA)_3$) in the presence of OAm at 200 °C for 25 min to form core-only InP QDs. As-prepared OAm-InP QDs were ligand exchanged with metal-solvent complex formed upon mixing $InCl_3$ in DMF (**Scheme 5.2**). It has been reported that Lewis acid group III metal halides ($MX_3$, M= Al, Ga, In; X = Cl, Br, I) tend to form hexacoordinated complexes in polar solvents such as NMF, DMF, DMSO, etc.[28] We chose $InCl_3$ as the Lewis acid salt as minimal etching of core-only InP QDs was observed compared to Al and Ga halides. Moreover, DMF was chosen as the polar solvent to form a coordination complex, as there was negligible interference in the quantification of $NH_3$. The success of ligand exchange was confirmed by the complete transfer of InP QDs from hexane to the DMF phase, as can be seen in the photographs (**Scheme 5.2**). To perform photocatalytic ammonia synthesis, InP QDs must be stable in aqueous medium. Consequently, place-exchanged InP QDs were transferred from DMF to the aqueous phase by precipitating with toluene, followed by

redispersion in water. Thus, colloidally stable dispersion of $[In(DMF)_6]^{3+}$-InP QDs (HDMFI-InP) were obtained for photocatalytic studies (**Scheme 5.2**).

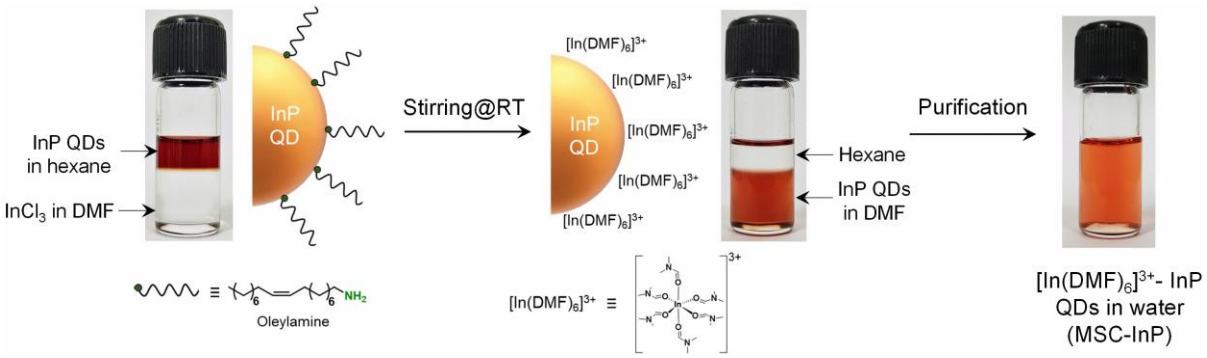


**Scheme 5.2.** Schematics showing the ligand exchange with positively charged $[In(DMF)_6]^{3+}$ complex on core-only InP QDs.

Absorption studies revealed changes in the position and nature of the first excitonic peak of [+] MSC-InP QDs compared to OAm-InP. Specifically, a blueshift of 15 nm was observed for [+] MSC-InP QDs, which can be attributed to surface etching because of the acidic nature of $InCl_3$. Moreover, the peak became broader, suggesting enhanced electron delocalization in [+] MSC-InP QDs compared to OAm-InP QDs (**Figure 5.5a**).[31] A higher delocalization of the electron wavefunction leads to a weaker coulombic attraction between the photoexcited electrons and holes, thereby enhancing the charge separation and extraction process.[32-34] The band gap of [+] MSC-InP QDs was estimated to be 2.07 eV from the Tauc plot (**Figure 5.6**). Detailed Fourier transform infrared spectroscopy (FTIR) studies revealed that characteristic stretching frequency bands for OAm-InP at 2921 and 2852 $cm^{-1}$ were absent from [+] MSC-InP QDs, suggesting negligible presence of OAm ligands on QD surface. The retention of characteristic carbonyl stretching frequency of $[In(DMF)_6]^{3+}$ on the InP QD surface indicates the successful functionalization of the metal-solvent complex. In comparison with pure DMF, carbonyl stretching frequency ($\nu_{CO}$) lowered to 1646 from 1654 $cm^{-1,}$ which indicates that DMF coordinates to the central $In^{3+}$ ion through the carbonyl oxygen atom. Moreover, a lower frequency of N-$CH_3$ bending mode ($\delta$(N-($CH_3$)) at 1370 $cm^{-1}$ for MSC-InP QDs compared to 1385 $cm^{-1}$ for pure DMF suggests the interaction between the amine group and InP surface (**Figure 5.5b**). A positive zeta potential value of +34.0±6.1 mV confirms the

presence of cationic In-DMF complex on InP QD surface (**Figure 5.5c**). High resolution transmission electron microscopy (HRTEM) studies confirm the formation of uniform-sized [+] MSC-InP QDs having an average diameter of 3.5 ± 0.5 nm (**Figures 5.5d, 5.11**). The elemental analysis (EDAX) from TEM revealed an increase in relative % of In to ~77 % for [+] MSC-InP QDs compared to ~60 % for OAm InP QD, suggesting the presence of cationic In complex on QD surface in [+] MSC-InP QDs (**Figure 5.12**).

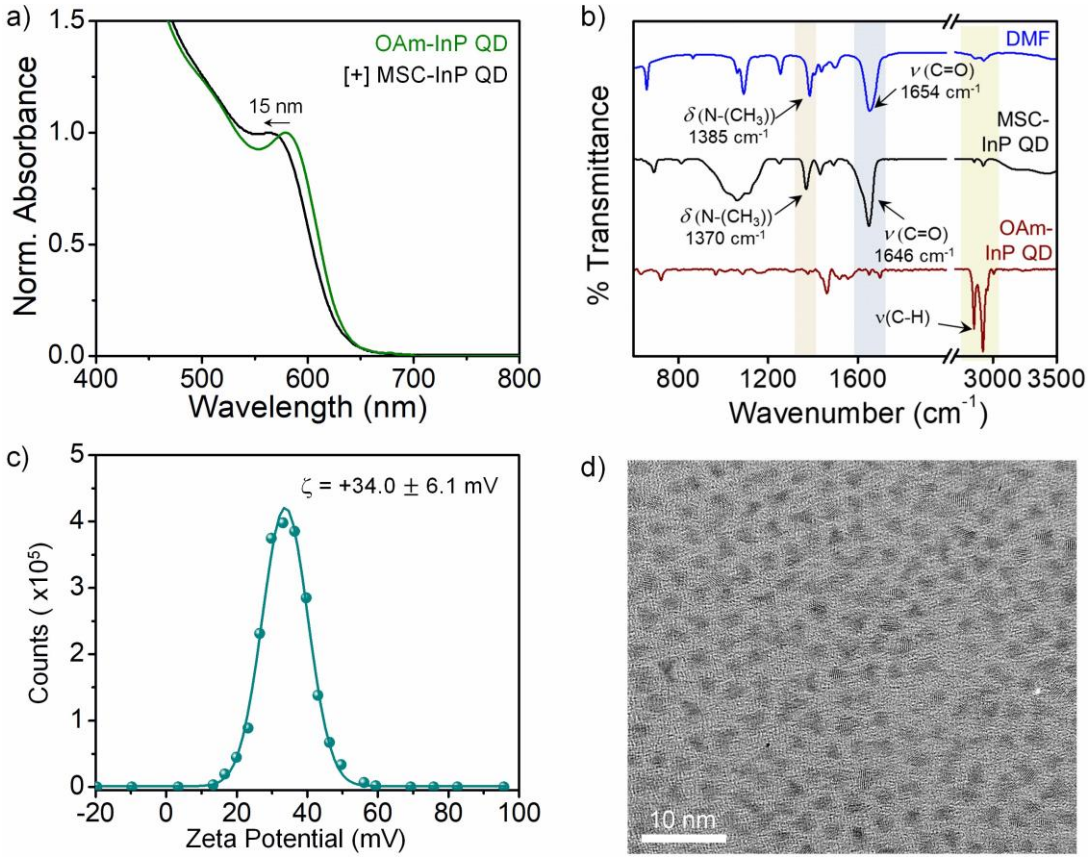


**Figure 5.5.** a) Absorption spectra of OAm-InP and [+] MSC-InP QDs. A slight change in the nature of first excitonic peak is observed after the ligand exchange. b) FTIR spectra of [+] MSC-InP QDs compared with OAm-InP QD and DMF. Absence of $\nu$(C-H) vibrational feature, characteristic of OAm, and retention of $\nu$(C=O), characteristic of DMF, confirms the successful ligand exchange with [+] MSC on InP QD surface. c) Zeta potential plot validating the presence of [+] MSC complex on the surface of InP QD. d) Representative HRTEM image of [+] MSC-InP QDs.

To evaluate the thermodynamic feasibility of photocatalytic $NO_3^-$ reduction to $NH_3$ with [+] MSC-InP QDs, we measured the band positions using cyclic voltammetry (CV) using ferrocene as the internal standard (**Figure 5.6a**). The oxidation features were observed for both OAm and [+] MSC InP QDs at 0.54 V and 1.20 V vs $Ag/AgNO_3$, respectively (**Figure 5.6b**), and were utilized to calculate the valence band positions. The

valence band positions were calculated to be -5.19 eV and -5.85 eV vs. vacuum for OAm InP QDs and [+] MSC InP QDs, respectively. In combination with Tauc plot (**Figure 5.6c**), the conduction band positions were estimated to be -3.16 eV and -3.78 eV vs vacuum for OAm InP QDs and [+] MSC InP QDs, respectively. As can been seen from **Figure 5.6d**, the band-edge energies were shifted to lower energy when the pristine OAm surface ligand was exchanged with $[In(DMF)_6]^{3+}$ complex. The shift in band positions due to changes in capping ligands and NC environment has been reported by other groups as well.[35-37] It must be noted that thermodynamic feasibility to perform $NO_3^-$ reduction (-5.69 eV vs vacuum) is retained despite the shifts in energy levels. After the successful synthesis, ligand exchange, and characterization of [+] MSC-InP QDs, we began the evaluation of photocatalytic $NH_3$ synthesis under visible light irradiation.

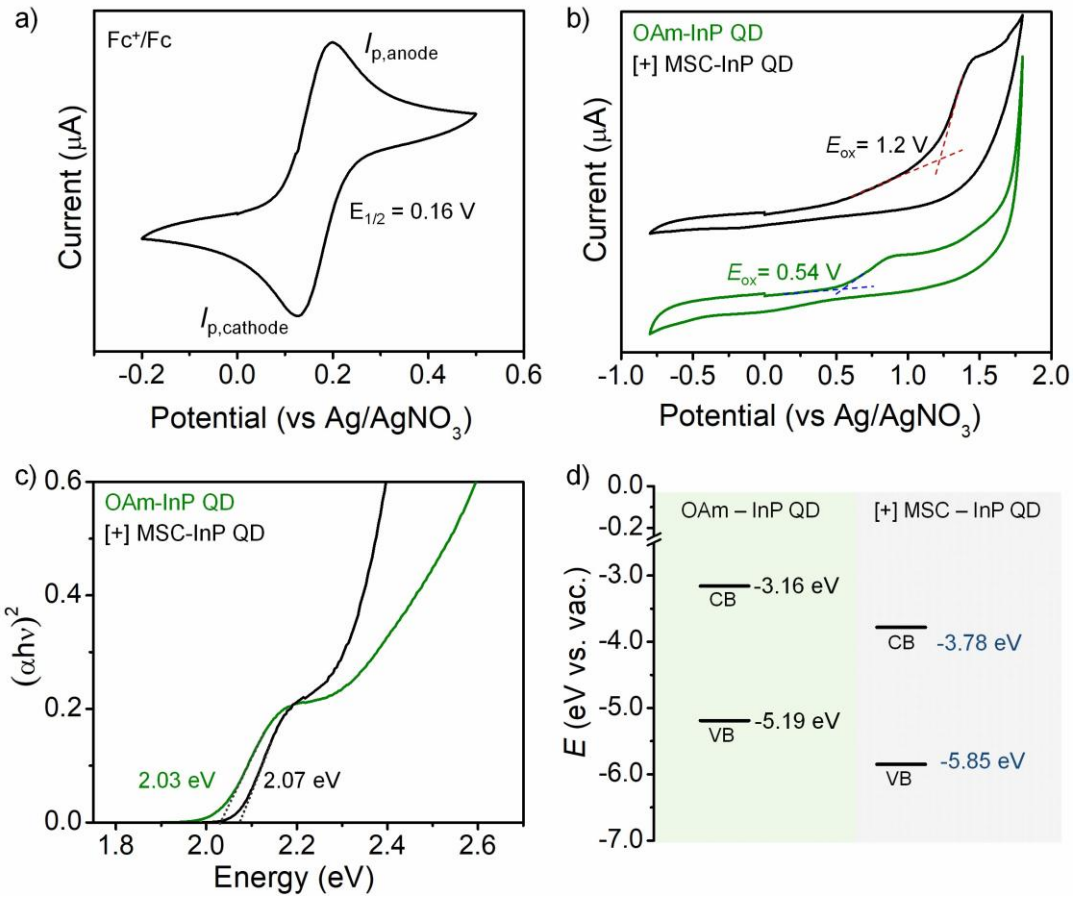


**Figure 5.6.** Estimation of the band-edge positions for InP QDs. Cyclic voltammograms of a) ferrocene (internal standard) and b) InP QDs functionalized with native oleylamine ligand and inorganic [+] MSC ligand. c) Tauc plot of OAm-InP and [+] MSC-InP QDs, showing a slight increase in band gap after ligand exchange with [+] MSC ligand. d) Energy level diagram comparing the band edge positions of OAm and [+] MSC InP QDs. A shift in band positions to lower energy was observed for [+] MSC-InP QDs.

## 5.4.2. Photocatalytic reduction of $NO_3^-$ to $NH_3$ with [+] MSC-InP QDs

A typical reaction mixture comprises 2.5 μM [+] MSC-InP QDs and 0.5 mM $KNO_3$ in water, which was illuminated with 2 x 10 W 450 nm LEDs (the total volume of the reaction mixture was 3 mL, pH was maintained ~5, and the total light intensity falling on the cuvette was ~200 mW $cm^{-2}$). Total $NO_3^-$ conversion and amount of $NH_4^+$ formed were analysed using ion chromatography (IC) using suitable cation and anion columns, respectively (**Figure 5.13**). The presence of a cationic complex on the InP QD surface is expected to install favorable catalyst-reactant interactions between the positively charged inorganic complex and negatively charged $NO_3^-$ ions (**Figure 5.7a**). Such favorable interactions will allow enhanced substrate channeling,[3-5,26] leading to higher local concentration of $NO_3^-$ near InP QDs, which in turn increases the probability of charge transfer from QD to $NO_3^-$ ions. With positively charged inorganic ligand on InP QD surface, $NO_3^-$ conversion reached 88.4±12 % with accumulation of 242±28 μM $NH_4^+$ in the aqueous phase within 2 h of visible light irradiation (**Figure 5.7b, 5.14**). Negligible $NO_3^-$ conversion in the absence of either light or InP QDs confirms the photocatalytic pathway for $NO_3^-$ to $NH_4^+$ conversion with [+] MSC-InP QDs (**Figure 5.7b, 5.15**). Isotope-labeled studies with $^{15}NO_3^-$ were performed to confirm the N-source for the observed $NH_4^+$ formation. $^1$H-NMR spectrum clearly revealed the presence of a doublet between 6.8-7.1 ppm with $J$ = 73.2 Hz, which is characteristic of $^{15}NH_4^+$ (**Figure 5.7c**). On the other hand, $^{14}NH_4^+$ shows a characteristic triplet with $J$ = 52.4 Hz. Thus, isotope-labeling experiments confirm $NO_3^-$ to be the sole proton source for $NH_3$ synthesis. Interestingly, we observed the sole presence of $NH_3$ in the gaseous phase as well, suggesting excellent selectivity of [+] MSC-InP QDs for $NO_3^-$ reduction to $NH_3$ (**Figure 5.7d**). The total amount of $NH_3$ formed in both aqueous (0.72±0.08 μmol) and gaseous phase (0.85±0.12 μmol) corroborates well with the total $NO_3^-$ converted and validates the claim of selective $NH_3$ formation from $NO_3^-$ ions. All these experiments clearly show excellent photocatalytic activity of inorganic ligand-capped InP QDs to drive multielectron reactions.

One of the most employed inorganic ligands is sulfide ions ($S^{2-}$), which are known to impart excellent charge mobility in NC assemblies.[24,38,39] However, the presence of negatively charged $S^{2-}$ on InP QD surface is expected to install electrostatic repulsions

between the QD and negatively charged $NO_3^-$ ions (**Figure 5.7a**). To verify the active role of ligands as gatekeepers in InP QD photocatalyzed $NH_3$ synthesis, we functionalized InP QDs with negatively charged inorganic ligand $S^{2-}$. Interestingly, the photocatalytic activity was completely switched OFF (**Figure 5.7b. 5.16**), even though $S^{2-}$ is not insulating in nature. This is due to the restricted access to the QD surface arising from strong electrostatic repulsions, which lead to a decrease in the local concentration of $NO_3^-$ ions. Consequently, the probability of charge transfer from $S^{2-}$-InP QD to $NO_3^-$ is reduced. This experiment clearly shows the power of favorable interactions emanating from surface ligands for challenging multielectron chemical transformations.

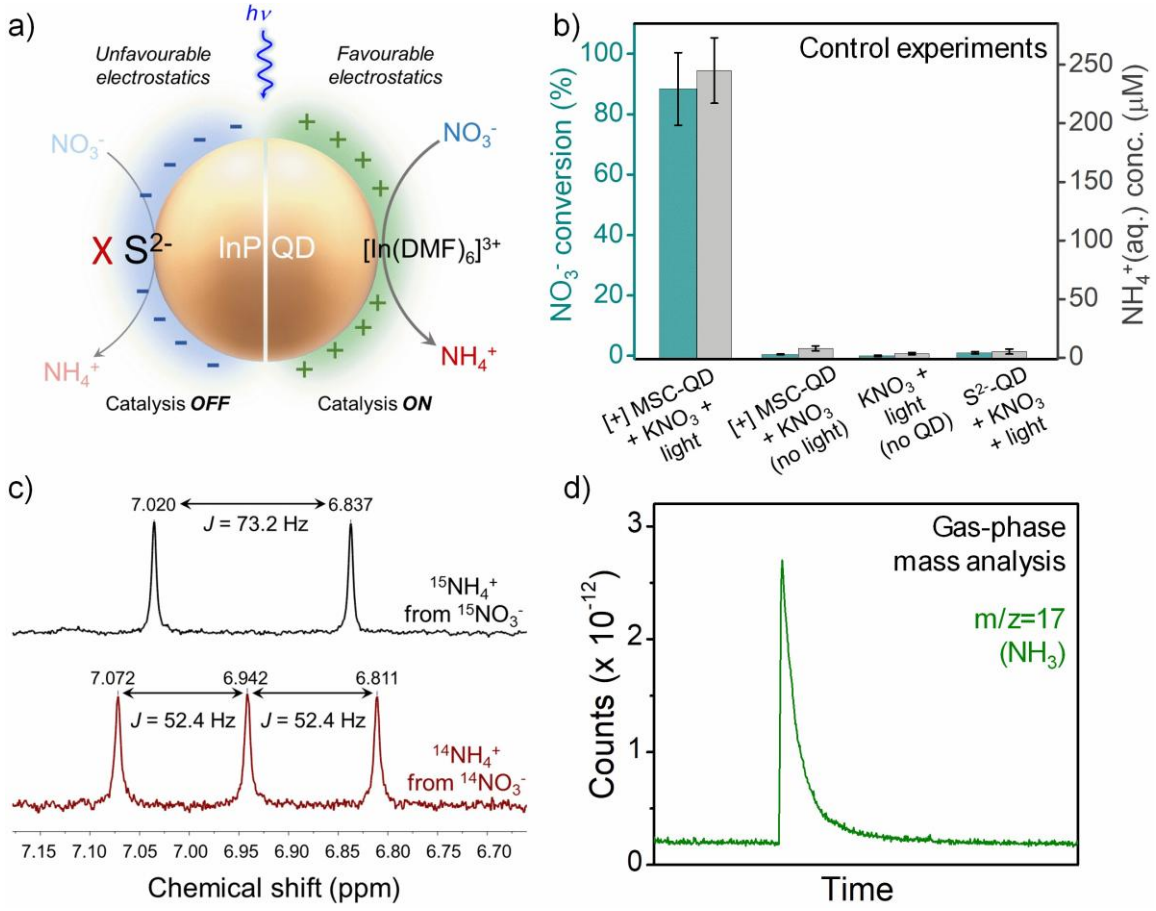


**Figure 5.7.** a) Schematics showing the modulation of photocatalytic activity by regulating the electrostatic forces emanating from surface ligands. The favorable catalyst-reactant interaction between InP QD and negatively charged $NO_3^-$ ions is the key to $NH_4^+$ synthesis. b) Bar diagram showing photocatalytic $NO_3^-$ conversion under different reaction conditions. A negligible conversion of $NO_3^-$ in the absence of either light or InP QDs confirms that the reaction indeed follows a photocatalytic pathway. Comparison of the photocatalytic $NO_3^-$ reduction activity with positively charged [+] MSC-InP QDs and negatively charged $S^{2-}$-InP QDs confirms the prodigious role of ligands as gatekeepers in $NH_3$ synthesis. c) $^1$H-NMR spectra of the photocatalytic reaction mixture performed with $^{14}NO_3^-$ and $^{15}NO_3^-$ as the N-source. The appearance of characteristic

triplet ($J$=52.4 Hz) and doublet ($J$=73.2 Hz) signals, corresponding to $^{14}NH_4^+$ and $^{15}NH_4^+$ formed from $^{14}NO_3^-$ and $^{15}NO_3^-$, respectively, confirms $NO_3^-$ to be the sole N-source. d) Gas phase mass analysis of the photocatalytic reaction mixture reveals the presence of m/z= 17 corresponding to $NH_3$.

### 5.4.3. Effect of inorganic ligands on $NH_3$ synthesis

It was seen in the previous Chapter that positively charged *N,N,N*-trimethyl(11-mercaptoundecyl) ammonium chloride ([+] TMA) ligands on InP QDs installs favorable electrostatic interactions between $NO_3^-$ ions and QD for photocatalytic $NH_3$ synthesis.[26] Even though a decent photocatalytic activity was observed under visible light irradiation with [+] TMA-InP QDs, [+] TMA is a long alkyl chain ligand comprising 11 carbons. Such long alkyl chains are often insulating in nature and pose steric hindrance for the substrates to access the catalyst surface.[21,22] As a result, we were interested in investigating the effect of inorganic ligands in photocatalytic applications. For this, we compared the photocatalytic activities of [+] MSC-InP QDs with [+] TMA-InP QDs (**Figure 5.8a**). Firstly, preliminary photocurrent experiments were performed to compare the charge separation and extraction process between [+] MSC-InP and [+] TMA-InP QDs. Interestingly, ~3.75-fold enhancement in the current density was observed for [+] MSC-InP QDs under 450 nm light illumination compared to [+] TMA-InP QDs (**Figure 5.8b**). This suggests enhanced charge separation and extraction in [+] MSC-InP QDs compared to InP QDs and indicates that a similar effect might appear in photocatalytic transformations. Such an enhancement in photocurrent for [+] MSC-InP QDs motivated us to compare the photocatalytic $NO_3^-$ reduction activity of these two positively charged InP QDs. With [+] MSC-InP QDs, we observed >90 % conversion within 30 min of visible light irradiation, whereas only ~15 % $NO_3^-$ conversion was observed with [+] TMA-InP QDs under similar reaction conditions (**Figure 5.8c**). This clearly suggests that the appropriate choice of surface ligands is crucial in achieving high photocatalytic efficiencies. Moreover, this comparison reveals the poisoning effect of long-chain alkyl ligands in photocatalysis. A detailed kinetic study was performed to evaluate various photocatalytic parameters such as reaction rate and apparent quantum yield (AQY). In the presence of inorganic [+] MSC ligand, the rate of $NO_3^-$ conversion to $NH_4^+$ reached $45\pm5$ μM $min^{-1}$, which was ~16-fold higher than [+] TMA-InP QDs ($2.8\pm0.4$ μM $min^{-1}$)

(**Figures 5.8d, 5.17-5.20**). Similarly, significant rate enhancement was observed even for core/shell InP/ZnS QDs when the [+] MSC ligand was used compared to the [+] TMA ligand (**Figure 5.8e**). As InP/ZnS QDs exhibit a type-I band structure,[40] the overall reaction rate is reduced for both cases (**Figure 5.8e**). Nevertheless, [+] MSC-InP/ZnS still outperformed [+] TMA-InP QDs to yield $NH_4^+$ under visible-light illumination (**Figures 5.8e, 5.21, and 5.22**), clearly suggesting the superior impact of appropriately chosen inorganic ligands in QD photocatalysis. The direct impact of such enhanced reaction rates was well-reflected in ~8-fold enhancement in AQY for [+] MSC-InP QDs (1.17 % @ 450 nm) compared with [+] TMA-InP QDs (0.15 % @450 nm). We anticipate that the enhanced electron delocalization leading to increased charge separation and extraction, along with the lower ligand density of [+] MSC on the InP QD surface results in excellent photocatalytic activity to drive challenging multielectron reactions.

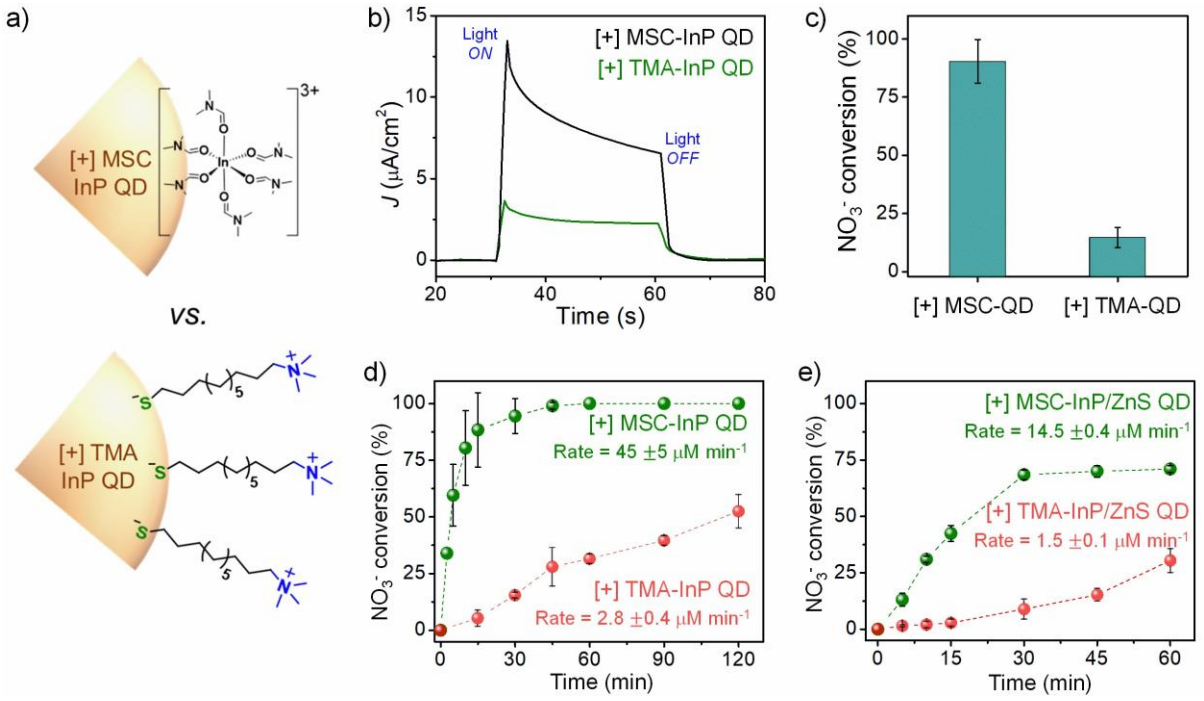


**Figure 5.8.** Comparison of the photocatalytic activity of [+] MSC-InP QDs with [+] TMA-InP QDs for $NO_3^-$ reduction to $NH_3$. a) Schematics of positively charged MSC and TMA ligands on the surface of InP QDs for photocatalytic $NH_3$ synthesis. b) Comparison of the photocurrent density of [+] MSC-InP QDs and [+] TMA-InP QDs under 450 nm light irradiation. A significant enhancement in the photocurrent density for inorganic [+] MSC-InP QDs was observed compared to long alkyl chain [+] TMA-InP QDs. For a fair comparison, the concentration of InP QDs was kept similar, and the light intensity was ~ 100 mW $cm^{-2}$. c) Bar diagram showing the photocatalytic $NO_3^-$ conversion activity with [+] MSC-InP QD and [+] TMA-InP QDs after 30 min of 450 nm light irradiation. A higher $NO_3^-$ conversion (>90 %) for [+] MSC-InP QDs than [+] TMA-InP QDs (~15 %) clearly suggests the enhanced charge separation and extraction process when

inorganic ligands are used. Photocatalytic $NO_3^-$ conversion to $NH_3$ as a function of time performed with d) core-only InP QDs and e) core/shell InP/ZnS QDs functionalized with [+] MSC and [+] TMA ligands. A higher reaction rate was observed for [+] MSC functionalized core/shell QDs as well compared to [+] TMA ligands, showcasing the impact of inorganic ligands in dictating the photoactivity activity.

Most of the multielectron reactions, including $NO_3^-$ reduction, proceed with a kinetically facile proton ($H^+$) reduction reaction to evolve hydrogen ($H_2$).[41] The simultaneous occurrence of $H_2$ evolution reaction with the desired product (here, $NH_3$) often leads to poor selectivity.[41] Consequently, we were interested in evaluating the effect of inorganic ligands on QD photocatalyzed reactions. From the energy level diagram, it is clear that both [+] MSC-InP QDs and [+] TMA-InP QDs satisfy the thermodynamics for $H_2$ evolution as well (**Figure 5.9a**). Interestingly, with an increase in $NO_3^-$ conversion to $NH_3$ with [+] MSC-InP QDs, we observed a significant enhancement in $H_2$ evolution as well compared to [+] TMA-InP QDs (**Figure 5.9b**), even though the thermodynamic feasibility of $H_2$ evolution with [+] MSC-InP QDs ($\Delta G$ = -63.67 kJ $mol^{-1}$) was lower than [+] TMA-InP QDs ($\Delta G$ = -86.84 kJ $mol^{-1}$). While the overall % of utilizable charge carriers were significantly higher when inorganic [+] MSC ligands were used instead of [+] TMA ligands, the proportion of charge carriers utilized for $NH_3$ significantly decreased from ~82.5 % for [+] TMA ligands to ~74 % for [+] MSC ligands (**Figure 5.9b**). This resulted in reduced selectivity of the desired $NH_3$ formation with respect to competing $H_2$ evolution. This tradeoff between overall yield and selectivity further calls for rational design and development of new NC surface chemistries in the future. As proton transfer is necessary for $NO_3^-$ conversion to $NH_3$, proton transfer needs to be regulated, where strategies from electrocatalysis may be adopted.[42-44] Nevertheless, it is clear that inorganic MSC ligands on the InP QD surface have a positive impact on the charge separation and utilization steps for driving multielectron photocatalytic transformations.

As $NO_3^-$ reduction to $NH_4^+$ is a proton-coupled electron transfer process, we investigated the proton source in our reaction mixture for $NH_4^+$ synthesis. Since DMF coordinates with the central In(III) ion to form MSC on the InP QD surface, the role of DMF as a proton source was analyzed first. As there are no ionizable protons in DMF, we expect DMF to play a non-innocent role in $NO_3^-$ reduction to $NH_4^+$. To prove this, a

photocatalytic reaction was performed in DMF instead of water using $^{15}NO_3^-$ as the N-source and analyzed through $^1$H-NMR spectroscopy. The absence of a characteristic doublet for $^{15}NH_4^+$ rules out the role of DMF as a proton source (**Figure 5.9c**). Since no additional proton sources are added to the reaction mixture, water emerges to be the sole proton source for $NH_3$ synthesis. Additional experiments were performed in $D_2O$ to verify the active participation of water as the proton source. Interestingly, a quantitatively similar $NO_3^-$ conversion (> 90 %) and $ND_4^+$ (~240 μM in the aqueous phase) formation to that of the photocatalytic reaction performed in $H_2O$ was observed (**Figures 5.9d, 5.23**). It must be noted that water was confirmed as the sole proton with [+] TMA-InP QDs in a previous study by our group. It can be concluded that the presence of inorganic ligands does not alter the reaction mechanism and only enhances the overall performance of the photocatalytic reactions by enhancing the charge extraction from QD photocatalysts.

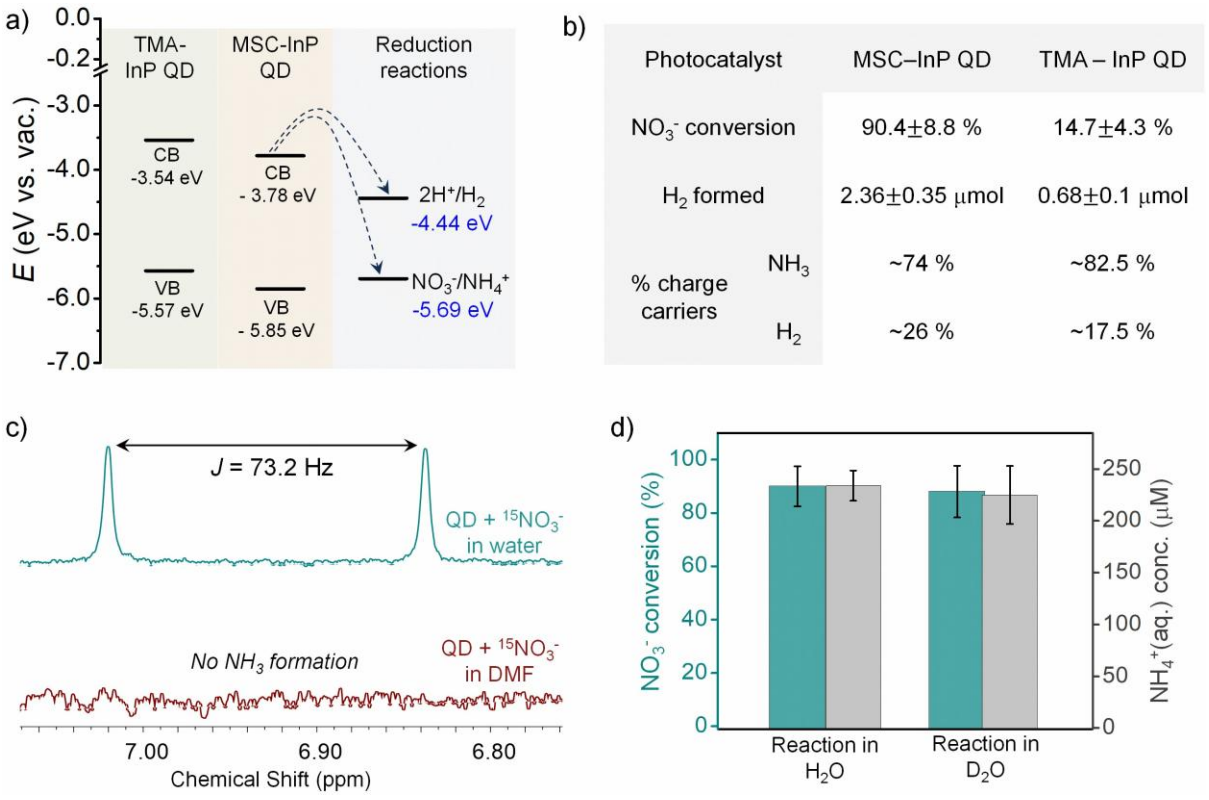


**Figure 5.9.** Effect of inorganic surface ligands on selectivity. a) Energy level diagram comparing the thermodynamic feasibility of driving $NO_3^-$ reduction to $NH_4^+$ and hydrogen evolution with positively charged TMA-InP QDs and MSC-InP QDs. b) Table comparing the effect of MSC and TMA ligands on $NH_4^+$ production and competing $H_2$ evolution reaction. Along with an increase in the total number of utilizable photoexcited charge carriers with inorganic MSC ligands, the selectivity for $NH_4^+$ production was lowered compared to alkyl TMA ligands. c) $^1$H-NMR spectra of the photocatalytic reaction mixture performed in aprotic solvent, DMF using $^{15}NO_3^-$ as the N-

source. The absence of characteristic doublet of $^{15}NH_4^+$ when reaction was performed in DMF suggests water to be the proton source. d) Photocatalytic reactions performed in deuterated water ($D_2O$) yield similar % $NO_3^-$ conversion and $NH_4^+$ formation, confirming water to be the sole proton source.

Next, we tested the applicability of other Lewis acid metal halide complexes as surface ligands on InP QDs for photocatalytic ammonia synthesis. We varied the halide counterpart from chloride to bromide and iodide to form cationic In(III) complexes on InP QD surface. The photocatalytic experiments performed with $InBr_3$ and $InI_3$ cationic complexes in DMF result in negligible change in the $NO_3^-$ conversion efficiency and $NH_4^+$ production (**Figures 5.10, 5.24**). This suggests that halide ions do not affect the photocatalytic activity, and it is purely the inorganic nature of the [+] MSC cationic ligand that boosts $NH_3$ production. When the Lewis acid metal was changed from In to Al, again, there was a negligible effect on the photocatalytic activity (**Figures 5.10, 5.25**), which suggests that the central ion does not play a major role in $NO_3^-$ reduction. Further elucidation of the role of the central metal ion in the metal-solvent complex in dictating photocatalytic activity requires extensive photophysical studies in the future. Moreover, it would be interesting to utilize this strategy to functionalize coordination complexes bearing redox-active metal ions such as $Fe^{2+}/Fe^{3+}$, which can lead to distinct charge carrier dynamics.[45,46]

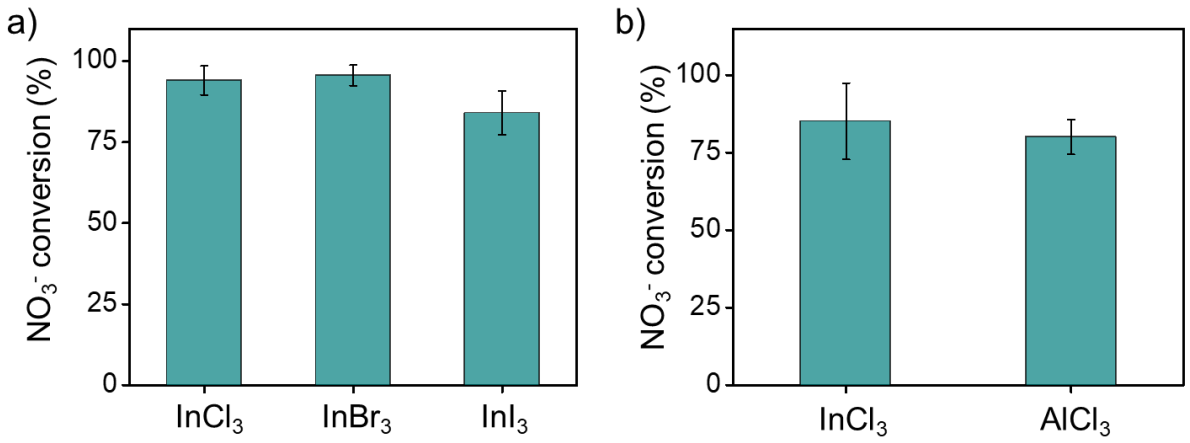


**Figure 5.10.** Extension to other Lewis metal halides as ligands on InP QDs for photocatalytic $NO_3^-$ to $NH_3$ conversion. Photocatalytic $NO_3^-$ conversion with InP QDs functionalized with cationic complexes formed from a) different indium halides and b) different Lewis metal chlorides. A similar photocatalytic $NO_3^-$ conversion suggests the negligible effect of halide counterions and central metal ions in dictating the photocatalytic activity of [+] MSC-InP QDs.

## 5.5. Conclusions

The present study implements new surface chemistries to attain high quantum efficiencies in QD photocatalysed multielectron/multiproton chemical transformations. The presence of an inorganic metal-solvent complex on InP QD surface boosted $NH_3$ production under visible-light irradiation. Compared to long-chain alkyl ligands, inorganic ligand-functionalized InP QDs exhibited ~16-fold and ~8-fold enhancement in reaction rate and AQY, respectively, with complete retention of selectivity for $NH_3$ formation. Through our work, we established the dominance of inorganic ligands over insulating alkyl ligands in outplaying ligand poisoning in visible-light photocatalysed chemical transformations. We posit that a similar ligand effect will be present to perform other challenging multielectron/multiproton chemical reactions, such as $CO_2$ reduction, $N_2$ fixation, urea synthesis, etc. As photocatalysis with QDs is an emerging area, and its full potential is unknown, all efforts made to enhance the quantum efficiencies will enable the development of practical photocatalytic platforms based on QDs.

## 5.6. References

1) Huang, Y.; Cohen, T. A.; Sperry, B. M.; Larson, H.; Nguyen, H. A.; Homer, M. K.; Dou, F. Y.; Jacoby, L. M.; Cossairt, B. M.; Gamelin, D. R.; Luscombe, C. K. Organic Building Blocks at Inorganic Nanomaterial Interfaces. *Mater. Horiz.* **2022**, *9*, 61-87.

2) Heuer-Jungemann, A.; Feliu, N.; Bakaimi, I.; Hamaly, M.; Alkilany, A.; Chakraborty, I.; Masood, A.; Casula, M. F.; Kostopoulou, A.; Oh, E.; Susumu, K.; Stewart, M. H.; Medintz, I. L.; Stratakis, E.; Parak, W. J.; Kanaras, A. G. The Role of Ligands in the Chemical Synthesis and Applications of Inorganic Nanoparticles. *Chem. Rev.* **2019**, *119*, 4819-4880.

3) Jain, V.; Roy, S.; Roy, P.; Pillai, P. P. When Design Meets Function: The Prodigious Role of Surface Ligands in Regulating Nanoparticle Chemistry. *Chem. Mater.* **2022**, *34*, 7579-7597.

4) Roy, S.; Roy, S.; Rao, A.; Devatha, G.; Pillai, P. P. Precise Nanoparticle-Reactant Interaction Outplays Ligand Poisoning in Visible-Light Photocatalysis. *Chem. Mater.* **2018**, *30*, 8415-8419.

5) Roy, S.; Jain, V.; Kashyap, R. K.; Rao, A.; Pillai, P. P. Electrostatically Driven Multielectron Transfer for the Photocatalytic Regeneration of Nicotinamide Cofactor. *ACS Catal.* **2020**, *10*, 5522-5528.

6) Kalyuzhny, G.; Murray, R. W. Ligand Effects on Optical Properties of CdSe Nanocrystals. *J. Phys. Chem. B* **2005**, *109*, 7012-7021.

7) Devatha, G.; Roy, S.; Rao, A.; Mallick, A.; Basu, S.; Pillai, P. P. Electrostatically driven resonance energy Transfer in “Cationic” Biocompatible Indium Phosphide Quantum Dots. *Chem. Sci.* **2017**, *8*, 3879-3884.

8) Roy, P.; Devatha, G.; Roy, S.; Rao, A.; Pillai, P. P. Electrostatically Driven Resonance Energy Transfer in an All-Quantum Dot Based Donor-Acceptor System. *J. Phys. Chem. Lett.* **2020**, *11*, 5354-5360.

9) Chakraborty, I. N.; Roy, P.; Rao, A.; Devatha, G.; Roy, S.; Pillai, P. P. The Unconventional Role of Surface Ligands in Dictating the Light Harvesting Properties of Quantum Dots. *J. Mater. Chem. A* **2021**, *9*, 7422-7457.

10) Hines, D. A.; Kamat, P. V. Quantum Dot Surface Chemistry: Ligand Effects and Electron Transfer Reactions. *J. Phys. Chem. C* **2013**, *117*, 14418-14426.

11) Sandeep, K.; Manoj, B.; Thomas, K. G. Gold Nanoparticle on Semiconductor Quantum Dot: Do Surface Ligands Influence Fermi Level Equilibration. *J. Chem. Phys.* **2020**, *152*, 044710.

12) Boles, M. A.; Ling, D.; Hyeon, T.; Talapin, D. V. The Surface Science of Nanocrystals. *Nat. Mater.* **2016**, *15*, 141-153.

13) Owen, J. The Coordination Chemistry of Nanocrystal Surfaces. *Science* **2015**, *347*, 615-616.

14) Peterson, M. D.; Cass, L. C.; Harris, R. D.; Edme, K.; Sung, K.; Weiss, E. A. The Role of Ligands in Determining the Exciton Relaxation Dynamics in Semiconductor Quantum Dots. *Annu. Rev. Phys. Chem.* **2014**, *65*, 317-339.

15) Weiss, E. A. Designing the Surfaces of Semiconductor Quantum Dots for Colloidal Photocatalysis. *ACS Energy Lett.* **2017**, *2*, 1005-1013.

16) Hines, D. A.; Forrest, R. P.; Corcelli, S. A.; Kamat, P. V. Predicting the Rate Constant of Electron Tunneling Reactions at the CdSe–$TiO_2$ Interface. *J. Phys. Chem. B* **2015**, *119*, 7439-7446.

17) Wang, H.; McNellis, E. R.; Kinge, S.; Bonn, M.; Canovas, E. Tuning Electron Transfer Rates through Molecular Bridges in Quantum Dot Sensitized Oxides. *Nano Lett.* **2013**, *13*, 5311-5315.

18) Kim, Y.; Wilson, A. J.; Jain, P. K. The Nature of Plasmonically Assisted Hot-Electron Transfer in a Donor–Bridge–Acceptor Complex. *ACS Catal.* **2017**, *7*, 4360-4365.

19) Dibbell, R. S.; Youker, D. G.; Watson, D. F. Excited-State Electron Transfer from CdS Quantum Dots to $TiO_2$ Nanoparticles via Molecular Linkers with Phenylene Bridges. *J. Phys. Chem. C* **2009**, *113*, 18643-18651.

20) Marcus, R. A.; Sutin, N. Electron Transfers in Chemistry and Biology. *Biochim. Biophys. Acta, Rev. Bioenerg.* **1985**, *811*, 265-322.

21) Smith, J. G.; Jain, P. K. The Ligand Shell as an Energy Barrier in Surface Reactions on Transition Metal Nanoparticles. *J. Am. Chem. Soc.* **2016**, *138*, 6765-6773.

22) Lu, L.; Zou, S.; Fang, B. The Critical Impacts of Ligands on Heterogeneous Nanocatalysis: A Review. *ACS Catal.* **2021**, *11*, 6020-6058.

23) Kovalenko, M. V.; Scheele, M.; Talapin, D. V. Colloidal Nanocrystals with Molecular Metal Chalcogenide Surface Ligands. *Science* **2009**, *324*, 1417-1420.

24) Nag, A.; Kovalenko, M. V.; Lee, J.-S.; Liu, W.; Spokoyny, B.; Talapin, D. V. Metal-Free Inorganic Ligands for Colloidal Nanocrystals: $S^{2-}$, $HS^{-}$, $Se^{2-}$, $HSe^{-}$, $Te^{2-}$, $HTe^{-}$, $TeS_3^{2-}$, $OH^{-}$, and $NH_2^{-}$ as Surface Ligands. *J. Am. Chem. Soc.* **2011**, *133*, 10612-10620.

25) Yu, S.; Fan, X.-B.; Wang, X.; Li, J.; Zhang, Q.; Xia, A.; Wei, S.; Wu, L.-Z.; Zhou, Y.; Patzke, G. R. Efficient Photocatalytic Hydrogen Evolution with Ligand Engineered All-Inorganic InP and InP/ZnS Colloidal Quantum Dots. *Nat. Commun.* **2018**, *9*, 4009.

26) Jain, V.; Tyagi, S.; Roy, P.; Pillai, P. P. Ammonia Synthesis with Visible Light and Quantum Dots. *J. Am. Chem. Soc.* **2024**, *146*, 32356-32365.

27) Dong, A.; Ye, X.; Chen, J.; Kang, Y.; Gordon, T.; Kikkawa, J. M.; Murray, C. B. A Generalized Ligand-Exchange Strategy Enabling Sequential Surface Functionalization of Colloidal Nanocrystals. *J. Am. Chem. Soc.* **2011**, *133*, 998- 1006.

28) Hai, Y.; Gahlot, K.; Tanchev, M.; Mutalik, S.; Tekelenburg, E. K.; Hong, J.; Ahmadi, M.; Piveteau, L.; Loi, M. A.; Protesescu, L. Metal-Solvent Complex Formation at the Surface of InP Colloidal Quantum Dots. *J. Am. Chem. Soc.* **2024**, *146*, 12808-12818.

29) Tessier, M. D.; Dupont, D.; De Nolf, K.; De Roo, J.; Hens, Z. Economic and Size-Tunable Synthesis of InP/ZnE (E = S,Se) Colloidal Quantum Dots. *Chem. Mater.* **2015**, *27*, 4893-4898.

30) Tessier, M. D.; De Nolf, K.; Dupont, D.; Sinnaeve, D.; De Roo, J.; Hens, Z. Aminophosphines: A Double Role in the Synthesis of Colloidal Indium Phosphide Quantum Dots. *J. Am. Chem. Soc.* **2016**, *138*, 5923-5929.

31) Okamoto, A.; Toda, S.; Tsujihata, T.; Kamada, T.; Huang, M.; Hashimoto, Y.; Isojima, S.; Kajii, H.; Seino, S.; Kurashiki, T. Enhanced Optical Properties of Green-Emitting InP Quantum Dots with Matched Junctions of the Core and Mn-Doped Novel Shells. *Adv. Mater. Interfaces* **2025**, *12*, 2400708.

32) Heath, J. R. Covalency in Semiconductor Quantum Dots. *Chem. Soc. Rev.* **1998**, *27*, 65-71.

33) Thomas, A.; Sandeep, K.; Somasundaran, S. M.; Thomas, K. G. How Trap States Affect Charge Carrier Dynamics of CdSe and InP Quantum Dots: Visualization through Complexation with Viologen. *ACS Energy Lett.* **2018**, *3*, 2368-2375.

34) Jang, D.; Han, Y.; Baek, S.; Kim, J. Theoretical Comparison of The Energies and Wave Functions of the Electron and Hole States Between CdSe- and InP-Based

Core/Shell/Shell Quantum Dots: Effect of the Bandgap Energy of the Core Material on the Emission Spectrum. *Opt. Mater. Express* **2019**, *9*, 1257-1270.

35) Brown, P. R.; Kim, D.; Lunt, R. R.; Zhao, N.; Bawendi, M. G.; Grossman, J. C.; Bulović, V. Energy Level Modification in Lead Sulfide Quantum Dot Thin Films Through Ligand Exchange. *ACS Nano* **2014**, *8*, 5863-5872.

36) Kroupa, D. M.; Vörös, M.; Brawand, N. P.; McNichols, B. W.; Miller, E. M.; Gu, J.; Nozik, A. J.; Sellinger, A.; Galli, G.; Beard, M. C. Tuning Colloidal Quantum Dot Band Edge Positions Through Solution-Phase Surface Chemistry Modification. *Nat. Commun.* **2017**, *8*, 15257.

37) Vogel, Y. B.; Pham, L. N.; Stam, M.; Ubbink, R. F.; Coote, M. L.; Houtepen, A. J. Solvation Shifts the Band-Edge Position of Colloidal Quantum Dots by Nearly 1 eV. *J. Am. Chem. Soc.* **2024**, *146*, 9928-9938.

38) Chung, D. S.; Lee, J.-S.; Huang, J.; Nag, A.; Ithurria, S.; Talapin, D. V. Low Voltage, Hysteresis Free, and High Mobility Transistors from All-Inorganic Colloidal Nanocrystals. *Nano Lett.* **2012**, *12*, 1813-1820.

39) Shanker, G. S.; Swarnkar, A.; Chatterjee, A.; Chakraborty, S.; Phukan, M.; Parveen, N.; Biswas, K.; Nag, A. Electronic Grade and Flexible Semiconductor Film Employing Oriented Attachment of Colloidal Ligand-Free PbS and PbSe Nanocrystals at Room Temperature. *Nanoscale* **2015**, *7*, 9204-9214.

40) Reiss, P.; Protière, M.; Li, L. Core/Shell Semiconductor Nanocrystals. *Small* **2009**, *5*, 154-168.

41) Meng, S.-L.; Ye, C.; Li, X.-B.; Tung, C.-H.; Wu, L.-Z. Photochemistry Journey to Multielectron and Multiproton Chemical Transformation. *J. Am. Chem. Soc.* **2022**, *144*, 16219-16231.

42) Kramer, W. W.; McCrory, C. C. L. Polymer Coordination Promotes Selective $CO_2$ Reduction by Cobalt Phthalocyanine. *Chem. Sci.* **2016**, *7*, 2506-2515.

43) Liu, Y.; McCrory, C. C. L. Modulating the Mechanism of Electrocatalytic $CO_2$ Reduction by Cobalt Phthalocyanine Through Polymer Coordination and Encapsulation. *Nat. Commun.* **2019**, *10*, 1683.

44) Zee, D. Z.; Nippe, M.; King, A. E.; Chang, C. J.; Long, J. R. Tuning Second Coordination Sphere Interactions in Polypyridyl–Iron Complexes to Achieve Selective Electrocatalytic Reduction of Carbon Dioxide to Carbon Monoxide. *Inorg. Chem.* **2020**, *59*, 5206-5217.

45) Tarafder, K.; Surendranath, Y.; Olshansky, J. H.; Alivisatos, A. P.; Wang, L. W. Hole Transfer Dynamics from a CdSe/CdS Quantum Rod to a Tethered Ferrocene Derivative. *J. Am. Chem. Soc.* **2014**, *136*, 5121-5131.

46) Dou, F. Y.; Harvey, S. M.; Mason, K. G.; Homer, M. K.; Gamelin, D. R.; Cossairt, B. M. Effect of a Redox-Mediating Ligand Shell on Photocatalysis by CdS Quantum Dots. *J. Chem. Phys.* **2023**, *158*, 184705.

# 5.7. Appendix

### Characterization of InP QDs

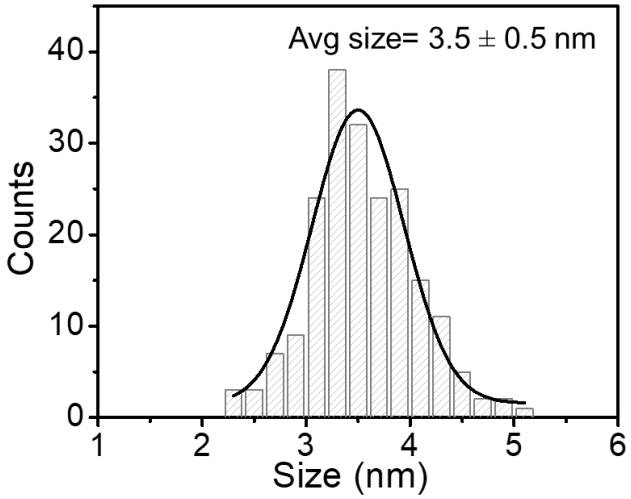


**Figure 5.11.** Size distribution histogram for core-only [+] MSC-InP QDs, measured from HRTEM images. The average size was calculated to be 3.5 ± 0.5 nm from ~ 200 InP QDs.

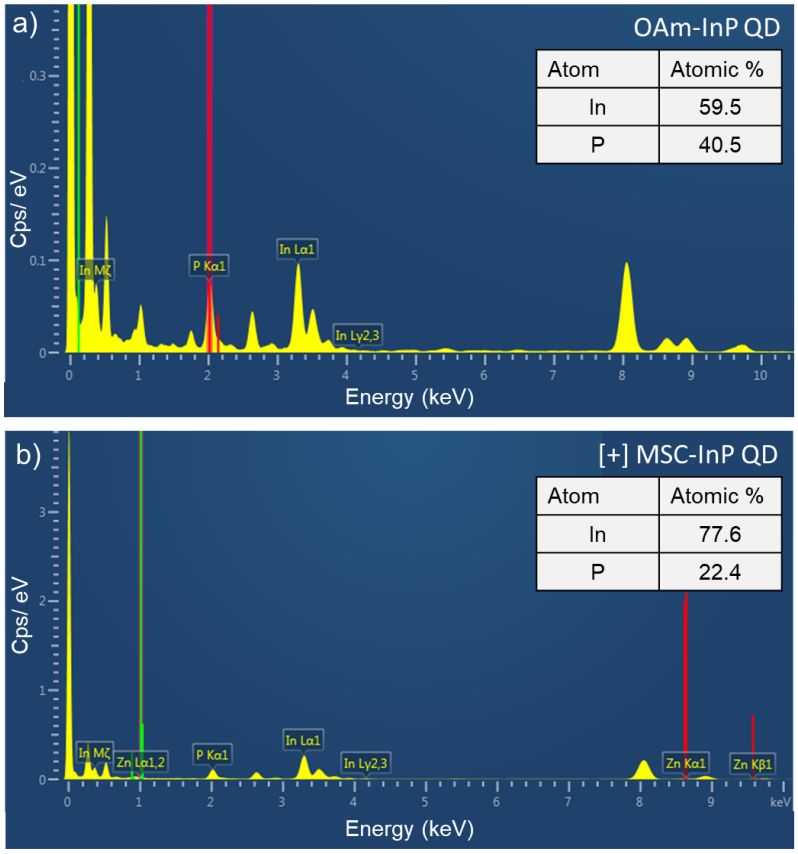


**Figure 5.12.** EDAX spectrum of a) OAm-InP QD and b) [+] MSC-InP QD. Inset shows the atomic percentages for In and P.

**Photocatalytic reaction performed with [+] MSC-InP QDs**

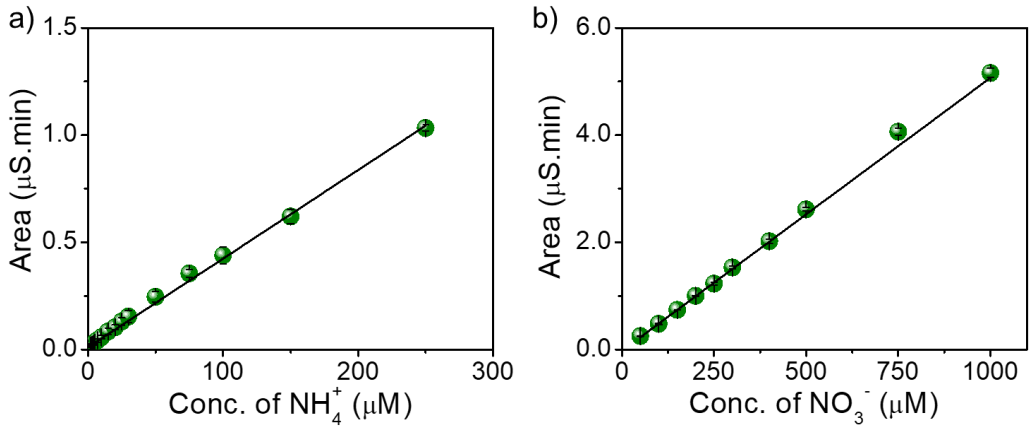


**Figure 5.13.** Calibration curves for a) $NH_4^+$ and b) $NO_3^-$ ions detection with ion chromatography.

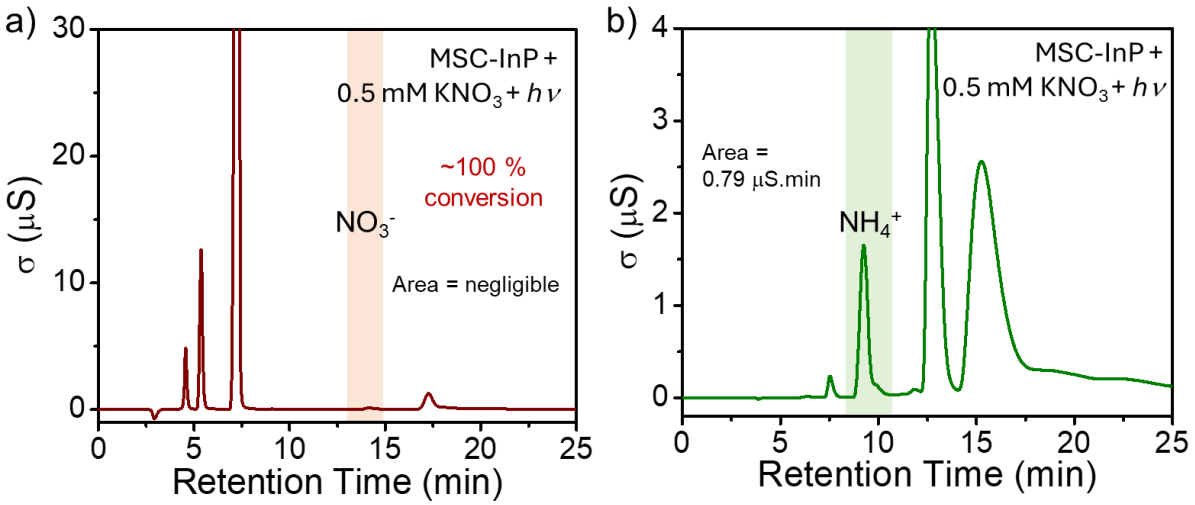


**Figure 5.14.** Photocatalytic reduction of $NO_3^-$ to $NH_4^+$ with [+] MSC-InP QDs. a) Anion and b) cation chromatograms of the photocatalytic reaction mixture after 2 h of visible-light irradiation.

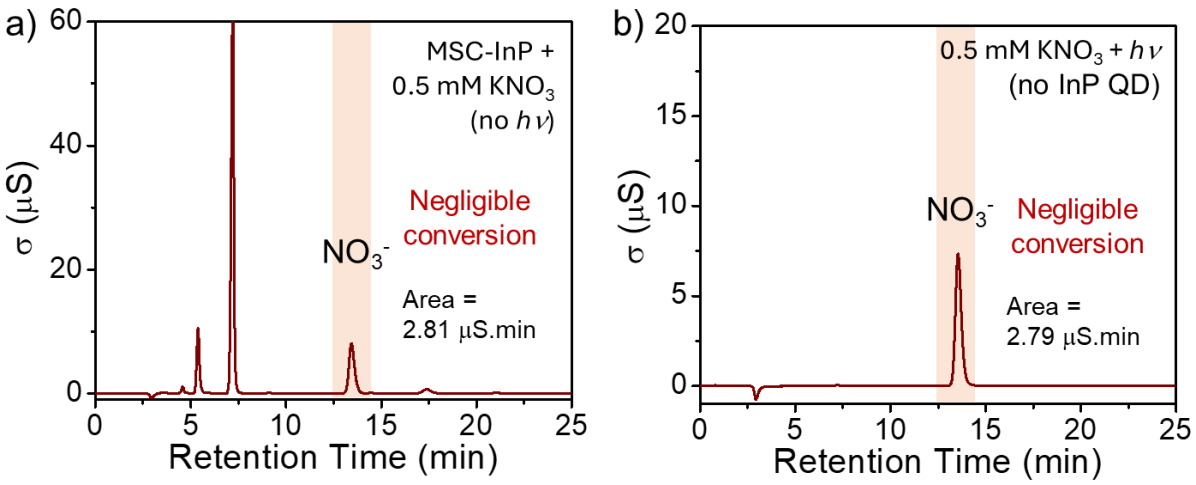


**Figure 5.15.** Anion chromatograms of the photocatalytic reactions performed in the absence of a) light and b) [+] MSC-InP QDs. A negligible $NO_3^-$ conversion confirms the need for both components for $NH_3$ synthesis.

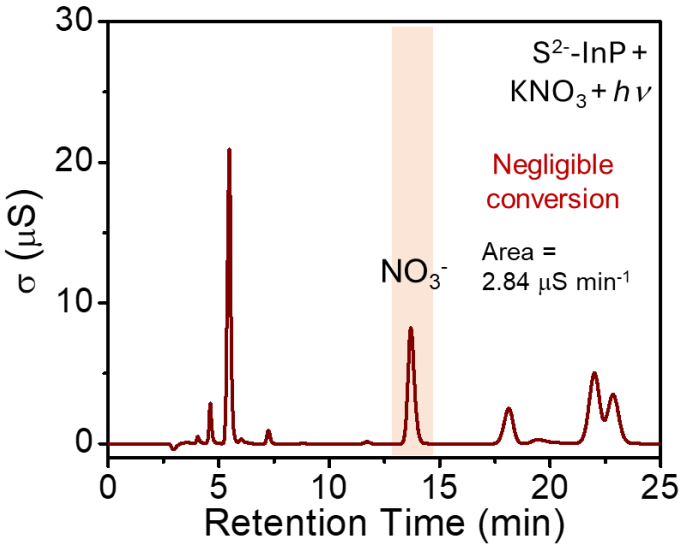


**Figure 5.16.** Proof of electrostatics. Anion chromatogram of the photocatalytic reaction mixture performed with negatively charged inorganic $S^{2-}$-functionalized InP QDs. A negligible $NO_3^-$ conversion was observed, suggesting the key role of favourable electrostatics in dictating photocatalytic activity.

**Comparison of the photocatalytic activity of inorganic ligand-capped [+] MSC-InP QDs with organic alkyl ligand-capped [+] TMA-InP QDs**

Time-dependent studies with core-only [+] MSC-InP QDs

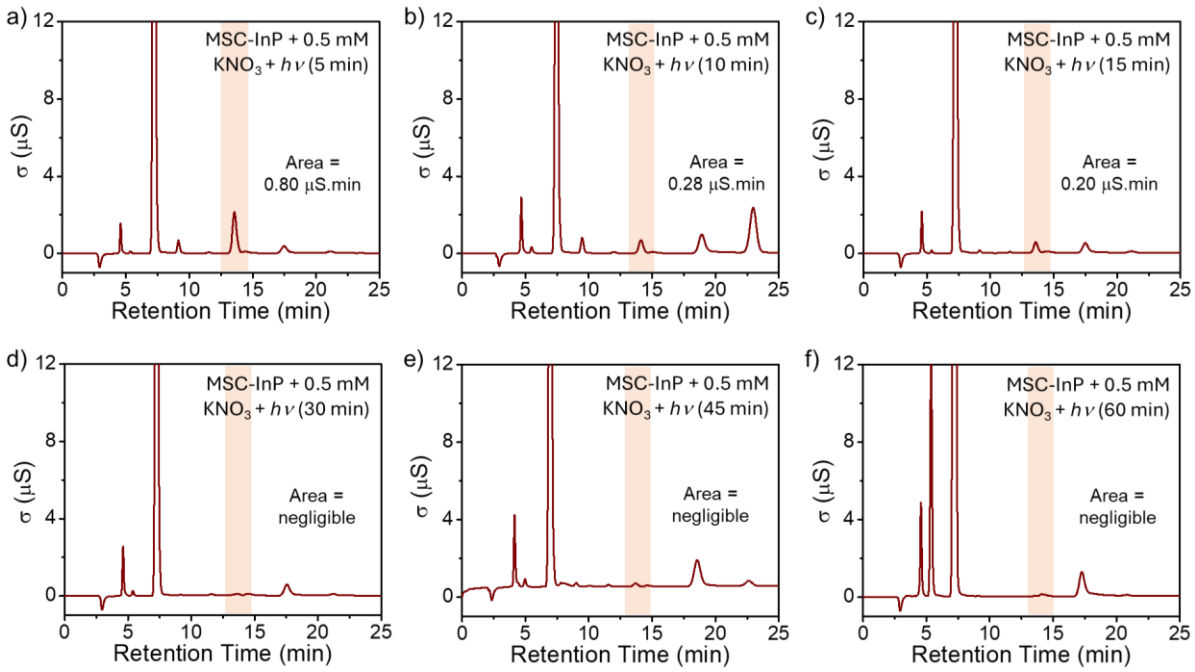


**Figure 5.17.** Anion chromatograms of the photocatalytic reaction mixture performed with [+] MSC-InP QDs for a) 5 min, b) 10 min, c) 15 min, d) 30 min, e) 45 min, and f) 60 min.

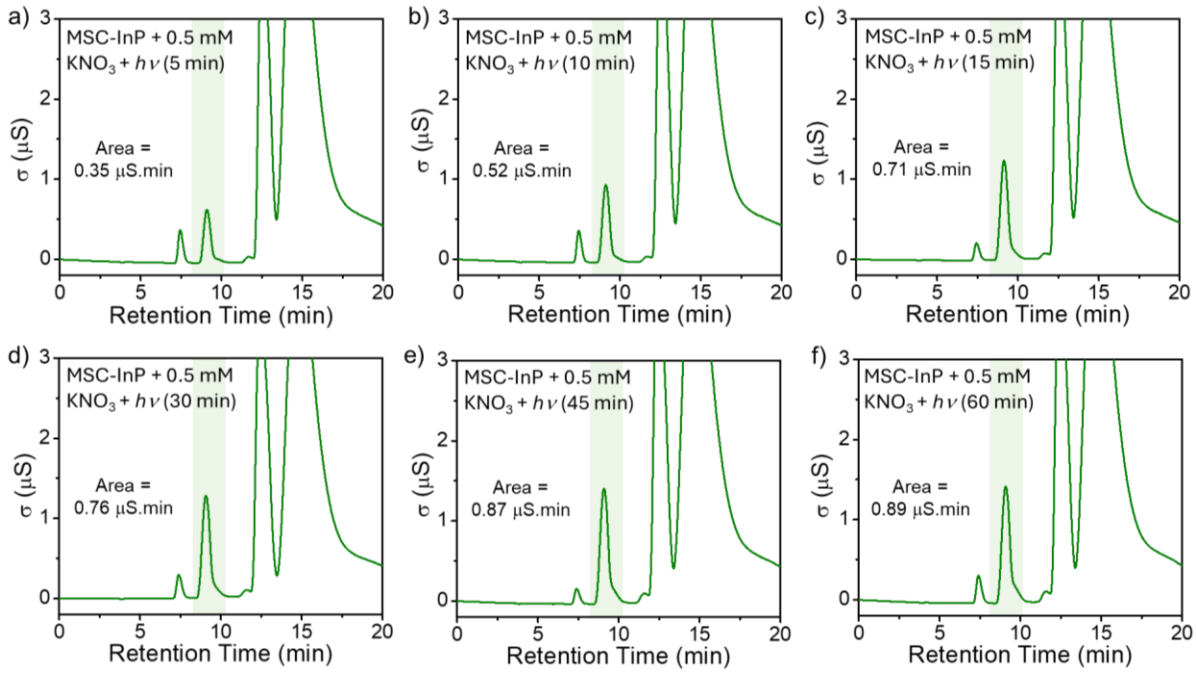


**Figure 5.18.** Cation chromatograms of the photocatalytic reaction mixture performed with [+] MSC-InP QDs for a) 5 min, b) 10 min, c) 15 min, d) 30 min, e) 45 min, and f) 60 min.

Time-dependent studies with core-only [+] TMA-InP QDs

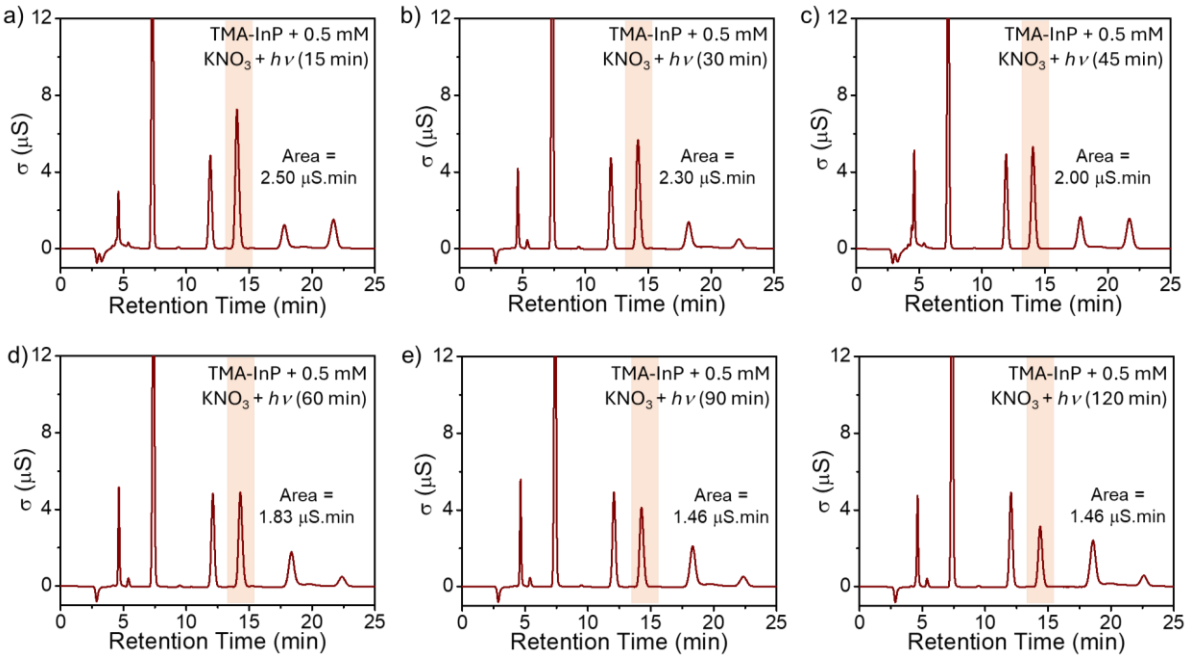


**Figure 5.19.** Anion chromatograms of the photocatalytic reaction mixture performed with [+] TMA-InP QDs for a) 15 min, b) 30 min, c) 45 min, d) 60 min, e) 90 min, and f) 120 min.

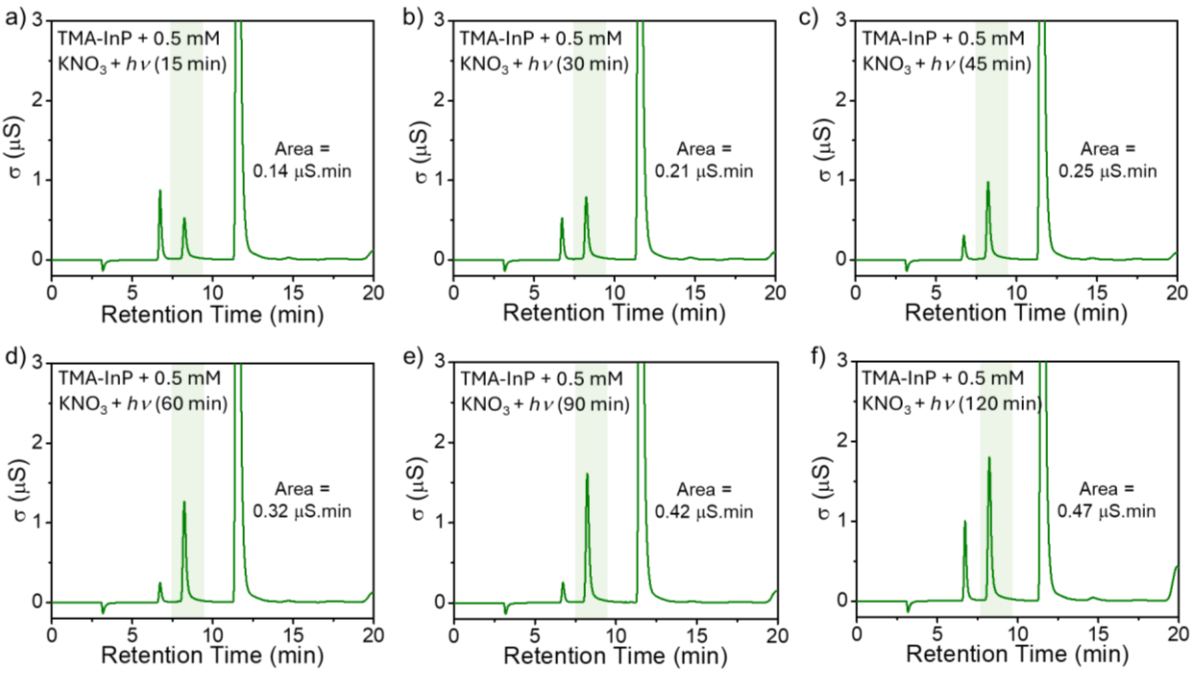


**Figure 5.20.** Cation chromatograms of the photocatalytic reaction mixture performed with [+] TMA-InP QDs for a) 15 min, b) 30 min, c) 45 min, d) 60 min, e) 90 min, and f) 120 min.

Time-dependent studies with core/shell [+] MSC-InP/ZnS QDs

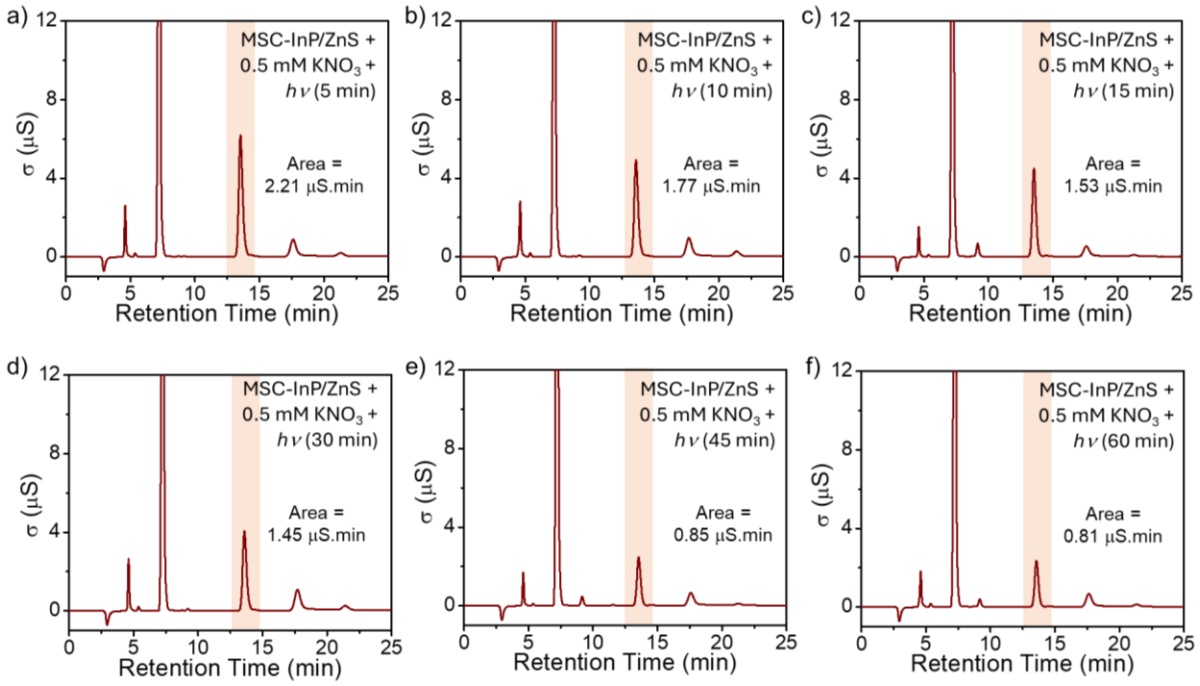


**Figure 5.21.** Anion chromatograms of the photocatalytic reaction mixture performed with [+] MSC-InP/ZnS QDs for a) 5 min, b) 10 min, c) 15 min, d) 30 min, e) 45 min, and f) 60 min.

Time-dependent studies with core/shell [+] TMA-InP/ZnS QDs

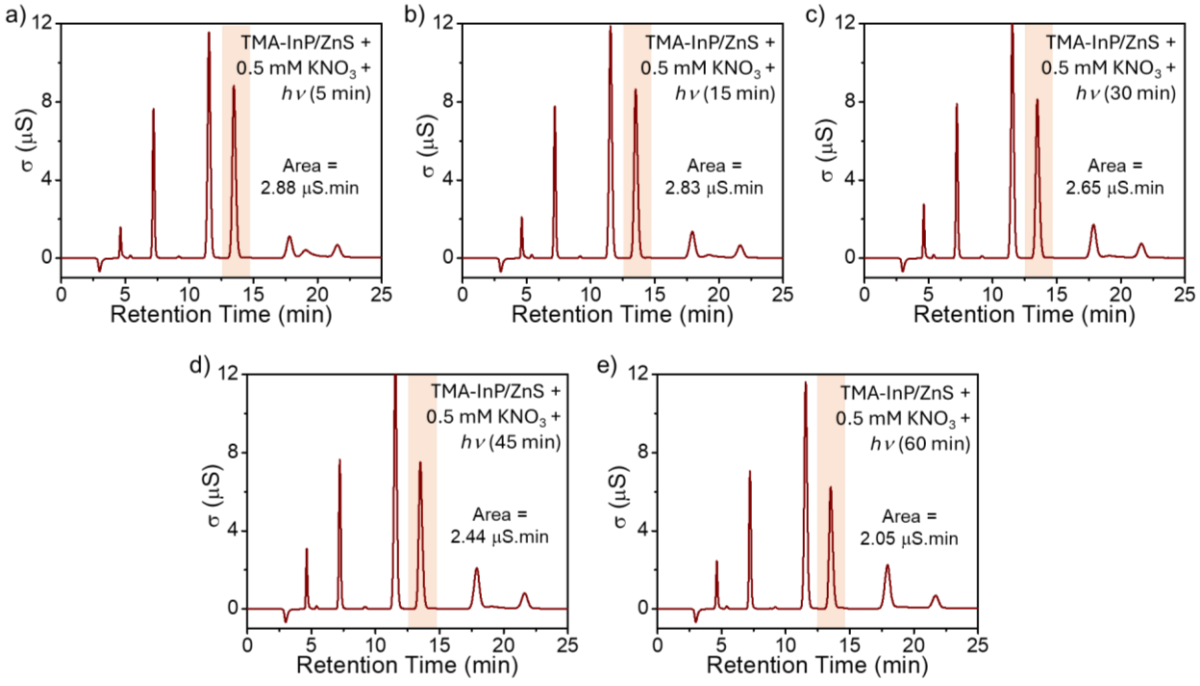


**Figure 5.22.** Anion chromatograms of the photocatalytic reaction mixture performed with [+] TMA-InP/ZnS QDs for a) 5 min, b) 15 min, c) 30 min, d) 45 min, and e) 60 min.

### Photocatalytic reaction performed in deuterated water

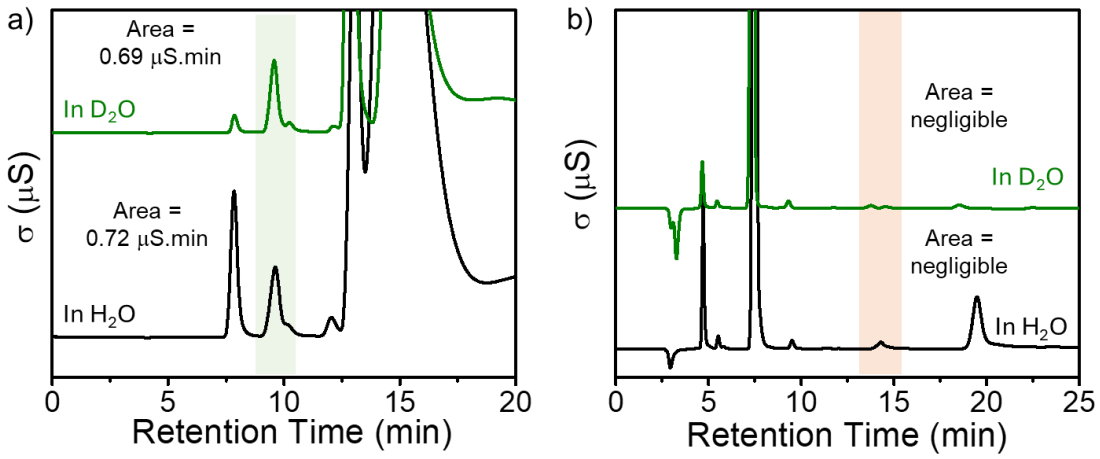


**Figure 5.23.** a) Cation and b) anion chromatograms of the photocatalytic reaction performed with [+] MSC-InP QDs in water and deuterated water, clearly showing the formation of ammonia and deuterated ammonia, respectively with complete conversion of $NO_3^-$ under both media. With no other source of proton present in the reaction mixture, this confirms the role of water as the proton source in ammonia synthesis with [+] MSC-InP QDs.

### Extension to other Lewis metal halides as surface ligands

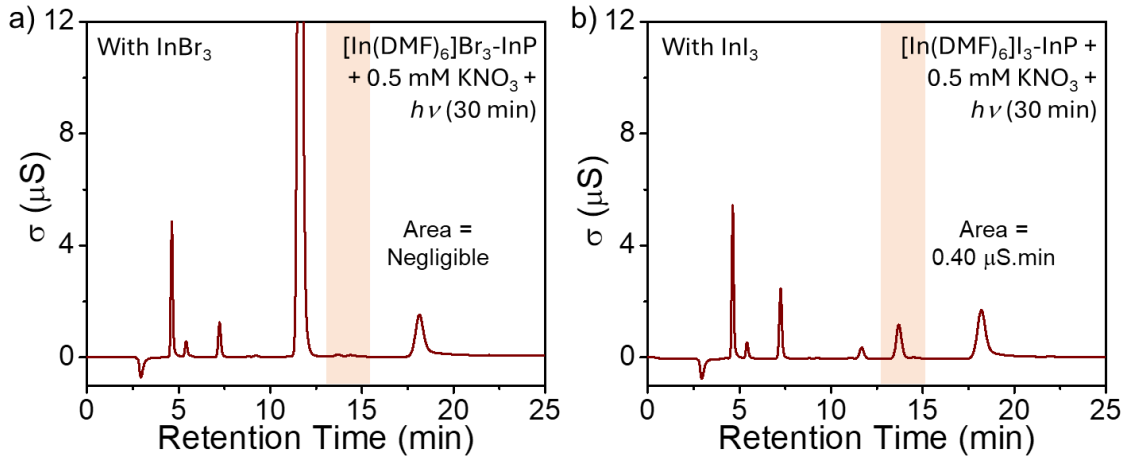


**Figure 5.24.** Anion chromatograms of the photocatalytic $NO_3^-$ conversion performed with InP QDs functionalized with different indium halides: a) $InBr_3$ and b) $InI_3$. Both these indium halides tend to form cationic complexes in DMF similar to $InCl_3$. A similar photocatalytic $NO_3^-$ conversion suggests the negligible effect of halide counterions in dictating the photocatalytic activity of [+] MSC-InP QDs under visible light illumination.

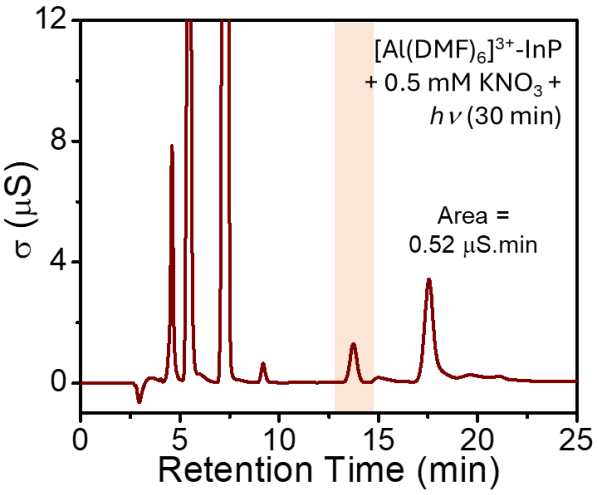


**Figure 5.25.** Anion chromatograms of the photocatalytic $NO_3^-$ conversion performed with InP QDs functionalized with different Lewis acid metal chloride, $AlCl_3$. Negligible effect of Lewis acid metal centre in dictating the photocatalytic activity of InP QDs under visible light illumination was observed.

# Chapter – 6

## Summary and Future Outlook

## 6.1. Thesis summary

The present Thesis deals with maximizing the efficiency of each fundamental step in photocatalysis: light absorption and charge generation, charge separation, and finally, charge extraction, to drive challenging and industrially relevant multielectron chemical transformations. This was achieved through the rational design of both the core and the surface of plasmonic metal nanoparticles (NPs) and semiconductor quantum dots (QDs), the photocatalysts of our choice.

**Thesis at a glance**

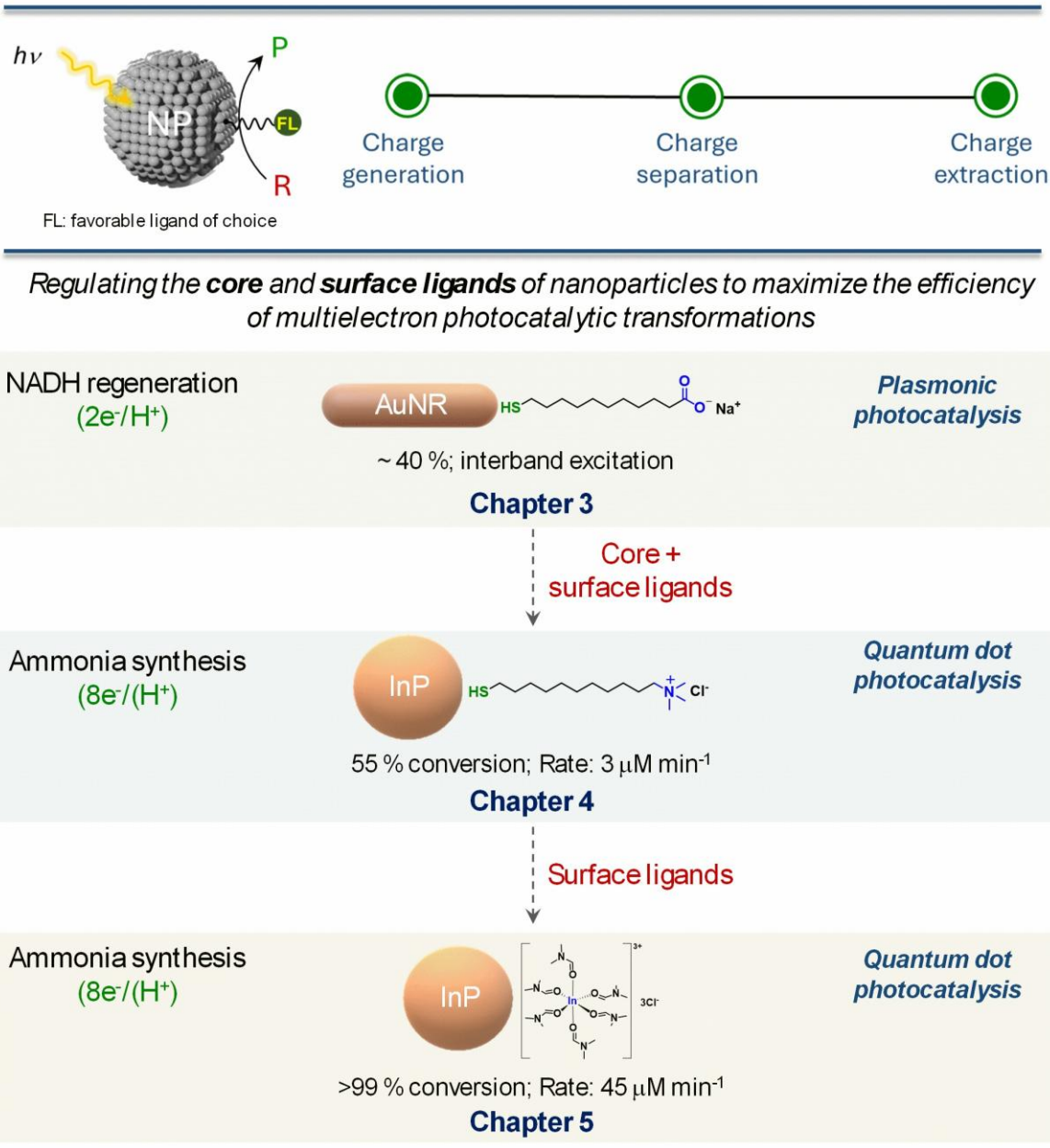

At a glance, we regulated the nanoparticle core and surface ligands to perform multielectron and multiproton reactions with the aim of maximizing photocatalytic efficiencies. **Chapter 3** focuses on understanding the role of light excitation attributes in light-driven nicotinamide cofactor regeneration with plasmonic metal nanoparticles. The appropriate choice of plasmonic nanoparticle core in the form of anisotropic nanorods and favorable surface ligand allowed us to understand the exclusive role of interband vs intraband transitions in maximizing the charge generation, separation, and extraction processes in NADH photoregeneration. Next, with the aim of synthesizing important commodity chemicals such as ammonia, we fine-tuned the photocatalyst design in **Chapter 4a** and switched the core from metal to semiconductor quantum dots (QDs) to overcome the challenges associated with the short lifetime of charge carriers. A rational choice of indium phosphide (InP) QDs, having a preferential affinity of N-sources towards surface In atoms and favorable ligands on InP QD photocatalysts, resulted in selective and efficient ammonia production from nitrate and nitrite ions under visible-light irradiation. This is one of the simplest photocatalytic systems comprising only the photocatalyst, the reactant, and water. The next part of this Chapter deals with elucidating the key mechanistic details involved in photocatalytic nitrate reduction to ammonia with InP QDs. In **Chapter 4b**, we listed our findings on reaction rate, competing reactions, proton source, fate of photoexcited holes, and recyclability aspects. In **Chapter 5**, we were successful in maximizing the efficiency of the charge extraction process by the appropriate choice of the *'less-explored'* inorganic surface ligands on the InP QDs for light-driven ammonia synthesis. The effect of surface chemistry was clearly seen in 16-fold and 8-fold enhancement in reaction rate and quantum yield, respectively. This is one of the first reports where cationic inorganic ligands are employed in quantum dot photocatalyzed multielectron chemical transformations.

## 6.2. Future outlook

The concepts developed in this thesis can be easily extended to one-pot complex molecule/material synthesis in a sustainable manner, including cascade coupling reactions and multicomponent reactions such as urea/ alkyl amines synthesis, amino acids synthesis, or synthesizing precursors for polymer synthesis (**Scheme 6.1**). Such ambitious work in the future requires dedicated efforts in alleviating the challenges associated at the fundamental level. For instance, stability under continuous light illumination is a long-standing challenge in QD photocatalysis. Overcoming this requires an in-depth understanding of the mechanisms of degradation under operating conditions, which is currently scarce in the literature.

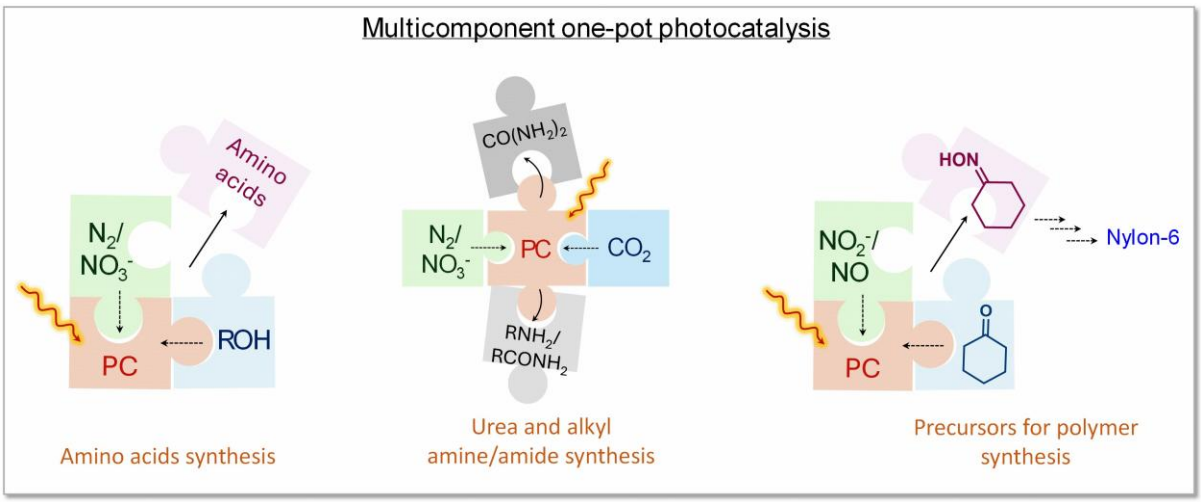


**Scheme 6.1.** Schematic representation of the multicomponent one-pot synthesis of value-added chemicals under photocatalytic conditions.

While arriving at the best photocatalyst design still relies upon the conventional route of the manual trial-and-error method, active learning can accelerate catalyst discovery and optimization of reaction parameters. The ultimate goal is to translate the photocatalytic process from laboratory to market-ready solar fuel platforms, which requires an increase in experimental replicability and standardization across different platforms by mitigating human error. In this direction, automation-driven photocatalysis or self-driving labs by integrating machine learning and robotics will turn out to be a game-changer.

# Scientific Output

## List of Publications

**Included in the thesis**

1. **Jain, V.**, Roy, S., Roy, P., and Pillai, P. P. When Design Meets Function: The Prodigious Role of Surface Ligands in Regulating Nanoparticle Chemistry. *Chem. Mater.* **2022**, *34*, 7579-7597.
2. **Jain, V.**, Kashyap, R. K., and Pillai, P. P. Plasmonic Photocatalysis: Activating Chemical Bonds through Light and Plasmon. *Adv. Opt. Mater.* **2022**, *10*, 2200463.
3. **Jain, V.**, Chakraborty, I. N., Raj, R. B., and Pillai, P. P. Deciphering the Role of Light Excitation Attributes in Plasmonic Photocatalysis: The Case of Nicotinamide Cofactor Regeneration. *J. Phys. Chem. C* **2023**, *127*, 5153-5161.
4. **Jain, V.**, Tyagi, S., Roy, P., and Pillai, P. P. Ammonia Synthesis with Visible Light and Quantum Dots. *J. Am. Chem. Soc.* **2024**, *146*, 32356-32365.
5. **Jain, V.** and Pillai, P. P. Metal-Solvent Complex on Quantum Dot Surface Enhances Ammonia Formation with Visible Light. *Manuscript Submitted*.

**Not included in the thesis**

6. **Jain, V.** and Pillai, P. P. A Path to Perpetual Chemical Synthesis Via Photocatalytic Cofactor Regeneration. *Chem. Sci.* **2025**. DOI: 10.1039/D5SC02770E (*corresponding author*)
7. Chakraborty, I. N., **Jain, V.**, Roy, P., Kumar, P., Vinod, C. P., and Pillai, P. P. Photoregeneration of Reactive Cofactors with InP Quantum Dots for the Continuous Chemical Synthesis. *ACS Catal.* **2024**, *14*, 6740-6748.
8. Deepak, N., **Jain, V.**, and Pillai, P. P. Metal-Semiconductor Heterojunction Accelerates the Plasmonically-Powered Photoregeneration of Biological Cofactors. *Photochem. Photobio.* **2024**, *100*, 1000-1009. (*corresponding author*)

9. Dhankhar, A., **Jain, V.**, Chakraborty, I. N., and Pillai, P. P. Enhancing the Photocatalytic Regeneration of Nicotinamide Cofactors with Surface Engineered Plasmonic Antenna-Reactor System. *J. Photochem. Photobio. A: Chem.* **2023**, *437*, 114472.
10. Rao, A., Roy, S., **Jain, V.**, and Pillai, P. P. Nanoparticle Self-Assembly: From Design Principles to Complex Matter to Functional Materials. *ACS Appl. Mater. Interfaces* **2023**, *15*, 25248-25274.
11. Roy, S., **Jain, V.**, Kashyap, R. K., Rao, A., and Pillai, P. P. Electrostatically Driven Multielectron Transfer for the Photocatalytic Regeneration of Nicotinamide Cofactor. *ACS Catal.* **2020**, *10*, 5522-5528.

## List of Conferences Attended

- Oral talk and poster presentation "*Ligands as Gatekeepers in Nanoparticles Photocatalyzed Chemical Transformations"* at **Gordon Research Seminar (GRS) and Gordon Research Conference (GRC) on Colloidal Semiconductor Nanocrystals 2024** held in **Les Diablerets, Switzerland**.
- Flash talk *"Photocatalysis with Surface Engineered Nanoparticles"* at **5th Alexander von Humboldt Kolleg 2024** held in **Goa, India**.
- Poster presentation *"Activating Chemical Bonds with Light and Plasmon"* at **PMRF Annual Symposium 2024** held at **Indian Institute of Technology Indore, India**.
- Poster presentation *"Channelizing the Flow of Reactants in Plasmonic Photocatalysis"* at **Nanomaterials and Molecules: From Spectroscopy to Bioimaging (NaMoSBio) 2024** held at **IISER Kolkata, India**.
- Oral talk *"Plasmon Driven Photocatalytic Regeneration of Biological Cofactors"* at **ChemSymphoria 2023** held at **IISER Pune, India**.
- Poster presentation *"Plasmon-Powered Regeneration of Nicotinamide Cofactor"* at **Mini-Symposium on Organometallic Chemistry and Catalysis** held at **IISER Pune, India**.
- Poster presentation *"Ligands as 'Gatekeepers' in Nanoparticle Photocatalysed Reactions"* at **Emerging Materials 2023** held at **IISER Pune, India**.
- Oral talk and poster presentation *"Plasmon Driven Photocatalytic Regeneration of Nicotinamide Cofactor"* at **Conference on Advances in Catalysis for Energy and Environment (CACEE) 2022 & $CO_2$ India Network 1st Annual Meet** held at **Tata Institute of Fundamental Research (TIFR) Mumbai, India.**
- Poster presentation *"Activating Chemical Bonds Through Plasmons"* at **Low-Dimensional Materials 2022** held at **IISER Pune, India**.

# Copyright Permissions

## Chapter 1

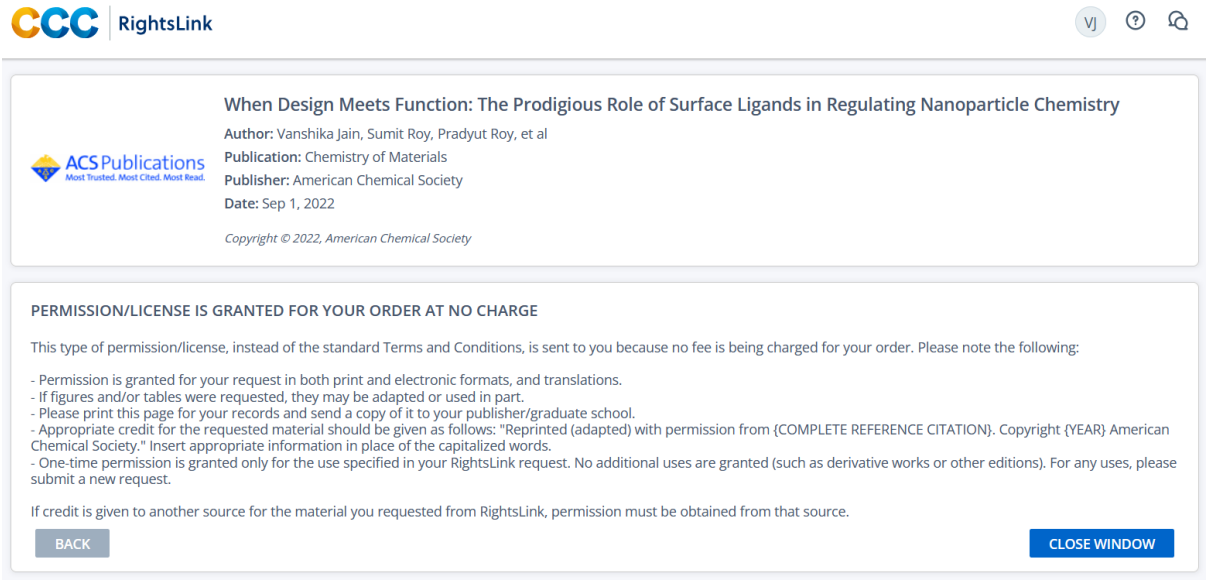

RightsLink

VJ

When Design Meets Function: The Prodigious Role of Surface Ligands in Regulating Nanoparticle Chemistry

**Author:** Vanshika Jain, Sumit Roy, Pradyut Roy, et al
**Publication:** Chemistry of Materials
**Publisher:** American Chemical Society
**Date:** Sep 1, 2022

*Copyright © 2022, American Chemical Society*

PERMISSION/LICENSE IS GRANTED FOR YOUR ORDER AT NO CHARGE

This type of permission/license, instead of the standard Terms and Conditions, is sent to you because no fee is being charged for your order. Please note the following:

- Permission is granted for your request in both print and electronic formats, and translations.
- If figures and/or tables were requested, they may be adapted or used in part.
- Please print this page for your records and send a copy of it to your publisher/graduate school.
- Appropriate credit for the requested material should be given as follows: "Reprinted (adapted) with permission from {COMPLETE REFERENCE CITATION}. Copyright {YEAR} American Chemical Society." Insert appropriate information in place of the capitalized words.
- One-time permission is granted only for the use specified in your RightsLink request. No additional uses are granted (such as derivative works or other editions). For any uses, please submit a new request.

If credit is given to another source for the material you requested from RightsLink, permission must be obtained from that source.

BACK

CLOSE WINDOW

**Figure 1.1**

## You are free to:

**Share** — copy and redistribute the material in any medium or format

The licensor cannot revoke these freedoms as long as you follow the license terms.

## Under the following terms:

**Attribution** — You must give appropriate credit , provide a link to the license, and indicate if changes were made . You may do so in any reasonable manner, but not in any way that suggests the licensor endorses you or your use.

**NonCommercial** — You may not use the material for commercial purposes .

**Figure 1.3a**

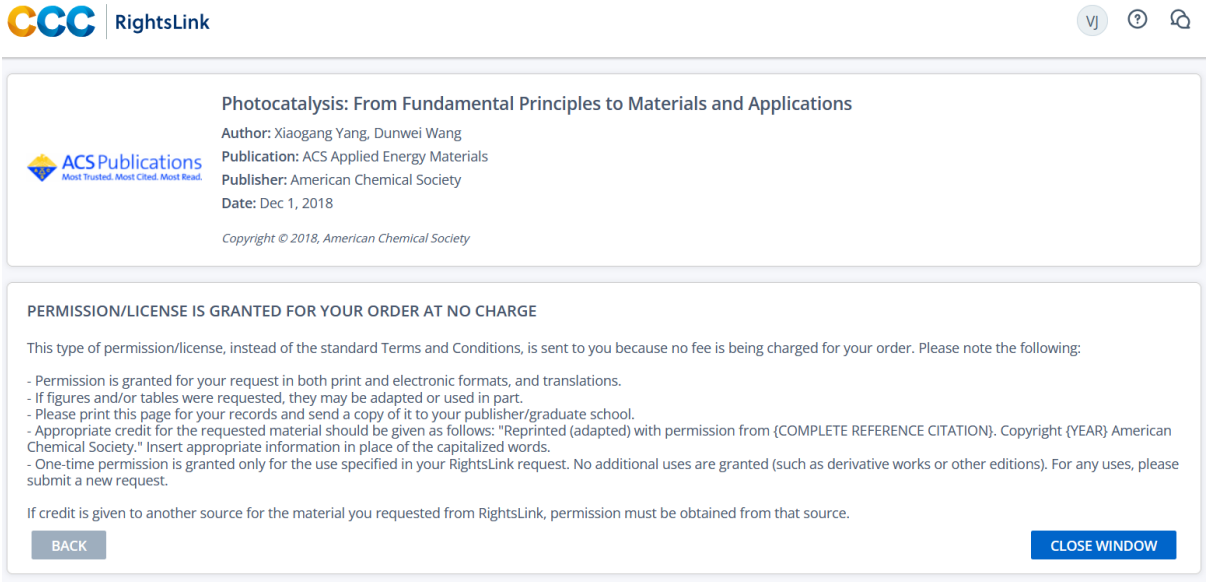
RightsLink
VJ
Photocatalysis: From Fundamental Principles to Materials and Applications
Author: Xiaogang Yang, Dunwei Wang
Publication: ACS Applied Energy Materials
Publisher: American Chemical Society
Date: Dec 1, 2018
Copyright © 2018, American Chemical Society
PERMISSION/LICENSE IS GRANTED FOR YOUR ORDER AT NO CHARGE
This type of permission/license, instead of the standard Terms and Conditions, is sent to you because no fee is being charged for your order. Please note the following:
- Permission is granted for your request in both print and electronic formats, and translations.
- If figures and/or tables were requested, they may be adapted or used in part.
- Please print this page for your records and send a copy of it to your publisher/graduate school.
- Appropriate credit for the requested material should be given as follows: "Reprinted (adapted) with permission from {COMPLETE REFERENCE CITATION}. Copyright {YEAR} American Chemical Society." Insert appropriate information in place of the capitalized words.
- One-time permission is granted only for the use specified in your RightsLink request. No additional uses are granted (such as derivative works or other editions). For any uses, please submit a new request.
If credit is given to another source for the material you requested from RightsLink, permission must be obtained from that source.
BACK
CLOSE WINDOW

Figure 1.3b

SPRINGER NATURE LICENSE
TERMS AND CONDITIONS

May 29, 2025

---

This Agreement between Vanshika Jain ("You") and Springer Nature ("Springer Nature") consists of your license details and the terms and conditions provided by Springer Nature and Copyright Clearance Center.

| | |
|---|---|
| License Number | 6038200305577 |
| License date | May 29, 2025 |
| Licensed Content Publisher | Springer Nature |
| Licensed Content Publication | Nature Catalysis |
| Licensed Content Title | Photocatalytic uphill conversion of natural gas beyond the limitation of thermal reaction systems |
| Licensed Content Author | Shusaku Shoji et al |
| Licensed Content Date | Jan 27, 2020 |
| Type of Use | Thesis/Dissertation |
| Requestor type | academic/university or research institute |
| Format | print and electronic |
| Portion | figures/tables/illustrations |
| Number of figures/tables/ illustrations | 1 |

| | |
|---|---|
| Would you like a high resolution image with your order? | no |
| Will you be translating? | no |
| Circulation/distribution | 1 - 29 |
| Author of this Springer Nature content | no |
| Title of new work | Light-Driven Multielectron Chemical Transformations with Tailored Nanoparticles |
| Institution name | Indian Institute of Science Education and Research (IISER) Pune |
| Expected presentation date | Jun 2025 |
| Portions | Figure 2 |
| The Requesting Person / Organization to Appear on the License | Vanshika Jain |
| Requestor Location | Ms. Vanshika Jain<br>Department of Chemistry, IISER Pune<br><br>Pune, 411008<br>India |
| Billing Type | Invoice |
| Billing Address | Ms. Vanshika Jain<br>Department of Chemistry, IISER Pune<br><br>Pune, India 411008 |
| Total | 0.00 USD |

Terms and Conditions

**Springer Nature Customer Service Centre GmbH Terms and Conditions**

The following terms and conditions ("Terms and Conditions") together with the terms specified in your [RightsLink] constitute the License ("License") between you as Licensee and Springer Nature Customer Service Centre GmbH as Licensor. By clicking 'accept' and completing the transaction for your use of the material ("Licensed Material"), you confirm your acceptance of and obligation to be bound by these Terms and Conditions.

**1. Grant and Scope of License**

1. 1. The Licensor grants you a personal, non-exclusive, non-transferable, non-sublicensable, revocable, world-wide License to reproduce, distribute, communicate to the public, make available, broadcast, electronically transmit or create derivative works using the Licensed Material for the purpose(s) specified in your RightsLink Licence Details only. Licenses are granted for the specific use requested in the order and for no other use, subject to these Terms and Conditions. You acknowledge and agree that the rights granted to you under this License do not include the right to modify, edit, translate, include in collective works, or create derivative works of the Licensed Material in whole or in part unless expressly stated in your RightsLink Licence Details. You may use the Licensed Material only as permitted under this Agreement and will not reproduce, distribute, display, perform, or otherwise use or exploit any Licensed Material in any way, in whole or in part, except as expressly permitted by this License.

1. 2. You may only use the Licensed Content in the manner and to the extent permitted by these Terms and Conditions, by your RightsLink Licence Details and by any applicable laws.

1. 3. A separate license may be required for any additional use of the Licensed Material, e.g. where a license has been purchased for print use only, separate permission must be obtained for electronic re-use. Similarly, a License is only valid in the language selected and does not apply for editions in other languages unless additional translation rights have been granted separately in the License.

1. 4. Any content within the Licensed Material that is owned by third parties is expressly excluded from the License.

1. 5. Rights for additional reuses such as custom editions, computer/mobile applications, film or TV reuses and/or any other derivative rights requests require additional permission and may be subject to an additional fee. Please apply to journalpermissions@springernature.com or bookpermissions@springernature.com for these rights.

**2. Reservation of Rights**

Licensor reserves all rights not expressly granted to you under this License. You acknowledge and agree that nothing in this License limits or restricts Licensor's rights in or use of the Licensed Material in any way. Neither this License, nor any act, omission, or statement by Licensor or you, conveys any ownership right to you in any Licensed Material, or to any element or portion thereof. As between Licensor and you,

Licensor owns and retains all right, title, and interest in and to the Licensed Material subject to the license granted in Section 1.1. Your permission to use the Licensed Material is expressly conditioned on you not impairing Licensor's or the applicable copyright owner's rights in the Licensed Material in any way.

**3. Restrictions on use**

3. 1. Minor editing privileges are allowed for adaptations for stylistic purposes or formatting purposes provided such alterations do not alter the original meaning or intention of the Licensed Material and the new figure(s) are still accurate and representative of the Licensed Material. Any other changes including but not limited to, cropping, adapting, and/or omitting material that affect the meaning, intention or moral rights of the author(s) are strictly prohibited.

3. 2. You must not use any Licensed Material as part of any design or trademark.

3. 3. Licensed Material may be used in Open Access Publications (OAP), but any such reuse must include a clear acknowledgment of this permission visible at the same time as the figures/tables/illustration or abstract and which must indicate that the Licensed Material is not part of the governing OA license but has been reproduced with permission. This may be indicated according to any standard referencing system but must include at a minimum 'Book/Journal title, Author, Journal Name (if applicable), Volume (if applicable), Publisher, Year, reproduced with permission from SNCSC'.

**4. STM Permission Guidelines**

4. 1. An alternative scope of license may apply to signatories of the STM Permissions Guidelines ("STM PG") as amended from time to time and made available at https://www.stm-assoc.org/intellectual-property/permissions/permissions-guidelines/.

4. 2. For content reuse requests that qualify for permission under the STM PG, and which may be updated from time to time, the STM PG supersede the terms and conditions contained in this License.

4. 3. If a License has been granted under the STM PG, but the STM PG no longer apply at the time of publication, further permission must be sought from the Rightsholder. Contact journalpermissions@springernature.com or bookpermissions@springernature.com for these rights.

**5. Duration of License**

5. 1. Unless otherwise indicated on your License, a License is valid from the date of purchase ("License Date") until the end of the relevant period in the below table:

| | |
|---|---|
| Reuse in a medical communications project | Reuse up to distribution or time period indicated in License |
| Reuse in a dissertation/ thesis | Lifetime of thesis |
| Reuse in a journal/ magazine | Lifetime of journal/magazine |
| Reuse in a book/ textbook | Lifetime of edition |

| | |
|---|---|
| Reuse on a website | 1 year unless otherwise specified in the License |
| Reuse in a presentation/ slide kit/poster | Lifetime of presentation/slide kit/poster. Note: publication whether electronic or in print of presentation/slide kit/poster may require further permission. |
| Reuse in conference proceedings | Lifetime of conference proceedings |
| Reuse in an annual report | Lifetime of annual report |
| Reuse in training/CME materials | Reuse up to distribution or time period indicated in License |
| Reuse in newsmedia | Lifetime of newsmedia |
| Reuse in coursepack/ classroom materials | Reuse up to distribution and/or time period indicated in license |

**6. Acknowledgement**

6. 1. The Licensor's permission must be acknowledged next to the Licensed Material in print. In electronic form, this acknowledgement must be visible at the same time as the figures/tables/illustrations or abstract and must be hyperlinked to the journal/book's homepage.

6. 2. Acknowledgement may be provided according to any standard referencing system and at a minimum should include "Author, Article/Book Title, Journal name/Book imprint, volume, page number, year, Springer Nature".

**7. Reuse in a dissertation or thesis**

7. 1. Where 'reuse in a dissertation/thesis' has been selected, the following terms apply: Print rights of the Version of Record are provided for; electronic rights for use only on institutional repository as defined by the Sherpa guideline (www.sherpa.ac.uk/romeo/) and only up to what is required by the awarding institution.

7. 2. For theses published under an ISBN or ISSN, separate permission is required. Please contact journalpermissions@springernature.com or bookpermissions@springernature.com for these rights.

7. 3. Authors must properly cite the published manuscript in their thesis according to current citation standards and include the following acknowledgement: '*Reproduced with permission from Springer Nature*'.

**8. License Fee**

You must pay the fee set forth in the License Agreement (the "License Fees"). All amounts payable by you under this License are exclusive of any sales, use, withholding, value added or similar taxes, government fees or levies or other assessments. Collection and/or remittance of such taxes to the relevant tax authority shall be the responsibility of the party who has the legal obligation to do so.

**9. Warranty**

9. 1. The Licensor warrants that it has, to the best of its knowledge, the rights to license reuse of the Licensed Material. **You are solely responsible for ensuring**

**that the material you wish to license is original to the Licensor and does not carry the copyright of another entity or third party (as credited in the published version).** If the credit line on any part of the Licensed Material indicates that it was reprinted or adapted with permission from another source, then you should seek additional permission from that source to reuse the material.

9. 2. EXCEPT FOR THE EXPRESS WARRANTY STATED HEREIN AND TO THE EXTENT PERMITTED BY APPLICABLE LAW, LICENSOR PROVIDES THE LICENSED MATERIAL "AS IS" AND MAKES NO OTHER REPRESENTATION OR WARRANTY. LICENSOR EXPRESSLY DISCLAIMS ANY LIABILITY FOR ANY CLAIM ARISING FROM OR OUT OF THE CONTENT, INCLUDING BUT NOT LIMITED TO ANY ERRORS, INACCURACIES, OMISSIONS, OR DEFECTS CONTAINED THEREIN, AND ANY IMPLIED OR EXPRESS WARRANTY AS TO MERCHANTABILITY OR FITNESS FOR A PARTICULAR PURPOSE. IN NO EVENT SHALL LICENSOR BE LIABLE TO YOU OR ANY OTHER PARTY OR ANY OTHER PERSON OR FOR ANY SPECIAL, CONSEQUENTIAL, INCIDENTAL, INDIRECT, PUNITIVE, OR EXEMPLARY DAMAGES, HOWEVER CAUSED, ARISING OUT OF OR IN CONNECTION WITH THE DOWNLOADING, VIEWING OR USE OF THE LICENSED MATERIAL REGARDLESS OF THE FORM OF ACTION, WHETHER FOR BREACH OF CONTRACT, BREACH OF WARRANTY, TORT, NEGLIGENCE, INFRINGEMENT OR OTHERWISE (INCLUDING, WITHOUT LIMITATION, DAMAGES BASED ON LOSS OF PROFITS, DATA, FILES, USE, BUSINESS OPPORTUNITY OR CLAIMS OF THIRD PARTIES), AND WHETHER OR NOT THE PARTY HAS BEEN ADVISED OF THE POSSIBILITY OF SUCH DAMAGES. THIS LIMITATION APPLIES NOTWITHSTANDING ANY FAILURE OF ESSENTIAL PURPOSE OF ANY LIMITED REMEDY PROVIDED HEREIN.

**10. Termination and Cancellation**

10. 1. The License and all rights granted hereunder will continue until the end of the applicable period shown in Clause 5.1 above. Thereafter, this license will be terminated and all rights granted hereunder will cease.

10. 2. Licensor reserves the right to terminate the License in the event that payment is not received in full or if you breach the terms of this License.

**11. General**

11. 1. The License and the rights and obligations of the parties hereto shall be construed, interpreted and determined in accordance with the laws of the Federal Republic of Germany without reference to the stipulations of the CISG (United Nations Convention on Contracts for the International Sale of Goods) or to Germany´s choice-of-law principle.

11. 2. The parties acknowledge and agree that any controversies and disputes arising out of this License shall be decided exclusively by the courts of or having jurisdiction for Heidelberg, Germany, as far as legally permissible.

11. 3. This License is solely for Licensor's and Licensee's benefit. It is not for the benefit of any other person or entity.

**Questions?** For questions on Copyright Clearance Center accounts or website issues

please contact springernaturesupport@copyright.com or +1-855-239-3415 (toll free in the US) or +1-978-646-2777. For questions on Springer Nature licensing please visit https://www.springernature.com/gp/partners/rights-permissions-third-party-distribution

**Other Conditions**:

Version 1.4 - Dec 2022

**Questions? customercare@copyright.com.**

Figure 1.3c

IISER PUNE

**Vanshika Jain <jain.vanshika@students.iiserpune.ac.in>**

# RE: THESIS/DISSERTATION USE – SCIENCE FIGURE – KIM ET AL 2024 DOI: 10.1126/science.adq6245

1 message

**Dana James** <djames@aaas.org> Tue, Jun 3, 2025 at 8:19 PM
To: "jain.vanshika@students.iiserpune.ac.in" <jain.vanshika@students.iiserpune.ac.in>
Cc: permissions <permissions@aaas.org>

**AAAS MATERIAL:**

Figure 2 (a, b) from Kim et al., *SCIENCE,* 3 Oct 2024

Vol 386, Issue 6717, pp. 99-105, DOI: 10.1126/science.adq6245

**YOUR RE-USE: THESIS/DISSERTATION**

Title: Light-Driven Multielectron Chemical Transformations with Tailored Nanoparticles

Publication date: July 2025

Dear Vanshika:

Thank you very much for your interest in the AAAS material identified in your request.

We are pleased to have you include this material in your thesis or dissertation subject to the following guidelines. These guidelines also appear on our website: https://www.science.org/content/page/reprints-and-permissions under the heading 'Using AAAS material in a thesis or dissertation'.

**REPRODUCING AAAS MATERIAL IN YOUR THESIS OR DISSERTATION**

AAAS permits the use of content published in its journals but only provided the following criteria are met:

1. If you are using figures/tables, permission is granted for use in print and electronic versions of your dissertation or thesis.

2. A full text article may be used only in print versions of a dissertation or thesis. AAAS does not permit the reproduction of full text articles in electronic versions of theses or dissertations.

3. The following credit line must be printed along with the AAAS material: "From [Insert Full Reference Citation]/ Reprinted with permission from AAAS".

4. All required credit lines and notices must be visible any time a user accesses any part of the AAAS material and must appear on any printed copies that an authorized user might make.

5. The AAAS material may not be modified or altered except that figures and tables may be modified with permission from the author. Author permission for any such changes must be secured prior to your use.

6. AAAS must publish the full paper prior to your use of any of its text or figures.

7. If the AAAS material covered by this permission was published in *Science* during the years 1974-1994, you must also obtain permission from the author, who may grant or withhold permission, and who may or may not charge a fee if permission is granted. See original article for author's address. This condition does not apply to the news articles published in *Science*.

8. Permission covers the distribution of your dissertation or thesis on demand by a third party distributor (eg ProQuest/UMI), provided the AAAS material covered by this permission remains in situ and is not distributed by that third party outside of the context of your thesis/dissertation.

9. Permission does not apply to figures/photos/artwork or any other content or material included in your work that are credited to non-AAAS sources. If the requested material is sourced to or references non-AAAS sources, you must obtain authorization from that source as well before using that material. You agree to hold harmless and indemnify AAAS against any claims arising from your use of any content in your work that is credited to non-AAAS sources.

10. By using the AAAS Material identified in your request, you agree to abide by all the terms & conditions herein.

11. AAAS makes no representations or warranties as to the accuracy of any information contained in the AAAS material covered by this permission, including any warranties of merchantability or fitness for a particular purpose.

If how you wish to use the content falls outside of these guidelines or if you have any questions, please let me know.

Kind regards,

Dana James

AAAS
AMERICAN ASSOCIATION FOR THE ADVANCEMENT OF SCIENCE

**Dana James** *(she/her)*
Rights and Licensing Coordinator, Office of Publishing
**American Association for the Advancement of Science**
1200 New York Avenue, NW | Washington, DC 20005
| djames@aaas.org | www.aaas.org | www.science.org

---

**From:** Vanshika Jain <jain.vanshika@students.iiserpune.ac.in>
**Sent:** Friday, May 30, 2025 3:13 AM
**To:** permissions <permissions@aaas.org>
**Subject:** Request for permission for figure reuse in PhD Thesis

[EXTERNAL EMAIL]

Dear AAAS Publications Team

We would like to get the copyright permission for the following article from Science.

The following are the details:

1. AAAS publication title (journal title or website name/URL): https://www.science.org/doi/10.1126/science.adq6245

2. Article title: Photocatalytic furan-to-pyrrole conversion
3. Authors' names: Donghyeon Kim, Jaehyun You, [Da%20Hye%20Lee]Da Hye Lee, Hojin Hong, Dongwook Kim , and Yoonsu Park
4. Volume number, issue date, page numbers, DOI (provide all that apply): Vol 386, Issue 6717, page no. 99-105, DOI: 10.1126/science.adq624
5. Specific figure numbers or portion of text (or supply a copy): Figure 2a and b

**Information about your publication/project:**

1. Type of work in which AAAS material will be used (e.g., book, journal, newsletter, poster, etc.): PhD Thesis/dissertation
2. Title of that work (the book/journal/newsletter, etc. in which you are reproducing the AAAS material): Light-Driven Multielectron Chemical Transformations with Tailored Nanoparticles
3. Title of the specific article/chapter in which you are reproducing the AAAS material (if applicable): Introduction to Photocatalysis with Designer Metal Nanoparticles and Quantum Dots
4. Author(s)/editor(s): Vanshika Jain
5. Expected publication date (or volume and issue number for journals): July 2025
6. Publishing company: Indian Institute of Science Education and Research Pune, India
7. Retail price (for books only)the – N/A
8. The formats your work will be distributed in (e.g., print, electronic, print and electronic): Print and electronic
9. The rights you are seeking: To reuse figure in the introduction chapter of my PhD thesis.

Please give us the required permission to re-use these images.

Thank you

--
Best regards,

Vanshika Jain | Ph.D. Student
Prof. Pramod Pillai Group
Department of Chemistry | IISER Pune
http://www.iiserpune.ac.in/~pramod/

## Figure 1.5a-d

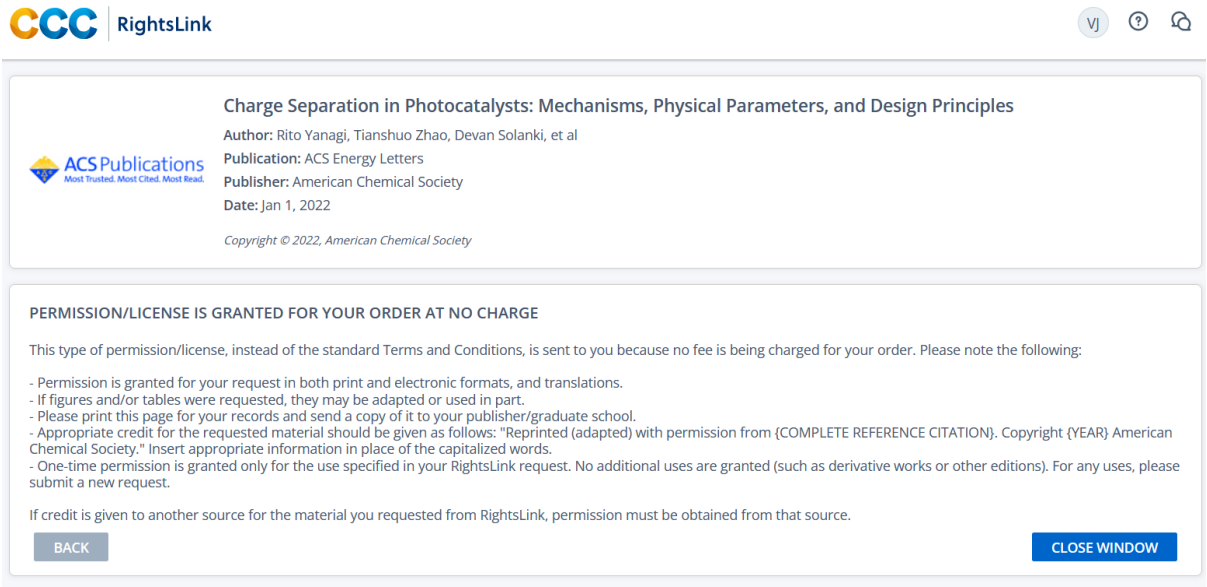
RightsLink
VJ
Charge Separation in Photocatalysts: Mechanisms, Physical Parameters, and Design Principles
Author: Rito Yanagi, Tianshuo Zhao, Devan Solanki, et al
Publication: ACS Energy Letters
Publisher: American Chemical Society
Date: Jan 1, 2022
Copyright © 2022, American Chemical Society
ACS Publications
Most Trusted. Most Cited. Most Read.
PERMISSION/LICENSE IS GRANTED FOR YOUR ORDER AT NO CHARGE
This type of permission/license, instead of the standard Terms and Conditions, is sent to you because no fee is being charged for your order. Please note the following:
- Permission is granted for your request in both print and electronic formats, and translations.
- If figures and/or tables were requested, they may be adapted or used in part.
- Please print this page for your records and send a copy of it to your publisher/graduate school.
- Appropriate credit for the requested material should be given as follows: "Reprinted (adapted) with permission from {COMPLETE REFERENCE CITATION}. Copyright {YEAR} American Chemical Society." Insert appropriate information in place of the capitalized words.
- One-time permission is granted only for the use specified in your RightsLink request. No additional uses are granted (such as derivative works or other editions). For any uses, please submit a new request.
If credit is given to another source for the material you requested from RightsLink, permission must be obtained from that source.
BACK
CLOSE WINDOW

**Figure 1.5 e**

## You are free to:

**Share** — copy and redistribute the material in any medium or format for any purpose, even commercially.

**Adapt** — remix, transform, and build upon the material for any purpose, even commercially.

The licensor cannot revoke these freedoms as long as you follow the license terms.

## Under the following terms:

**Attribution** — You must give appropriate credit , provide a link to the license, and indicate if changes were made . You may do so in any reasonable manner, but not in any way that suggests the licensor endorses you or your use.

# Figure 1.6 a,b

SPRINGER NATURE LICENSE
TERMS AND CONDITIONS

May 29, 2025

---

This Agreement between Vanshika Jain ("You") and Springer Nature ("Springer Nature") consists of your license details and the terms and conditions provided by Springer Nature and Copyright Clearance Center.

| | |
|---|---|
| License Number | 6038220237483 |
| License date | May 29, 2025 |
| Licensed Content Publisher | Springer Nature |
| Licensed Content Publication | Nature Catalysis |
| Licensed Content Title | Catalytic conversion of solar to chemical energy on plasmonic metal nanostructures |
| Licensed Content Author | Umar Aslam et al |
| Licensed Content Date | Sep 12, 2018 |
| Type of Use | Thesis/Dissertation |
| Requestor type | academic/university or research institute |
| Format | print and electronic |
| Portion | figures/tables/illustrations |
| Number of figures/tables/illustrations | 1 |
| Would you like a high resolution image with your order? | no |

| | |
|---|---|
| Will you be translating? | no |
| Circulation/distribution | 1 - 29 |
| Author of this Springer Nature content | no |
| Title of new work | Light-Driven Multielectron Chemical Transformations with Tailored Nanoparticles |
| Institution name | Indian Institute of Science Education and Research (IISER) Pune |
| Expected presentation date | Jun 2025 |
| Portions | Figure1a,b |
| The Requesting Person / Organization to Appear on the License | Vanshika Jain |
| Requestor Location | Ms. Vanshika Jain<br>Department of Chemistry, IISER Pune<br><br>Pune, 411008<br>India |
| Billing Type | Invoice |
| Billing Address | Ms. Vanshika Jain<br>Department of Chemistry, IISER Pune<br><br>Pune, India 411008 |
| Total | 0.00 USD |

Terms and Conditions

**Springer Nature Customer Service Centre GmbH Terms and Conditions**

The following terms and conditions ("Terms and Conditions") together with the terms specified in your [RightsLink] constitute the License ("License") between you as

Licensee and Springer Nature Customer Service Centre GmbH as Licensor. By clicking 'accept' and completing the transaction for your use of the material ("Licensed Material"), you confirm your acceptance of and obligation to be bound by these Terms and Conditions.

**1. Grant and Scope of License**

1. 1. The Licensor grants you a personal, non-exclusive, non-transferable, non-sublicensable, revocable, world-wide License to reproduce, distribute, communicate to the public, make available, broadcast, electronically transmit or create derivative works using the Licensed Material for the purpose(s) specified in your RightsLink Licence Details only. Licenses are granted for the specific use requested in the order and for no other use, subject to these Terms and Conditions. You acknowledge and agree that the rights granted to you under this License do not include the right to modify, edit, translate, include in collective works, or create derivative works of the Licensed Material in whole or in part unless expressly stated in your RightsLink Licence Details. You may use the Licensed Material only as permitted under this Agreement and will not reproduce, distribute, display, perform, or otherwise use or exploit any Licensed Material in any way, in whole or in part, except as expressly permitted by this License.

1. 2. You may only use the Licensed Content in the manner and to the extent permitted by these Terms and Conditions, by your RightsLink Licence Details and by any applicable laws.

1. 3. A separate license may be required for any additional use of the Licensed Material, e.g. where a license has been purchased for print use only, separate permission must be obtained for electronic re-use. Similarly, a License is only valid in the language selected and does not apply for editions in other languages unless additional translation rights have been granted separately in the License.

1. 4. Any content within the Licensed Material that is owned by third parties is expressly excluded from the License.

1. 5. Rights for additional reuses such as custom editions, computer/mobile applications, film or TV reuses and/or any other derivative rights requests require additional permission and may be subject to an additional fee. Please apply to journalpermissions@springernature.com or bookpermissions@springernature.com for these rights.

**2. Reservation of Rights**

Licensor reserves all rights not expressly granted to you under this License. You acknowledge and agree that nothing in this License limits or restricts Licensor's rights in or use of the Licensed Material in any way. Neither this License, nor any act, omission, or statement by Licensor or you, conveys any ownership right to you in any Licensed Material, or to any element or portion thereof. As between Licensor and you, Licensor owns and retains all right, title, and interest in and to the Licensed Material subject to the license granted in Section 1.1. Your permission to use the Licensed Material is expressly conditioned on you not impairing Licensor's or the applicable copyright owner's rights in the Licensed Material in any way.

**3. Restrictions on use**

3. 1. Minor editing privileges are allowed for adaptations for stylistic purposes or

formatting purposes provided such alterations do not alter the original meaning or intention of the Licensed Material and the new figure(s) are still accurate and representative of the Licensed Material. Any other changes including but not limited to, cropping, adapting, and/or omitting material that affect the meaning, intention or moral rights of the author(s) are strictly prohibited.

3. 2. You must not use any Licensed Material as part of any design or trademark.

3. 3. Licensed Material may be used in Open Access Publications (OAP), but any such reuse must include a clear acknowledgment of this permission visible at the same time as the figures/tables/illustration or abstract and which must indicate that the Licensed Material is not part of the governing OA license but has been reproduced with permission. This may be indicated according to any standard referencing system but must include at a minimum 'Book/Journal title, Author, Journal Name (if applicable), Volume (if applicable), Publisher, Year, reproduced with permission from SNCSC'.

**4. STM Permission Guidelines**

4. 1. An alternative scope of license may apply to signatories of the STM Permissions Guidelines ("STM PG") as amended from time to time and made available at https://www.stm-assoc.org/intellectual-property/permissions/permissions-guidelines/.

4. 2. For content reuse requests that qualify for permission under the STM PG, and which may be updated from time to time, the STM PG supersede the terms and conditions contained in this License.

4. 3. If a License has been granted under the STM PG, but the STM PG no longer apply at the time of publication, further permission must be sought from the Rightsholder. Contact journalpermissions@springernature.com or bookpermissions@springernature.com for these rights.

**5. Duration of License**

5. 1. Unless otherwise indicated on your License, a License is valid from the date of purchase ("License Date") until the end of the relevant period in the below table:

| | |
|---|---|
| Reuse in a medical communications project | Reuse up to distribution or time period indicated in License |
| Reuse in a dissertation/ thesis | Lifetime of thesis |
| Reuse in a journal/ magazine | Lifetime of journal/magazine |
| Reuse in a book/ textbook | Lifetime of edition |
| Reuse on a website | 1 year unless otherwise specified in the License |
| Reuse in a presentation/ slide kit/poster | Lifetime of presentation/slide kit/poster. Note: publication whether electronic or in print of presentation/slide kit/poster may require further permission. |
| Reuse in conference proceedings | Lifetime of conference proceedings |

| | |
|---|---|
| Reuse in an annual report | Lifetime of annual report |
| Reuse in training/CME materials | Reuse up to distribution or time period indicated in License |
| Reuse in newsmedia | Lifetime of newsmedia |
| Reuse in coursepack/ classroom materials | Reuse up to distribution and/or time period indicated in license |

**6. Acknowledgement**

6. 1. The Licensor's permission must be acknowledged next to the Licensed Material in print. In electronic form, this acknowledgement must be visible at the same time as the figures/tables/illustrations or abstract and must be hyperlinked to the journal/book's homepage.

6. 2. Acknowledgement may be provided according to any standard referencing system and at a minimum should include "Author, Article/Book Title, Journal name/Book imprint, volume, page number, year, Springer Nature".

**7. Reuse in a dissertation or thesis**

7. 1. Where 'reuse in a dissertation/thesis' has been selected, the following terms apply: Print rights of the Version of Record are provided for; electronic rights for use only on institutional repository as defined by the Sherpa guideline (www.sherpa.ac.uk/romeo/) and only up to what is required by the awarding institution.

7. 2. For theses published under an ISBN or ISSN, separate permission is required. Please contact journalpermissions@springernature.com or bookpermissions@springernature.com for these rights.

7. 3. Authors must properly cite the published manuscript in their thesis according to current citation standards and include the following acknowledgement: '*Reproduced with permission from Springer Nature*'.

**8. License Fee**

You must pay the fee set forth in the License Agreement (the "License Fees"). All amounts payable by you under this License are exclusive of any sales, use, withholding, value added or similar taxes, government fees or levies or other assessments. Collection and/or remittance of such taxes to the relevant tax authority shall be the responsibility of the party who has the legal obligation to do so.

**9. Warranty**

9. 1. The Licensor warrants that it has, to the best of its knowledge, the rights to license reuse of the Licensed Material. **You are solely responsible for ensuring that the material you wish to license is original to the Licensor and does not carry the copyright of another entity or third party (as credited in the published version).** If the credit line on any part of the Licensed Material indicates that it was reprinted or adapted with permission from another source, then you should seek additional permission from that source to reuse the material.

9. 2. EXCEPT FOR THE EXPRESS WARRANTY STATED HEREIN AND TO

THE EXTENT PERMITTED BY APPLICABLE LAW, LICENSOR PROVIDES THE LICENSED MATERIAL "AS IS" AND MAKES NO OTHER REPRESENTATION OR WARRANTY. LICENSOR EXPRESSLY DISCLAIMS ANY LIABILITY FOR ANY CLAIM ARISING FROM OR OUT OF THE CONTENT, INCLUDING BUT NOT LIMITED TO ANY ERRORS, INACCURACIES, OMISSIONS, OR DEFECTS CONTAINED THEREIN, AND ANY IMPLIED OR EXPRESS WARRANTY AS TO MERCHANTABILITY OR FITNESS FOR A PARTICULAR PURPOSE. IN NO EVENT SHALL LICENSOR BE LIABLE TO YOU OR ANY OTHER PARTY OR ANY OTHER PERSON OR FOR ANY SPECIAL, CONSEQUENTIAL, INCIDENTAL, INDIRECT, PUNITIVE, OR EXEMPLARY DAMAGES, HOWEVER CAUSED, ARISING OUT OF OR IN CONNECTION WITH THE DOWNLOADING, VIEWING OR USE OF THE LICENSED MATERIAL REGARDLESS OF THE FORM OF ACTION, WHETHER FOR BREACH OF CONTRACT, BREACH OF WARRANTY, TORT, NEGLIGENCE, INFRINGEMENT OR OTHERWISE (INCLUDING, WITHOUT LIMITATION, DAMAGES BASED ON LOSS OF PROFITS, DATA, FILES, USE, BUSINESS OPPORTUNITY OR CLAIMS OF THIRD PARTIES), AND WHETHER OR NOT THE PARTY HAS BEEN ADVISED OF THE POSSIBILITY OF SUCH DAMAGES. THIS LIMITATION APPLIES NOTWITHSTANDING ANY FAILURE OF ESSENTIAL PURPOSE OF ANY LIMITED REMEDY PROVIDED HEREIN.

**10. Termination and Cancellation**

10. 1. The License and all rights granted hereunder will continue until the end of the applicable period shown in Clause 5.1 above. Thereafter, this license will be terminated and all rights granted hereunder will cease.

10. 2. Licensor reserves the right to terminate the License in the event that payment is not received in full or if you breach the terms of this License.

**11. General**

11. 1. The License and the rights and obligations of the parties hereto shall be construed, interpreted and determined in accordance with the laws of the Federal Republic of Germany without reference to the stipulations of the CISG (United Nations Convention on Contracts for the International Sale of Goods) or to Germany´s choice-of-law principle.

11. 2. The parties acknowledge and agree that any controversies and disputes arising out of this License shall be decided exclusively by the courts of or having jurisdiction for Heidelberg, Germany, as far as legally permissible.

11. 3. This License is solely for Licensor's and Licensee's benefit. It is not for the benefit of any other person or entity.

**Questions?** For questions on Copyright Clearance Center accounts or website issues please contact springernaturesupport@copyright.com or +1-855-239-3415 (toll free in the US) or +1-978-646-2777. For questions on Springer Nature licensing please visit https://www.springernature.com/gp/partners/rights-permissions-third-party-distribution

**Other Conditions**:

Version 1.4 - Dec 2022

**Questions? customercare@copyright.com.**

# Figure 1.6c

JOHN WILEY AND SONS LICENSE
TERMS AND CONDITIONS

May 29, 2025

---

This Agreement between Vanshika Jain ("You") and John Wiley and Sons ("John Wiley and Sons") consists of your license details and the terms and conditions provided by John Wiley and Sons and Copyright Clearance Center.

| | |
|---|---|
| License Number | 6038221499882 |
| License date | May 29, 2025 |
| Licensed Content Publisher | John Wiley and Sons |
| Licensed Content Publication | Wiley Books |
| Licensed Content Title | Theory of Plasmonic Excitations |
| Licensed Content Author | Alexander O. Govorov, Zhiming M. Wang, Xiang-Tian Kong, et al |
| Licensed Content Date | Jun 11, 2021 |
| Licensed Content Pages | 35 |
| Type of use | Dissertation/Thesis |
| Requestor type | University/Academic |
| Format | Print and electronic |
| Portion | Figure/table |
| Number of figures/tables | 1 |

| | |
|---|---|
| Will you be translating? | No |
| Title of new work | Light-Driven Multielectron Chemical Transformations with Tailored Nanoparticles |
| Institution name | Indian Institute of Science Education and Research (IISER) Pune |
| Expected presentation date | Jun 2025 |
| Portions | Figure 1.6c |
| The Requesting Person / Organization to Appear on the License | Vanshika Jain |
| Requestor Location | Ms. Vanshika Jain<br>Department of Chemistry, IISER Pune<br><br>Pune, 411008<br>India |
| Publisher Tax ID | EU826007151 |
| Total | 0.00 USD |

Terms and Conditions

**TERMS AND CONDITIONS**

This copyrighted material is owned by or exclusively licensed to John Wiley & Sons, Inc. or one of its group companies (each a"Wiley Company") or handled on behalf of a society with which a Wiley Company has exclusive publishing rights in relation to a particular work (collectively "WILEY"). By clicking "accept" in connection with completing this licensing transaction, you agree that the following terms and conditions apply to this transaction (along with the billing and payment terms and conditions established by the Copyright Clearance Center Inc., ("CCC's Billing and Payment terms and conditions"), at the time that you opened your RightsLink account (these are available at any time at http://myaccount.copyright.com).

**Terms and Conditions**

- The materials you have requested permission to reproduce or reuse (the "Wiley Materials") are protected by copyright.

- You are hereby granted a personal, non-exclusive, non-sub licensable (on a stand-alone basis), non-transferable, worldwide, limited license to reproduce the Wiley Materials for the purpose specified in the licensing process. This license, **and any CONTENT (PDF or image file) purchased as part of your order,** is for a one-time use only and limited to any maximum distribution number specified in the license. The first instance of republication or reuse granted by this license must be completed within two years of the date of the grant of this license (although copies prepared before the end date may be distributed thereafter). The Wiley Materials shall not be used in any other manner or for any other purpose, beyond what is granted in the license. Permission is granted subject to an appropriate acknowledgement given to the author, title of the material/book/journal and the publisher. You shall also duplicate the copyright notice that appears in the Wiley publication in your use of the Wiley Material. Permission is also granted on the understanding that nowhere in the text is a previously published source acknowledged for all or part of this Wiley Material. Any third party content is expressly excluded from this permission.

- With respect to the Wiley Materials, all rights are reserved. Except as expressly granted by the terms of the license, no part of the Wiley Materials may be copied, modified, adapted (except for minor reformatting required by the new Publication), translated, reproduced, transferred or distributed, in any form or by any means, and no derivative works may be made based on the Wiley Materials without the prior permission of the respective copyright owner.**For STM Signatory Publishers clearing permission under the terms of the STM Permissions Guidelines only, the terms of the license are extended to include subsequent editions and for editions in other languages, provided such editions are for the work as a whole in situ and does not involve the separate exploitation of the permitted figures or extracts,** You may not alter, remove or suppress in any manner any copyright, trademark or other notices displayed by the Wiley Materials. You may not license, rent, sell, loan, lease, pledge, offer as security, transfer or assign the Wiley Materials on a stand-alone basis, or any of the rights granted to you hereunder to any other person.

- The Wiley Materials and all of the intellectual property rights therein shall at all times remain the exclusive property of John Wiley & Sons Inc, the Wiley Companies, or their respective licensors, and your interest therein is only that of having possession of and the right to reproduce the Wiley Materials pursuant to Section 2 herein during the continuance of this Agreement. You agree that you own no right, title or interest in or to the Wiley Materials or any of the intellectual property rights therein. You shall have no rights hereunder other than the license as provided for above in Section 2. No right, license or interest to any trademark, trade name, service mark or other branding ("Marks") of WILEY or its licensors is granted hereunder, and you agree that you shall not assert any such right, license or interest with respect thereto

- NEITHER WILEY NOR ITS LICENSORS MAKES ANY WARRANTY OR REPRESENTATION OF ANY KIND TO YOU OR ANY THIRD PARTY, EXPRESS, IMPLIED OR STATUTORY, WITH RESPECT TO THE MATERIALS OR THE ACCURACY OF ANY INFORMATION CONTAINED IN THE MATERIALS, INCLUDING, WITHOUT LIMITATION, ANY IMPLIED WARRANTY OF MERCHANTABILITY, ACCURACY, SATISFACTORY QUALITY, FITNESS FOR A PARTICULAR PURPOSE, USABILITY, INTEGRATION OR NON-INFRINGEMENT AND ALL SUCH WARRANTIES

ARE HEREBY EXCLUDED BY WILEY AND ITS LICENSORS AND WAIVED BY YOU.

- WILEY shall have the right to terminate this Agreement immediately upon breach of this Agreement by you.

- You shall indemnify, defend and hold harmless WILEY, its Licensors and their respective directors, officers, agents and employees, from and against any actual or threatened claims, demands, causes of action or proceedings arising from any breach of this Agreement by you.

- IN NO EVENT SHALL WILEY OR ITS LICENSORS BE LIABLE TO YOU OR ANY OTHER PARTY OR ANY OTHER PERSON OR ENTITY FOR ANY SPECIAL, CONSEQUENTIAL, INCIDENTAL, INDIRECT, EXEMPLARY OR PUNITIVE DAMAGES, HOWEVER CAUSED, ARISING OUT OF OR IN CONNECTION WITH THE DOWNLOADING, PROVISIONING, VIEWING OR USE OF THE MATERIALS REGARDLESS OF THE FORM OF ACTION, WHETHER FOR BREACH OF CONTRACT, BREACH OF WARRANTY, TORT, NEGLIGENCE, INFRINGEMENT OR OTHERWISE (INCLUDING, WITHOUT LIMITATION, DAMAGES BASED ON LOSS OF PROFITS, DATA, FILES, USE, BUSINESS OPPORTUNITY OR CLAIMS OF THIRD PARTIES), AND WHETHER OR NOT THE PARTY HAS BEEN ADVISED OF THE POSSIBILITY OF SUCH DAMAGES. THIS LIMITATION SHALL APPLY NOTWITHSTANDING ANY FAILURE OF ESSENTIAL PURPOSE OF ANY LIMITED REMEDY PROVIDED HEREIN.

- Should any provision of this Agreement be held by a court of competent jurisdiction to be illegal, invalid, or unenforceable, that provision shall be deemed amended to achieve as nearly as possible the same economic effect as the original provision, and the legality, validity and enforceability of the remaining provisions of this Agreement shall not be affected or impaired thereby.

- The failure of either party to enforce any term or condition of this Agreement shall not constitute a waiver of either party's right to enforce each and every term and condition of this Agreement. No breach under this agreement shall be deemed waived or excused by either party unless such waiver or consent is in writing signed by the party granting such waiver or consent. The waiver by or consent of a party to a breach of any provision of this Agreement shall not operate or be construed as a waiver of or consent to any other or subsequent breach by such other party.

- This Agreement may not be assigned (including by operation of law or otherwise) by you without WILEY's prior written consent.

- Any fee required for this permission shall be non-refundable after thirty (30) days from receipt by the CCC.

- These terms and conditions together with CCC's Billing and Payment terms and conditions (which are incorporated herein) form the entire agreement between you and WILEY concerning this licensing transaction and (in the absence of fraud) supersedes all prior agreements and representations of the parties, oral or written. This Agreement may not be amended except in writing signed by both parties. This Agreement shall be binding upon and inure to the benefit of the parties' successors, legal representatives, and authorized assigns.

- In the event of any conflict between your obligations established by these terms and conditions and those established by CCC's Billing and Payment terms and conditions, these terms and conditions shall prevail.

- WILEY expressly reserves all rights not specifically granted in the combination of (i) the license details provided by you and accepted in the course of this licensing transaction, (ii) these terms and conditions and (iii) CCC's Billing and Payment terms and conditions.

- This Agreement will be void if the Type of Use, Format, Circulation, or Requestor Type was misrepresented during the licensing process.

- This Agreement shall be governed by and construed in accordance with the laws of the State of New York, USA, without regards to such state's conflict of law rules. Any legal action, suit or proceeding arising out of or relating to these Terms and Conditions or the breach thereof shall be instituted in a court of competent jurisdiction in New York County in the State of New York in the United States of America and each party hereby consents and submits to the personal jurisdiction of such court, waives any objection to venue in such court and consents to service of process by registered or certified mail, return receipt requested, at the last known address of such party.

**WILEY OPEN ACCESS TERMS AND CONDITIONS**

Wiley Publishes Open Access Articles in fully Open Access Journals and in Subscription journals offering Online Open. Although most of the fully Open Access journals publish open access articles under the terms of the Creative Commons Attribution (CC BY) License only, the subscription journals and a few of the Open Access Journals offer a choice of Creative Commons Licenses. The license type is clearly identified on the article.

**The Creative Commons Attribution License**

The Creative Commons Attribution License (CC-BY) allows users to copy, distribute and transmit an article, adapt the article and make commercial use of the article. The CC-BY license permits commercial and non-

**Creative Commons Attribution Non-Commercial License**

The Creative Commons Attribution Non-Commercial (CC-BY-NC)License permits use, distribution and reproduction in any medium, provided the original work is properly cited and is not used for commercial purposes.(see below)

**Creative Commons Attribution-Non-Commercial-NoDerivs License**

The Creative Commons Attribution Non-Commercial-NoDerivs License (CC-BY-NC-ND) permits use, distribution and reproduction in any medium, provided the original work is properly cited, is not used for commercial purposes and no modifications or adaptations are made. (see below)

**Use by commercial "for-profit" organizations**

Use of Wiley Open Access articles for commercial, promotional, or marketing purposes requires further explicit permission from Wiley and will be subject to a fee.

Further details can be found on Wiley Online Library http://olabout.wiley.com/WileyCDA/Section/id-410895.html

**Other Terms and Conditions:**

**v1.10 Last updated September 2015**

**Questions? customercare@copyright.com.**

---

Figure 1.7

SPRINGER NATURE LICENSE
TERMS AND CONDITIONS

May 29, 2025

---

This Agreement between Vanshika Jain ("You") and Springer Nature ("Springer Nature") consists of your license details and the terms and conditions provided by Springer Nature and Copyright Clearance Center.

| | |
|---|---|
| License Number | 6038221040563 |
| License date | May 29, 2025 |
| Licensed Content Publisher | Springer Nature |
| Licensed Content Publication | Nature Materials |
| Licensed Content Title | Photochemical transformations on plasmonic metal nanoparticles |
| Licensed Content Author | Suljo Linic et al |
| Licensed Content Date | May 20, 2015 |
| Type of Use | Thesis/Dissertation |
| Requestor type | academic/university or research institute |
| Format | print and electronic |
| Portion | figures/tables/illustrations |
| Number of figures/tables/illustrations | 1 |
| Would you like a high resolution image with your order? | no |

| | |
|---|---|
| Will you be translating? | no |
| Circulation/distribution | 1 - 29 |
| Author of this Springer Nature content | no |
| Title of new work | Light-Driven Multielectron Chemical Transformations with Tailored Nanoparticles |
| Institution name | Indian Institute of Science Education and Research (IISER) Pune |
| Expected presentation date | Jun 2025 |
| Portions | figure 5 |
| The Requesting Person / Organization to Appear on the License | Vanshika Jain |
| Requestor Location | Ms. Vanshika Jain<br>Department of Chemistry, IISER Pune<br><br>Pune, 411008<br>India |
| Billing Type | Invoice |
| Billing Address | Ms. Vanshika Jain<br>Department of Chemistry, IISER Pune<br><br>Pune, India 411008 |
| Total | 0.00 USD |

Terms and Conditions

**Springer Nature Customer Service Centre GmbH Terms and Conditions**

The following terms and conditions ("Terms and Conditions") together with the terms specified in your [RightsLink] constitute the License ("License") between you as

Licensee and Springer Nature Customer Service Centre GmbH as Licensor. By clicking 'accept' and completing the transaction for your use of the material ("Licensed Material"), you confirm your acceptance of and obligation to be bound by these Terms and Conditions.

**1. Grant and Scope of License**

1. 1. The Licensor grants you a personal, non-exclusive, non-transferable, non-sublicensable, revocable, world-wide License to reproduce, distribute, communicate to the public, make available, broadcast, electronically transmit or create derivative works using the Licensed Material for the purpose(s) specified in your RightsLink Licence Details only. Licenses are granted for the specific use requested in the order and for no other use, subject to these Terms and Conditions. You acknowledge and agree that the rights granted to you under this License do not include the right to modify, edit, translate, include in collective works, or create derivative works of the Licensed Material in whole or in part unless expressly stated in your RightsLink Licence Details. You may use the Licensed Material only as permitted under this Agreement and will not reproduce, distribute, display, perform, or otherwise use or exploit any Licensed Material in any way, in whole or in part, except as expressly permitted by this License.

1. 2. You may only use the Licensed Content in the manner and to the extent permitted by these Terms and Conditions, by your RightsLink Licence Details and by any applicable laws.

1. 3. A separate license may be required for any additional use of the Licensed Material, e.g. where a license has been purchased for print use only, separate permission must be obtained for electronic re-use. Similarly, a License is only valid in the language selected and does not apply for editions in other languages unless additional translation rights have been granted separately in the License.

1. 4. Any content within the Licensed Material that is owned by third parties is expressly excluded from the License.

1. 5. Rights for additional reuses such as custom editions, computer/mobile applications, film or TV reuses and/or any other derivative rights requests require additional permission and may be subject to an additional fee. Please apply to journalpermissions@springernature.com or bookpermissions@springernature.com for these rights.

**2. Reservation of Rights**

Licensor reserves all rights not expressly granted to you under this License. You acknowledge and agree that nothing in this License limits or restricts Licensor's rights in or use of the Licensed Material in any way. Neither this License, nor any act, omission, or statement by Licensor or you, conveys any ownership right to you in any Licensed Material, or to any element or portion thereof. As between Licensor and you, Licensor owns and retains all right, title, and interest in and to the Licensed Material subject to the license granted in Section 1.1. Your permission to use the Licensed Material is expressly conditioned on you not impairing Licensor's or the applicable copyright owner's rights in the Licensed Material in any way.

**3. Restrictions on use**

3. 1. Minor editing privileges are allowed for adaptations for stylistic purposes or

formatting purposes provided such alterations do not alter the original meaning or intention of the Licensed Material and the new figure(s) are still accurate and representative of the Licensed Material. Any other changes including but not limited to, cropping, adapting, and/or omitting material that affect the meaning, intention or moral rights of the author(s) are strictly prohibited.

3. 2. You must not use any Licensed Material as part of any design or trademark.

3. 3. Licensed Material may be used in Open Access Publications (OAP), but any such reuse must include a clear acknowledgment of this permission visible at the same time as the figures/tables/illustration or abstract and which must indicate that the Licensed Material is not part of the governing OA license but has been reproduced with permission. This may be indicated according to any standard referencing system but must include at a minimum 'Book/Journal title, Author, Journal Name (if applicable), Volume (if applicable), Publisher, Year, reproduced with permission from SNCSC'.

**4. STM Permission Guidelines**

4. 1. An alternative scope of license may apply to signatories of the STM Permissions Guidelines ("STM PG") as amended from time to time and made available at https://www.stm-assoc.org/intellectual-property/permissions/permissions-guidelines/.

4. 2. For content reuse requests that qualify for permission under the STM PG, and which may be updated from time to time, the STM PG supersede the terms and conditions contained in this License.

4. 3. If a License has been granted under the STM PG, but the STM PG no longer apply at the time of publication, further permission must be sought from the Rightsholder. Contact journalpermissions@springernature.com or bookpermissions@springernature.com for these rights.

**5. Duration of License**

5. 1. Unless otherwise indicated on your License, a License is valid from the date of purchase ("License Date") until the end of the relevant period in the below table:

| | |
|---|---|
| Reuse in a medical communications project | Reuse up to distribution or time period indicated in License |
| Reuse in a dissertation/ thesis | Lifetime of thesis |
| Reuse in a journal/ magazine | Lifetime of journal/magazine |
| Reuse in a book/ textbook | Lifetime of edition |
| Reuse on a website | 1 year unless otherwise specified in the License |
| Reuse in a presentation/ slide kit/poster | Lifetime of presentation/slide kit/poster. Note: publication whether electronic or in print of presentation/slide kit/poster may require further permission. |
| Reuse in conference proceedings | Lifetime of conference proceedings |

| | |
|---|---|
| Reuse in an annual report | Lifetime of annual report |
| Reuse in training/CME materials | Reuse up to distribution or time period indicated in License |
| Reuse in newsmedia | Lifetime of newsmedia |
| Reuse in coursepack/ classroom materials | Reuse up to distribution and/or time period indicated in license |

**6. Acknowledgement**

6. 1. The Licensor's permission must be acknowledged next to the Licensed Material in print. In electronic form, this acknowledgement must be visible at the same time as the figures/tables/illustrations or abstract and must be hyperlinked to the journal/book's homepage.

6. 2. Acknowledgement may be provided according to any standard referencing system and at a minimum should include "Author, Article/Book Title, Journal name/Book imprint, volume, page number, year, Springer Nature".

**7. Reuse in a dissertation or thesis**

7. 1. Where 'reuse in a dissertation/thesis' has been selected, the following terms apply: Print rights of the Version of Record are provided for; electronic rights for use only on institutional repository as defined by the Sherpa guideline (www.sherpa.ac.uk/romeo/) and only up to what is required by the awarding institution.

7. 2. For theses published under an ISBN or ISSN, separate permission is required. Please contact journalpermissions@springernature.com or bookpermissions@springernature.com for these rights.

7. 3. Authors must properly cite the published manuscript in their thesis according to current citation standards and include the following acknowledgement: '*Reproduced with permission from Springer Nature*'.

**8. License Fee**

You must pay the fee set forth in the License Agreement (the "License Fees"). All amounts payable by you under this License are exclusive of any sales, use, withholding, value added or similar taxes, government fees or levies or other assessments. Collection and/or remittance of such taxes to the relevant tax authority shall be the responsibility of the party who has the legal obligation to do so.

**9. Warranty**

9. 1. The Licensor warrants that it has, to the best of its knowledge, the rights to license reuse of the Licensed Material. **You are solely responsible for ensuring that the material you wish to license is original to the Licensor and does not carry the copyright of another entity or third party (as credited in the published version).** If the credit line on any part of the Licensed Material indicates that it was reprinted or adapted with permission from another source, then you should seek additional permission from that source to reuse the material.

9. 2. EXCEPT FOR THE EXPRESS WARRANTY STATED HEREIN AND TO

THE EXTENT PERMITTED BY APPLICABLE LAW, LICENSOR PROVIDES THE LICENSED MATERIAL "AS IS" AND MAKES NO OTHER REPRESENTATION OR WARRANTY. LICENSOR EXPRESSLY DISCLAIMS ANY LIABILITY FOR ANY CLAIM ARISING FROM OR OUT OF THE CONTENT, INCLUDING BUT NOT LIMITED TO ANY ERRORS, INACCURACIES, OMISSIONS, OR DEFECTS CONTAINED THEREIN, AND ANY IMPLIED OR EXPRESS WARRANTY AS TO MERCHANTABILITY OR FITNESS FOR A PARTICULAR PURPOSE. IN NO EVENT SHALL LICENSOR BE LIABLE TO YOU OR ANY OTHER PARTY OR ANY OTHER PERSON OR FOR ANY SPECIAL, CONSEQUENTIAL, INCIDENTAL, INDIRECT, PUNITIVE, OR EXEMPLARY DAMAGES, HOWEVER CAUSED, ARISING OUT OF OR IN CONNECTION WITH THE DOWNLOADING, VIEWING OR USE OF THE LICENSED MATERIAL REGARDLESS OF THE FORM OF ACTION, WHETHER FOR BREACH OF CONTRACT, BREACH OF WARRANTY, TORT, NEGLIGENCE, INFRINGEMENT OR OTHERWISE (INCLUDING, WITHOUT LIMITATION, DAMAGES BASED ON LOSS OF PROFITS, DATA, FILES, USE, BUSINESS OPPORTUNITY OR CLAIMS OF THIRD PARTIES), AND WHETHER OR NOT THE PARTY HAS BEEN ADVISED OF THE POSSIBILITY OF SUCH DAMAGES. THIS LIMITATION APPLIES NOTWITHSTANDING ANY FAILURE OF ESSENTIAL PURPOSE OF ANY LIMITED REMEDY PROVIDED HEREIN.

**10. Termination and Cancellation**

10. 1. The License and all rights granted hereunder will continue until the end of the applicable period shown in Clause 5.1 above. Thereafter, this license will be terminated and all rights granted hereunder will cease.

10. 2. Licensor reserves the right to terminate the License in the event that payment is not received in full or if you breach the terms of this License.

**11. General**

11. 1. The License and the rights and obligations of the parties hereto shall be construed, interpreted and determined in accordance with the laws of the Federal Republic of Germany without reference to the stipulations of the CISG (United Nations Convention on Contracts for the International Sale of Goods) or to Germany´s choice-of-law principle.

11. 2. The parties acknowledge and agree that any controversies and disputes arising out of this License shall be decided exclusively by the courts of or having jurisdiction for Heidelberg, Germany, as far as legally permissible.

11. 3. This License is solely for Licensor's and Licensee's benefit. It is not for the benefit of any other person or entity.

**Questions?** For questions on Copyright Clearance Center accounts or website issues please contact springernaturesupport@copyright.com or +1-855-239-3415 (toll free in the US) or +1-978-646-2777. For questions on Springer Nature licensing please visit https://www.springernature.com/gp/partners/rights-permissions-third-party-distribution

**Other Conditions**:

Version 1.4 - Dec 2022

**Questions? customercare@copyright.com.**

**Figure 1.8**

## You are free to:

**Share** — copy and redistribute the material in any medium or format for any purpose, even commercially.

**Adapt** — remix, transform, and build upon the material for any purpose, even commercially.

The licensor cannot revoke these freedoms as long as you follow the license terms.

## Under the following terms:

**Attribution** — You must give appropriate credit , provide a link to the license, and indicate if changes were made . You may do so in any reasonable manner, but not in any way that suggests the licensor endorses you or your use.

**Figure 1.9**

## You are free to:

**Share** — copy and redistribute the material in any medium or format for any purpose, even commercially.

**Adapt** — remix, transform, and build upon the material for any purpose, even commercially.

The licensor cannot revoke these freedoms as long as you follow the license terms.

## Under the following terms:

**Attribution** — You must give appropriate credit , provide a link to the license, and indicate if changes were made . You may do so in any reasonable manner, but not in any way that suggests the licensor endorses you or your use.

## Chapter 1

Figure 1.10

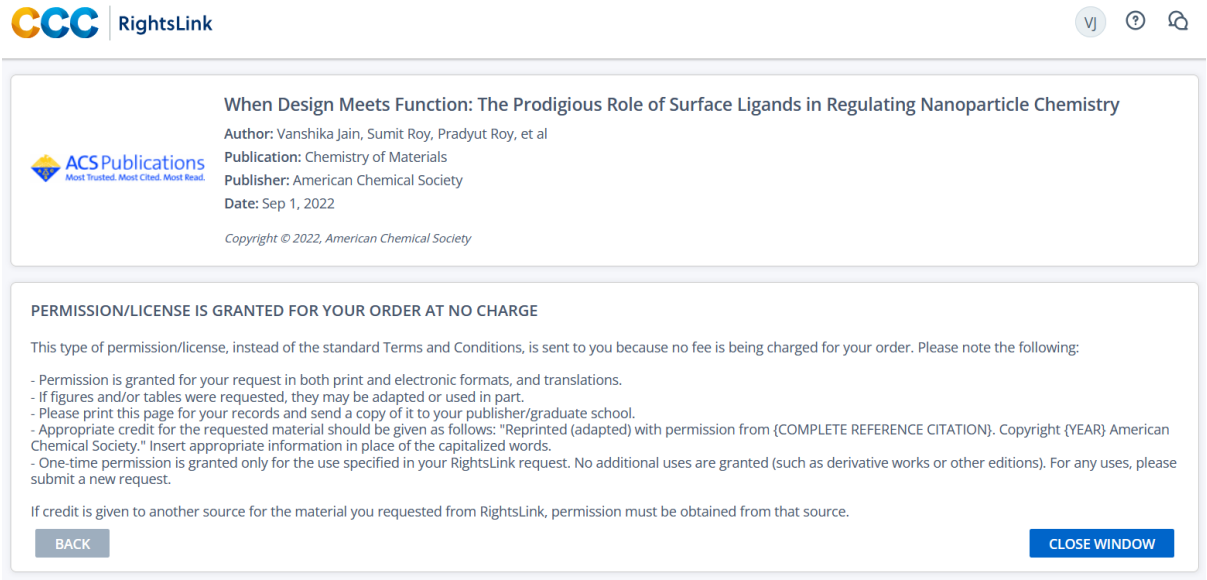

**Figure 1.11a**

# Imidazolium-modification enhances photocatalytic $CO_2$ reduction on ZnSe quantum dots

C. D. Sahm, E. Mates-Torres, N. Eliasson, K. Sokołowski, A. Wagner, K. E. Dalle, Z. Huang, O. A. Scherman, L. Hammarström, M. García-Melchor and E. Reisner, *Chem. Sci.*, 2021, **12**, 9078 **DOI:** 10.1039/D1SC01310F

This article is licensed under a Creative Commons Attribution 3.0 Unported Licence. You can use material from this article in other publications without requesting further permissions from the RSC, provided that the correct acknowledgement is given.

Read more about how to correctly acknowledge RSC content.

## Figure 1.11b

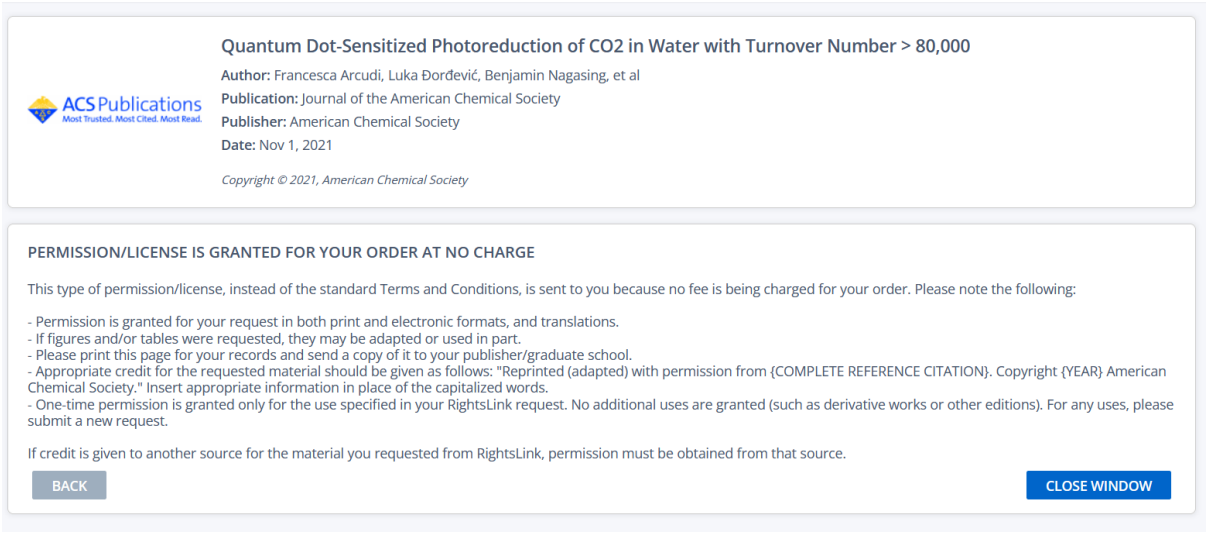

Quantum Dot-Sensitized Photoreduction of CO2 in Water with Turnover Number > 80,000

**Author:** Francesca Arcudi, Luka Đorđević, Benjamin Nagasing, et al

**Publication:** Journal of the American Chemical Society

**Publisher:** American Chemical Society

**Date:** Nov 1, 2021

*Copyright © 2021, American Chemical Society*

**PERMISSION/LICENSE IS GRANTED FOR YOUR ORDER AT NO CHARGE**

This type of permission/license, instead of the standard Terms and Conditions, is sent to you because no fee is being charged for your order. Please note the following:

- Permission is granted for your request in both print and electronic formats, and translations.
- If figures and/or tables were requested, they may be adapted or used in part.
- Please print this page for your records and send a copy of it to your publisher/graduate school.
- Appropriate credit for the requested material should be given as follows: "Reprinted (adapted) with permission from {COMPLETE REFERENCE CITATION}. Copyright {YEAR} American Chemical Society." Insert appropriate information in place of the capitalized words.
- One-time permission is granted only for the use specified in your RightsLink request. No additional uses are granted (such as derivative works or other editions). For any uses, please submit a new request.

If credit is given to another source for the material you requested from RightsLink, permission must be obtained from that source.

BACK CLOSE WINDOW

# Chapter 3

RightsLink

Sign in/Register

ACS Publications
Most Trusted. Most Cited. Most Read.

Deciphering the Role of Light Excitation Attributes in Plasmonic Photocatalysis: The Case of Nicotinamide Cofactor Regeneration

**Author:** Vanshika Jain, Indra Narayan Chakraborty, Rohit B. Raj, et al
**Publication:** The Journal of Physical Chemistry C
**Publisher:** American Chemical Society
**Date:** Mar 1, 2023

*Copyright © 2023, American Chemical Society*

PERMISSION/LICENSE IS GRANTED FOR YOUR ORDER AT NO CHARGE

This type of permission/license, instead of the standard Terms and Conditions, is sent to you because no fee is being charged for your order. Please note the following:

- Permission is granted for your request in both print and electronic formats, and translations.
- If figures and/or tables were requested, they may be adapted or used in part.
- Please print this page for your records and send a copy of it to your publisher/graduate school.
- Appropriate credit for the requested material should be given as follows: "Reprinted (adapted) with permission from {COMPLETE REFERENCE CITATION}. Copyright {YEAR} American Chemical Society." Insert appropriate information in place of the capitalized words.
- One-time permission is granted only for the use specified in your RightsLink request. No additional uses are granted (such as derivative works or other editions). For any uses, please submit a new request.

If credit is given to another source for the material you requested from RightsLink, permission must be obtained from that source.

BACK

CLOSE WINDOW

## Figure 3.2

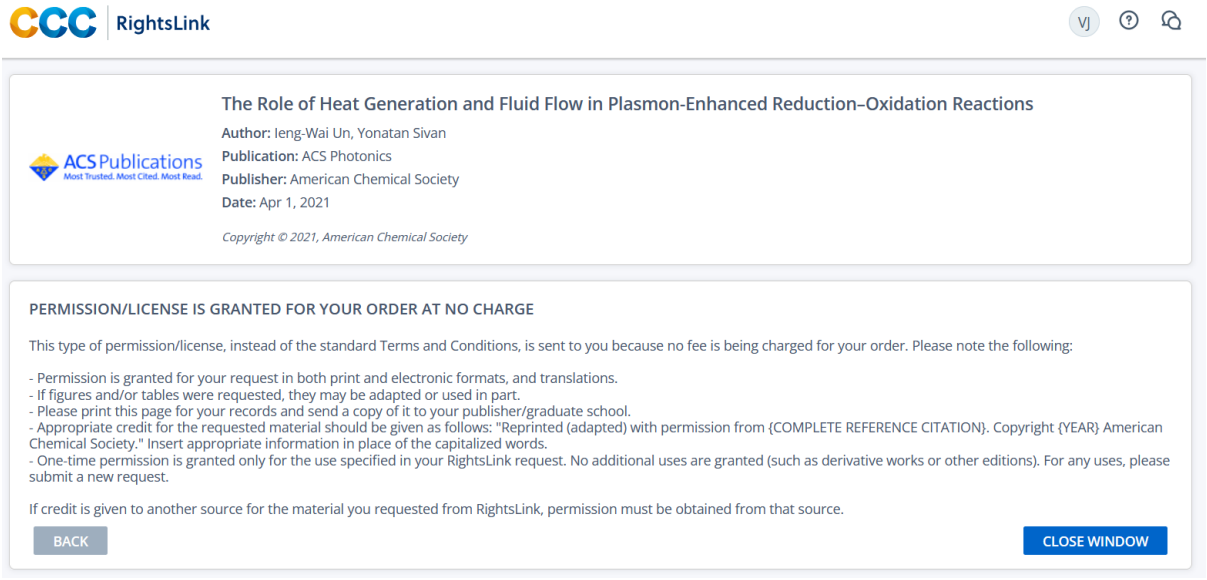

RightsLink

VJ

ACS Publications
Most Trusted. Most Cited. Most Read.

The Role of Heat Generation and Fluid Flow in Plasmon-Enhanced Reduction–Oxidation Reactions

**Author:** Ieng-Wai Un, Yonatan Sivan
**Publication:** ACS Photonics
**Publisher:** American Chemical Society
**Date:** Apr 1, 2021

*Copyright © 2021, American Chemical Society*

PERMISSION/LICENSE IS GRANTED FOR YOUR ORDER AT NO CHARGE

This type of permission/license, instead of the standard Terms and Conditions, is sent to you because no fee is being charged for your order. Please note the following:

- Permission is granted for your request in both print and electronic formats, and translations.
- If figures and/or tables were requested, they may be adapted or used in part.
- Please print this page for your records and send a copy of it to your publisher/graduate school.
- Appropriate credit for the requested material should be given as follows: "Reprinted (adapted) with permission from {COMPLETE REFERENCE CITATION}. Copyright {YEAR} American Chemical Society." Insert appropriate information in place of the capitalized words.
- One-time permission is granted only for the use specified in your RightsLink request. No additional uses are granted (such as derivative works or other editions). For any uses, please submit a new request.

If credit is given to another source for the material you requested from RightsLink, permission must be obtained from that source.

BACK

CLOSE WINDOW

## Figure 3.5

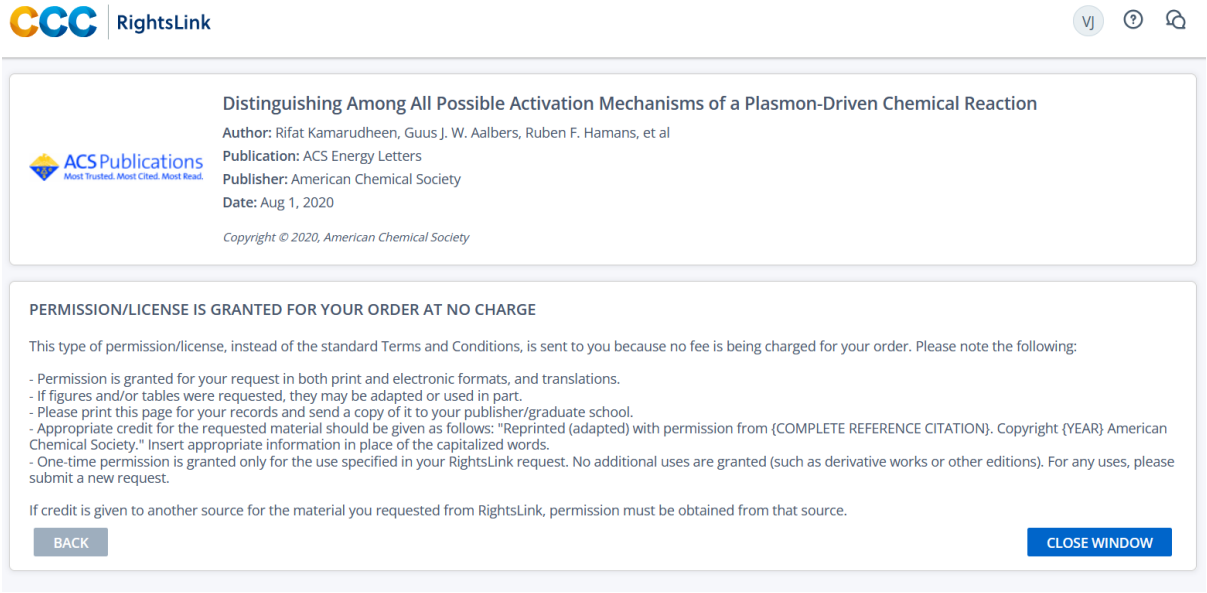

RightsLink

VJ

ACS Publications
Most Trusted. Most Cited. Most Read.

Distinguishing Among All Possible Activation Mechanisms of a Plasmon-Driven Chemical Reaction

**Author:** Rifat Kamarudheen, Guus J. W. Aalbers, Ruben F. Hamans, et al
**Publication:** ACS Energy Letters
**Publisher:** American Chemical Society
**Date:** Aug 1, 2020

*Copyright © 2020, American Chemical Society*

PERMISSION/LICENSE IS GRANTED FOR YOUR ORDER AT NO CHARGE

This type of permission/license, instead of the standard Terms and Conditions, is sent to you because no fee is being charged for your order. Please note the following:

- Permission is granted for your request in both print and electronic formats, and translations.
- If figures and/or tables were requested, they may be adapted or used in part.
- Please print this page for your records and send a copy of it to your publisher/graduate school.
- Appropriate credit for the requested material should be given as follows: "Reprinted (adapted) with permission from {COMPLETE REFERENCE CITATION}. Copyright {YEAR} American Chemical Society." Insert appropriate information in place of the capitalized words.
- One-time permission is granted only for the use specified in your RightsLink request. No additional uses are granted (such as derivative works or other editions). For any uses, please submit a new request.

If credit is given to another source for the material you requested from RightsLink, permission must be obtained from that source.

BACK

CLOSE WINDOW

# Chapter 4a: Permission

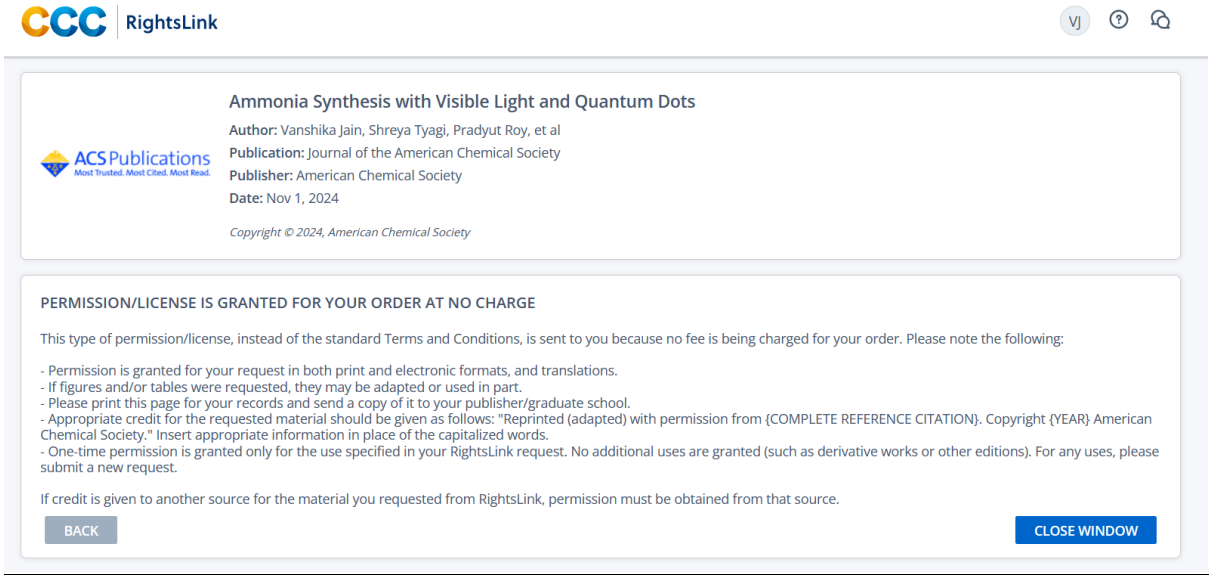

RightsLink

VJ

ACS Publications
Most Trusted. Most Cited. Most Read.

## Ammonia Synthesis with Visible Light and Quantum Dots

**Author:** Vanshika Jain, Shreya Tyagi, Pradyut Roy, et al
**Publication:** Journal of the American Chemical Society
**Publisher:** American Chemical Society
**Date:** Nov 1, 2024

*Copyright © 2024, American Chemical Society*

**PERMISSION/LICENSE IS GRANTED FOR YOUR ORDER AT NO CHARGE**

This type of permission/license, instead of the standard Terms and Conditions, is sent to you because no fee is being charged for your order. Please note the following:

- Permission is granted for your request in both print and electronic formats, and translations.
- If figures and/or tables were requested, they may be adapted or used in part.
- Please print this page for your records and send a copy of it to your publisher/graduate school.
- Appropriate credit for the requested material should be given as follows: "Reprinted (adapted) with permission from {COMPLETE REFERENCE CITATION}. Copyright {YEAR} American Chemical Society." Insert appropriate information in place of the capitalized words.
- One-time permission is granted only for the use specified in your RightsLink request. No additional uses are granted (such as derivative works or other editions). For any uses, please submit a new request.

If credit is given to another source for the material you requested from RightsLink, permission must be obtained from that source.

BACK

CLOSE WINDOW

# Figure 4a.2 (a-d)

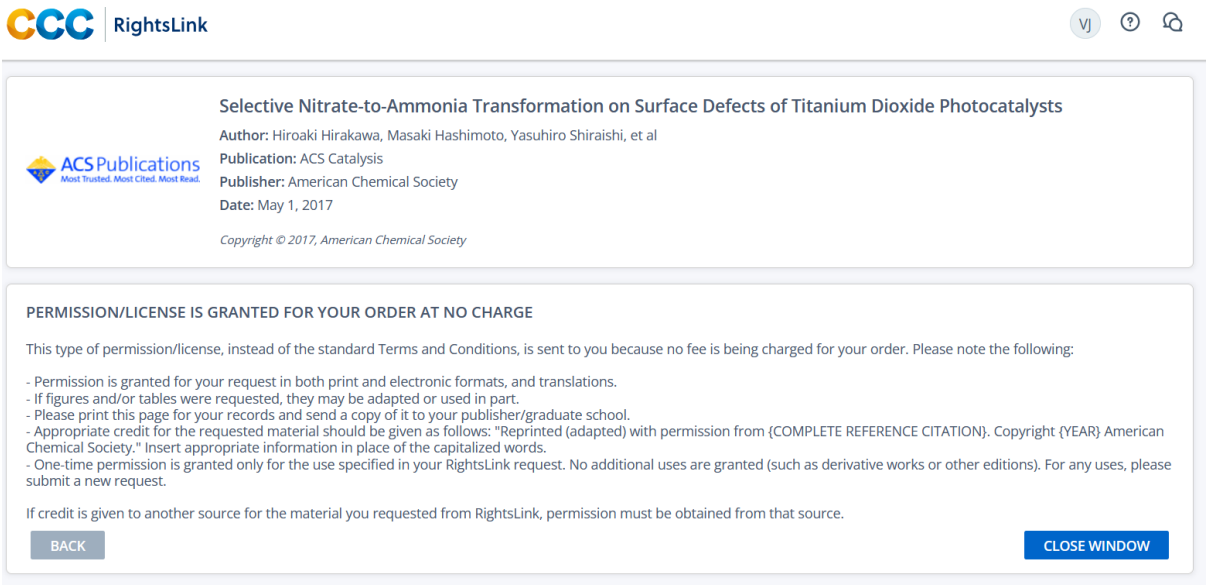

## Figure 4a.3a

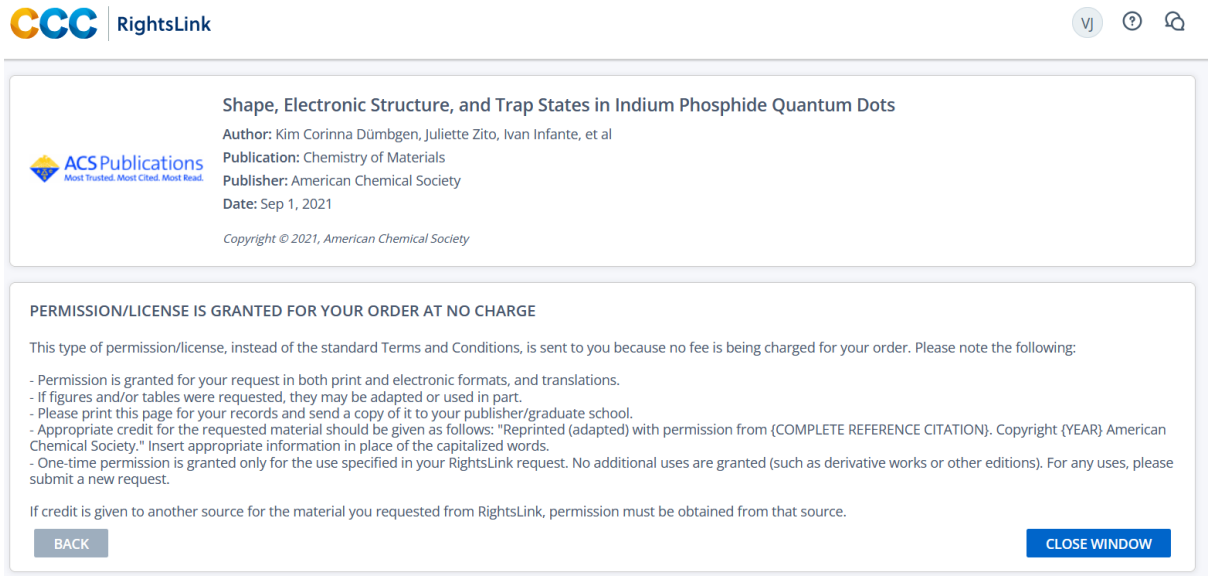


## Figure 4a.3d

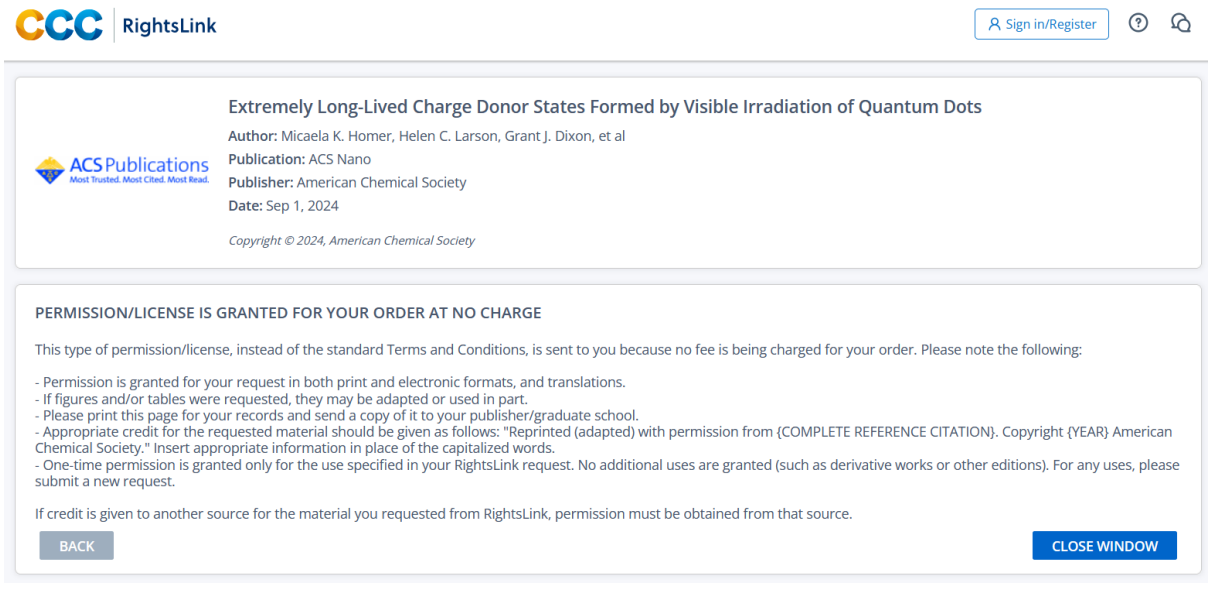

# Figure 4a.3e

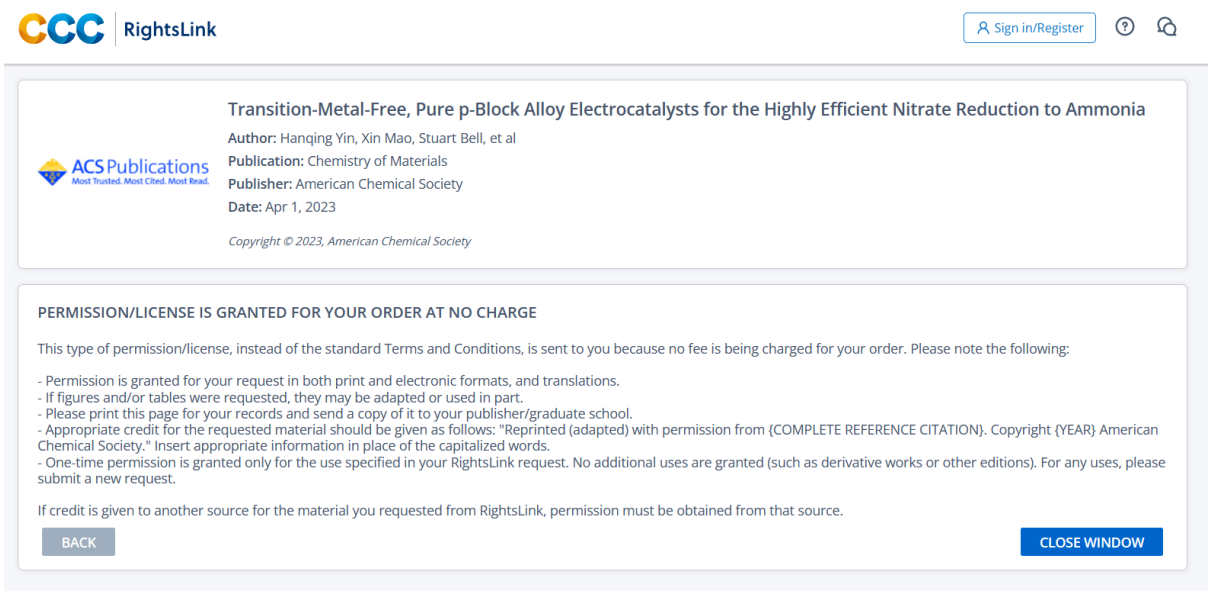
RightsLink
Sign in/Register
Transition-Metal-Free, Pure p-Block Alloy Electrocatalysts for the Highly Efficient Nitrate Reduction to Ammonia
Author: Hanqing Yin, Xin Mao, Stuart Bell, et al
Publication: Chemistry of Materials
Publisher: American Chemical Society
Date: Apr 1, 2023
Copyright © 2023, American Chemical Society
PERMISSION/LICENSE IS GRANTED FOR YOUR ORDER AT NO CHARGE
This type of permission/license, instead of the standard Terms and Conditions, is sent to you because no fee is being charged for your order. Please note the following:
- Permission is granted for your request in both print and electronic formats, and translations.
- If figures and/or tables were requested, they may be adapted or used in part.
- Please print this page for your records and send a copy of it to your publisher/graduate school.
- Appropriate credit for the requested material should be given as follows: "Reprinted (adapted) with permission from {COMPLETE REFERENCE CITATION}. Copyright {YEAR} American Chemical Society." Insert appropriate information in place of the capitalized words.
- One-time permission is granted only for the use specified in your RightsLink request. No additional uses are granted (such as derivative works or other editions). For any uses, please submit a new request.
If credit is given to another source for the material you requested from RightsLink, permission must be obtained from that source.
BACK
CLOSE WINDOW

# Figure 4a.2 e-,f

ELSEVIER LICENSE
TERMS AND CONDITIONS

Mar 03, 2025

---

This Agreement between Vanshika Jain/ IISER Pune ("You") and Elsevier ("Elsevier") consists of your license details and the terms and conditions provided by Elsevier and Copyright Clearance Center.

| | |
|---|---|
| License Number | 5981280416476 |
| License date | Mar 03, 2025 |
| Licensed Content Publisher | Elsevier |
| Licensed Content Publication | Applied Catalysis B: Environment and Energy |
| Licensed Content Title | A facile preparation of Ag2O/P25 photocatalyst for selective reduction of nitrate |
| Licensed Content Author | Hai-Tao Ren,Shao-Yi Jia,Ji-Jun Zou,Song-Hai Wu,Xu Han |
| Licensed Content Date | Oct 1, 2015 |
| Licensed Content Volume | 176 |
| Licensed Content Issue | n/a |
| Licensed Content Pages | 9 |
| Start Page | 53 |
| End Page | 61 |
| Type of Use | reuse in a thesis/dissertation |

| | |
|---|---|
| Portion | figures/tables/illustrations |
| Number of figures/tables/illustrations | 1 |
| Format | both print and electronic |
| Are you the author of this Elsevier article? | No |
| Will you be translating? | No |
| Title of new work | Light-Driven Multielectron Chemical Transformations with Tailored Nanoparticles |
| Institution name | Indian Institute of Science Education and Research (IISER) Pune |
| Expected presentation date | Jun 2025 |
| Portions | Scheme 1 |
| The Requesting Person / Organization to Appear on the License | Vanshika Jain/ IISER Pune |
| Requestor Location | Ms. Vanshika Jain<br>Department of Chemistry, IISER Pune<br><br>Pune, 411008<br>India |
| Publisher Tax ID | GB 494 6272 12 |
| Total | 0.00 USD |

Terms and Conditions

**INTRODUCTION**

1. The publisher for this copyrighted material is Elsevier. By clicking "accept" in connection with completing this licensing transaction, you agree that the following terms

and conditions apply to this transaction (along with the Billing and Payment terms and conditions established by Copyright Clearance Center, Inc. ("CCC"), at the time that you opened your RightsLink account and that are available at any time at https://myaccount.copyright.com).

## GENERAL TERMS

2. Elsevier hereby grants you permission to reproduce the aforementioned material subject to the terms and conditions indicated.

3. Acknowledgement: If any part of the material to be used (for example, figures) has appeared in our publication with credit or acknowledgement to another source, permission must also be sought from that source. If such permission is not obtained then that material may not be included in your publication/copies. Suitable acknowledgement to the source must be made, either as a footnote or in a reference list at the end of your publication, as follows:

"Reprinted from Publication title, Vol /edition number, Author(s), Title of article / title of chapter, Pages No., Copyright (Year), with permission from Elsevier [OR APPLICABLE SOCIETY COPYRIGHT OWNER]." Also Lancet special credit - "Reprinted from The Lancet, Vol. number, Author(s), Title of article, Pages No., Copyright (Year), with permission from Elsevier."

4. Reproduction of this material is confined to the purpose and/or media for which permission is hereby given. The material may not be reproduced or used in any other way, including use in combination with an artificial intelligence tool (including to train an algorithm, test, process, analyse, generate output and/or develop any form of artificial intelligence tool), or to create any derivative work and/or service (including resulting from the use of artificial intelligence tools).

5. Altering/Modifying Material: Not Permitted. However figures and illustrations may be altered/adapted minimally to serve your work. Any other abbreviations, additions, deletions and/or any other alterations shall be made only with prior written authorization of Elsevier Ltd. (Please contact Elsevier's permissions helpdesk here). No modifications can be made to any Lancet figures/tables and they must be reproduced in full.

6. If the permission fee for the requested use of our material is waived in this instance, please be advised that your future requests for Elsevier materials may attract a fee.

7. Reservation of Rights: Publisher reserves all rights not specifically granted in the combination of (i) the license details provided by you and accepted in the course of this licensing transaction, (ii) these terms and conditions and (iii) CCC's Billing and Payment terms and conditions.

8. License Contingent Upon Payment: While you may exercise the rights licensed immediately upon issuance of the license at the end of the licensing process for the transaction, provided that you have disclosed complete and accurate details of your proposed use, no license is finally effective unless and until full payment is received from you (either by publisher or by CCC) as provided in CCC's Billing and Payment terms and conditions. If full payment is not received on a timely basis, then any license preliminarily granted shall be deemed automatically revoked and shall be void as if never granted. Further, in the event that you breach any of these terms and conditions or any of CCC's Billing and Payment terms and conditions, the license is automatically revoked and shall be void as if never granted. Use of materials as described in a revoked license, as well as any use of the materials beyond the scope of an unrevoked license, may constitute copyright infringement and publisher reserves the right to take any and all action to

protect its copyright in the materials.

9. Warranties: Publisher makes no representations or warranties with respect to the licensed material.

10. Indemnity: You hereby indemnify and agree to hold harmless publisher and CCC, and their respective officers, directors, employees and agents, from and against any and all claims arising out of your use of the licensed material other than as specifically authorized pursuant to this license.

11. No Transfer of License: This license is personal to you and may not be sublicensed, assigned, or transferred by you to any other person without publisher's written permission.

12. No Amendment Except in Writing: This license may not be amended except in a writing signed by both parties (or, in the case of publisher, by CCC on publisher's behalf).

13. Objection to Contrary Terms: Publisher hereby objects to any terms contained in any purchase order, acknowledgment, check endorsement or other writing prepared by you, which terms are inconsistent with these terms and conditions or CCC's Billing and Payment terms and conditions. These terms and conditions, together with CCC's Billing and Payment terms and conditions (which are incorporated herein), comprise the entire agreement between you and publisher (and CCC) concerning this licensing transaction. In the event of any conflict between your obligations established by these terms and conditions and those established by CCC's Billing and Payment terms and conditions, these terms and conditions shall control.

14. Revocation: Elsevier or Copyright Clearance Center may deny the permissions described in this License at their sole discretion, for any reason or no reason, with a full refund payable to you. Notice of such denial will be made using the contact information provided by you. Failure to receive such notice will not alter or invalidate the denial. In no event will Elsevier or Copyright Clearance Center be responsible or liable for any costs, expenses or damage incurred by you as a result of a denial of your permission request, other than a refund of the amount(s) paid by you to Elsevier and/or Copyright Clearance Center for denied permissions.

## LIMITED LICENSE

The following terms and conditions apply only to specific license types:

15. **Translation**: This permission is granted for non-exclusive world **English** rights only unless your license was granted for translation rights. If you licensed translation rights you may only translate this content into the languages you requested. A professional translator must perform all translations and reproduce the content word for word preserving the integrity of the article.

16. **Posting licensed content on any Website**: The following terms and conditions apply as follows: Licensing material from an Elsevier journal: All content posted to the web site must maintain the copyright information line on the bottom of each image; A hyper-text must be included to the Homepage of the journal from which you are licensing at http://www.sciencedirect.com/science/journal/xxxxx or the Elsevier homepage for books at http://www.elsevier.com; Central Storage: This license does not include permission for a scanned version of the material to be stored in a central repository such as that provided by Heron/XanEdu.

Licensing material from an Elsevier book: A hyper-text link must be included to the Elsevier homepage at http://www.elsevier.com . All content posted to the web site must

maintain the copyright information line on the bottom of each image.

**Posting licensed content on Electronic reserve**: In addition to the above the following clauses are applicable: The web site must be password-protected and made available only to bona fide students registered on a relevant course. This permission is granted for 1 year only. You may obtain a new license for future website posting.

17. **For journal authors:** the following clauses are applicable in addition to the above:

**Preprints:**

A preprint is an author's own write-up of research results and analysis, it has not been peer-reviewed, nor has it had any other value added to it by a publisher (such as formatting, copyright, technical enhancement etc.).

Authors can share their preprints anywhere at any time. Preprints should not be added to or enhanced in any way in order to appear more like, or to substitute for, the final versions of articles however authors can update their preprints on arXiv or RePEc with their Accepted Author Manuscript (see below).

If accepted for publication, we encourage authors to link from the preprint to their formal publication via its DOI. Millions of researchers have access to the formal publications on ScienceDirect, and so links will help users to find, access, cite and use the best available version. Please note that Cell Press, The Lancet and some society-owned have different preprint policies. Information on these policies is available on the journal homepage.

**Accepted Author Manuscripts:** An accepted author manuscript is the manuscript of an article that has been accepted for publication and which typically includes author-incorporated changes suggested during submission, peer review and editor-author communications.

Authors can share their accepted author manuscript:

- immediately
    - via their non-commercial person homepage or blog
    - by updating a preprint in arXiv or RePEc with the accepted manuscript
    - via their research institute or institutional repository for internal institutional uses or as part of an invitation-only research collaboration work-group
    - directly by providing copies to their students or to research collaborators for their personal use
    - for private scholarly sharing as part of an invitation-only work group on commercial sites with which Elsevier has an agreement
- After the embargo period
    - via non-commercial hosting platforms such as their institutional repository
    - via commercial sites with which Elsevier has an agreement

In all cases accepted manuscripts should:

- link to the formal publication via its DOI
- bear a CC-BY-NC-ND license - this is easy to do
- if aggregated with other manuscripts, for example in a repository or other site, be shared in alignment with our hosting policy not be added to or enhanced in any way to appear more like, or to substitute for, the published journal article.

**Published journal article (JPA):** A published journal article (PJA) is the definitive final

record of published research that appears or will appear in the journal and embodies all value-adding publishing activities including peer review co-ordination, copy-editing, formatting, (if relevant) pagination and online enrichment.

Policies for sharing publishing journal articles differ for subscription and gold open access articles:

**Subscription Articles:** If you are an author, please share a link to your article rather than the full-text. Millions of researchers have access to the formal publications on ScienceDirect, and so links will help your users to find, access, cite, and use the best available version.

Theses and dissertations which contain embedded PJAs as part of the formal submission can be posted publicly by the awarding institution with DOI links back to the formal publications on ScienceDirect.

If you are affiliated with a library that subscribes to ScienceDirect you have additional private sharing rights for others' research accessed under that agreement. This includes use for classroom teaching and internal training at the institution (including use in course packs and courseware programs), and inclusion of the article for grant funding purposes.

**Gold Open Access Articles:** May be shared according to the author-selected end-user license and should contain a CrossMark logo, the end user license, and a DOI link to the formal publication on ScienceDirect.

Please refer to Elsevier's posting policy for further information.

18. **For book authors** the following clauses are applicable in addition to the above: Authors are permitted to place a brief summary of their work online only. You are not allowed to download and post the published electronic version of your chapter, nor may you scan the printed edition to create an electronic version. **Posting to a repository:** Authors are permitted to post a summary of their chapter only in their institution's repository.

19. **Thesis/Dissertation**: If your license is for use in a thesis/dissertation your thesis may be submitted to your institution in either print or electronic form. Should your thesis be published commercially, please reapply for permission. These requirements include permission for the Library and Archives of Canada to supply single copies, on demand, of the complete thesis and include permission for Proquest/UMI to supply single copies, on demand, of the complete thesis. Should your thesis be published commercially, please reapply for permission. Theses and dissertations which contain embedded PJAs as part of the formal submission can be posted publicly by the awarding institution with DOI links back to the formal publications on ScienceDirect.

## Elsevier Open Access Terms and Conditions

You can publish open access with Elsevier in hundreds of open access journals or in nearly 2000 established subscription journals that support open access publishing. Permitted third party re-use of these open access articles is defined by the author's choice of Creative Commons user license. See our open access license policy for more information.

**Terms & Conditions applicable to all Open Access articles published with Elsevier:**

Any reuse of the article must not represent the author as endorsing the adaptation of the article nor should the article be modified in such a way as to damage the author's honour or reputation. If any changes have been made, such changes must be clearly indicated.

The author(s) must be appropriately credited and we ask that you include the end user license and a DOI link to the formal publication on ScienceDirect.

If any part of the material to be used (for example, figures) has appeared in our publication with credit or acknowledgement to another source it is the responsibility of the user to ensure their reuse complies with the terms and conditions determined by the rights holder.

**Additional Terms & Conditions applicable to each Creative Commons user license:**

**CC BY:** The CC-BY license allows users to copy, to create extracts, abstracts and new works from the Article, to alter and revise the Article and to make commercial use of the Article (including reuse and/or resale of the Article by commercial entities), provided the user gives appropriate credit (with a link to the formal publication through the relevant DOI), provides a link to the license, indicates if changes were made and the licensor is not represented as endorsing the use made of the work. The full details of the license are available at http://creativecommons.org/licenses/by/4.0.

**CC BY NC SA:** The CC BY-NC-SA license allows users to copy, to create extracts, abstracts and new works from the Article, to alter and revise the Article, provided this is not done for commercial purposes, and that the user gives appropriate credit (with a link to the formal publication through the relevant DOI), provides a link to the license, indicates if changes were made and the licensor is not represented as endorsing the use made of the work. Further, any new works must be made available on the same conditions. The full details of the license are available at http://creativecommons.org/licenses/by-nc-sa/4.0.

**CC BY NC ND:** The CC BY-NC-ND license allows users to copy and distribute the Article, provided this is not done for commercial purposes and further does not permit distribution of the Article if it is changed or edited in any way, and provided the user gives appropriate credit (with a link to the formal publication through the relevant DOI), provides a link to the license, and that the licensor is not represented as endorsing the use made of the work. The full details of the license are available at http://creativecommons.org/licenses/by-nc-nd/4.0. Any commercial reuse of Open Access articles published with a CC BY NC SA or CC BY NC ND license requires permission from Elsevier and will be subject to a fee.

Commercial reuse includes:

- Associating advertising with the full text of the Article
- Charging fees for document delivery or access
- Article aggregation
- Systematic distribution via e-mail lists or share buttons

Posting or linking by commercial companies for use by customers of those companies.

20. **Other Conditions**:

v1.10

**Questions? customercare@copyright.com.**

# Chapter 4b: Permission

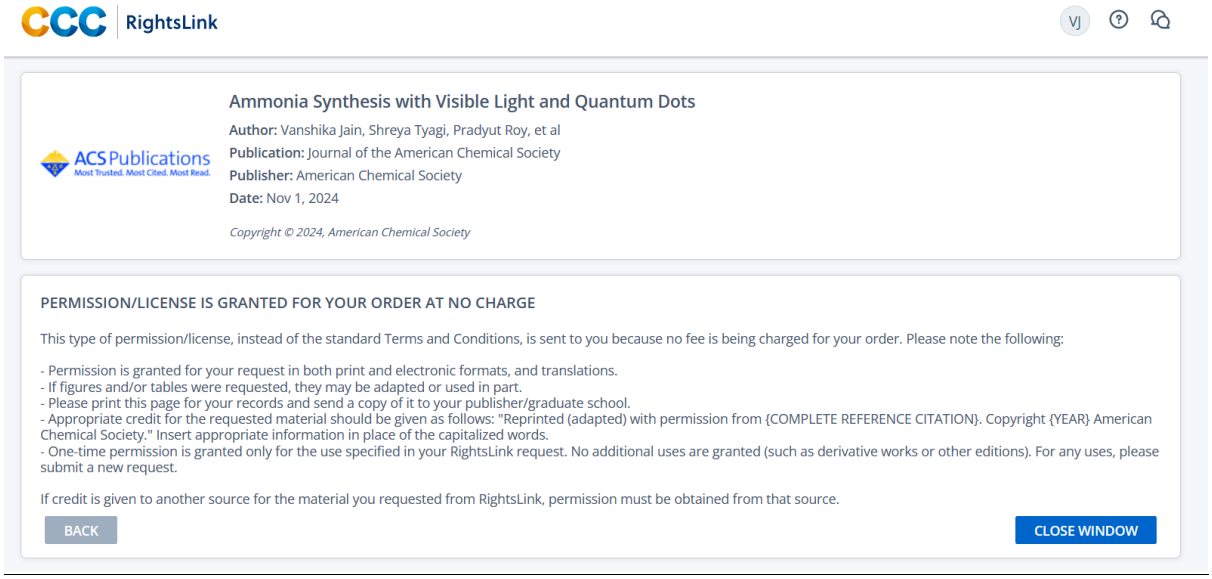

**Figure 4b.1**

## Reaction mechanism and selectivity regulation of photocatalytic nitrate reduction for wastewater purification: progress and challenges

W. Yang, J. Wang, R. Chen, L. Xiao, S. Shen, J. Li and F. Dong, *J. Mater. Chem. A*, 2022, **10**, 17357 **DOI:** 10.1039/D2TA04611C

To request permission to reproduce material from this article, please go to the Copyright Clearance Center request page.

If you are an author contributing to an RSC publication, you do not need to request permission provided correct acknowledgement is given.

If you are the author of this article, you do not need to request permission to reproduce figures and diagrams provided correct acknowledgement is given. If you want to reproduce the whole article in a third-party publication (excluding your thesis/dissertation for which permission is not required) please go to the Copyright Clearance Center request page.

Read more about how to correctly acknowledge RSC content.

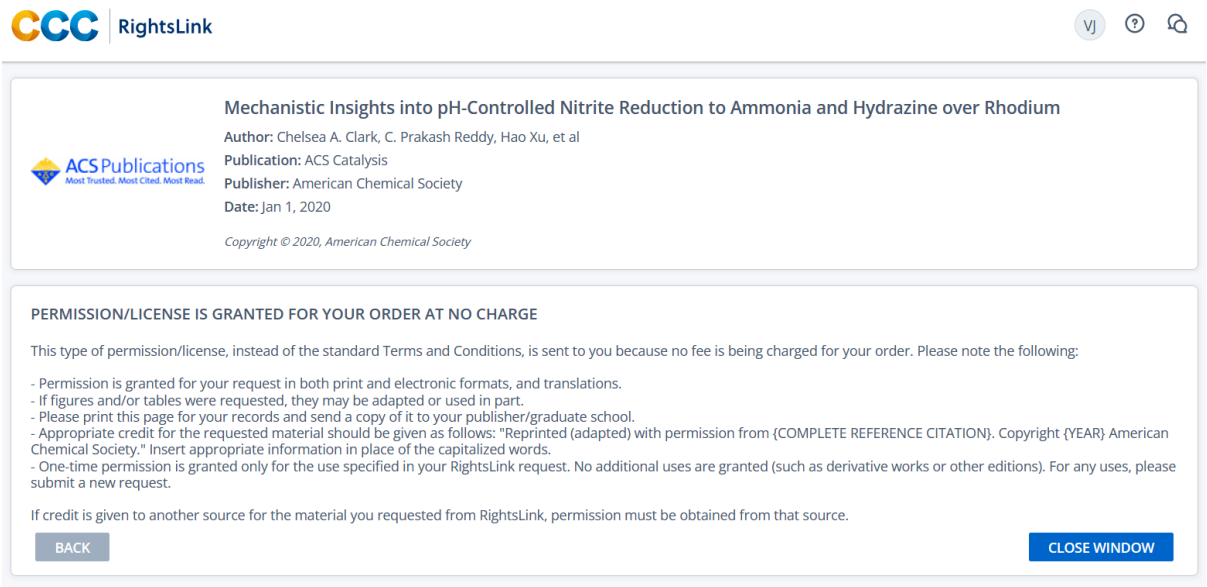

## Figure 4b.2

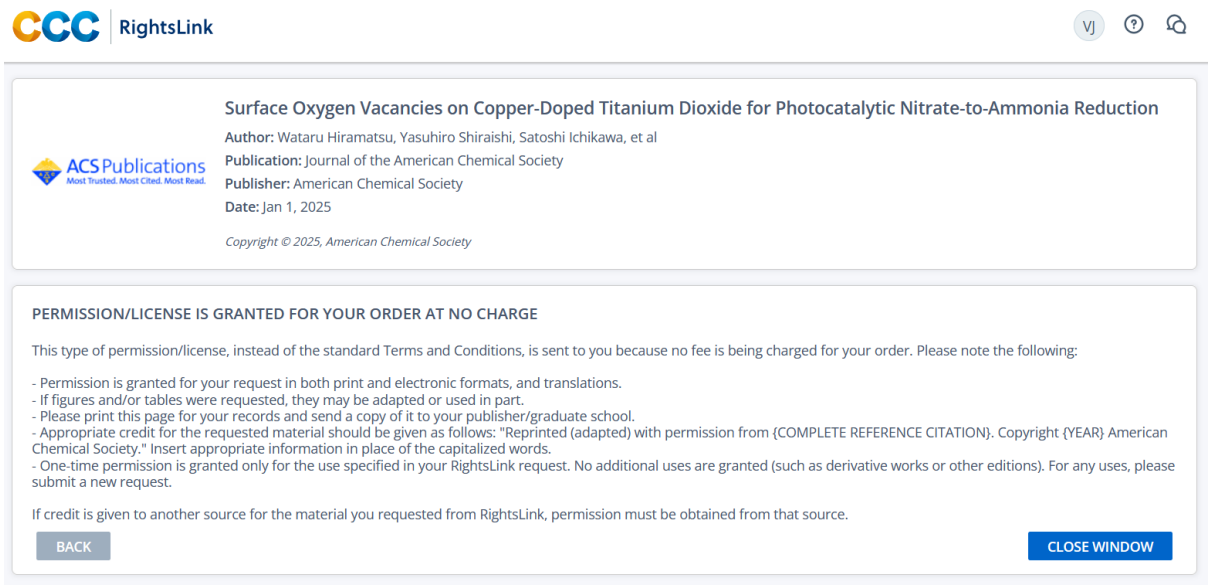


## Figure 4b.3a

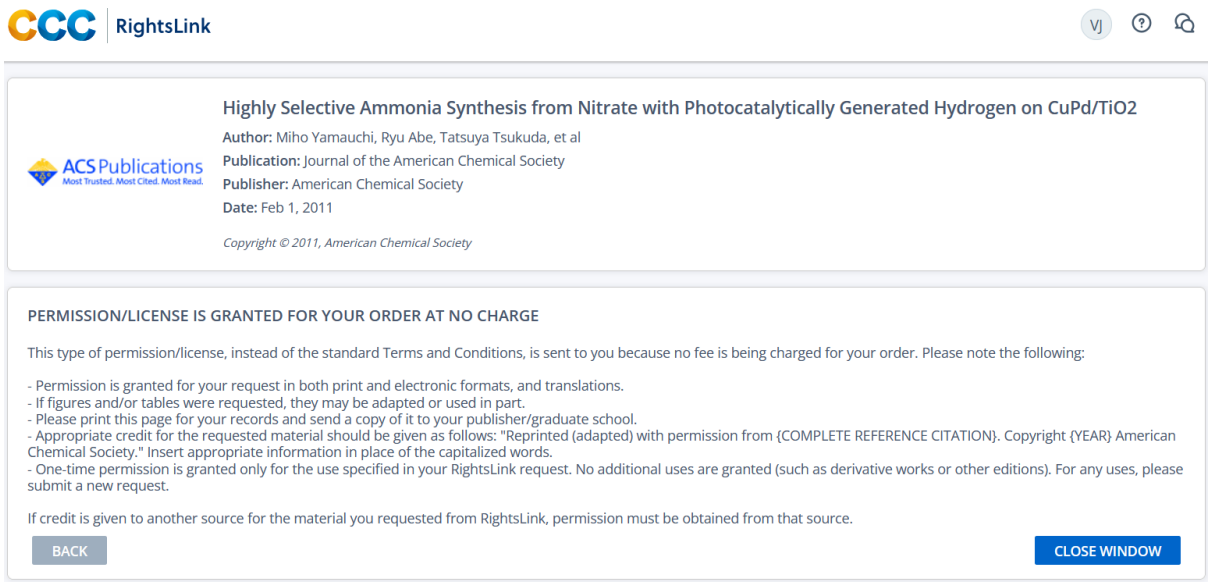

# Figure 4b.3b

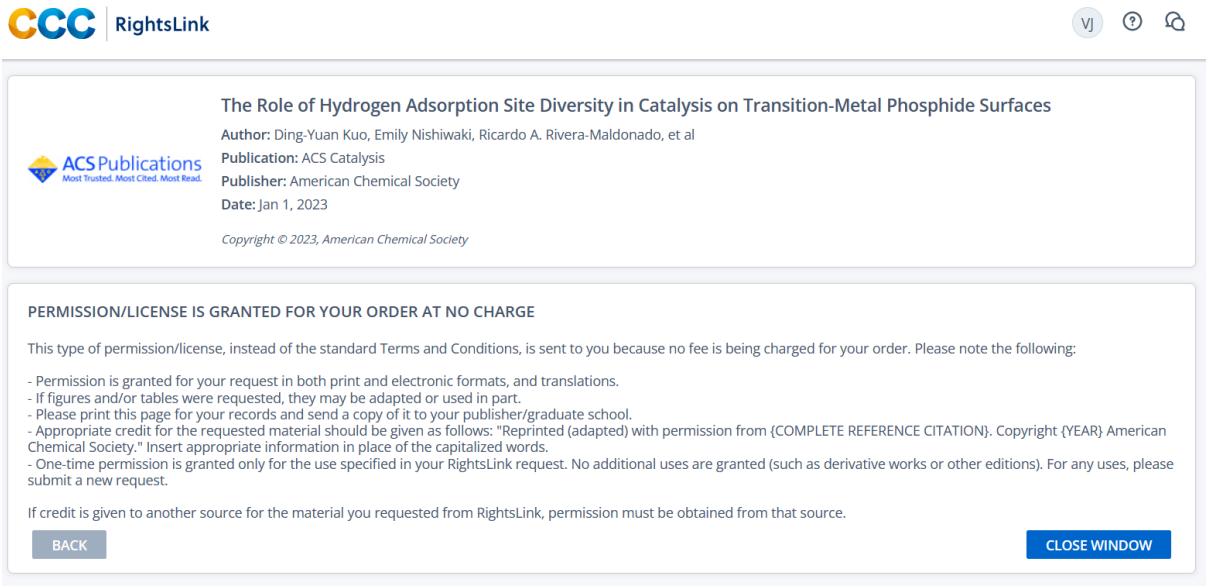

RightsLink

VJ

The Role of Hydrogen Adsorption Site Diversity in Catalysis on Transition-Metal Phosphide Surfaces

**Author:** Ding-Yuan Kuo, Emily Nishiwaki, Ricardo A. Rivera-Maldonado, et al

**Publication:** ACS Catalysis

**Publisher:** American Chemical Society

**Date:** Jan 1, 2023

*Copyright © 2023, American Chemical Society*

ACS Publications
Most Trusted. Most Cited. Most Read.

PERMISSION/LICENSE IS GRANTED FOR YOUR ORDER AT NO CHARGE

This type of permission/license, instead of the standard Terms and Conditions, is sent to you because no fee is being charged for your order. Please note the following:

- Permission is granted for your request in both print and electronic formats, and translations.
- If figures and/or tables were requested, they may be adapted or used in part.
- Please print this page for your records and send a copy of it to your publisher/graduate school.
- Appropriate credit for the requested material should be given as follows: "Reprinted (adapted) with permission from {COMPLETE REFERENCE CITATION}. Copyright {YEAR} American Chemical Society." Insert appropriate information in place of the capitalized words.
- One-time permission is granted only for the use specified in your RightsLink request. No additional uses are granted (such as derivative works or other editions). For any uses, please submit a new request.

If credit is given to another source for the material you requested from RightsLink, permission must be obtained from that source.

BACK

CLOSE WINDOW

# Figure 5.1a and 5.1b

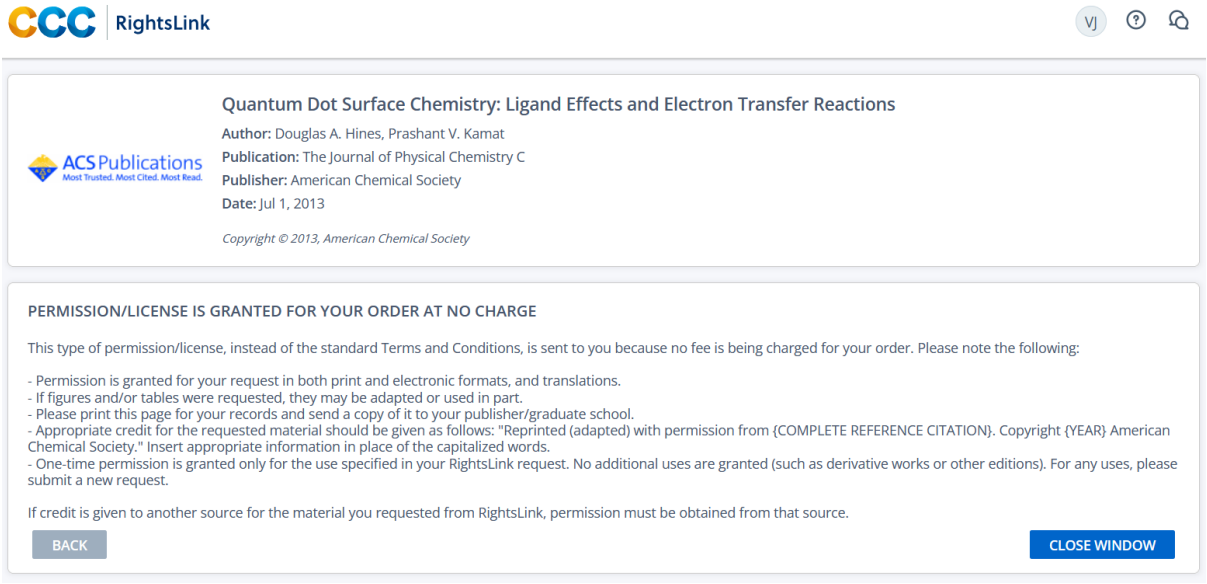

CCC RightsLink

VJ

ACS Publications
Most Trusted. Most Cited. Most Read.

Quantum Dot Surface Chemistry: Ligand Effects and Electron Transfer Reactions

**Author:** Douglas A. Hines, Prashant V. Kamat
**Publication:** The Journal of Physical Chemistry C
**Publisher:** American Chemical Society
**Date:** Jul 1, 2013

*Copyright © 2013, American Chemical Society*

PERMISSION/LICENSE IS GRANTED FOR YOUR ORDER AT NO CHARGE

This type of permission/license, instead of the standard Terms and Conditions, is sent to you because no fee is being charged for your order. Please note the following:

- Permission is granted for your request in both print and electronic formats, and translations.
- If figures and/or tables were requested, they may be adapted or used in part.
- Please print this page for your records and send a copy of it to your publisher/graduate school.
- Appropriate credit for the requested material should be given as follows: "Reprinted (adapted) with permission from {COMPLETE REFERENCE CITATION}. Copyright {YEAR} American Chemical Society." Insert appropriate information in place of the capitalized words.
- One-time permission is granted only for the use specified in your RightsLink request. No additional uses are granted (such as derivative works or other editions). For any uses, please submit a new request.

If credit is given to another source for the material you requested from RightsLink, permission must be obtained from that source.

BACK

CLOSE WINDOW

Figure 5.1 c,d

AIP PUBLISHING LICENSE
TERMS AND CONDITIONS

May 30, 2025

---

This Agreement between Vanshika Jain ("You") and AIP Publishing ("AIP Publishing") consists of your license details and the terms and conditions provided by AIP Publishing and Copyright Clearance Center.

| | |
|---|---|
| License Number | 6038690797626 |
| License date | May 30, 2025 |
| Licensed Content Publisher | AIP Publishing |
| Licensed Content Publication | Journal of Chemical Physics |
| Licensed Content Title | Gold nanoparticle on semiconductor quantum dot: Do surface ligands influence Fermi level equilibration |
| Licensed Content Author | Sandeep, K.; Manoj, B. |
| Licensed Content Date | Jan 27, 2020 |
| Licensed Content Volume | 152 |
| Licensed Content Issue | 4 |
| Type of Use | Thesis/Dissertation |
| Requestor type | University or Educational Institution |
| Format | Print and electronic |
| Portion | Figure/Table |

| | |
|---|---|
| Number of figures/tables | 1 |
| Will you be translating? | No |
| Title of new work | Light-Driven Multielectron Chemical Transformations with Tailored Nanoparticles |
| Institution name | Indian Institute of Science Education and Research (IISER) Pune |
| Expected presentation date | Jun 2025 |
| Portions | Figure 3 |
| The Requesting Person / Organization to Appear on the License | Vanshika Jain |
| Requestor Location | Ms. Vanshika Jain<br>Department of Chemistry, IISER Pune<br><br>Pune, 411008<br>India |
| Billing Type | Invoice |
| Billing Address | Ms. Vanshika Jain<br>Department of Chemistry, IISER Pune<br><br>Pune, India 411008 |
| Total | 0.00 USD |

Terms and Conditions

AIP Publishing -- Terms and Conditions: Permissions Uses

AIP Publishing hereby grants to you the non-exclusive right and license to use and/or distribute the Material according to the use specified in your order, on a one-time basis, for the specified term, with a maximum distribution equal to the number that you have

ordered. Any links or other content accompanying the Material are not the subject of this license.

1. You agree to include the following copyright and permission notice with the reproduction of the Material: "Reprinted from [FULL CITATION], with the permission of AIP Publishing." For an article, the credit line and permission notice must be printed on the first page of the article or book chapter. For photographs, covers, or tables, the notice may appear with the Material, in a footnote, or in the reference list.
2. If you have licensed reuse of a figure, photograph, cover, or table, it is your responsibility to ensure that the material is original to AIP Publishing and does not contain the copyright of another entity, and that the copyright notice of the figure, photograph, cover, or table does not indicate that it was reprinted by AIP Publishing, with permission, from another source. Under no circumstances does AIP Publishing purport or intend to grant permission to reuse material to which it does not hold appropriate rights.
   You may not alter or modify the Material in any manner. You may translate the Material into another language only if you have licensed translation rights. You may not use the Material for promotional purposes.
3. The foregoing license shall not take effect unless and until AIP Publishing or its agent, Copyright Clearance Center, receives the Payment in accordance with Copyright Clearance Center Billing and Payment Terms and Conditions, which are incorporated herein by reference.
4. AIP Publishing or Copyright Clearance Center may, within two business days of granting this license, revoke the license for any reason whatsoever, with a full refund payable to you. Should you violate the terms of this license at any time, AIP Publishing, or Copyright Clearance Center may revoke the license with no refund to you. Notice of such revocation will be made using the contact information provided by you. Failure to receive such notice will not nullify the revocation.
5. AIP Publishing makes no representations or warranties with respect to the Material. You agree to indemnify and hold harmless AIP Publishing, and their officers, directors, employees or agents from and against any and all claims arising out of your use of the Material other than as specifically authorized herein.
6. The permission granted herein is personal to you and is not transferable or assignable without the prior written permission of AIP Publishing. This license may not be amended except in a writing signed by the party to be charged.
7. If purchase orders, acknowledgments or check endorsements are issued on any forms containing terms and conditions which are inconsistent with these provisions, such inconsistent terms and conditions shall be of no force and effect. This document, including the CCC Billing and Payment Terms and Conditions, shall be the entire agreement between the parties relating to the subject matter hereof.

This Agreement shall be governed by and construed in accordance with the laws of the State of New York. Both parties hereby submit to the jurisdiction of the courts of New York County for purposes of resolving any disputes that may arise hereunder.

**Special Terms:**

V1.2

**Questions? customercare@copyright.com.**

## Figure 5.2

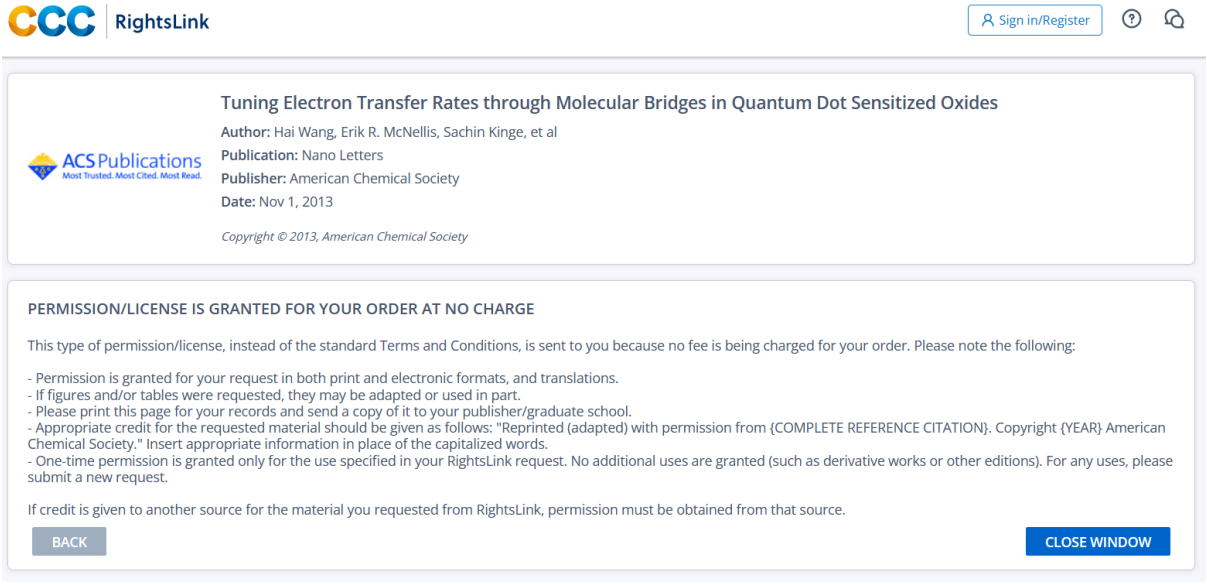
RightsLink
Sign in/Register
Tuning Electron Transfer Rates through Molecular Bridges in Quantum Dot Sensitized Oxides
Author: Hai Wang, Erik R. McNellis, Sachin Kinge, et al
Publication: Nano Letters
Publisher: American Chemical Society
Date: Nov 1, 2013
Copyright © 2013, American Chemical Society
ACS Publications
Most Trusted. Most Cited. Most Read.
PERMISSION/LICENSE IS GRANTED FOR YOUR ORDER AT NO CHARGE
This type of permission/license, instead of the standard Terms and Conditions, is sent to you because no fee is being charged for your order. Please note the following:
- Permission is granted for your request in both print and electronic formats, and translations.
- If figures and/or tables were requested, they may be adapted or used in part.
- Please print this page for your records and send a copy of it to your publisher/graduate school.
- Appropriate credit for the requested material should be given as follows: "Reprinted (adapted) with permission from {COMPLETE REFERENCE CITATION}. Copyright {YEAR} American Chemical Society." Insert appropriate information in place of the capitalized words.
- One-time permission is granted only for the use specified in your RightsLink request. No additional uses are granted (such as derivative works or other editions). For any uses, please submit a new request.
If credit is given to another source for the material you requested from RightsLink, permission must be obtained from that source.
BACK
CLOSE WINDOW

Figure 5.3 a,b

Vanshika Jain <jain.vanshika@students.iiserpune.ac.in>

# RE: THESIS/DISSERTATION USE – SCIENCE FIGURE – KOVALENKO ET AL 2009 DOI: 10.1126/science.1170524

1 message

**Dana James** <djames@aaas.org> Wed, Jun 4, 2025 at 12:21 AM
To: "jain.vanshika@students.iiserpune.ac.in" <jain.vanshika@students.iiserpune.ac.in>
Cc: permissions <permissions@aaas.org>

**AAAS MATERIAL:**

Figure 1 (a, b) from Kovalenko et al., *SCIENCE,* 12 Jun 2009

Vol 324, Issue 5933, pp. 1417-1420, DOI: 10.1126/science.1170524

**YOUR RE-USE: THESIS/DISSERTATION**

Title: Light-Driven Multielectron Chemical Transformations with Tailored Nanoparticles

Publication date: July 2025

Dear Vanshika:

Thank you very much for your interest in the AAAS material identified in your request.

We are pleased to have you include this material in your thesis or dissertation subject to the following guidelines. These guidelines also appear on our website: https://www.science.org/content/page/reprints-and-permissions under the heading 'Using AAAS material in a thesis or dissertation'.

**REPRODUCING AAAS MATERIAL IN YOUR THESIS OR DISSERTATION**

AAAS permits the use of content published in its journals but only provided the following criteria are met:

1. If you are using figures/tables, permission is granted for use in print and electronic versions of your dissertation or thesis.

2. A full text article may be used only in print versions of a dissertation or thesis. AAAS does not permit the reproduction of full text articles in electronic versions of theses or dissertations.

3. The following credit line must be printed along with the AAAS material: "From [Insert Full Reference Citation]/ Reprinted with permission from AAAS".

4. All required credit lines and notices must be visible any time a user accesses any part of the AAAS material and must appear on any printed copies that an authorized user might make.

5. The AAAS material may not be modified or altered except that figures and tables may be modified with permission from the author. Author permission for any such changes must be secured prior to your use.

6. AAAS must publish the full paper prior to your use of any of its text or figures.

7. If the AAAS material covered by this permission was published in *Science* during the years 1974-1994, you must also obtain permission from the author, who may grant or withhold permission, and who may or may not charge a fee if permission is granted. See original article for author's address. This condition does not apply to the news articles published in *Science*.

8. Permission covers the distribution of your dissertation or thesis on demand by a third party distributor (eg ProQuest/UMI), provided the AAAS material covered by this permission remains in situ and is not distributed by that third party outside of the context of your thesis/dissertation.

9. Permission does not apply to figures/photos/artwork or any other content or material included in your work that are credited to non-AAAS sources. If the requested material is sourced to or references non-AAAS sources, you must obtain authorization from that source as well before using that material. You agree to hold harmless and indemnify AAAS against any claims arising from your use of any content in your work that is credited to non-AAAS sources.

10. By using the AAAS Material identified in your request, you agree to abide by all the terms & conditions herein.

11. AAAS makes no representations or warranties as to the accuracy of any information contained in the AAAS material covered by this permission, including any warranties of merchantability or fitness for a particular purpose.

If how you wish to use the content falls outside of these guidelines or if you have any questions, please let me know.

Kind regards,

Dana James

AAAS
AMERICAN ASSOCIATION FOR THE ADVANCEMENT OF SCIENCE

**Dana James** *(she/her)*
Rights and Licensing Coordinator, Office of Publishing
**American Association for the Advancement of Science**
1200 New York Avenue, NW | Washington, DC 20005
| djames@aaas.org | www.aaas.org | www.science.org

---

**From:** Vanshika Jain <jain.vanshika@students.iiserpune.ac.in>
**Sent:** Friday, May 30, 2025 5:20 AM
**To:** permissions <permissions@aaas.org>
**Subject:** Request for permission for figure reuse in PhD Thesis

**[EXTERNAL EMAIL]**

Dear AAAS Publications Team

We would like to get the copyright permission for the following article from Science.

The following are the details:

AAAS publication title (journal title or website name/URL): https://www.science.org/doi/full/10.1126/science.1170524
Article title: **Colloidal Nanocrystals with Molecular Metal Chalcogenide Surface Ligands**
Authors' names: Maksym V. Kovalenko, Marcus Scheele, and Dmitri V. Talapin
Volume number, issue date, page numbers, DOI (provide all that apply): Vol 324, Issue 5933, page no. 1417-1420, **DOI: 10.1126/science.1170524**

Specific figure numbers or portion of text (or supply a copy): Figure 1a and b

Following information about your publication/project:

Type of work in which AAAS material will be used (e.g., book, journal, newsletter, poster, etc.): **PhD Thesis/dissertation**
Title of that work (the book/journal/newsletter, etc. in which you are reproducing the AAAS material): **Light-Driven Multielectron Chemical Transformations with Tailored Nanoparticles**
Title of the specific article/chapter in which you are reproducing the AAAS material (if applicable): **Metal-Solvent Complex on Quantum Dot Surface Enhances Ammonia Formation with Visible Light**
Author(s)/editor(s): Vanshika Jain
Expected publication date (or volume and issue number for journals): July 2025
Publishing company: **Indian Institute of Science Education and Research Pune, India**
Retail price (for books only)the – N/A
The formats your work will be distributed in (e.g., print, electronic, print and electronic): Print and electronic
The rights you are seeking: **To reuse figure in my PhD thesis.**

Please give us the required permission to re-use these images.

Thank you

--
Best regards,

Vanshika Jain | Ph.D. Student
Prof. Pramod Pillai Group
Department of Chemistry | IISER Pune
http://www.iiserpune.ac.in/~pramod/

## Figure 5.3c and 5.3d

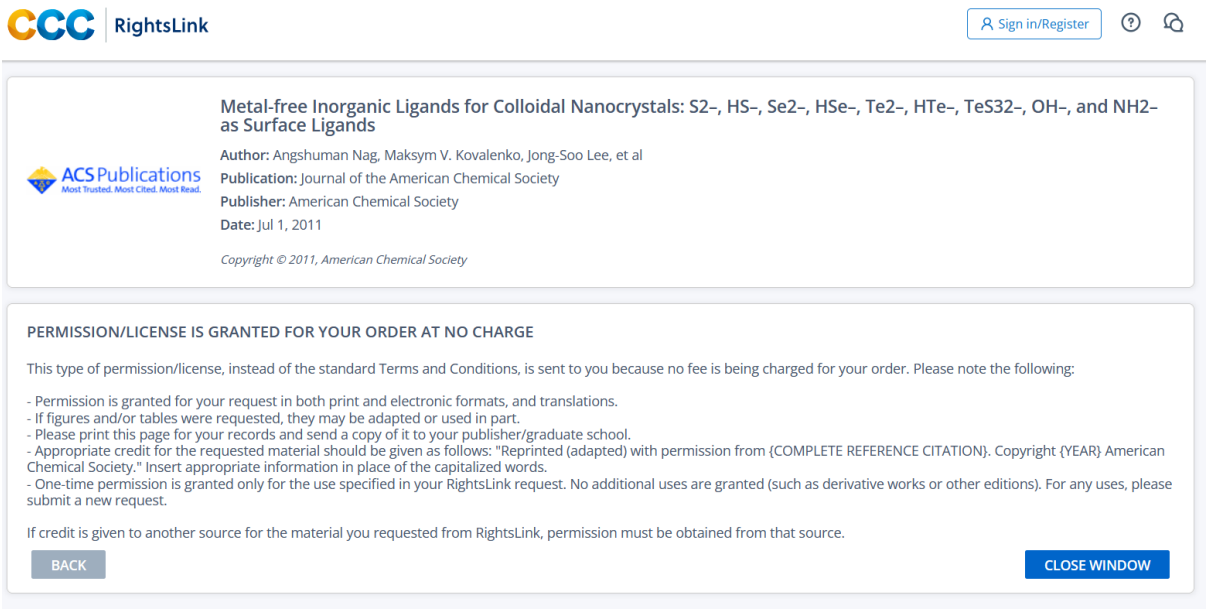

RightsLink

Sign in/Register

ACS Publications
Most Trusted. Most Cited. Most Read.

**Metal-free Inorganic Ligands for Colloidal Nanocrystals: S2–, HS–, Se2–, HSe–, Te2–, HTe–, TeS32–, OH–, and NH2– as Surface Ligands**

**Author:** Angshuman Nag, Maksym V. Kovalenko, Jong-Soo Lee, et al
**Publication:** Journal of the American Chemical Society
**Publisher:** American Chemical Society
**Date:** Jul 1, 2011

*Copyright © 2011, American Chemical Society*

PERMISSION/LICENSE IS GRANTED FOR YOUR ORDER AT NO CHARGE

This type of permission/license, instead of the standard Terms and Conditions, is sent to you because no fee is being charged for your order. Please note the following:

- Permission is granted for your request in both print and electronic formats, and translations.
- If figures and/or tables were requested, they may be adapted or used in part.
- Please print this page for your records and send a copy of it to your publisher/graduate school.
- Appropriate credit for the requested material should be given as follows: "Reprinted (adapted) with permission from {COMPLETE REFERENCE CITATION}. Copyright {YEAR} American Chemical Society." Insert appropriate information in place of the capitalized words.
- One-time permission is granted only for the use specified in your RightsLink request. No additional uses are granted (such as derivative works or other editions). For any uses, please submit a new request.

If credit is given to another source for the material you requested from RightsLink, permission must be obtained from that source.

BACK

CLOSE WINDOW

## Figure 5.3e and 5.3f

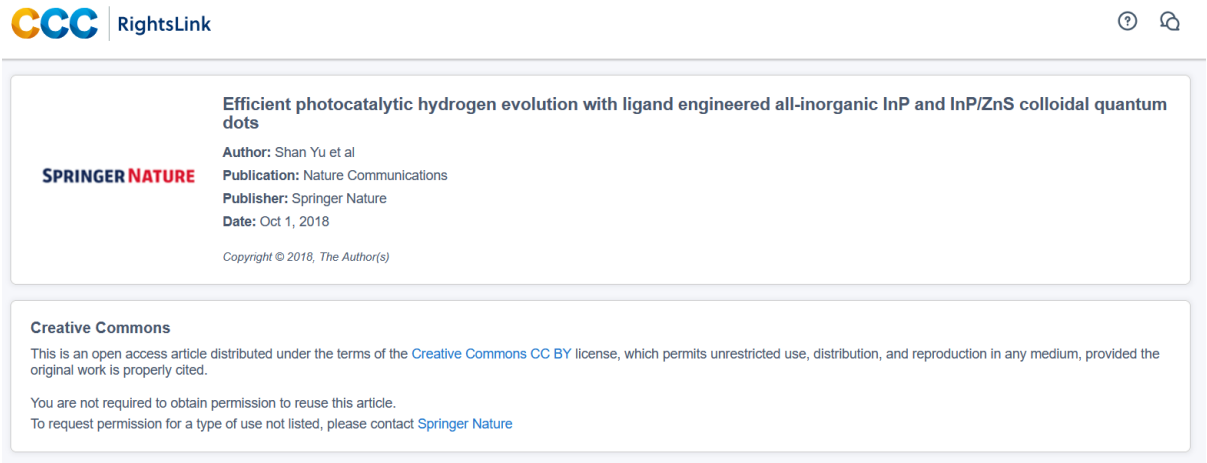

RightsLink

**Efficient photocatalytic hydrogen evolution with ligand engineered all-inorganic InP and InP/ZnS colloidal quantum dots**

**Author:** Shan Yu et al
**Publication:** Nature Communications
**Publisher:** Springer Nature
**Date:** Oct 1, 2018

*Copyright © 2018, The Author(s)*

**Creative Commons**

This is an open access article distributed under the terms of the Creative Commons CC BY license, which permits unrestricted use, distribution, and reproduction in any medium, provided the original work is properly cited.

You are not required to obtain permission to reuse this article.
To request permission for a type of use not listed, please contact Springer Nature